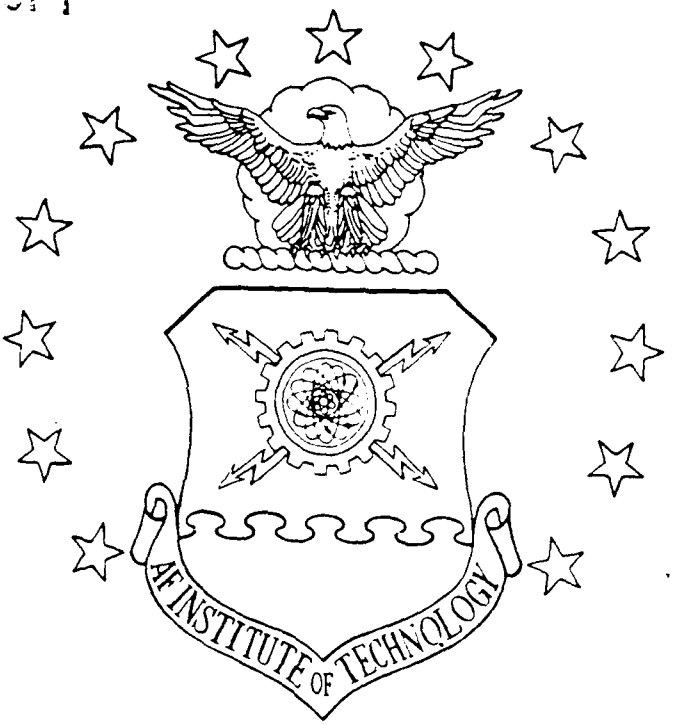

MEASUREMENT AND ANALYSIS OF THE ELECTROMAGNETIC SCATTERING OF A GEODESIC ARRAY OF TRIANGULAR TRIHEDRAL CORNER REFLECTORS

THESIS

Richard E. Hamilton, B.S.E.
Captain, USAF

AFIT/GE/ENG/90M-3

DEPARTMENT OF THE AIR FORCE
AIR UNIVERSITY
AIR FORCE INSTITUTE OF TECHNOLOGY
Wright-Patterson Air Force Base, Ohio

(1)

MEASUREMENT AND ANALYSIS OF THE ELECTROMAGNETIC SCATTERING OF A GEODESIC ARRAY OF TRIANGULAR TRIHEDRAL CORNER REFLECTORS

THESIS

Richard E. Hamilton, B.S.E.
Captain, USAF

AFIT/GE/ENG/90M-3

AFIT/GE/ENG/90M-3

MEASUREMENT AND ANALYSIS OF THE ELECTROMAGNETIC SCATTERING OF A GEODESIC ARRAY OF TRIANGULAR TRIHEDRAL CORNER REFLECTORS

THESIS

Presented to the Faculty of the School of Engineering
of the Air Force Institute of Technology
Air University
In Partial Fulfillment of the
Requirements for the Degree of
Master of Science in Electrical Engineering

Richard E. Hamilton, B.S.E.
Captain, USAF

March 1990

Preface

The purpose of this research was to investigate the electromagnetic scattering of a Geodesic Array of triangular trihedral corner reflectors. This research effort could not have been accomplished without the assistance of several persons to whom I would like to express my gratitude.

First, I would like to thank my thesis advisor, Dr Vittal Pyati, for his guidance and support. Second, I am indebted to Mr Ron Ruley and Mr Tim Hancock of the AFIT Fabrication Shop who constructed the targets and target mounting assemblies. Third, I would like to thank Mr Robert J. Puskar of Mission Research Corporation (MRC) for making the software package available for my use and Mr Stan Bashore, and Mr Richard Porter also of MRC for their support during the radar cross section (RCS) measurement phase of this research. I would especially like to thank Dr Tipton N. Patton for his friendship, genuine interest and continuous help throughout this endeavor.

Finally, I would like to thank my son Scott and wife Barbara for their assistance and companionship during the many hours required to obtain the RCS measurements; and my daughter Regina for her love and patience during this extremely long year.

Table of Contents

List of Figures

List of Tables

Abstract

This thesis investigated the electromagnetic (EM) scattering of a Geodesic Array consisting of a cluster of twenty trihedral corner reflectors held together by hinges. This target was designed to provide a large radar return with a spatial coverage greater than that due to an array of eight corner reflectors.

Radar cross section (RCS), or echo area, was chosen as a means of investigating the EM scattering of a scaled model version of the Geodesic Array. The RCS of the individual components of the Geodesic Array (i.e. the single corner reflectors) and the RCS of the Geodesic Array were measured using a continuous wave measurement technique. For the purpose of comparison the RCS of an eight corner reflector array was also measured. In order to gather as much spatial scattering information as possible, a unique target support mount was designed, constructed, and used to collect conical cut RCS patterns. The measured RCS patterns of the targets are included in the appendixes of this document.

A comparative analysis between the measured RCS of the Geodesic Array and that of the eight corner reflector array was performed to determine how well the Geodesic Array met its designed goal. Based on certain criteria it was found

that in almost all cases, the measured spatial RCS coverage for the Geodesic Array was equal to or better than the measured spatial RCS coverage of the array of eight corner reflectors. The only exception was for broadside incidence for which the Geodesic Array spatial coverage was slightly less.

The overall conclusion of this research effort was that the Geodesic Array is a viable target for the purpose of providing a large radar return over a large number of aspect angles. The recommendations stemming from this research are, to first compare the results presented in this document to results of other targets designed for this purpose, and based on this future comparison to decide if field testing of a full scale version of the Geodesic Array is warranted.

MEASUREMENT AND ANALYSIS OF THE ELECTROMAGNETIC SCATTERING OF A GEODESIC ARRAY OF TRIANGULAR TRIHEDRAL CORNER REFLECTORS

I. Introduction

Overview

The overall goal of this research effort was to characterize the electromagnetic scattering (EM) associated with an array of twenty triangular trihedral corner reflectors. Throughout this document this configuration of corner reflectors will be referred to as the "Geodesic Array". In this chapter we introduce the Geodesic Array by presenting its purpose and origin. This is followed by a discussion of radar cross section (RCS). The problem statement and general approach are given in the overview section and the chapter concludes with an preview of the chapters contained within this document.

Background

Since the inception of radar guided weapon systems as viable threats to airborne platforms, much effort has been concentrated on developing countermeasures against such threats. The use of chaff and electronic jamming have been developed and employed by airborne platforms as effective countermeasures against the radar assisted weapon systems.

Ground and sea based installations are also susceptible to attack from radar guided weapons and passive countermeasure devices are being developed to provide protection from the radar assisted threats (1:64). The purpose of these passive countermeasure devices can be to either conceal a potential target from detection by a surveillance type radar or to serve as a decoy against radar guided missiles. The concealment type devices are designed to enhance the radar clutter environment surrounding a target and should produce radar returns that are indistinguishable from the target it is protecting (1:64). The decoy type countermeasure device is designed to shift the radar centroid associated with a radar guided missile thereby causing the missile to miss its intended target (1:64). The later type devices have been traditionally called "radar decoys" and the Geodesic Array under investigation has been designed with this application in mind.

Radar decoys. The first characteristic that all radar decoys have in common is that when the energy from a radar impinges on their surface they must be capable of re-radiating a large amount of this energy in the direction of the radar's receiver. A measure of the amount of radar energy (incident on a target) that is reradiated in the direction of the radar's receive antenna is known as the

target's RCS. If the radar's transmit and receive antennas are located together the RCS is called monostatic RCS, otherwise the term bistatic RCS is used. Only the monostatic RCS was investigated during this research and all remaining references to RCS imply the monostatic case. Typically, the radar decoy is designed to present an RCS that is much greater than the object it is designed to protect (2:1).

The second requirement of a radar decoy is that the large RCS remain relatively constant over a wide range of radar operating frequencies (2:1). Additionally, if the radar decoy is to function without prior knowledge as to the location of the radar threat (no decoy steering capability is employed) it must be capable of providing the large RCS characteristic over a wide range of radar viewing angles (2:1).

Classical radar decoys. The basic building blocks used in the construction of typical radar decoys are the three sided (trihedral) square, circular, and triangular corner reflectors. These corner reflectors are used because of their ability to redirect a large portion of the incident radar energy, back toward a monostatic radar, and over a wide range of radar viewing angles (3:72). Traditionally, the individual corner reflectors have been arranged into a set of eight corner reflectors by effectively placing the

reflectors back to back with four reflectors on top and four inverted reflectors on the bottom. The classical configuration of a set of eight triangular corner reflectors is shown in Figure 1.1.

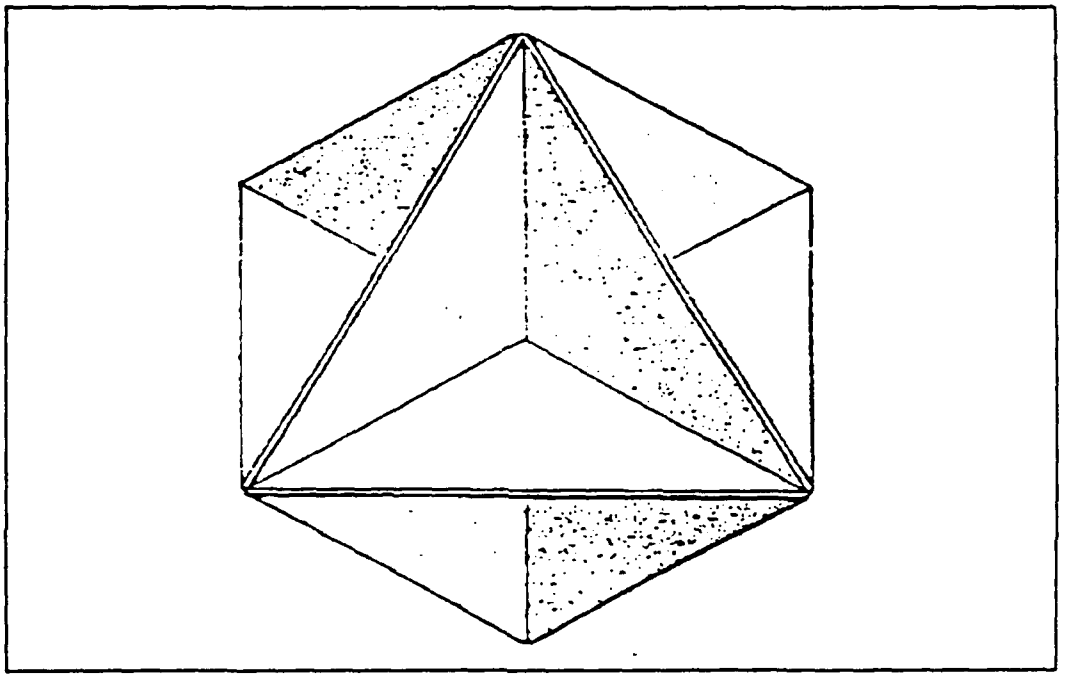

Figure 1.1 Classical Radar Decoy Configuration of Eight Triangular Corner Reflectors (3:90)

The Geodesic Array. The Geodesic Array of corner reflectors being examined in this research effort is an extension of the traditional approach. The Geodesic Array design was formulated by Mr E. E. Decker who has a full disclosure of a detailed design with the United States Patent Office (2:2).

The Geodesic Array is formed by putting 20 of the

triangular type corner reflectors together. Each of the corner reflectors has interior angles equal to 90 degrees. As designed, the corner reflectors are envisioned to be attached to one another using a hinge type of arrangement. By orienting the corner reflectors as described, no two adjacent corner reflectors have their side plates touching. This characteristic of the design is intended to yield a superior spatial coverage (with regards to the monostatic scattering for arbitrary viewing angles) over the traditional radar decoys (2:1).

The Geodesic Array of twenty corner reflectors is extremely difficult to depict using a two-dimensional drawing and the visual representation is reserved for the pictures of the RCS measurement targets to be presented in Chapter II.

As with the traditional radar decoys, the main function of the Geodesic Array is to decoy a radar guided missile away from its intended target (by either presenting an effectively larger target to the radar or by shifting the radar centroid) and as such, an operationally fielded Geodesic Array should be designed to present an RCS that is equivalent to or greater than the object it is designed to protect (2:1). Depending on the application, each corner reflector could typically have side dimensions on the order of several feet in length.

Radar Cross Section

The ability of a radar system to detect and track a target depends on many variables of which one is the target's RCS. The RCS itself is a function of several variables which include both radar parameters and target properties. The radar parameters of interest are the operating frequency, transmit/receive antenna separation distance, and antenna polarizations. The target properties include it's material composition, roughness, reflectivity, shape, size, and orientation. This section introduces the concept of RCS by first presenting a formal definition and then discussing the methods by which the RCS of a target can be assessed; namely, by theoretical prediction and by measurement techniques.

Formal definition of RCS. As discussed earlier, RCS is a measure of the amount of the energy incident on a target to the amount of energy scattered in the direction of the radar receiver. Formally it is defined in terms of the power density relationship between the incident and scattered electric fields and is defined as (4:157):

$$\sigma = 4\pi \lim_{R\to\infty} R^2 \frac{|E_s|^2}{|E_i|^2} \qquad (1.1)$$

where:

σ = radar cross section (in square meters)

R = separation distance of radar and target (in meters)

E_s= scattered electric field intensity

E_i= incident electric field intensity

In practice the RCS is normalized to remove the dependence of the RCS with respect to the radar and target separation distance. The units of RCS in the above expression are indicative of the units associated with an area, and as such the RCS is often interpreted as an equivalent area which would scatter the same amount of power back to the radar if the area were to radiate isotropically (5:33).

The limiting process in equation 1.1 requires that the EM field from the radar be planar in nature when it arrives at the target. In operational scenarios where the radar and target are separated by large distances this is indeed the case, but as will be seen in Chapter II, this requirement has a large impact on the conditions surrounding the RCS measurements.

Theoretical prediction. Various methods exist for predicting the EM scattering from material bodies. These methods are generally divided into three scattering regimes that depend on the ratio of the characteristic dimension of

the target to the wavelength of the incident EM field. The three regimes are known as the Rayleigh, the Resonance, and the Optical (or high frequency) regimes. The characteristic dimension of a trihedral triangular corner reflector is the distance measured along the junction of two of the sides and is denoted as a_{CR}. As pointed out earlier this dimension could be on the order of several feet for an operationally fielded Geodesic Array. The wavelength (λ) is defined in the usual manner as c/f where c is the velocity of the incident wave and f is the corresponding frequency. For free space propagation, the wavelength range associated with the 2 to 18 GHz radar frequency band therefore extends from 15.0 to 1.67 centimeters, respectfully. For a corner reflector with a characteristic dimension of 3 feet, the corresponding ratio of a_{CR} to λ ranges from 6 to 55. This ratio implies that the optical (or high frequency) type scattering prediction methods apply to an operationally fielded Geodesic Array.

The optical scattering method can be further divided into the following EM scattering theories:

a. Geometrical Optics.

b. Geometrical Theory of Diffraction.

c. Uniform Theory of Diffraction.

d. Method of Equivalent Currents.

e. Physical Optics.

f. Physical Theory of Diffraction.

g. Incremental Length Diffraction Coefficients.

These methods were investigated for applicability in predicting the RCS of the Geodesic Array.

RCS measurement. The measurement of the RCS of a target requires the determination of the ratio between the amount of power incident on an object and the amount of power reradiated from the object in a given direction. RCS measurements can generally be classified into two types, outdoor and indoor measurements. Outdoor measurements are usually associated with full scale targets and operational radars, while indoor measurements are often performed using scaled versions of the actual target and low-power radar simulators (4:318).

An indoor RCS measurement range was used to perform the measurements associated with this research. The particular variety of indoor range used is commonly referred to as a spherical range. In this arrangement a horn antenna is typically employed to produce the incident EM wave onto a scaled target model (6:905).

As mentioned, an operationally fielded Geodesic Array would be a large target and therefore the RCS measurements had to be performed on a scaled model of the array. The greatest limitations in performing representative and accurate measurements of the EM scattering qualities of

full-scale targets using an indoor measurement facility and scaled models are the ability to produce an incident EM wave that is approximately planar in the region occupied by the target and the proper scaling of the target/frequency relationship. (6:906) The impact of these limitations will be addressed in Chapter II.

Thesis Overview

This section presents a statement of the thesis problem, the approach followed during the research effort, and a summary of the chapters that follow.

Problem statement. Quantitatively determine the EM scattering characteristics of the Geodesic Array through the use of both measured results and theoretical predictions. Explain any differences between the measured and calculated results and provide a value assessment of the relative performance of Geodesic Array.

Approach. The monostatic RCS was decided on as the means for describing the EM scattering characteristics of the targets addressed in this research effort. The targets selected for examination were single triangular corner reflectors, an array of four triangular corner reflectors, an array of eight triangular corner reflectors, and the Geodesic Array. The maximum size of the Geodesic Array (and thus the size of the corner reflectors) was driven by the maximum target size which could be measured in the RCS

measurement facility. RCS measurements were performed on the various configurations of corner reflectors at the Air Force Wright Research and Development Center's Far-Field RCS Measurement Range. The measured RCS results were then used to assess the performance of the Geodesic Array. The various options for predicting the RCS of the Geodesic Array were considered. The option chosen was to start with an existing computer model for corner reflectors and to modify the software routines to allow the prediction of the RCS of the Geodesic Array. The measured results were then compared to the predicted results to verify the adequateness of the prediction model.

Document Preview.

Chapter II continues the discussion of the RCS concepts involved in the research effort and further defines the targets investigated. Chapter III discusses the RCS measurement facility and the different RCS measurement range configurations used during the measurements. Chapter IV presents the RCS measurement results for the selected targets. Chapter V presents an assessment of the Geodesic Array as compared to an array of eight corner reflectors. Chapter VI discusses the RCS predictions and presents some comparisons of the measured and predicted RCS results. Finally, Chapter VII provides the conclusions and recommendations.

II. RCS Measurement Concepts and Target Selection

Overview

The overall purpose of this research effort was to characterize the EM scattering associated with the Geodesic Array. One method of characterizing the EM scattering of the array is to examine it's RCS. The RCS can be assessed through the use of both theoretical prediction and RCS measurements.

The final goal of the theoretical effort, which will be presented in Chapter VI, was to develop a tool for predicting the RCS of the Geodesic Array. The complex nature of the Geodesic Array led to a three phase theoretical approach. The first phase was to develop the ability to predict the RCS of a single trihedral triangular corner reflector. The second phase was to expand this ability to the prediction of the classical configuration of a set of eight triangular corner reflectors. The final phase was to develop the Geodesic Array prediction. Before these predictions can be used with an acceptable certainty in regards to the results, the theoretical results need to be verified. The means for verifying the theoretical results is the comparison of these results with the results obtained through actual RCS measurements.

This chapter first develops the RCS measurement concepts that impacted the selection of the measurement targets. The selected targets and target fabrication are presented next. The chapter also contains a discussion of the various types of RCS pattern measurements used during the research effort and a discussion of the scaling up of the RCS measurement results. The chapter concludes with a presentation of the target naming convention to be used throughout the remainder of the document.

RCS Measurement Concepts Affecting Target Selection

If proven to be an acceptable means of providing a target with a large radar return, a operationally fielded Geodesic Array is envisioned to be very large. Each corner reflector could be as large as three to eight feet on a side. Such a large target could not have been measured in the spherical type indoor RCS measurement range used during this research and thus the Geodesic Array had to be scaled down to an acceptable size. The factors affecting the scaling of the array were the measurement facility parameters, the plane wave illumination requirement, and the optical region type scattering requirement.

RCS measurement facility parameters. The relevant target scaling parameters of the spherical type range are the maximum antenna to target separation distance and the available measurement frequencies. The maximum separation

distance was approximately 50 feet while the possible measuring frequencies (available for the range configurations used) ranged from 2 to 18 GHz.

Incident Plane Wave Illumination. To exactly satisfy the RCS definition given in (1.1) the incident EM wave must be planar in the region occupied by the target. In order to achieve perfect plane wave illumination the target would have to be separated from the measuring antenna by a very large distance (infinity in the limit). In actual RCS measurements, the plane wave illumination is approximated. The degree of approximation depends on the target size, the measuring frequency, the antenna to target separation distance, and the acceptable limits for the amplitude and phase variations within the region occupied by the target. Derivation of the plane wave requirements requires the consideration of the cross range phase, down range amplitude, and cross range amplitude variations across the target. Figure 2.1 depicts a point source model for determining the cross range phase and down range amplitude variations.

Cross range phase variation. The quantities associated with the cross range phase are:

a. the separation distance between the antennas amplitude and phase center and the target centroid (R).

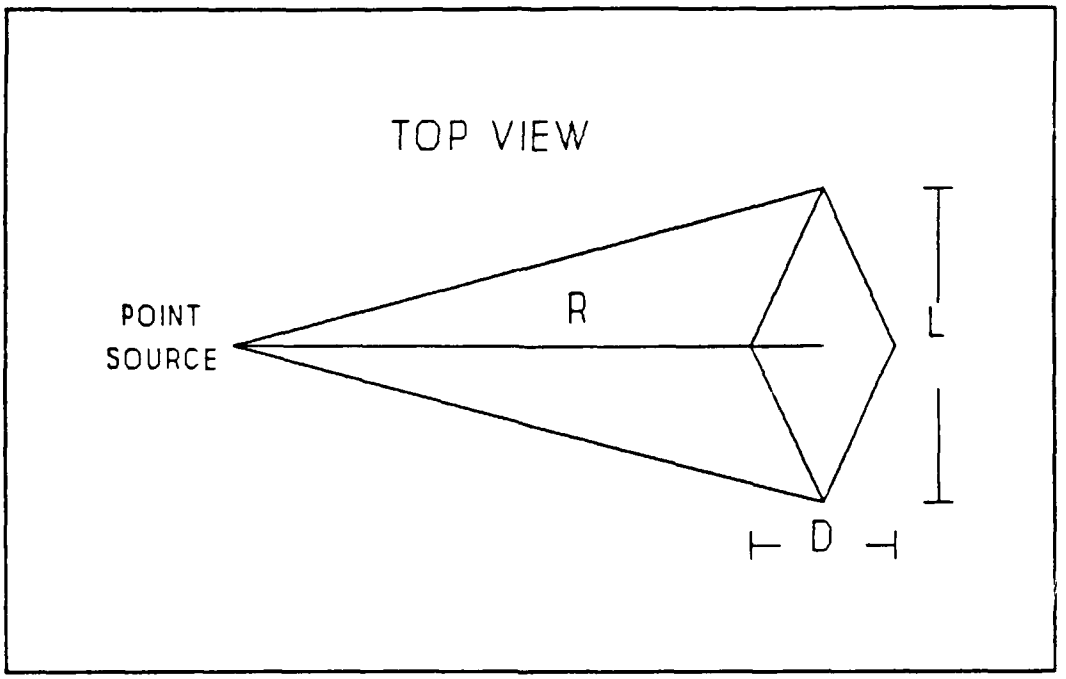

Figure 2.1 Geometry Associated with the Cross Range Phase Variation and Down Range Amplitude Variation Plane Wave Requirements

b. the cross range phase variation (ϕ).

c. the operating wavelength of the radar (λ).

d. the cross range extent of the target (L).

The expression relating these parameters is given as (7:922):

$$R = \frac{\pi (L)^2}{4 \phi \lambda} \qquad (2.1)$$

Selecting a maximum acceptable phase variation of 22.5 degrees ($\pi/8$ radian), equation 2.1 can be rewritten as:

$$R_{min} \geq \frac{2 L^2}{\lambda} \qquad (2.2)$$

Down range amplitude variation. If the down range extent (front to back) of the target is defined as "D" and assuming that R is large enough such that the incident field varies as 1/R in the region occupied by the target, and an acceptable amplitude variation is chosen as 1 dB, then the relationship between R and D is given by (8:16):

$$R_{min2} \geq 8.2\ D \qquad (2.3)$$

Cross range amplitude variation. The consideration of the cross range amplitude variation would require a model that includes a specific antenna. The analysis is not pursued here, because it is suffice to say that the result would lead to a result for R_{min} that is less restrictive than the result given by equation 2.2 (8:17).

Target size versus plane wave illumination requirements. The Geodesic Array is a symmetrical target with respect to it's centroid and therefore the quantities L and D in the above equations are equivalent. Replacing D with L in equation 2.3 yields a pair of equations with which the largest dimension of the Geodesic Array can be determined. The resulting two equations are:

$$R_{min1} \geq (2/\lambda)(L^2) \qquad (2.4)$$

or

$$R_{min2} \geq 8.2\ L \qquad (2.5)$$

For a given L, the required separation distance between the measuring antenna and the target is the larger of the two distances determined by equations 2.4 and 2.5.

Figure 2.2 depicts the minimum ranges calculated using equation 2.4 for various values of L (L = 6, 12, 18,and 24 inches). Since the maximum separation distance of the RCS measurement facility was 50 feet, the frequency corresponding to the intersection point of a given line with the top of the graph is the maximum frequency that a measurement could be accomplished and still fulfill the cross range phase/plane wave requirement.

Figure 2.3 represents the results for equation 2.5. When compared with Figure 2.2, the graph easily depicts the fact that the cross range phase/plane wave requirement is the dominate consideration for most frequency and target dimension considerations. The exceptions to this rule occur at the lower limits of the frequency range.

After considering the next topic, these results, will be used to determine the scale model size for the Geodesic Array.

Optical region type scattering requirement. As mentioned in Chapter I, the ratio of the characteristic dimension of an object to the wavelength of the incident EM wave defines the type of EM scattering associated with an

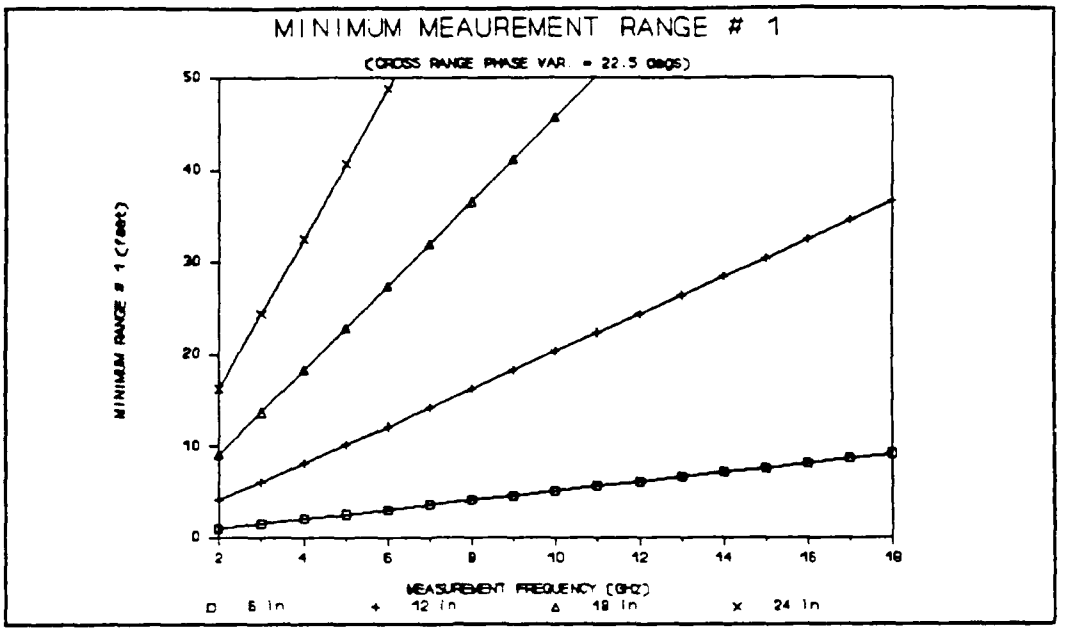

Figure 2.2 Minimum Antenna to Target Separation Distance for Different Size Targets (results based on 22.5 degree phase variation)

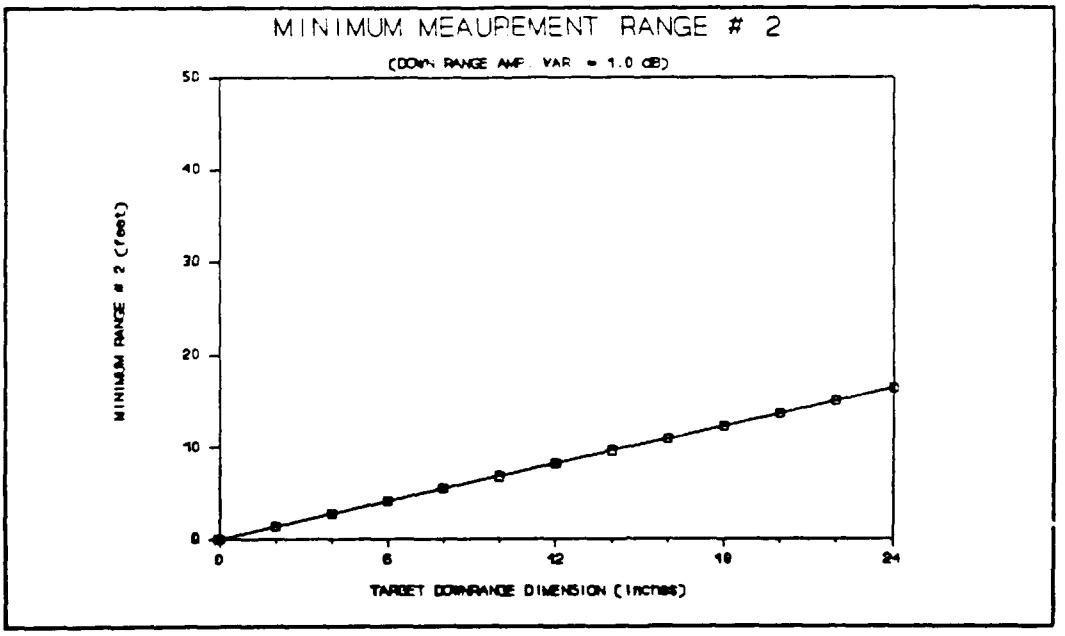

Figure 2.3 Minimum Antenna to Target Separation Distance for Different Size Targets (results based on a 1 dB down range amplitude variation)

object. Typically, if this ratio is larger than 5, the type scattering is considered to be optical (or high frequency). Since the Geodesic Array is comprised of a symmetrically arranged pattern of corner reflectors, scaling of the characteristic dimension a_{CR} of a single corner reflector in turn scales the overall dimension of the array by an equal amount. The overall type of scattering was assumed to be defined by the type of scattering associated with the individual corner reflectors. This was the approach used in Chapter I to determine that the scattering associated with an operationally fielded Geodesic Array would be of the optical type.

This being the case, the corner reflectors associated with the scaled down model of the Geodesic Array and the associated measurement frequencies needed to be chosen in a manner that would yield the high frequency type scattering. Based on the overall target dimensions used to create Figure 2.2 (i.e. L = 6, 12, 18, and 24 inches), the characteristic dimensions of the individual reflectors required to generate an array of these sizes are 2.125, 4.25, 6.375, and 8.5 inches respectfully. Figure 2.4 is a graph of the ratio between these characteristic dimensions and the available measurement wavelengths (Note: the results are plotted versus frequency so that the results were comparable with Figure 2.2). Any portion of a line above the a/λ equal 5

line represents the optical type scattering case and is therefore an applicant for further consideration.

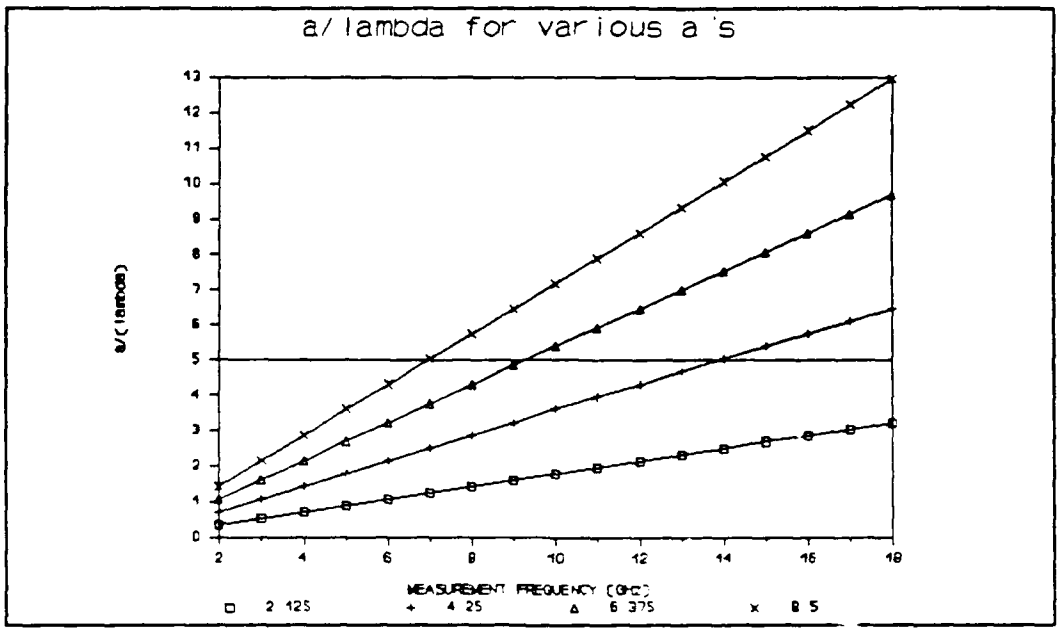

Figure 2.4 Ratio of Characteristic Dimension a_{CR}/λ for Various Values of a_{CR} Given in inches

Target Selection

The actual selection of the scaled down model of the Geodesic Array was a trade off demanded by the results depicted in Figures 2.2 and 2.4. The scaled model had to be chosen in order to simultaneously fulfill the plane wave illumination requirement and the optical type scattering requirement.

A 24 inch target would have satisfied the optical scattering requirement for frequencies above 7 GHz; however, it would have only satisfied the plane wave requirement for frequencies below 6 GHz and was thus eliminated from

consideration. Similarly, the 6 inch target would have always satisfied the plane wave requirement but would have never satisfied the optical type scattering criteria. The 18 inch target would have satisfied both criteria from approximately 9 to 11 GHz but was also eliminated in lieu of the broader frequency coverage afforded by the 12 inch target.

The 12 inch scaled model of the Geodesic Array satisfied both criteria as long as the RCS measurements were performed between 14 and 18 GHz. The 12 inch model Geodesic Array target was selected for the RCS measurements.

The characteristic dimension of the corner reflectors for a Geodesic Array of largest dimension equal to 12 inches is 4.25 inches. The interior angles of each corner reflector were chosen as 90 degrees. A means for connecting the corner reflectors in a manner to form such an array was required. Following the basic design of Mr E. E. Decker, it was decided to use a hinge arrangement to assemble the corner reflectors into an array. The hinge arrangement was chosen because it enabled any combination of corner reflectors to be connected together and because it was envisioned as a acceptable alternative for assembling the array operationally. A 3/16 inch (cylindrical diameter) piano type metal hinge was selected. The arrangement of the hinge around the outside edges of the corner reflector was

chosen such that any two corner reflectors could be picked up and arbitrarily put together. It was expected that the scattering from the hinges would be difficult to model precisely, and that their effect should be examined during the measurements. To accomplish this goal, corner reflectors with and without hinges were required.

Recalling that one of the underlying reasons for performing the measurements was to be able to compare the measured results with the predicted results, the following set of targets was selected.

a. A 4.25 inch single corner reflector without hinge.

b. A 4.25 inch single corner reflector with hinge.

c. An array of four corner reflectors formed using the 4.25 inch corner reflectors without hinges.

d. An array of four corner reflectors formed using the 4.25 inch corner reflectors with hinges.

e. An array of eight corner reflectors formed using the 4.25 inch corner reflectors with hinges.

f. A 12 inch scaled model Geodesic Array formed using twenty 4.25 inch corner reflectors with hinges.

Target Fabrication

In order to produce the desired targets, a total of 5 corner reflectors without hinges, and 33 corner reflectors with hinges were fabricated by the AFIT Fabrication Shop. The material used was 60/1000 inch soft aluminum (type O). The corners were made by first cutting the aluminum into the pattern shown in Figure 2.5 (a = 4.25 inches). The 90 degree interior angles were made by bending the aluminum using a 90 degree press. The overlapping section was wrapped under one of the sides and then flush mount riveted using a single rivet. The hinges were cut to the appropriate shape and size and were also flush mount riveted in place using two rivets per side. The rivet heads were polished so as to present a continuously smooth interior surface. A single corner reflector with and without the hinge attached is depicted in Figure 2.6.

The array of eight corner reflectors with hinges was constructed using the hinged design. Figure 2.7 shows the 8 corner reflector array.

The scaled model Geodesic Array was constructed using the hinge design and is shown in Figure 2.8. The orientation shown will be termed the "upright" orientation. In this orientation the array can be described as a three tier object. The top tier is comprised of five corner

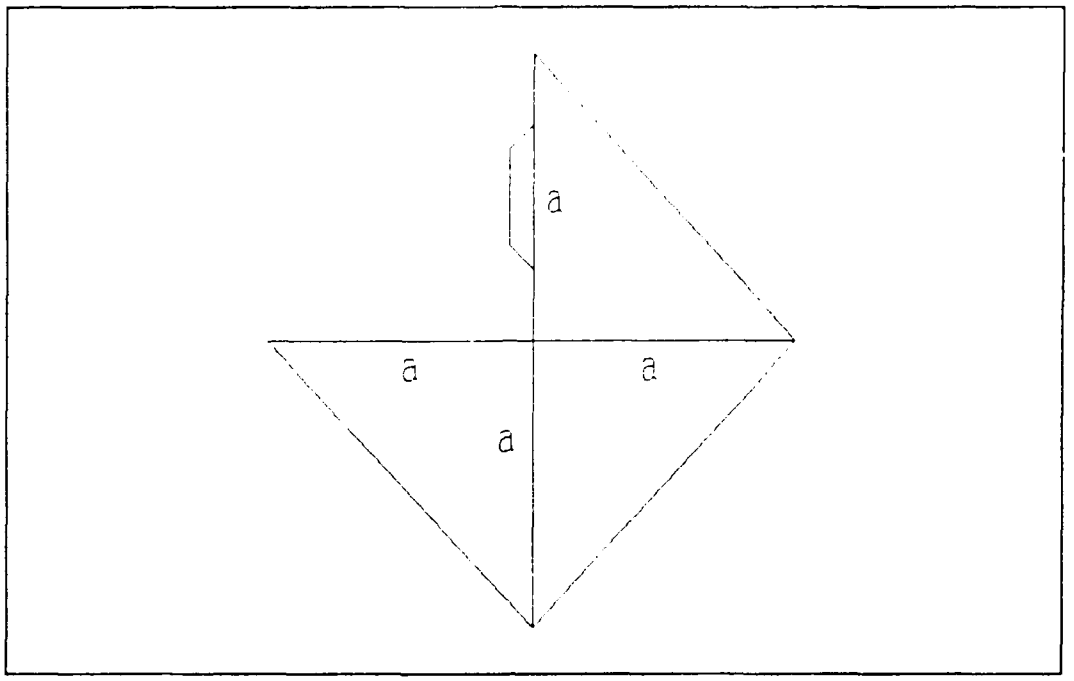

Figure 2.5 Single Corner Reflector Fabrication Pattern (a = 4.25 inches)

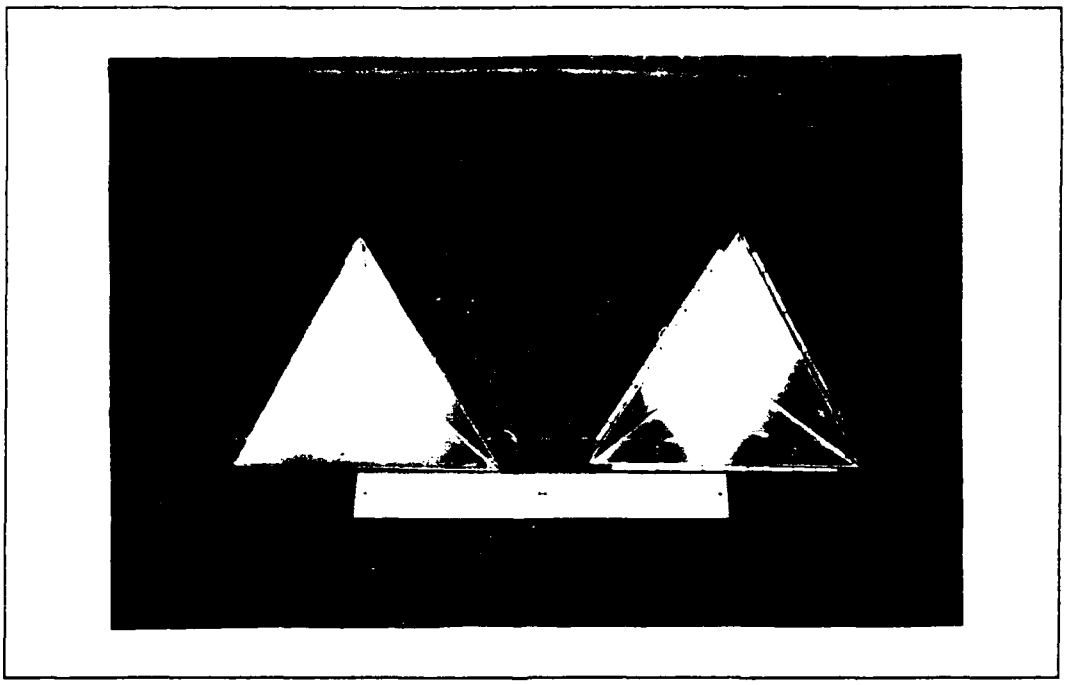

Figure 2.6 Single Corner Reflector With and Without Hinges Attached

reflectors. The bottom tier is also comprised of five corner reflectors with each corner reflector inverted. The middle tier is a set of 10 corner reflectors with alternating reflectors inverted.

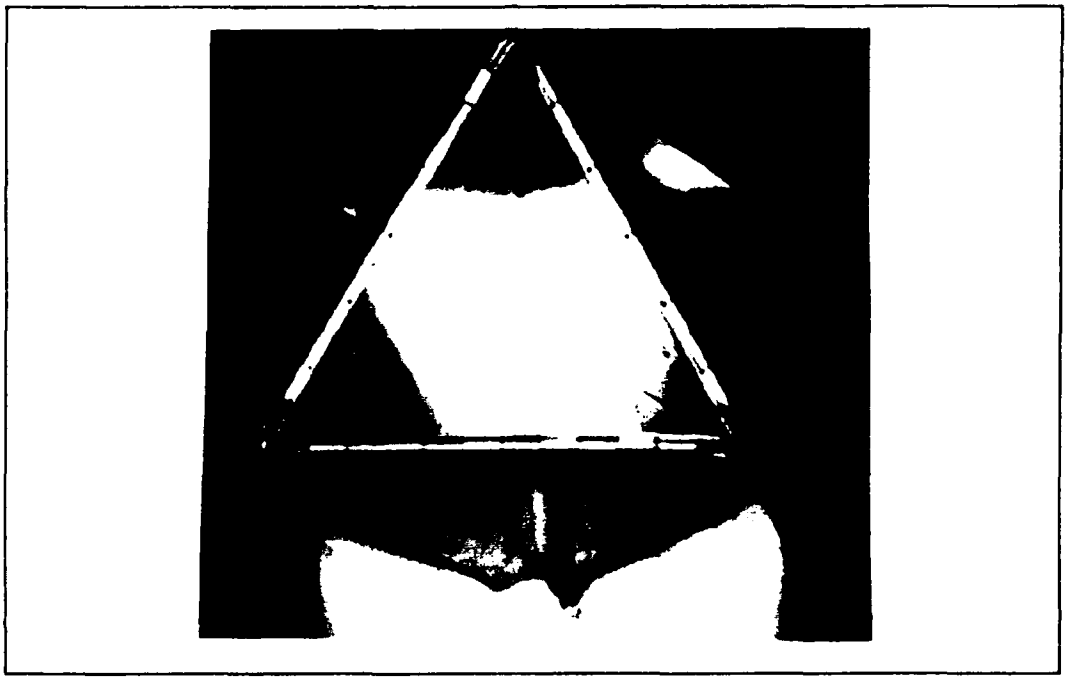

Figure 2.7 Eight Corner Reflector Array

RCS Measurement Patterns

The RCS of an object depends on the attitude at which the object is presented with respect to the incident EM wave and is therefore a strongly angular dependent property of the object (4:156). One of the requirements of a radar decoy type target is to present a large RCS over a wide region of radar to target viewing angles. In order to measure the spatial coverage provided by the selected

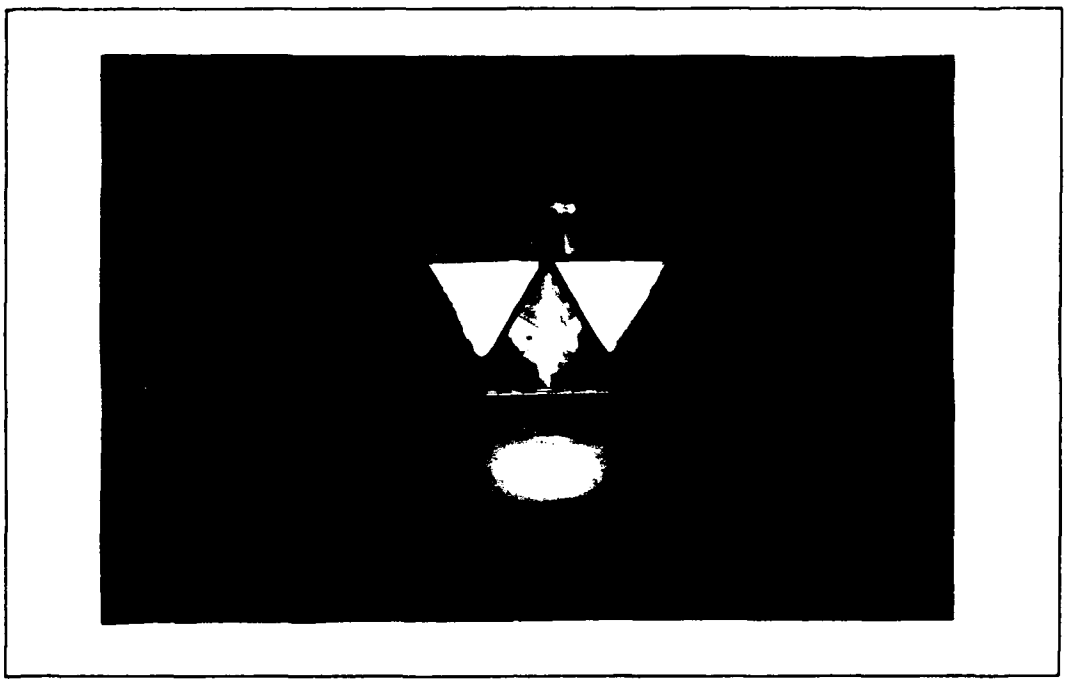

Figure 2.8 The Scaled Model Geodesic Array Shown in an Upright Orientation

targets, the RCS measurements performed in this thesis were of the pattern cut variety. The term pattern cut (or cut) refers to a plot of the target's RCS for a complete revolution of the target (4:328). There are various types of pattern cuts one can perform. The two types used during the RCS measurements associated with this research were the conical cut, and the great circle cut.

The type cut can be distinguished by the angle between the target rotation axis and a horizontal plane. The target positioning and rotation axis geometries associated with the conical and great circle type cuts are depicted in Figure 2.9.

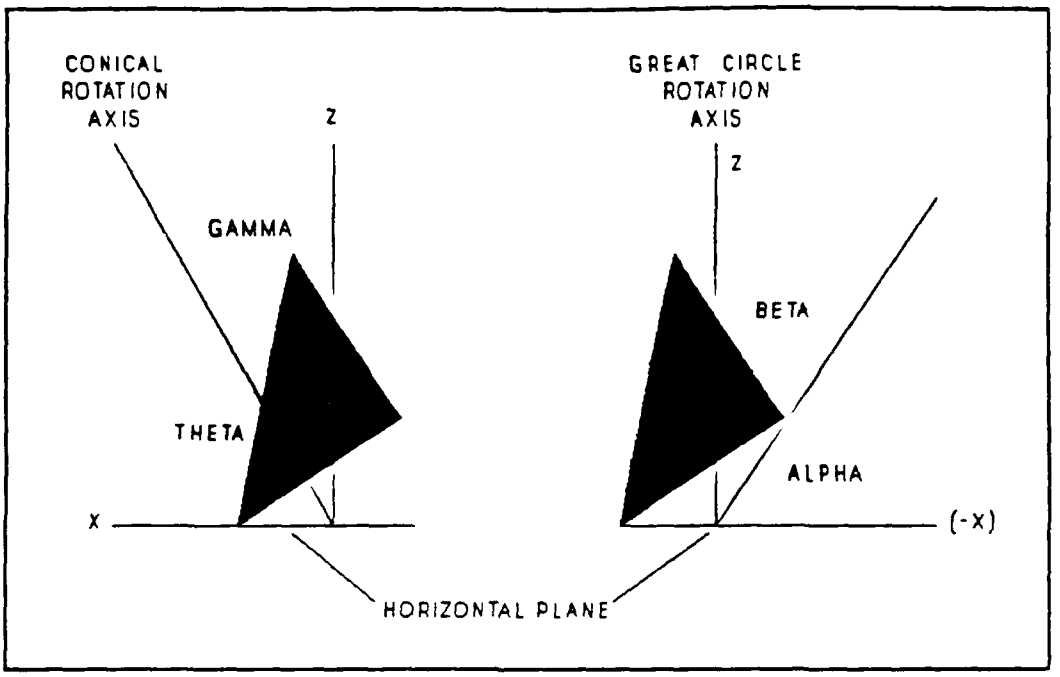

Figure 2.9 Target Positioning and Rotation Axis Geometries Associated with Conical and Great Circle Cuts.

Conical cuts. The target in the left portion of Figure 2.9 depicts the conical cut target configuration. The angles theta and gamma are the angles between the rotation axis and the x and z axis, respectfully. The angles are measured in the plane of the paper (the xz plane). As the target is rotated about it's rotation axis, the angles theta and gamma remain constant. With the measuring antennas located to the left of the target and the target tilted forward (by an amount equal to gamma degrees) in the direction of the measuring antennas, this type rotation yields the same result as if the target were oriented perpendicular to the horizontal plane (gamma = 0 degrees)

and the measuring antennas were rotated by an amount equal to the angle gamma above the horizontal plane.

If theta is considered in the context of the traditional angle used by engineers to represent the angle down from a z-directed axis, the angle theta in combination with the rotation angle phi represents the radar to target viewing angle. This consequence of the conical cut pattern measurements makes it easier to relate the results to an operational environment.

The conical cut is the favored type measurement because it provides a larger amount of spatial coverage information than the great circle cuts, however the mounting of the target in this manner presents it's own challenges (4:330). The mounting approach is presented in Chapter III.

Great circle cuts. The target in the right portion of Figure 2.9 represents the configuration associated with a great circle cut. The angles depicted as alpha and beta are again measured in the plane of the paper ((-x)z plane). The angle alpha (as depicted in Figure 2.9) is the angle from the horizontal plane to the lower and outer extremity of the target. As the target is rotated around it's rotation axis, the angle alpha (as well as the angle gamma) does not remain fixed. In order to obtain the same amount of spatial information as afforded by the conical cuts, a larger amount of great circle cuts (accompanied with the tilting of the

target into and out of the paper) would be required (4:330).

It may be noteworthy to point out that measurements performed using a conical cut with theta = 90 degrees or using a great circle cut with alpha always equal to zero degrees will obviously produce equal results. RCS measurements performed in this manner are often referred to simply as "pattern cuts".

RCS Measurement Result Scaling

As mentioned in the scattering regime discussions, EM scattering phenomena are a function of the frequency associated with the incident EM wave and the dimensions of the target. In order to relate the RCS measurements using scaled models to a full scale target, the relationship l/λ, must remain constant during the effort (9:1369). In this relationship, l is any dimension of the target and the corresponding scale model. Defining l_f as any dimension of the full scale target and l_s as the corresponding dimension of the scaled model, the scale factor (ρ) is given by the ratio of l_f/l_s. Further defining f_f as the full scale frequency of interest and f_s as the scaled model measurement frequency, the relationship between the two frequencies can be derived by considering the previously defined relationship between λ and f. The result is given simply by:

$$f_f = f_s / (l_f/l_s) = f_s / \rho \qquad (2.6)$$

A similar relationship exists for relating the corresponding measured RCS of the scaled model (σ_s) to the RCS of the full scale target (σ_f) at a frequency of interest given by (2.6). The resulting expression is given below (9:1369).

$$\sigma_f = \rho^2 \sigma_s \qquad (2.7)$$

As a typical example, if interested in relating the RCS of the 1 foot scaled model Geodesic Array measured at 18 GHz to a 6 foot full scale Geodesic Array (scale factor equal six), the RCS of the full scale array would be 36 times the scaled model measured RCS and would be associated with a full scale frequency of 3 GHz.

An additional single corner reflector with characteristic dimension of 8.5 inches was fabricated to verify the above relationships.

Target Naming Convention

The following acronyms are used in the remaining chapters to identify the selected targets.

a. HSSCR = half scale single corner reflector = the 4.25 inch corner reflector without hinges.

b. HSSWH = half scale single corner reflector = the 4.25 inch characteristic dimension corner reflector with hinges.

c. FSSCR = full scale single corner reflector = the 8.5 inch characteristic dimension corner reflector.

d. HSQCR = half scale quad corner reflector array = the four corner reflector array constructed using the 4.25 inch corner reflectors "without" the hinge arrangement.

e. HSQWH = half scale quad corner reflector array with hinge = the four corner reflector array constructed using the 4.25 inch corner reflectors "with" the hinge arrangement.

f. HS8WH = half scale eight corner reflector array with hinge = the eight corner reflector array constructed using the 4.25 inch corner reflectors "with" the hinge arrangement.

g. HSGA = half scale Geodesic Array = the twelve inch array constructed using 20 of the 4.25 inch corner reflectors with the hinge arrangement.

(Note: the terms half and full scale used in the target naming conventions simply distinguish the 4.25 inch corner reflector from the 8.5 inch corner reflector and should not be confused with any reference to a full scale operationally fielded Geodesic Array.)

III. WRDC Far Field RCS Measurement Range

Overview

The RCS measurements were performed at the Air Force Wright Research and Development Center (WRDC) microwave measurement facility, located on Wright-Patterson Air Force Base, Ohio. The measurements were accomplished using the "Far-Field" RCS Measurement Range housed within the facility. This chapter provides an overview of the Far-Field range and discusses the different range configurations used during the RCS measurements.

Concept of Operation

The WRDC Far-Field RCS measurement system is based on the continuous wave (CW) nulling RCS measurement technique. In all RCS measurement techniques the EM scattering returns associated with the measurement environment must in some manner be isolated from the EM scattering returns associated with the target of interest plus measurement environment. The CW nulling technique is based on the ability to effectively cancel the returns from the measurement chamber and the target mounting structure prior to the insertion of the target onto the mounting structure. Once this is

accomplished and the target of interest is positioned onto the mounting structure, the resulting measured EM scattering returns will (in theory) be associated with the target of interest only.

Far-Field Range Physical Dimensions.

The WRDC microwave measurement facility is contained in a large barn shaped, arched roof structure. The Far-Field range consists of a 30 foot by 60 foot rectangular area inside the facility. On the four sides, the range is isolated from the remainder of the building's interior through the use of walls lined with radar absorbing material (RAM). The height of the RAM walls varies but are a minimum of 12 feet above the floor. An overhead view of the Far-Field range is shown in Figure 3.1. The top of the range is not directly enclosed and extends upwards to the building's arched roof (approximately 90 feet).

RCS Measurement Systems

During the experimental measurements two distinct measurement system configurations were used. The discussion that follows is divided into a "general" system description, a "pedestal" system configuration, and a "conical cut" system configuration.

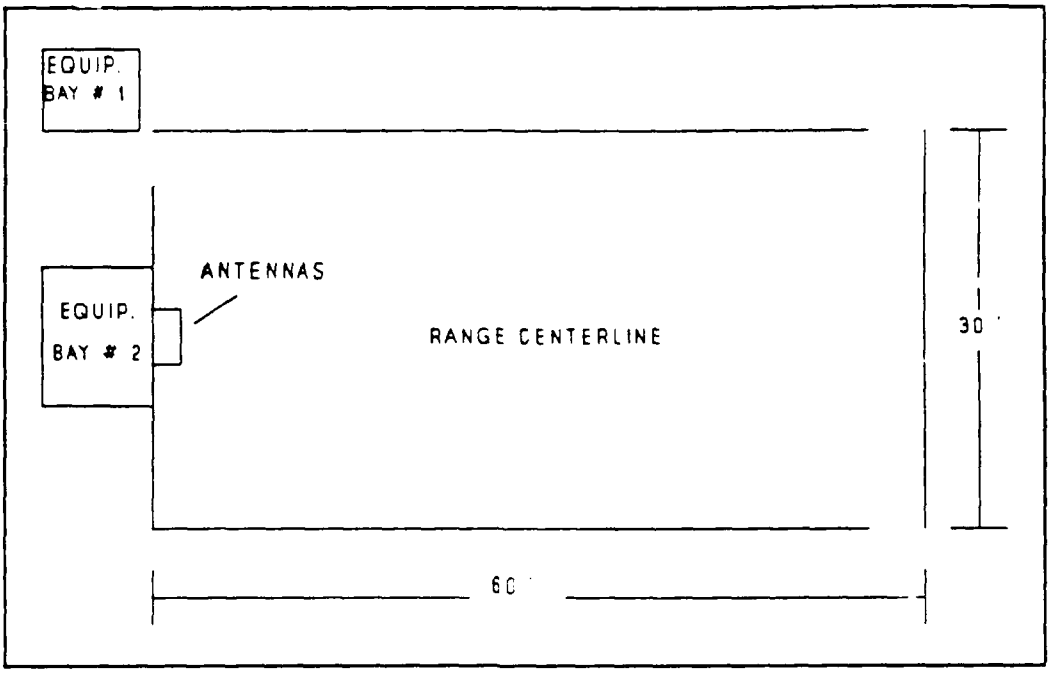

Figure 3.1 Overhead view of the Far-Field Range (Dimensions are in Feet)

General system description. The general RCS measurement system can be broken down into the subsystems depicted in Figure 3.2. The transmit subsystem consists of a signal source, a power amplifier, and one of four pyramidal shaped standard gain horn antennas. The receive subsystem consists of one of four pyramidal shaped standard gain horn antennas, a phase amplitude receiver, and two harmonic mixers. The CW nulling subsystem consists of three direct current power supplies, three RF couplers, two variable attenuators, a variable phase adjuster, one of four isolation filters, one oscilloscope, and a multimeter. The HPIB interface subsystem consists of two HPIB interface

extenders and a IEEE 488 bus strip.

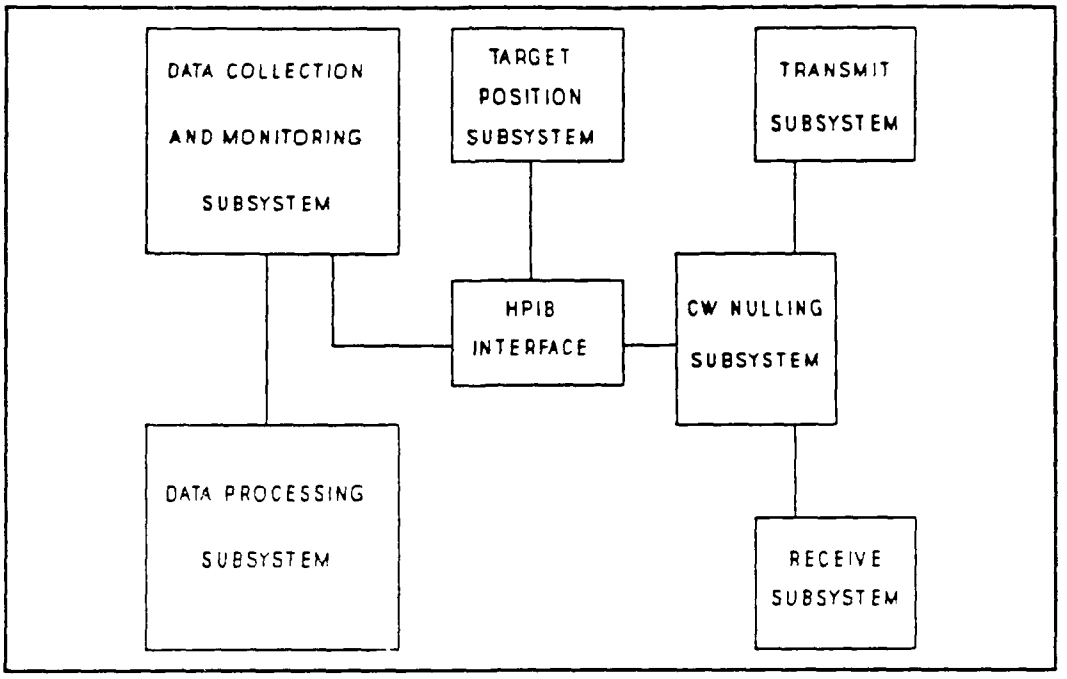

Figure 3.2 Far-Field Range Measurement System Flow Diagram

The data collection and monitoring subsystem consists of a Hewlett Packard (HP) series 9000 computer (HP computer #1), an external hard drive, a general purpose bus monitor, and a multimeter. The HP operating system was Basic 5.0 and the original software program used to control the measurement equipment was entitled "FFRANGE", dated November 1989.

The data processing subsystem initially consisted of a HP printer connected to the HP computer (#1) listed above and a second HP series 9000 computer (#2) connected to a HP

plotter. This arrangement gave the ability to obtain a quick look data product (using HP computer # 1 and the HP printer) or to obtain a plot of the data off-line from the actual measuring equipment (using HP computer #2 and the HP plotter). In order to provide a greater capability for analyzing the test results, a personal computer (PC) configuration was added to the data processing subsystem. The PC was interfaced to the HP computer (#1) through the use of a HP RS-232 serial interface card, a null modem, a gender changer, and the appropriate interface cables. The HP controlling software was modified so that the HP formatted test results were converted to the standard ASCII format and then transferred to the PC computer. The modified HP program was still entitled "FFRANGE" but was dated 05 December 1990. This additional capability allowed the processing of the data through the use of PC application software packages.

The target position subsystem consisted of a target position controller, a target rotator, and a target support structure. Two distinctly different target position subsystems were used during the experimental measurements. The RCS measurement system configuration depended on which of these target position subsystems was being used.

The equipment manufacturer, model numbers, and serial numbers of all the equipment used in the measurements is

given in Appendix A.

Pedestal system configuration. In this configuration the positioning subsystem utilized a Scientific Atlanta (SA) controller and a SA target rotator. The target rotator was located inside the base of an ogive-cylinder shaped target support pedestal. The ogive-cylinder shaped pedestal was designed to minimize the scattering returns from the target support structure (10:19). An open cell polystyrene mounting fixture was designed and built using a standard lathe. The polystyrene mounting fixture, depicted in Figure 3.3, was placed on the top of the ogive-cylinder pedestal to provide a platform for target placement. The target support pedestal with the polystyrene mounting fixture installed is depicted in figure 3.4. This configuration, termed the "pedestal configuration" was used to collect the great circle pattern cuts (introduced in Chapter II).

Conical cut system configuration. The second target position subsystem was designed and constructed in order to allow the rotation axis and the target of interest to be tilted toward the measuring antennas. The RCS measurements performed using this configuration resulted in the conical pattern cuts (also introduced in Chapter II). A Newport programmable target position controller and a Newport target rotator were used. The target rotator was attached to a

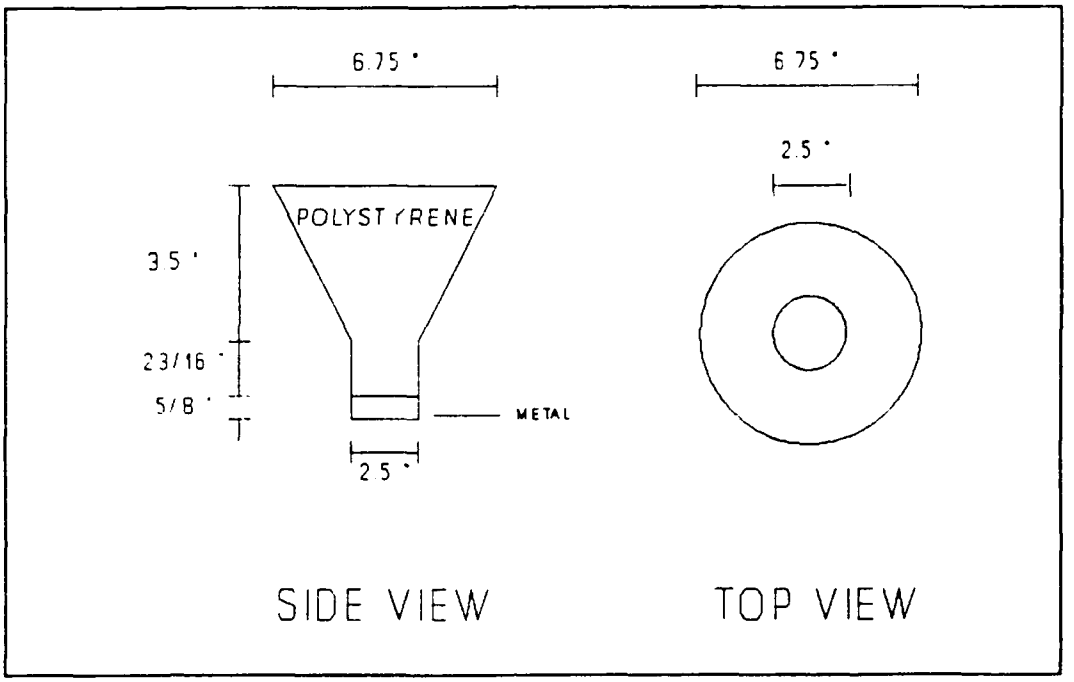

Figure 3.3 Polystyrene Mounting Fixture (All Dimensions are in inches)

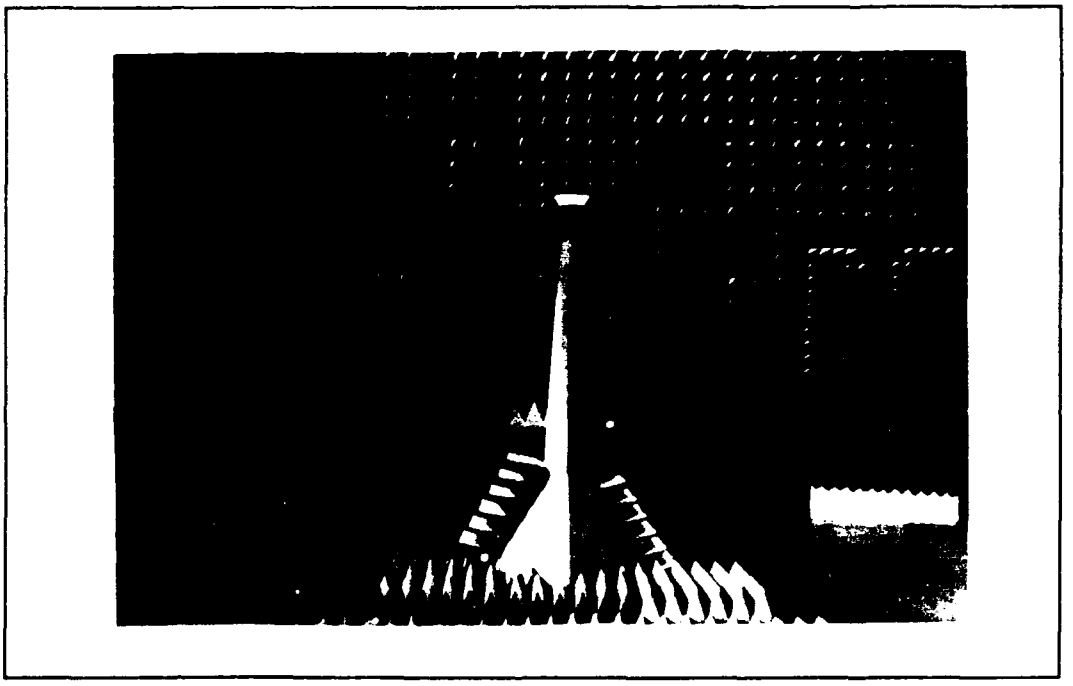

Figure 3.4 Ogive-Cylinder Shaped Target Support Pedestal with Pclystyrene Target Fixture

rotator mounting assembly as shown in Figure 3.5. The target rotator mounting assembly was designed to take the stress off the rotator as the complete assembly (with target attached on the top of the target mount rod) was tilted down and toward the antennas. The rotator mounting assembly was fabricated by the AFIT Fabrication Shop using three eighths inch thick aluminum. The rotator mounting assembly was then attached to the top of a Quickset model 4-62225-A tripod stand. The final conical cut target mount structure, shown in Figure 3.6, allowed the target of interest to be positioned with three degrees of freedom.

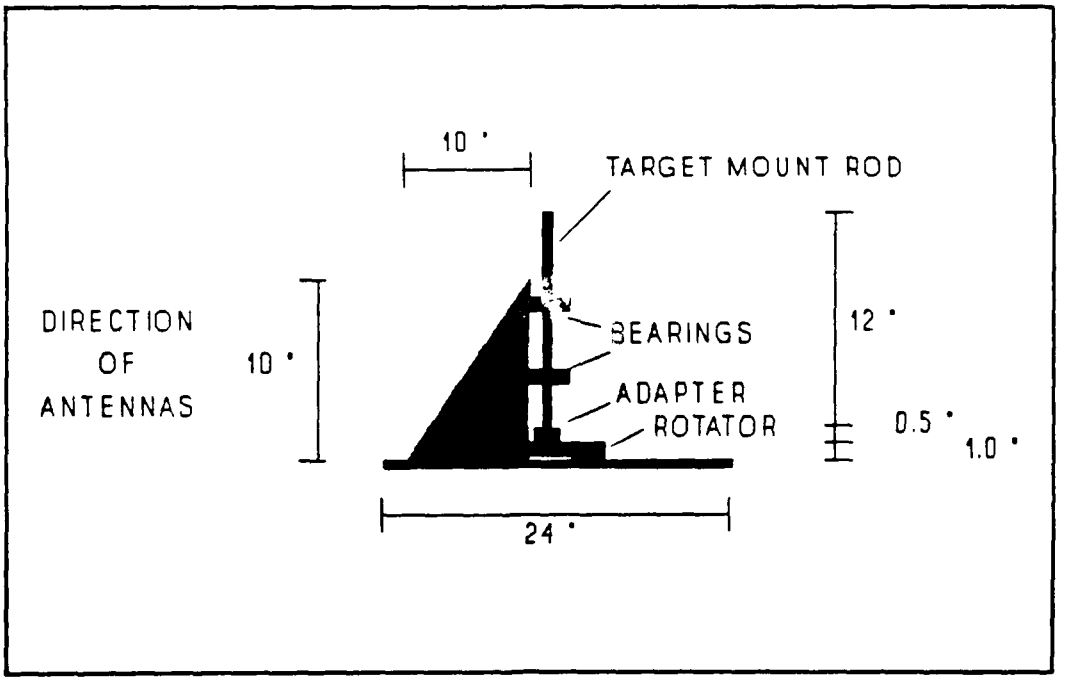

Figure 3.5 Side View of the Conical Cut Rotator Mounting Assembly (All Dimensions are in inches)

It was obvious that the conical cut mount structure by

itself would have produced a much larger EM scattered field than the ogive shaped pedestal target mount structure. To alleviate the problem of having to "null" this larger return from the measurement environment, a RAM enclosure was designed and constructed. The underlying structure of the RAM enclosure was first built out of one half inch plywood. The dimensions of the underlying structure are shown in Figure 3.7. RAM was then added to the sides and top of the underlying structure. The RAM used was manufactured by Emerson and Cuming Inc and came in the standard two foot by two foot square sections. The RAM used on the top of the enclosure was eight inch thick wedge shaped WG-8 material. The RAM used on the three sides of the enclosure was twelve

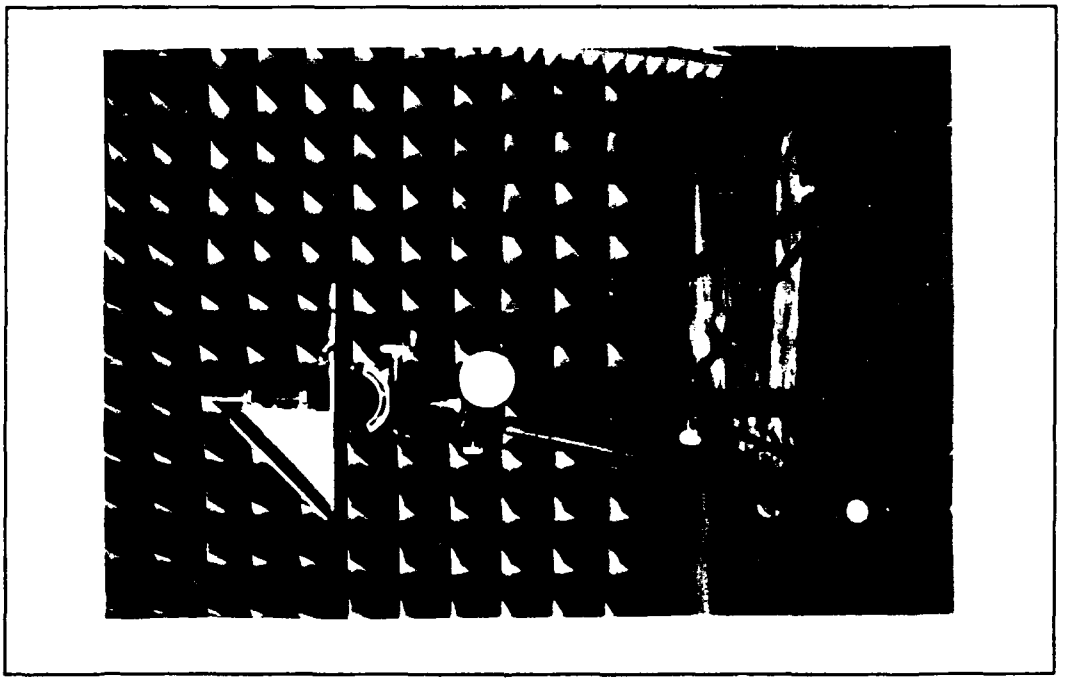

Figure 3.6 Conical Cut Target Mount Structure

inch thick pyramidal shaped AAP-12 FR material and was positioned so that an eight inch portion of the RAM extended above the top of the underlying structure. This extension above the underlying structure prevented the wedge RAM from presenting a flat face in the direction of the measuring antennas. The RAM enclosure is shown in Figure 3.8.

When used during the conical cut measurements, the RAM enclosure was positioned in the chamber with the open side facing the opposite direction from the measuring antennas. The conical cut target mount structure was then placed inside the RAM enclosure as shown in Figure 3.9. To help eliminate any scattering from the conical cut mount structure through the slot in front of the enclosure, a twelve inch by twelve inch section of ECCOSORB AN-75 RAM was attached to the slanted portion of the rotator mount assembly.

The final modification required for the conical cut measurements was the modification of the data collection software. The software was modified to allow the interfacing between the HP computer and the Newport programmable target position controller. This version of software was entitled "FFRANGE2" and was dated 20 January 1990.

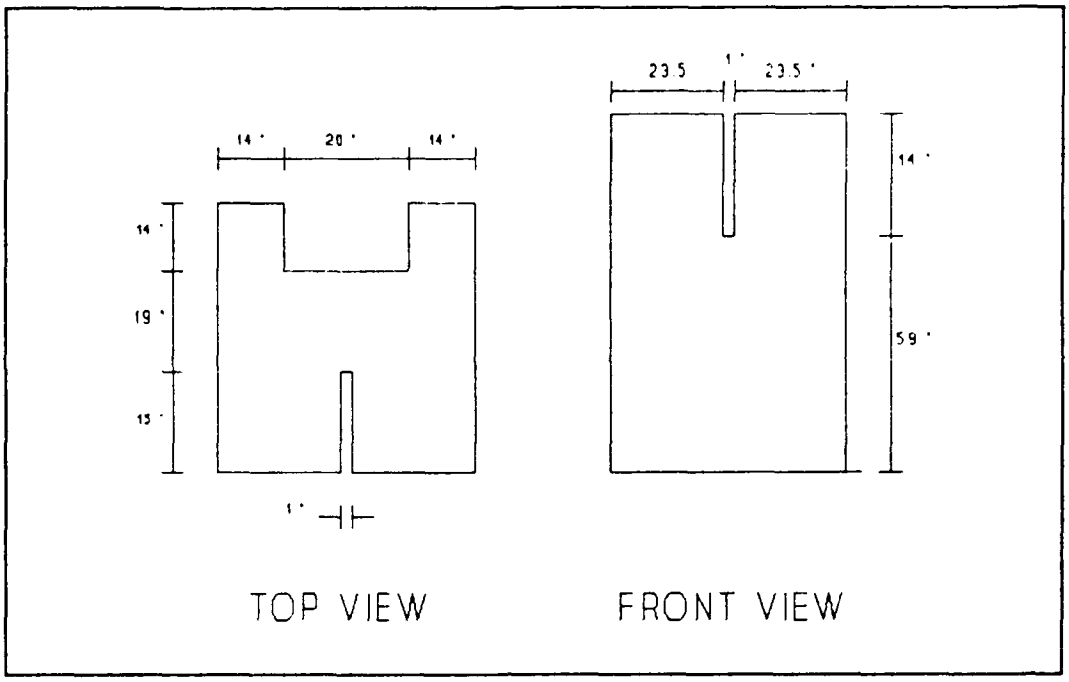

Figure 3.7 Dimensions of the Underlying Structure of the RAM Enclosure (All Dimensions are in inches)

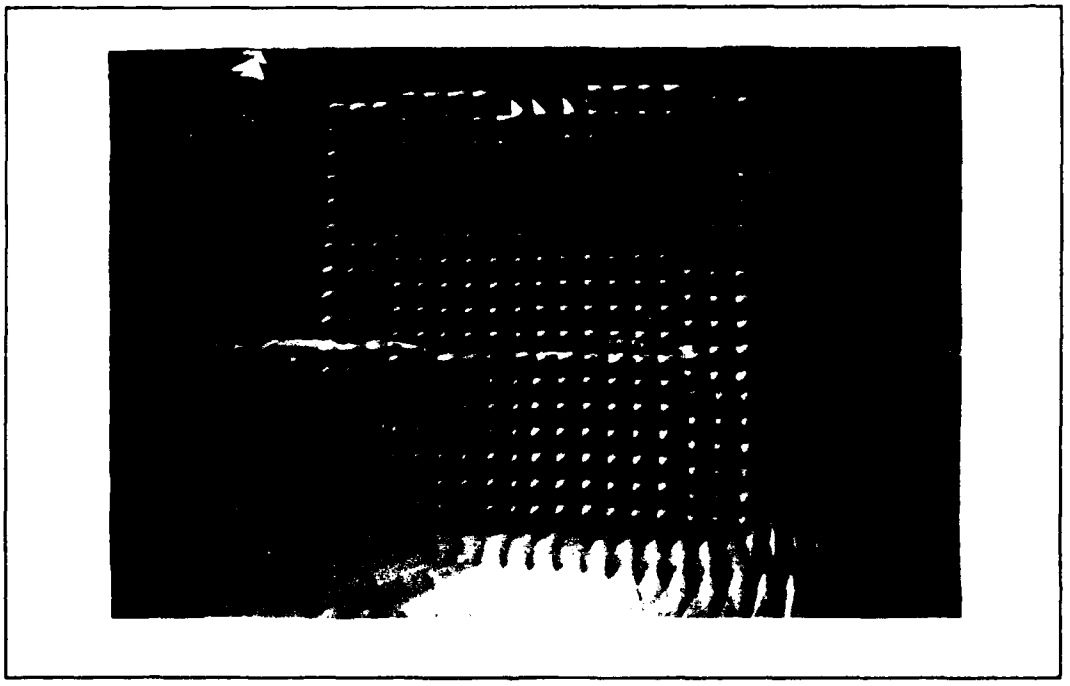

Figure 3.8 RAM Enclosure as Viewed from the Measuring Antennas

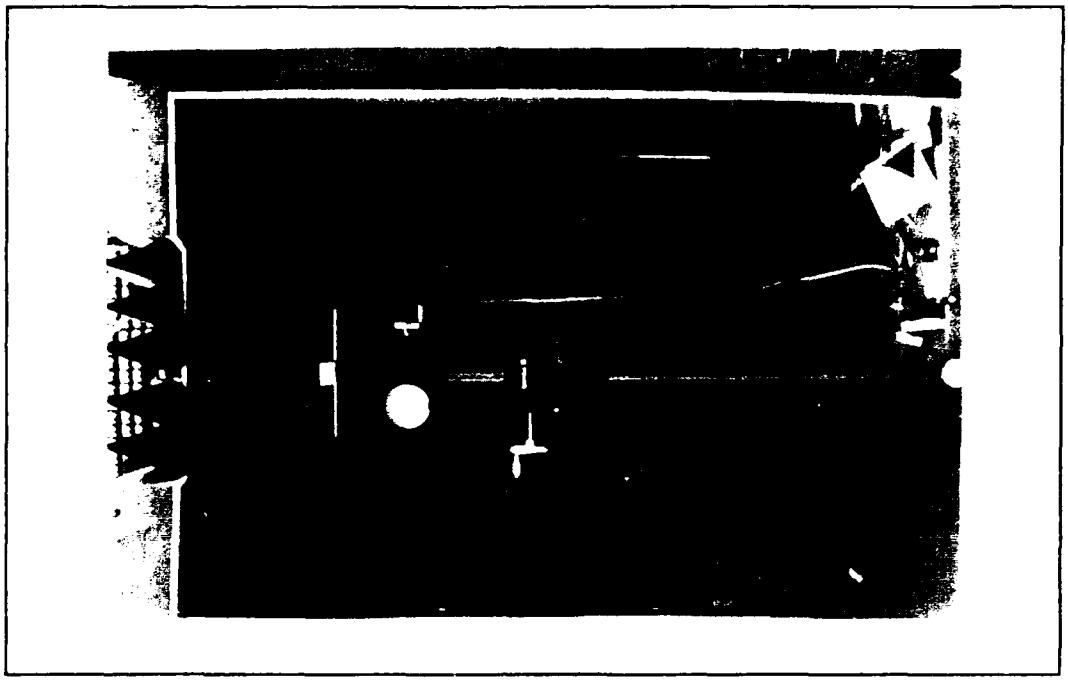

Figure 3.9 Conical Cut Mount Structure Installed Inside The Ram Enclosure

IV. RCS Measurement Results

Overview

The Geodesic Array being investigated is comprised of twenty corner reflectors configured as in Figure 2.8. The purpose of the Geodesic Array design is to provide a target with a large radar return over a larger spatial coverage than that afforded by the classical array of eight corner reflectors. The objective of this research effort was to characterize the EM scattering of the Geodesic Array through the use of both RCS measurement and theoretical prediction techniques. To achieve the objective, a comprehensive set of RCS measurements were performed on the various types of targets introduced in Chapter II. The RCS measurements were accomplished during the period from December 1989 to February 1990. All measurements were of the monostatic variety and involved the collection of EM scattering amplitude data. Following a discussion of the major measurement concerns, the measurement results for each type of target are presented and discussed.

Measurement Concerns

The measurement topics to be addressed in this section are the measurement frequency, the antenna polarization, the antenna to target separation distance, and the measurement

accuracy.

Measurement frequency. Two measurement frequencies were used to obtain the RCS measurement results reported in this document. As discussed previously, the frequencies were chosen based on the high frequency type scattering requirement. A frequency of 18 GHz was used for all measurements involving the half scale (a_{CR} = 4.25 inches) corner reflector configurations while a frequency of 9 GHz was used for the full scale (a_{CR} = 8.5 inches) corner reflector. Measurements at other frequencies were also performed but the results were omitted from this document as the results were comparable with the results performed at 9 and 18 GHz.

Antenna polarization. Two types of antenna polarizations; namely, vertical and horizontal polarization, were used during the measurements. The type of antennas used are referred to as pyramidal horns. The transmitted EM fields were generated using a dipole fed rectangular waveguide coupled to the antenna. The feed was oriented perpendicular to the broadest side of the waveguide and horn. If the broadest side of the waveguide and antenna are then oriented parallel to the ground, the resulting polarization of the EM field is termed as linear and vertical (11:398). During the RCS measurements the vertical polarization was achieved when both the transmit and receive

antennas were located side by side with their broadest side parallel to the ground. The horizontal polarization was achieved by rotating the pair of antennas 90 degrees from the vertical position. In the presentations of the RCS measurement results the symbols V for vertical and H for horizontal are used to designate the appropriate polarization.

Antenna to target range. Under the restrictions discussed in the plane wave illumination section of Chapter II, the minimum antenna to scaled model Geodesic Array separation distance was determined to be approximately 36.5 feet. The RCS measurements reported in this document were accomplished with each of the targets located approximately 37 feet from the phase center of the measuring antennas.

Measurement accuracy. RCS measurements will in general contain errors that depend on the planarity of the incident EM wave and on the measurement technique employed to perform the measurements. Under the restrictions of $\pi/8$ radian maximum cross range phase variation and 1 dB down range amplitude variation (used to determine the aforementioned measurement antenna to target separation distance) the expected measurement error associated with the target's main lobe return is less than 1 dB (7:921). For the case of pattern nulls located approximately 20 dB down from the main lobe the phase variation can result in some

filling of the nulls.

As mentioned, the RCS measurement technique employed during this research was of the CW nulling type. The general procedure is to first illuminate the measurement chamber (with target support apparatus in place but no target) and sample the resulting return. A CW nulling loop is then used to generate a "nulling" signal equal in amplitude but opposite in phase to the sampled chamber return. The nulling signal when added to the chamber return, effectively cancels the chamber return. After the chamber return is "nulled" the target of interest is placed in the chamber and the resulting backscattered return is measured. The final step of the measurement is to replace the target of interest with a calibration target of known RCS and repeat the measurement. The calibration target measurement is used to properly scale the RCS of the target of interest. An eight inch diameter sphere was used as the calibration target.

When the above technique is used, the measured returns associated with both the target of interest measurement and the calibration sphere measurement will be due approximately to the return from the item being measured alone. The term approximately is required here because the measured returns will inherently include some returns due to the target (whether target of interest or calibration sphere) and

chamber interactions. If the relative level between the measured return and the level of the target/chamber interaction return were known precisely, the measurement accuracy could be estimated as (6:907):

$$\sigma_e = \pm 10 \log (1 + 2s_e\cos(\phi) + s_e^2) \qquad (4.1)$$

where:

σ_e = the RCS measurement error (in dB)

s_e = the error in the measured voltage signal

ϕ = the relative phase error term (set to zero for amplitude measurements)

and:

$$s_e = 10^{-(\Delta/20)} \qquad (4.2)$$

where:

Δ = the difference between the measured target return and the target/chamber interaction return (in dB)

Unfortunately, the target/chamber interaction return can not easily be separated from the measured target return and therefore to assess the overall accuracy the difference between the measured target return and the "nulled" chamber return is considered first and then a qualitative estimate of the interaction term will be added.

Measured target to nulled chamber levels. A Scientific Atlanta model 1783 receiver was used to measure the relative levels of the signals of interest. The system noise level of the receiver is specified as approximately

-60 dB relative to the receiver's internal intermediate frequency (IF) stage. The output of the receiver IF was monitored through the use of an oscilloscope and a multimeter. During the chamber nulling process a -63 dB nulled chamber level was obtained for all measurements. Table 4-1 illustrates the typical target peak levels (measured at 18 GHz) and the difference between these levels and the "nulled" chamber levels obtained during the measurements. The difference term identified in Table 4-1 is the term identified as Δ in equation 4.2.

Table 4-1 Recorded Target Peak Signal Levels and the Difference Between the Signal Levels and the "Nulled" Chamber Level.

TARGET NOMENCLATURE	MEASURED TARGET "IF" SIGNAL LEVEL (dB)	DIFFERENCE BETWEEN TARGET AND "NULLED" CHAMBER (dB)
HSSCR	- 17	46
HSQCR	- 14	49
HSQWH	- 14	49
HS8WH	- 9	54
HSGA	- 14	49
FSSCR	- 10	53
8 in DIAM. CALIBRATION SPHERE	- 31	32

Since both the target of interest measurement and the calibration sphere measurement are used in determining the RCS of the target of interest the overall measurement accuracy can not be any greater than the accuracy associated with the measurement for which the difference value (Δ) is the least. The difference level associated with the calibration sphere measurements was always the smallest level (Δ = 32 dB) and therefore the overall accuracy of the measurements can not be better than the accuracy associated with the measurement of the sphere.

Target/Chamber interaction term. If the target/chamber interaction term were ideally zero the measurement accuracy associated with the calibration sphere is found from equations 4.2 and 4.1 as ± .22 dB. For a chamber the size of the Far-Field range (where the target can be placed away from the chamber walls) the dominating factor associated with the target/chamber interaction term will be due to possible target and target mount interactions. The target mounting structures were designed to minimize the target and mount interactions and therefore the target/chamber interactions are considered to be minimal. Even if the interaction term contributed 6 dB, the resulting difference term for the calibration sphere would be Δ = 26 and the resulting measurement error would be ± .42 dB. This being the case, the accuracy of the RCS

measurements presented in this document are estimated as being no worse than ± 0.5 dB.

RCS Measurement Results

The major objectives of the RCS measurements were to collect RCS measurement data for use in assessing:

a. the applicability of equation 2.7 to RCS measurement scaling of corner reflectors.

b. the impact that the hinge arrangement had on the RCS of the corner reflector configurations.

c. the RCS of the Geodesic Array over a large number of radar aspect angles.

d. the RCS provided by the Geodesic Array as compared to the RCS afforded by an array of eight corner reflectors.

e. the applicability of the theoretical RCS model (to be discussed in Chapter VI) for use in predicting the RCS of the Geodesic Array.

To accomplish these objectives, two different measurement range configurations, each producing a distinct type of RCS pattern cut, were used. The initial measurements were performed with the Far-Field range configured in the "Pedestal" configuration and addressed the first two of these objectives. Once the initial measurements were accomplished, the Far-Field range was configured in the "conical-cut" configuration and the bulk

of the measurements were obtained using this configuration.

Pedestal configuration measurements. The pedestal configuration measurements were the first type of measurements performed during the research effort. These measurements addressed the first two major objectives listed above and also provided a baseline with which the initial results of the conical cut configuration could be compared. The Far-Field range was configured in the pedestal system configuration described in Chapter II. The targets measured using this range configuration were the half scale single corner reflector (with (HSSWH) and without (HSSCR) hinges), a quad array of the half scale corner reflectors (with (HSQWH) and without (HSQCR) hinges), and the full scale single corner reflector (FSSCR). The chamber was first "nulled" as described above and then each target was placed on the ogive-cylinder shaped target support pedestal with polystyrene target fixture (see Figure 3.4) and rotated counter-clockwise (as viewed from above) 360 degrees in azimuth. In this range configuration the amplitude data was sampled in 0.1 degree increments. After each target measurement was completed, the target was removed and the nulled chamber level was checked to verify the nulling had remained constant during the measurements. The calibration sphere was then placed on the target fixture and the scattered return measured. The results for each class of

target are discussed separately.

Single corner reflector targets. The individual results for the HSSCR, HSSWH, and FSSCR RCS measurements are contained in Appendix B in Figures B.1 through B.14. Since only the return associated with the frontal lobe of the individual corners is important for the investigations of this research, a 110 degree sector is shown for each single corner reflector measurement. The results are of the great circle cut variety (see Figure 2.9 and accompanying discussion) and the angle alpha listed on the measurement plots is actually the angle measured from the base of the target fixture to the centerline of the base plate of the corner reflector. An angle of alpha = zero indicates that the reflector was placed with it's base plate lying flat on the target fixture.

HSSCR vs FSSCR. The result of the HSSCR measured at 18 GHz and the FSSCR measured at 9 GHz were compared to assess the applicability of the scaling of the corner reflector RCS measurements. Figure 4.1 depicts a comparative plot of the results obtained for a horizontal polarization and alpha = 0° test case. The difference between the two measurements is approximately 6 dB (i.e. a factor of 4) which is in agreement to the calculated result obtained using equation 2.7 with the scale factor equal to 2.

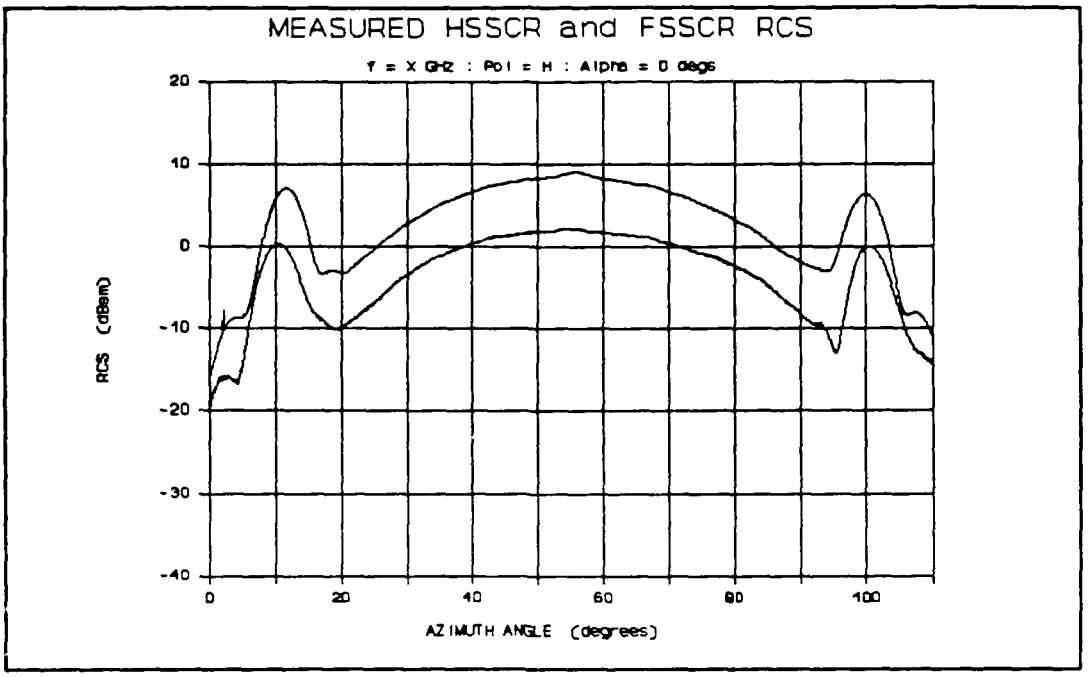

Figure 4.1 RCS of the HSSCR (@ 18 GHz) and the FSSCR (@ 9 GHz) for the Horizontal Polarization and Alpha = 0° Case (Top Curve is FSSCR)

HSSCR vs HSSWH results. The results of the single corner reflector with and without hinges were compared to assess the impact of the hinge arrangement on the RCS of a single corner reflector. The results for the horizontal polarization and alpha = 0° and 45° test cases are shown in Figures 4.2 and 4.3 respectfully. The results indicate the presence of the hinge had a minimal effect on the RCS of the single corner reflector with the only noticeable effect being to cause a slight rippling of the RCS of the main lobe. When the vertical polarization case is examined the results, though not as pronounced, are

basically the same.

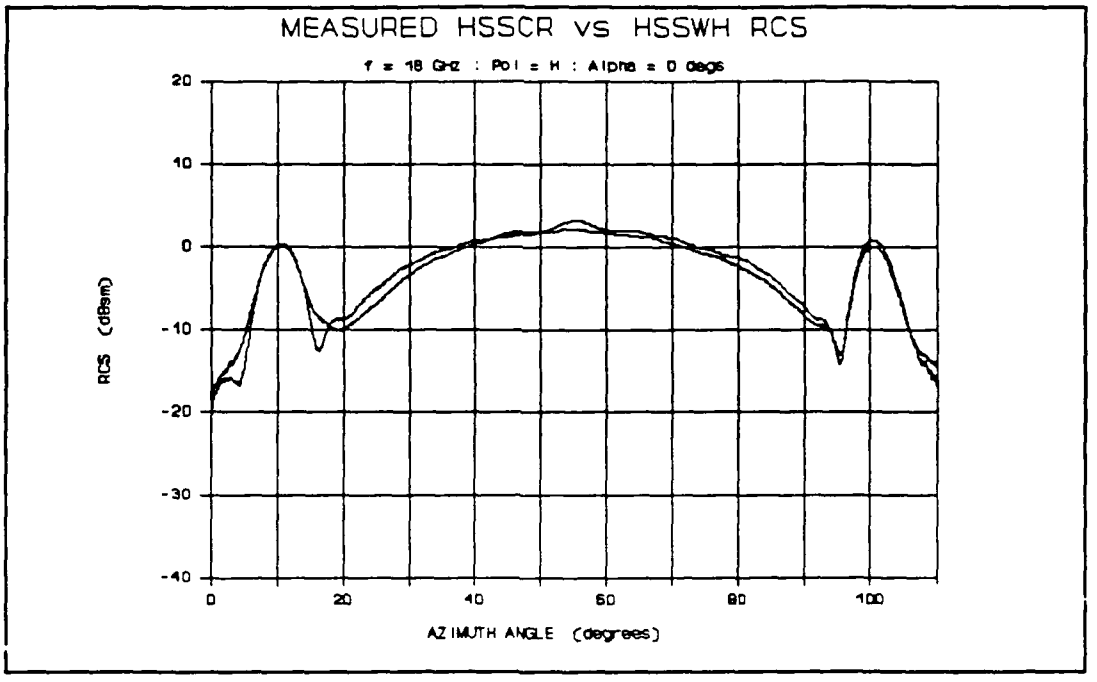

Figure 4.2 RCS of the Single Corner Reflector with (HSSWH) and without (HSSCR) Hinge for the Horizontal and Alpha = 0° Case (Top Curve is HSSWH)

Quad array targets. Two different arrays containing four corner reflectors were also measured to examine the effect of the hinge arrangement on the RCS associated with multiple corner reflectors. Measurements were performed on each type using vertical and horizontal polarizations for the case of alpha = 0°. A 110° sector of the results for both the non-hinged quad array (HSQCR) and the hinged quad array (HSQWH) are contained in Appendix B, Figures B.15 through B.18. When the results are overlaid the same conclusions reached for the single corner reflector

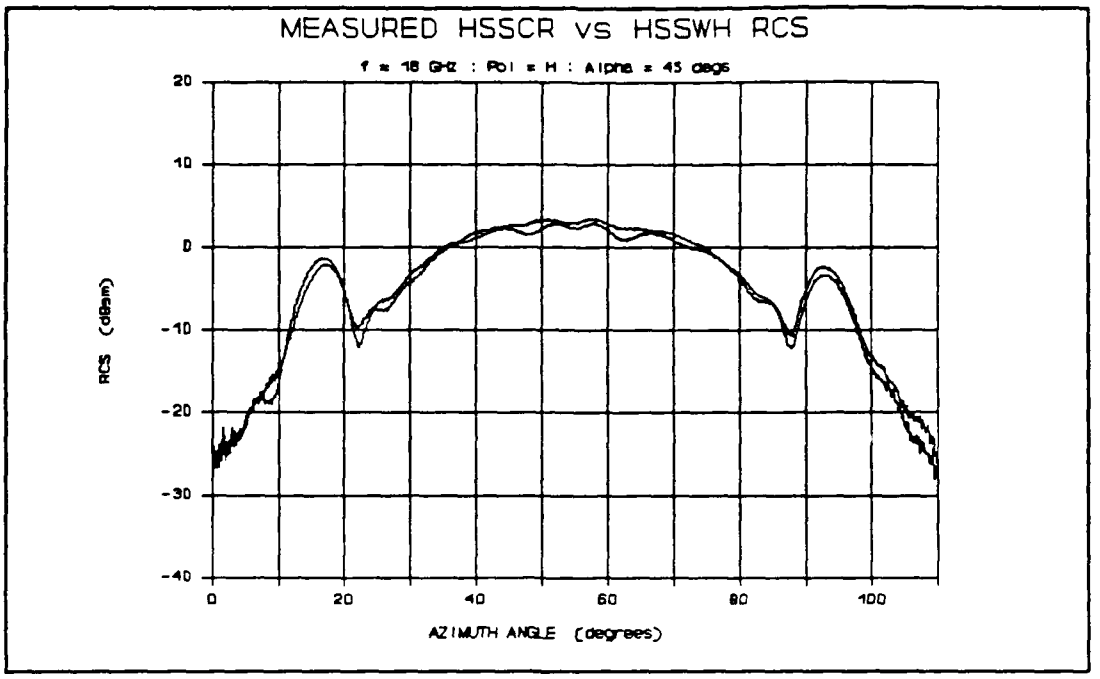

Figure 4.3 RCS of the Single Corner Reflector with (HSSWH) and without (HSSCR) Hinge for the Horizontal and Alpha = 45° Case (Top Curve is HSSCR)

comparisons apply.

Conical Cut configuration measurements. In order to collect test data over a large spatial coverage the Far Field range was converted into the conical cut system configuration as described in Chapter II. The ogive shaped pedestal mount was replaced with the conical cut target mount structure surrounded by the RAM enclosure. The targets measured using this range configuration were the single corner reflector without hinges (HSSCR), an array of eight corner reflectors constructed using the hinged arrangement (HS8WH), and the scaled model Geodesic ARRAY

(HSGA). The mounting of the targets was provided through the use of a matched set of 5/8 inch diameter, 12 inch long steel rods. One rod (termed the target mount rod in Figure 3.5) was permanently attached to the rotator assembly and protruded slightly above the slot in the RAM enclosure. Each of the targets and the calibration sphere were attached to it's own rod (called a target support rod in the discussions below) which could be threaded into the target mount rod. An additional nulling rod (with no target attached) was required during the chamber nulling process.

The measurements were performed by first threading the nulling rod to the target mount rod and then subsequently tilting the target rotation axis toward the measuring antennas until the desired viewing angle with respect to the measuring antennas was obtained. The chamber return was then "nulled" in the described manner. The nulling rod was then replaced by the target and target support rod and the target rotated clockwise (as viewed from above the rotation axis) 360° in azimuth around the rotation axis. In this configuration, the amplitude data was collected in 0.5° increments. After the target measurement was complete the target and target support rod were removed, the nulling rod reinstalled, and the chamber nulling verified. The nulling rod was then replaced by the calibration sphere and it's support rod and the calibration sphere return measured.

discussion of these results will be delayed until Chapter VI (the theoretical comparisons).

The data collected using the pedestal configuration was collected with the target rotating counter-clockwise while the data collected using the conical cut configuration was collected with the target rotating clockwise. Therefore before a comparative plot could be generated the order of one of the measurement results had to be inverted. This was accomplished for the pedestal results and the comparative plots for the HSSCR for theta = 90° (conical cut) and alpha = 0° (pedestal configuration) are presented in Figures 4.4 and 4.5 for the horizontal and vertical polarizations respectfully. The difference between the results obtained using both procedures is practically indistinguishable. The slightly higher value of the single bounce peaks for the conical cut horizontal case might be attributed to the fact that the three degrees of freedom afforded by the conical cut target support structure enabled the targets to be leveled with a higher degree of precision.

Eight corner reflector array target. The array of eight corner reflectors constructed using the hinged arrangement (HS8WH) was measured to provide the data set to which the results of the scaled model Geodesic Array could be compared in order to assess how well the Geodesic Array achieved its design objective. The measurements were again

Initial test runs were performed to ensure that the nulling rods and target support rods were sufficiently matched so that the replacement of one rod with another did not affect the "nulled" chamber return. Initial tests were also performed to ensure that the rods could not only be successfully nulled but that this return remained nulled during the rotation of the rods. Although the initial tests indicated that it wasn't necessary, a strip of RAM was placed in front of the protruding portion of the target support rods as a precautionary measure for the test cases when the rods were near perpendicular to the ground.

The results for each type of target will be discussed separately. The angle theta presented in the RCS measurement results should be interpreted as the elevation angle down from a vertically oriented z-axis to a viewing radar's line of sight.

Single corner reflector target. The purpose of the single corner reflector conical cut measurements was to collect data for comparison to the pedestal configuration measurements and for use in assessing the theoretical model. Measurements were performed for elevation angles (theta) from 90° to 15° in 15° increments for both vertical and horizontal polarizations. The 110° degree sector results are given in Figures C.1 through C.12. Except for the comparison to the pedestal configuration measurements, the

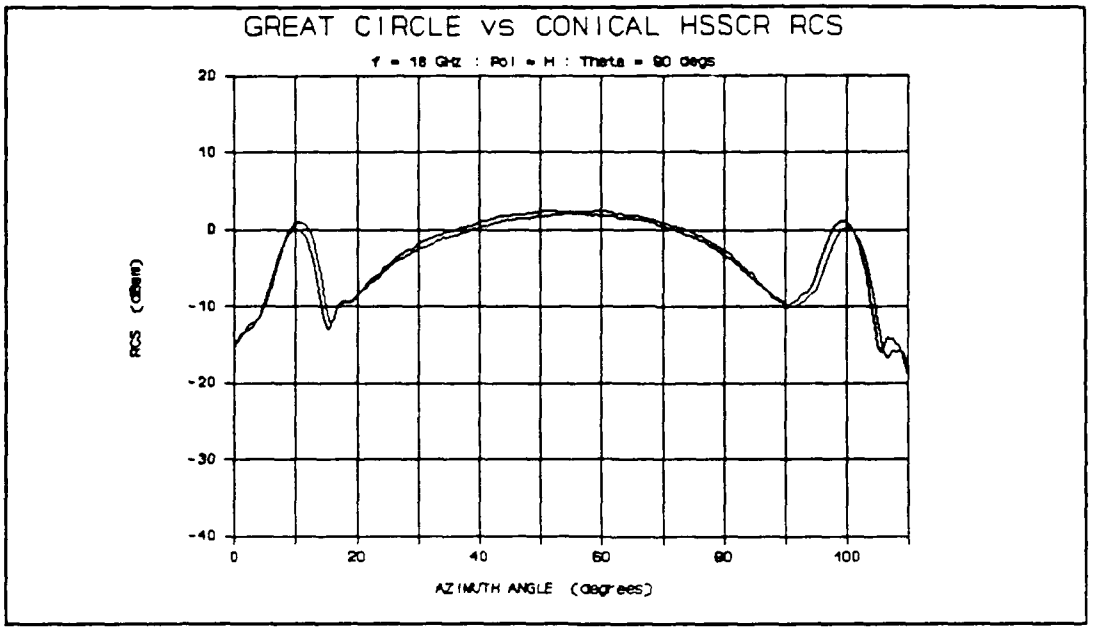

Figure 4.4 Comparison of the Pedestal Configuration and Conical Cut Configuration RCS Results for the HSSCR Horizontal Polarization Case

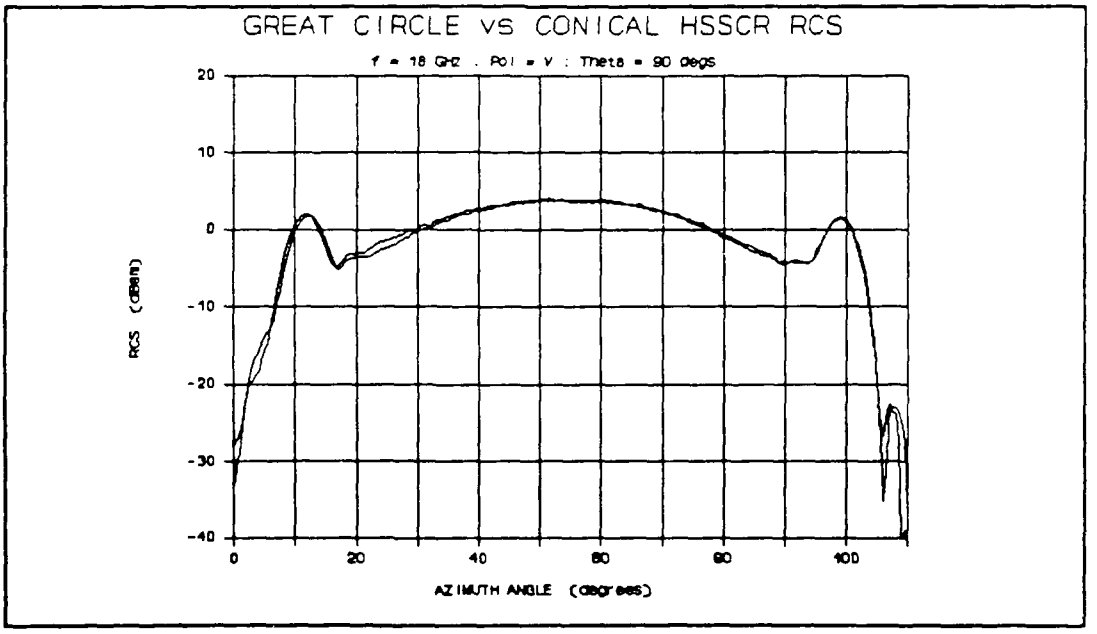

Figure 4.5 Comparison of the Pedestal Configuration and Conical Cut Configuration RCS Results for the HSSCR Vertical Polarization Case

performed in 15° increments from theta = 90° to 15° for both polarizations.

Use of the hinged arrangement to construct the eight corner reflector array turned out not to be an optimal way to fabricate this type target. Because all sides of the individual reflectors are parallel to a side of an adjacent reflector the use of the hinges resulted in some non-symmetrical quadrants existing in the array. The 110° sector results presented in Appendix D, Figures D.1 through D.12, were chosen using the array quadrant that best exhibited the RCS characteristics typical of this type target. These results will be compared to the Geodesic Array RCS results in the following chapter.

Scaled model Geodesic Array target. During the RCS measurements of the scaled model Geodesic Array (denoted as HSGA), the array was oriented in an upright orientation (see Figure 2.8) with respect to the rotation axis. In other words the rotation axis extended from the lower tip of the array, through the middle of the array, to the upper tip of the array. Since the scaled model Geodesic Array was the primary target of interest a more comprehensive set of RCS measurements were obtained. The measurements were again performed for both the vertical and horizontal polarizations however the measurements were performed in 7.5° increments from theta = 90° to theta = 15°. To allow comparisons

between the different measurements, the starting azimuthal position of the Geodesic Array (azimuth angle = 0 degrees in the plots) was always the same. This starting orientation will become evident in the pictures that follow. The complete set of RCS measurement results for the full 360° azimuth rotation are presented in Figures E.1 through E.22 of Appendix E. Before discussing the measurement results it is appropriate to consider the construction and geometry of the HSGA in a little more detail.

HSGA construction. The construction of the HSGA using the hinged arrangement did not impose the physical constraints encountered during the construction of the array of eight corner reflectors. This is because the geometry of the Geodesic Array is such that none of the sides of adjacent corner reflectors are parallel. Starting with twenty hinged single corner reflectors, the array could be put together from scratch in about five minutes.

HSGA geometry. For the purpose of discussion a z-axis will be defined as an axis which extends through the middle of the array from bottom to top. A horizontal plane is also required for the discussion and is defined as any plane perpendicular to the z-axis. When the Geodesic Array is viewed in an upright orientation the array can be visualized as being comprised of three separate tiers (top, middle, and bottom) of corner reflectors.

The top tier of the array is comprised of a set of five corner reflectors. The five corner reflectors are equally spaced at 72° intervals around the z-axis. Each of the vertices of the five reflectors is displaced 1.502 inches from the z-axis and the top tip of each reflector is tilted back toward the z-axis. The result of this backwards canter is that each of the top tier corner reflector base plates lies in a plane that is oriented at an angle of 17.358° above a horizontal plane. The bottom tier is also comprised of five corner reflectors and is the inverted case of the top tier. The result is that the base plates of the bottom tier reflectors are oriented at an angle 17.358° below a horizontal plane. It is also important to note that the vertices of the bottom tier reflectors are also located at 72° intervals but are shifted 36° with respect to the vertices of the top tier reflectors.

The middle tier of the array is comprised of a set of 10 corner reflectors. The vertices of each middle tier corner are located at 36° intervals around the z-axis and every other middle tier corner reflector is inverted. The radial distance from the z-axis to the vertices of the middle tier corners is 2.286 inches. The geometry of the array is such that the leading edge of the base plate associated with each of the non-inverted middle corners is coincident with the leading edge of the base plate of a

bottom tier corner reflector. The leading edge of the base plate of the inverted middle corners is therefore coincident with the leading edge of the base plate of a top tier corner. This arrangement results in the fact that the base plates of the middle tier non-inverted and inverted corner reflectors lie in planes ± 46.077° with respect to a horizontal plane.

HSGA RCS results. As can be seen in Figure 2.8, each tip of a corner reflector is adjacent to the tips of four other corner reflectors. Because the hinges occupy space between the corner reflectors, there is an empty space (of approximately 1/2 inch circular diameter) where the tips come together. The effect of this empty space on the RCS of the Geodesic Array was expected to be minimal but was examined anyway. The results contained in Figures E.1 through E.22 were obtained with the empty space left alone. Subsequent to these measurements the empty spaces were filled with RAM material and the measurements for the vertical polarization and theta = 90°, 75°, 60°, and 45° cases were repeated. This configuration of the HSGA (with the RAM filling) is actually the configuration pictured in Figure 2.8. The results for these measurements are given in Figures E.23 through E.26. When these results are overlaid onto the results contained in Figures E.2, E.6, E.10, and E.14 an exact match is found for each case, indicating that

the empty spacing was indeed not a factor in the RCS of the scaled model Geodesic Array results obtained at a frequency of 18 GHz.

The RCS measurement results presented in Appendix E depict the fact that the RCS of the Geodesic Array is a consequence of the complex interaction between the returns from the individual corner reflectors. Ignoring the diffraction terms (considered small relative to the main lobe corner reflector returns), a detailed analysis of the results for a single azimuth angle would require the consideration of the single bounce, double bounce, and triple bounce phenomena of "each" corner reflector that is within the measuring antennas line of sight. This level of detail is not pursued here. Instead, two measurement cases are examined to hopefully provide some insight to the reader as to the nature and complexity of the scattering phenomena.

The result for the vertical polarization and theta = 90° case is the first case to be investigated. Figure 4.6 depicts the orientation of the Geodesic Array at the beginning of a test run for an elevation angle of 90°. Figure 4.7 is the resulting RCS pattern for the vertical polarization measurement. For the 90° elevation angle case the top tier and bottom tier corner reflectors are tilted 17.358° away from the viewing radar and contribute little from their main lobes. The middle tier corner reflectors

are spaced 36° apart and are the primary reason for the 36° repeating pattern shown in Figure 4.7. Starting at an azimuth angle of 0°, the first 36° sector will be examined.

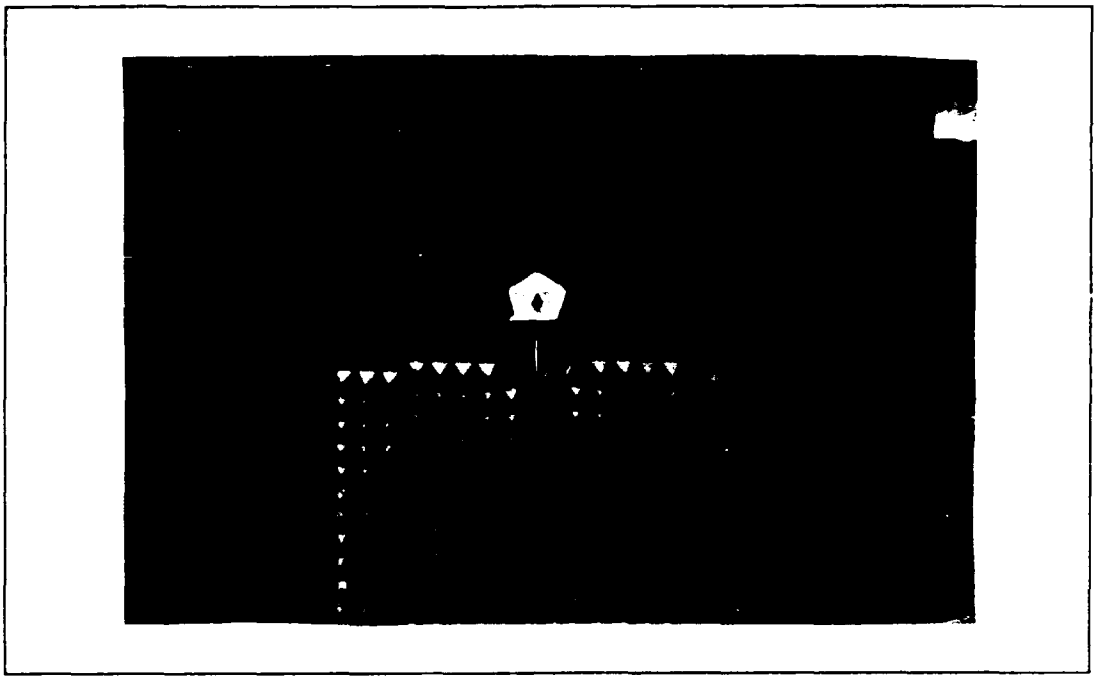

Figure 4.6 The Scaled Model Geodesic Array Viewed at an Elevation Angle (Theta) = 90° and Azimuth Angle = 0°

To predict the peak to null to peak pattern of the first 36° sector, four of the middle tier corner reflectors are considered. As depicted in Figure 4.6 the centermost middle tier corner reflector (non-inverted) will be labeled as corner "B". The inverted corner to it's left will be labeled as corner "A" while the inverted corner on the right will be labeled corner "C". The fourth corner reflector that must be considered is the non-inverted corner located to the right of corner "C" and will be called corner "D".

Establishing a phase center for the return from each corner reflector at the vertex of the reflector, the relative phase between the returns from each of the four corners being considered can be calculated.

The relative phase calculation was performed by first calculating the downrange path difference associated with the backscattered returns for each of the four corners relative to a point located on the radar to target centroid line of sight. The ratio of the path difference and the wavelength associated with the 18 GHz signal (1.66 cm) was then calculated and multiplied times 360 degrees. The resulting relative phase for each of the corners was plotted

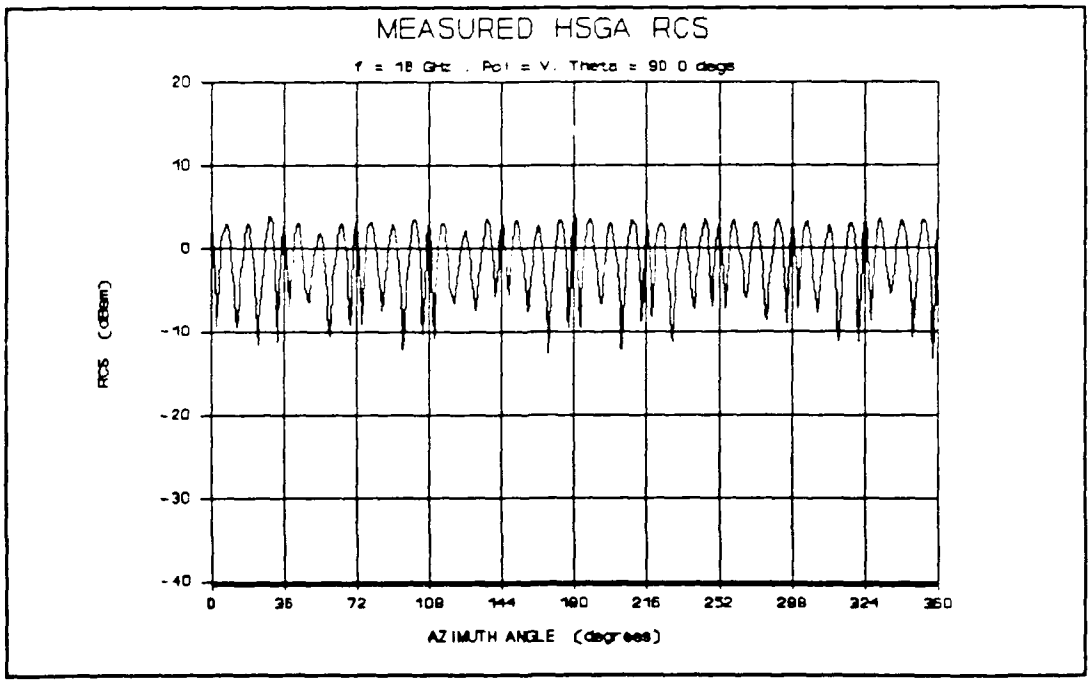

Figure 4.7 RCS of the Scaled Model Geodesic Array for the Vertical Polarization and Theta = 90° case

for the first 36° of azimuth rotation (clockwise when viewed from above). The result is shown in Figure 4.8. Note that since the corners "A" and "D" are not physically viewable for the full 36° of rotation their relative phases were not plotted for the full sector.

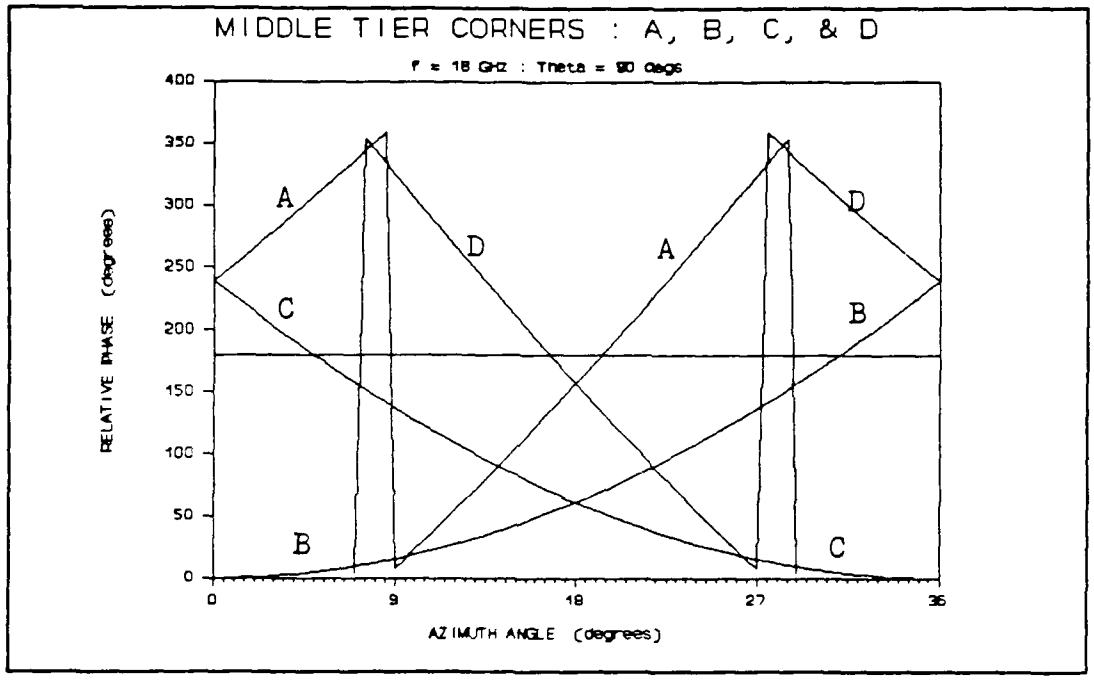

Figure 4.8 Calculated Relative Phase of the Scattered Returns from Four Middle Tier Corner Reflectors

By comparing the relative phase between the different returns, the source of the relative maxima and minimum of the RCS plot depicted in Figure 4.7 can be identified. The first peak at 0° is mainly due to the return from corner "B". The first null occurring at 4.5° is where the returns from corners "B" and "C" are 180° out of phase. The second

peak occurring around 8° is where three of the four returns are in phase. The second null occurring at 14.5° is associated with the returns from "B" and "D" being 180° out of phase. The third peak at 18° is where the returns from "B" and "C" are exactly in phase. Continuing the comparison the remaining nulls and peaks are mirror images of the ones just discussed.

A second measurement case to consider is the measurement performed for a vertical polarization and theta = 60°. For this measurement the rotation axis was tilted toward the measuring antennas at an angle of 30° from vertical. The starting orientation is shown in Figure 4.9 and the resulting measured RCS is shown in Figure 4.10. The resulting RCS pattern is now seen to repeat at 72° intervals. Each of the five main pattern lobes is the result of a pair of corner reflectors. Each pair is comprised of one top tier corner and one inverted middle tier corner reflector. Two of these pairs are visible in Figure 4.9, one pair on the left and one pair on the right side of the array. The minor lobes are due to the interactions of the returns from the other corners visible to the measuring antennas.

The preceding discussions were aimed at giving the reader some insight into the complexity of the scattering phenomena associated with the Geodesic Array. A complete

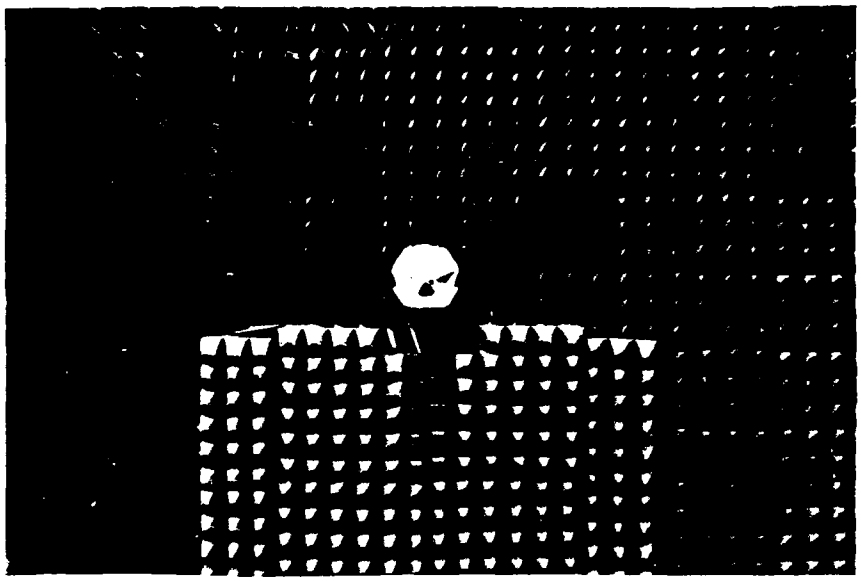

Figure 4.9 The Scaled Model Geodesic Array Viewed at an Elevation Angle (Theta) = 60° and Azimuth Angle = 0°

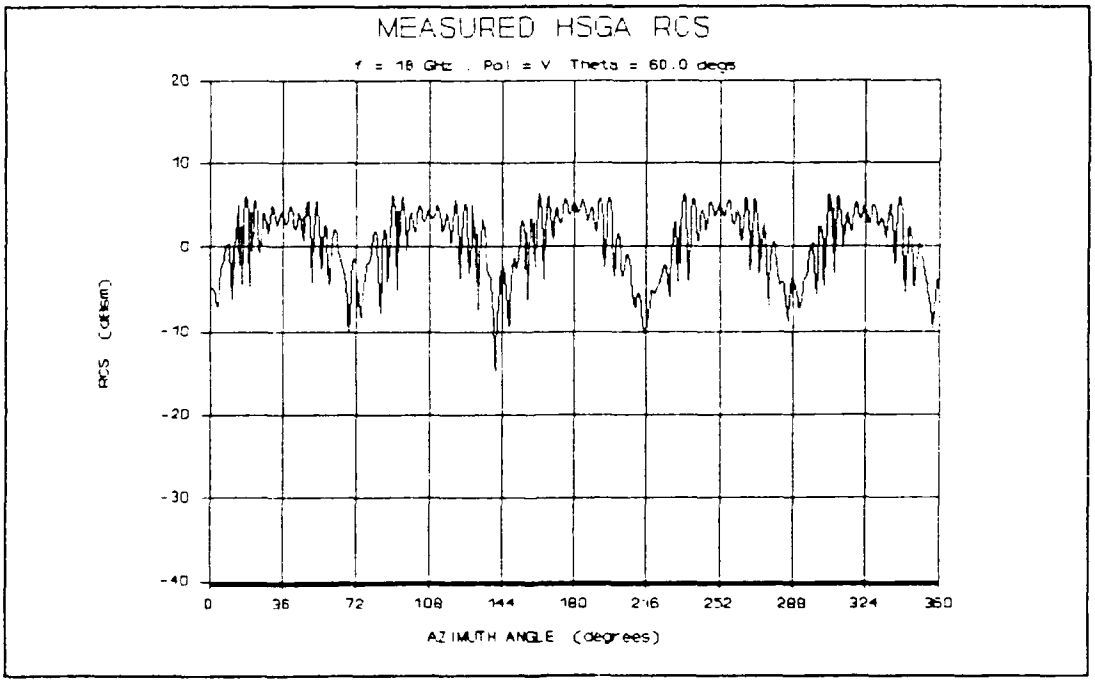

Figure 4.10 RCS of the Scaled Model Geodesic Array for the Vertical Polarization and Theta = 60° case

examination of all the results presented in Appendix E is beyond the scope of this document. It is suffice to conclude at this point that the RCS of this type of target is extremely dependent on the viewing angle of the measuring radar. The subject to be addressed next is the interpretation of the RCS measurements in terms of the relative performance of the Geodesic Array as a target for providing a large radar return over a wide number of viewing angles. This is the subject of Chapter V.

V. Geodesic Array Value Assessment

Overview

The Geodesic Array was designed to present a large radar return over a greater spatial coverage than the coverage afforded by an array of eight corner reflectors. This chapter uses the RCS measurement results of the preceding chapter to assess how well the Geodesic Array fulfilled this design objective. Discussions of the assessment criteria, assessment methodology, and assessment results are presented.

Assessment Criteria

The measurement results introduced in the preceding chapter serve to document the RCS of both the HSGA and the eight corner reflector array over a wide variety of radar viewing angles. The question that remains unanswered is; which target is better suited for the purpose of providing a large radar return over the greatest spatial coverage. If the RCS patterns of the two classes of targets are compared for a given elevation angle, the decision as to which target best fulfills this purpose is sometimes apparent and sometimes not so apparent. For example, if Figures D.3 (noting that the eight corner reflector array would have a repeating pattern every 90°) and E.5 are compared it is

readily apparent that the HSGA resulted in a larger and more consistent RCS and as such would be the preferred target for the stated purpose at the 75° elevation angle and horizontal polarization. Examination of Figures D.5 and E.9 however does not lead to such an undisputable conclusion.

The criteria of the analysis of this chapter was to provide a means with which the spatial coverage provided by each of the targets could be more readily interpreted.

Assessment Methodology.

Before a meaningful analysis of the RCS measurement data could be performed, the data had to first be put in a format more suited for this purpose. This was accomplished through the use of the modification to the normal data processing subsystem of the Far-Field range, as discussed in Chapter III. The RCS data originally collected and stored in HP format was converted to the standard ASCII format and then transferred to a PC computer system. With the data now in ASCII format, subsequent processing could be performed using standard PC software packages.

The next decision was to decide on what intervals of azimuth angles the additional data processing should be performed. Since the eight corner reflector array data was limited to a 110° sector, the subsequent processing was performed on the 90° peak lobe to peak lobe quadrant. Since the results for any array of eight corner reflectors has a

repeating RCS pattern every 90° any results applicable to one quadrant would also be applicable to the other quadrants. The choice of the interval with which to consider the HSGA RCS results was not so straightforward. Because the symmetry of the RCS patterns varies from 36° or 72° increments depending on the elevation angle, any selection of an azimuth sector that was a multiple of 72° may have biased the results in favor of one of the targets. The one exception to this case is if the complete 360° of azimuth coverage were included and as such, the subsequent analysis of the HSGA RCS results was performed on the complete 360° data set.

The RCS results presented in the appendices are seen to contain an occasional wild point. The wild points are typical of most RCS measurements and were attributed to the receiver processing circuitry. Before any further data processing was performed these wild points were examined. The wild points were found to exist for a single measurement interval (0.5°) at a time and were accounted for by replacing the wild point value with a value that fell in the middle of the two adjacent data points.

To provide a more visual means for interpreting the RCS measurement results, the distribution of the RCS results for both targets was calculated for the horizontal and vertical polarizations and for theta = 90°, 75°, 60°, 45°, 30°, and

15° test cases. The number of the RCS data points that occurred within the 3 dB intervals between 15, 12, 9, 6, 3, 0, -3, -6, -9, -12, and -15 dB as well as the number of points that were below -15 dBsm were calculated. The numerical distribution was then converted to a percentage so that the resulting distributions were comparable between targets.

Assessment Results

The data distribution percentages were plotted in bar graph form and are presented in Appendix F for the test cases mentioned. Figures 5.1 and 5.2 are the resulting distribution plots that correspond to Figures D.4 and E.9 mentioned in the beginning of this chapter.

As an example of how to interpret the bar graph form of the distribution plot, consider the tallest bar of Figure 5.1. From the data set point of view, the bar should be interpreted to mean that approximately 36% (36.11% to be exact) of the data points in the 90° interval considered had a measured value between 0 and 3 dBsm. From a spatial coverage point of view, the same bar can be interpreted to mean that the RCS of the eight corner reflector array will be between 0 and 3 dBsm for 36% of the 90° spatial interval analyzed (or 32.4°). Since the RCS pattern approximately repeats itself every 90° for an eight corner reflector array

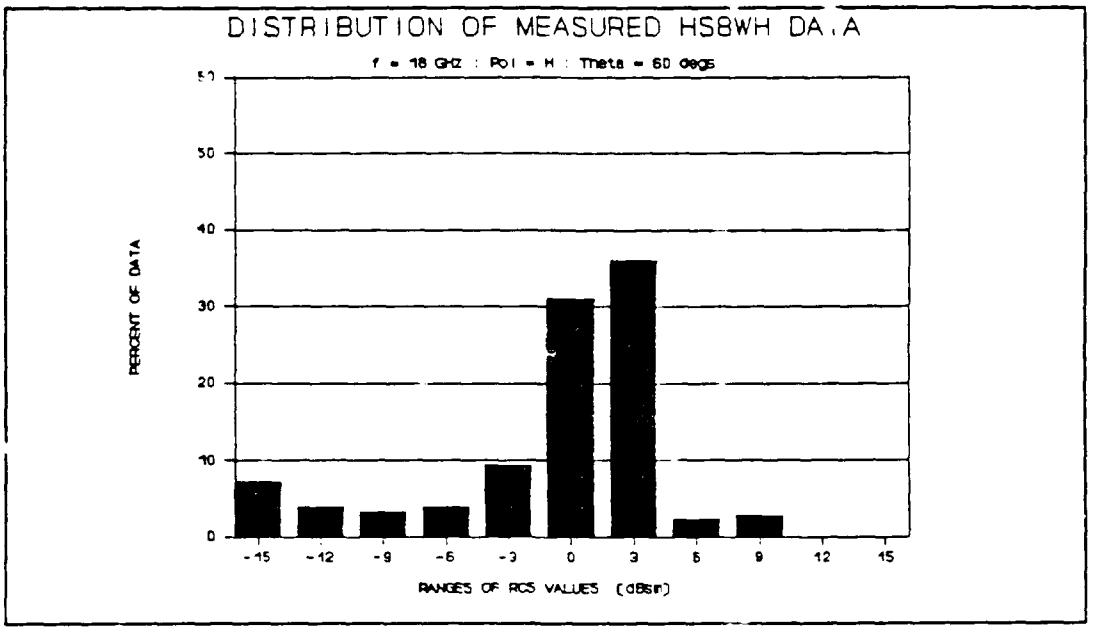

Figure 5.1 Distribution of the Measured Eight Corner Reflector Array RCS Results, Theta = 60°, Horz Pol

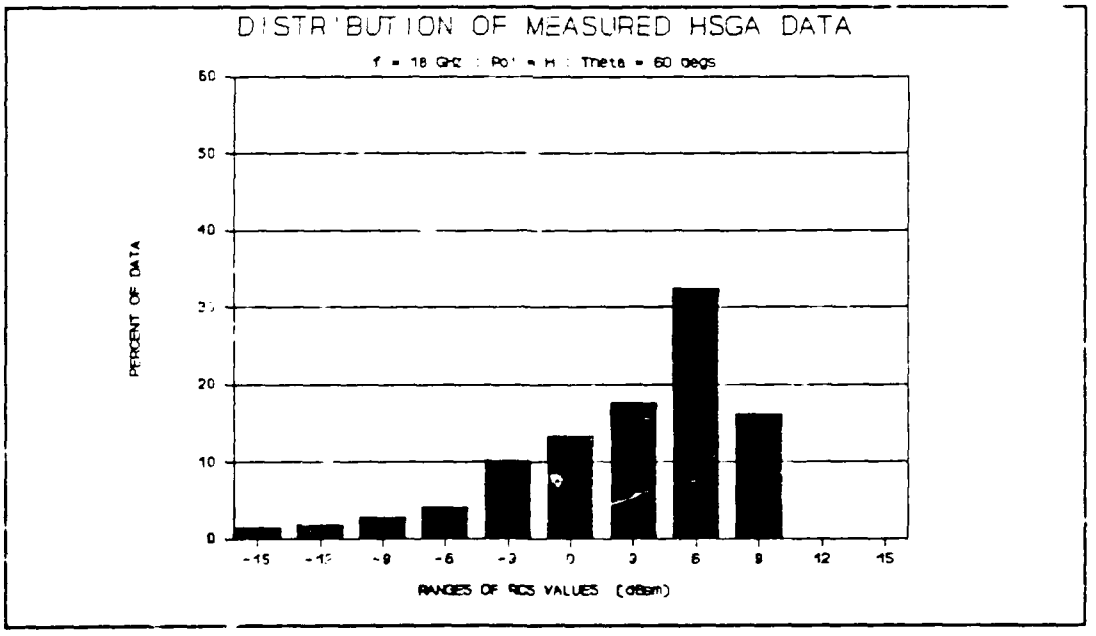

Figure 5.2 Distribution of the Measured Scaled Model Geodesic Array RCS Results, Theta = 60°, Horz Pol

this percentage is comparable to a corresponding percentage associated with the scaled model Geodesic Array.

The distribution plots when combined with an additional criteria can be used as an effective tool in assessing the relative performance between the two type of targets. When one is selecting a target to be used for the purpose of providing a large radar return, some minimal acceptable RCS is often established based on the desired application. With this in mind Table 5-1 was created by selecting a minimal acceptable RCS to be 0 dBsm. The resulting spatial coverage percentage for which each target provided a RCS equal to or greater than 0 dBsm was calculated from the distribution plots of Appendix F by adding the percentages for each bar that was above 0 dBsm.

The results indicate that except for the theta = 90° cases (where the eight array is designed for a maximum return) the HSGA performed as well as or better than the eight array. One should be cautioned that the results of such a comparison will depend on the selection of the minimum acceptable RCS. Regardless of the minimum value selected, the distribution plots of Appendix F clearly indicate that the Geodesic Array oriented in the upright position, when compared to an array of eight corner reflectors, provided a more superior spatial coverage for the elevation angles of theta = 75° and theta ≤ 30°.

Table 5-1 Spatial Coverage Percentages of the Array Targets for a Minimum Acceptable RCS of 0 dBsm

ELEVATION ANGLE THETA (degs)	HORZ POLARIZATION		VERT POLARIZATION	
	EIGHT ARRAY	GEODESIC ARRAY	EIGHT ARRAY	GEODESIC ARRAY
90	66 %	55 %	88 %	45 %
75	4 %	81 %	1 %	37 %
60	41 %	66 %	56 %	61 %
45	64 %	67 %	57 %	56 %
30	9 %	63 %	8 %	70 %
15	16 %	53 %	0 %	60 %

The results presented in this chapter indicate the Geodesic Array investigated in this research is a viable candidate as a target for providing a large radar return over a wide variety of viewing angles.

VI. Theoretical Prediction

Overview

If the capability of predicting the RCS of the Geodesic Array could be developed and verified through the use of the scaled model Geodesic Array RCS measurements presented in this document, the model could in turn be used as a tool for predicting and analyzing the RCS of much larger Geodesic Arrays. As mentioned throughout this document the type of EM scattering associated with a operational size Geodesic Array is of the high frequency (optical regime) type and therefore the prediction capability was directed toward the use of one of the high frequency prediction techniques. An excellent overview of the high frequency scattering techniques is given by Eugene Knott in reference 12 and is not pursued here.

Since obtaining the RCS measurements was a very time intensive effort, the approach taken toward developing the capability to predict the RCS of the Geodesic Array was to first obtain an existing computer code, to verify how well the code predicted the RCS of the targets it was designed for, and then to modify the code such that the desired Geodesic Array RCS could be predicted.

The "CLUSTR" Computer Model

A physical optics based computer model called CLUSTR was obtained through Mr Robert Puskar of the Mission Research Corporation. The Fortran based computer model developed by Tracor Inc in the early 1980's was designed to predict the RF scattering characteristics of various configurations of corner reflectors. The mathematical basis for the model as well as a description of the codes capabilities, limitations, input requirements, and output options can be obtained through the thesis sponsor.

Of interest to this research, was the model's ability to predict the monostatic RCS of rigidly connected triangular shaped trihedral corner reflectors. In it's original configuration the CLUSTR computer model was capable of predicting the RCS of arrays comprised of up to eight of these corner reflectors. As mentioned above, the goal was to successfully modify the model in a manner that would allow the prediction of the RCS of a Geodesic Array.

Modification #1

In it's original form the CLUSTR computer model was written for execution using a vax computer. Because this author is more familiar with Fortran applications using personal computers (PC) the first modification was to convert the CLUSTR program so that it could be executed on a PC. The input portion of the code was first modified so

that the required inputs are prompted on the monitor and entered from the keyboard. The program output statements were then modified so that the calculated results are written to both the monitor and to an ASCII file named RESULT.PRN. The four vax specific plotting subroutines were also deleted during this modification. The resulting PC version was renamed as CL.FOR.

Several test cases were generated using the CLUSTR program and a vax computer and the CL program and a PC. The numerical outputs were compared to verify the modification to the PC compatible version was successful. Next the CL version was used to obtain the RCS predictions for the single corner reflector and array of eight corner reflectors used in this research. The theoretical predictions were then plotted against the measured results and these comparative plots are included in Appendix G. The results depicted in Appendix G indicate that the predictions compare reasonably well with the measured results.

Modification #2

Having verified the ability of the computer model to adequately predict the RCS of the single corner reflector and the array of eight corner reflectors the next step was to modify the model to predict the RCS of the Geodesic Array. To accomplish this step a feature of the code that allows the inputing of individual corner reflectors at

different locations in space was utilized. The code initially places each of the corner reflectors at the origin of a fixed coordinate system with the base plate of the reflector lying in a xy plane and the two side plates lying in a xz plane and yz plane. Using the geometry discussed in Chapter 4 a set of successive yaw (CCW about the z-axis), pitch (CCW about the y axis), and roll (CCW about the x-axis) rotations coupled with an xyz translation vector can be used to place each of the twenty corner reflectors at its appropriate position in the Geodesic Array. Once each of the corners is properly positioned the remaining task is to define the viewing angles (by considering both the elevation and azimuthal aspects) for which to include the contribution from each of the twenty corner reflectors.

During the modification process this author mistakenly defined the rotations (yaw, pitch, and roll) with respect to a moving coordinate system instead of defining them with respect to the original fixed coordinate system as required by the current implementation of the computer model. Unfortunately, this violation of the defined rotation requirements was not identified until the last few days allotted for the research effort and therefore the correct rotations could not be accomplished in the remaining time.

It turns out that this violation had the least effect on the placement of the five corner reflectors occupying the

top tier of the Geodesic Array. Since the RCS for angles of theta less than 35° (viewing angles looking down near the top of the array) is only dependent on the top tier corner reflectors the predicted RCS (although not totally correct yet) of the Geodesic Array is included here to show that the computer model once corrected should yield adequate results. Figures 6.1 and 6.2 represent the predicted results for the theta = 30° case and for the vertical and horizontal polarizations. Comparison of these results with the measured results depicted in Figures E.17 and E.18 indicate that the predicted results once the rotation discrepancy is resolved can be expected to agree reasonably well with the measured RCS results.

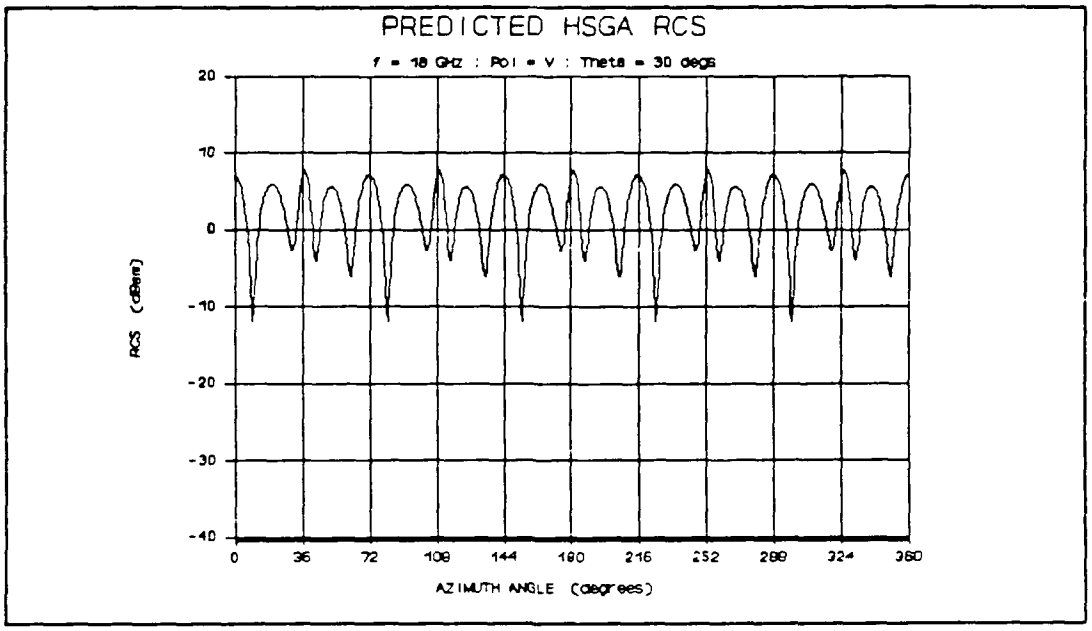

Figure 6.1 Predicted RCS of the Scaled Model Geodesic Array Obtained Using the Incorrect Corner Reflector Rotations (Vertical Polarization)

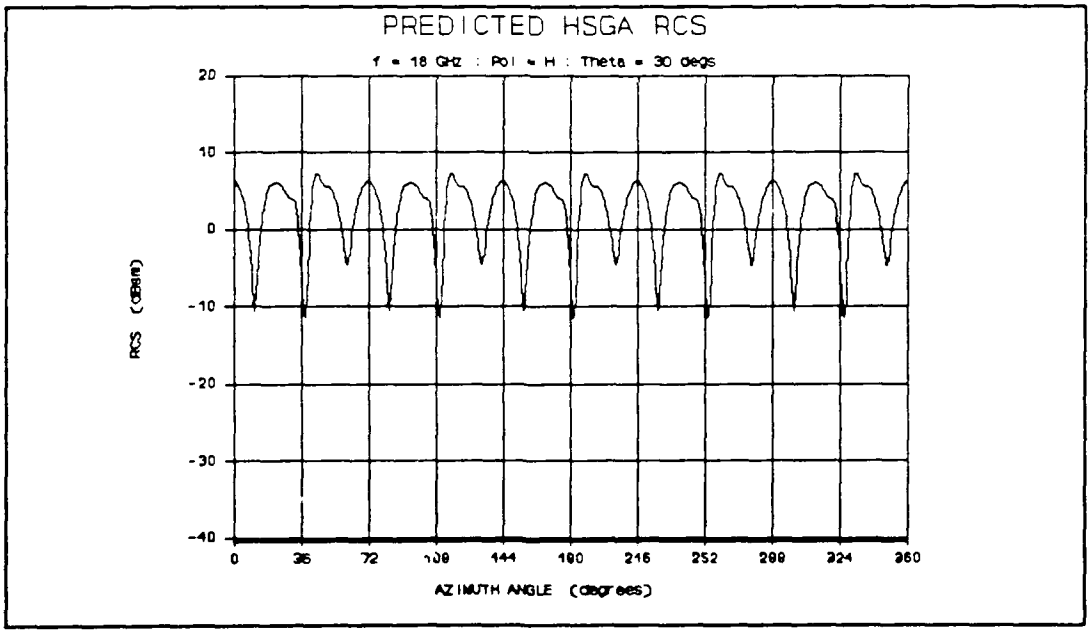

Figure 6.2 Predicted RCS of the Scaled Model Geodesic Array Obtained Using the Incorrect Corner Reflector Rotations (Horizontal Polarization)

VII. Conclusions and Recommendations

Review

The objective of this research effort was to investigate the EM scattering of the Geodesic Array. The problem statement identified the need to quantitatively measure and predict the scattering properties of the Geodesic Array and the need to assess the relative performance of the Geodesic Array.

The radar cross section (RCS) was chosen as the means of investigating the EM scattering of a scaled model version of Geodesic Array. In order to gather as much spatial scattering information as possible, a unique target support mount was designed, constructed, and used to measure the conical cut RCS patterns. The RCS of the individual components of the Geodesic Array (i.e. the single corner reflectors), the RCS of a eight corner reflector array, and the RCS of the Geodesic Array were measured using the CW nulling RCS measurement technique. A comparative analysis between the measured RCS of the Geodesic Array and the measured RCS of the eight corner reflector array was performed. The approach of starting with an existing RCS prediction model and then modifying to model to allow the prediction of the RCS of the Geodesic Array was attempted.

Conclusions

The conical cut RCS pattern measurements provided a large amount of spatial coverage information for the targets examined in this research effort and as such were very useful in characterizing the radar return from the targets.

The CW nulling RCS measurement technique combined with the conical cut mounting structure and RAM enclosure proved to be a successful method of obtaining the required conical cut RCS patterns. The conical cut target mounting structure designed, constructed, and used during the measurements adequately fulfilled the purpose of rotating the targets about the non-vertical rotation axis.

Without a specific application being stated for the use of a large radar return target, it is difficult to assess what an acceptable spatial coverage of the target should be. The large amount of spatial coverage RCS results for the scaled model Geodesic Array presented in this document is intended to provide a comprehensive set of information which can be used to evaluate the usefulness of the Geodesic Array during any subsequent consideration of the array for a specific application. The data distribution plots generated from the RCS measurement data can serve as a useful tool for assessing the relative spatial coverage of the Geodesic Array.

Under the restrictions of the criteria selected for the assessment, the comparative analysis using the data distribution plots, found that for all but one of the elevation angles examined, the measured spatial RCS coverage for the Geodesic Array was equal to or better than that for the array of eight corner reflectors. This stated result was dependent on the minimum acceptable RCS level established during the analysis, however the data distribution plots allow the interested reader to set their on criteria and perform their own judgement. Regardless of the criteria chosen, the spatial coverage of the Geodesic Array was found to be superior to the coverage afforded by the array of eight corner reflectors for the elevation angles of 75° and elevation angles $\leq$ 30°.

The approach taken in predicting the RCS of the Geodesic Array is believed to be appropriate for large RCS targets comprised on multiple corner reflectors. The RCS predictions of the CLUSTR computer model and the modified version for the PC (CL.FOR) agreed reasonably well with the single corner reflector and eight corner reflector array RCS measurements. The computer model was successfully modified to allow the simulation of the Geodesic Array through the rotation and translation of each of the twenty individual corner reflectors of the array. Due to time constraints,

the final resolution of the appropriate rotation angles required for this simulation was not accomplished.

The overall conclusion of this research effort was that the Geodesic Array is a viable target for the purpose of providing a large radar return over a large number of aspect angles.

Recommendations

1. Complete the modification of the PC version simulation model and compare the prediction results to the measured results obtained during this thesis.
2. Provided the first recommendation is accomplished, subsequently modify the model to allow the prediction of an operational size Geodesic Array.
3. Compare the results presented in this document to corresponding results of other targets designed for the purpose of providing a large RCS over a wide range of aspect angles.
4. Based on the results of the above recommendations, decide if field testing of a full scale version of the Geodesic Array is warranted.

APPENDIX A: Equipment Listing

This appendix contains a listing of all the equipment used to perform the RCS measurements. The equipment listing is organized by the subsystems discussed in Chapter III. The equipment manufacturer, equipment model number, and equipment serial number is included for each item.

Transmit Subsystem

Synthesized Sweep Oscillator (Signal Source)

Manufacturer : Hewlett Packard
Model Number : HP - 8340A
Serial Number: 2430A00661

Power Amplifier

Manufacturer : Hewlett Packard
Model Number : HP - 8349A
Serial Number: 2441A00498

Transmit Antennas

Manufacturer : Scientific Atlanta

2.60 to 3.95 GHz

Model Number : 12 - 2.6
Serial Number: 4488 BH

3.95 to 5.85 GHz

Model Number : 12 - 3.9
Serial Number: 3827 BF

8.20 to 12.0 GHz

Model Number : 12 - 8.2
Serial Number: 4061 BG

12.0 to 18.0 GHz

Model Number : 12 - 12
Serial Number: 4651 BH

Receive Subsystem

Receive Antennas

Manufacturer : Scientific Atlanta

2.60 to 3.95 GHz

Model Number : 12 - 2.6
Serial Number: 4489 BH

3.95 to 5.85 GHz

Model Number : 12 - 3.9
Serial Number: 3830 BF

8.20 to 12.0 GHz

Model Number : 12 - 8.2
Serial Number: 4062 BG

12.0 to 18.0 GHz

Model Number : 12 - 12
Serial Number: 4650 BH

Harmonic Mixer # 1 and # 2

Manufacturer : Scientific Atlanta
Model Number : 14 - 5
Serial Number: 1384 and 1391

Phase Amplitude Receiver

Manufacturer : Scientific Atlanta
Model Number : 1783
Serial Number: 252 and 4215

CW Nulling Subsystem

DC Power Supply # 1

Manufacturer : Hewlett Packard
Model Number : HP - 6284A
Serial Number: 1931A-06039

DC Power Supply # 2

Manufacturer : Hewlett Packard
Model Number : HP - 6205C
Serial Number: 2411A-09179

DC Power Supply # 3

Manufacturer : Hewlett Packard
Model Number : HP - 6289A
Serial Number: 1931A-05424

RF Couplers # 1 and # 2

Manufacturer : Omni-Spectra
Model Number : 2026-6006-20
Serial Number: N/A

RF Coupler # 3

Manufacturer : Narda
Model Number : 322-16
Serial Number: N/A

Variable Attenuators # 1 and # 2

Manufacturer : ARRA
Model Number : 8752-35D
Serial Number: 556 and 557

Phase Adjuster

Manufacturer : ARRA
Model Number : 9428A
Serial Number: 6244

Isolation Filters

Manufacturer : Innowave

2 to 4 GHz

Model Number : 1030HQ
Serial Number: 52

3 to 6 GHz

Model Number : 1045HQ
Serial Number: 52

6 to 12 GHz

Model Number : 1090HQ
Serial Number: 52

12 to 18 GHz

Model Number : 1145HQ
Serial Number: 52

Oscilloscope

Manufacturer : Textronic
Model Number : 485
Serial Number: B192528

Multimeter

Manufacturer : Hewlett Packard
Model Number : HP - 3478A
Serial Number: 2619A48851

HBIP Interface Subsystem

HP-IB Interface Extenders # 1 and # 2

Manufacturer : Hewlett Packard
Model Number : HP - 37203
Serial Number: 2325O10297 and 2325U13388

IEEE 488 Buss Strip

Manufacturer : ICS Electronic Corp.
Model Number : 4801
Serial Number: N/A

Data Collection and Monitoring Subsystem

HP Series 9000 computer # 1

Manufacturer : Hewlett Packard
Model Number : HP - 236
Serial Number: 2441A04644

External Hard Drive

Manufacturer : Hewlett Packard
Model Number : HP - 9133H
Serial Number: 2621A37273

General Purpose Buss Monitor

Manufacturer : ZIA Tech
Model Number : ZT - 488
Serial Number: N/A

Multimeter

Manufacturer : Hewlett Packard
Model Number : HP - 3478A
Serial Number: 2619A48856

Data Processing Subsystem

HP Data Printing and Plotting

HP Printer

Manufacturer : Hewlett Packard
Model Number : HP - 9876A
Serial Number: 1834A08642

HP Series 9000 computer # 2

Manufacturer : Hewlett Packard
Model Number : HP - 236
Serial Number: 2143A00601

HP Plotter

Manufacturer : Hewlett Packard
Model Number : HP - 7470A
Serial Number: 2210411809

ASCII Data Transfer and Processing

RS 232 Serial Interface Card

Manufacturer : Hewlett Packard
Model Number : HP - 98626A
Serial Number: 2210411809

Null Modem

Manufacturer : GC Electronics
Model Number : 43 - 105
Serial Number: N/A

PC Computer

Manufacturer : Everex
Model Number : EXO - 2802A - 00+
Serial Number: 25G03-849-22582

PC Monitor

Manufacturer : NEC Corp
Model Number : JC1401P3A
Serial Number: 71C07582C

PC Keyboard

Manufacturer : Everex
Model Number : 2186035E
Serial Number: 00042752

PC "Pinwriter" Printer

Manufacturer : NEC Corp
Model Number : P 5200
Serial Number: 6030536658

Target Position Subsystem

"Pedestal Configuration" System

Target Position Controller

Manufacturer : Scientific Atlanta
Model Number : 4131
Serial Number: 1044697

Target Position Rotator

Manufacturer : Scientific Atlanta
Model Number : N/A
Serial Number: N/A

Ogive-Cylinder Shaped Target Support Pedestal

"Conical Cut Configuration" System

Target Position Controller

Manufacturer : Newport
Model Number : 855C
Serial Number: R8734

Target Position Rotator

Manufacturer : Newport
Model Number : 495
Serial Number: 336

Quickset Tripod Stand

Manufacturer : Quickset
Model Number : 4 - 62225 - A
Serial Number: 1086016

APPENDIX B: Pedestal Configuration RCS Measurement Results

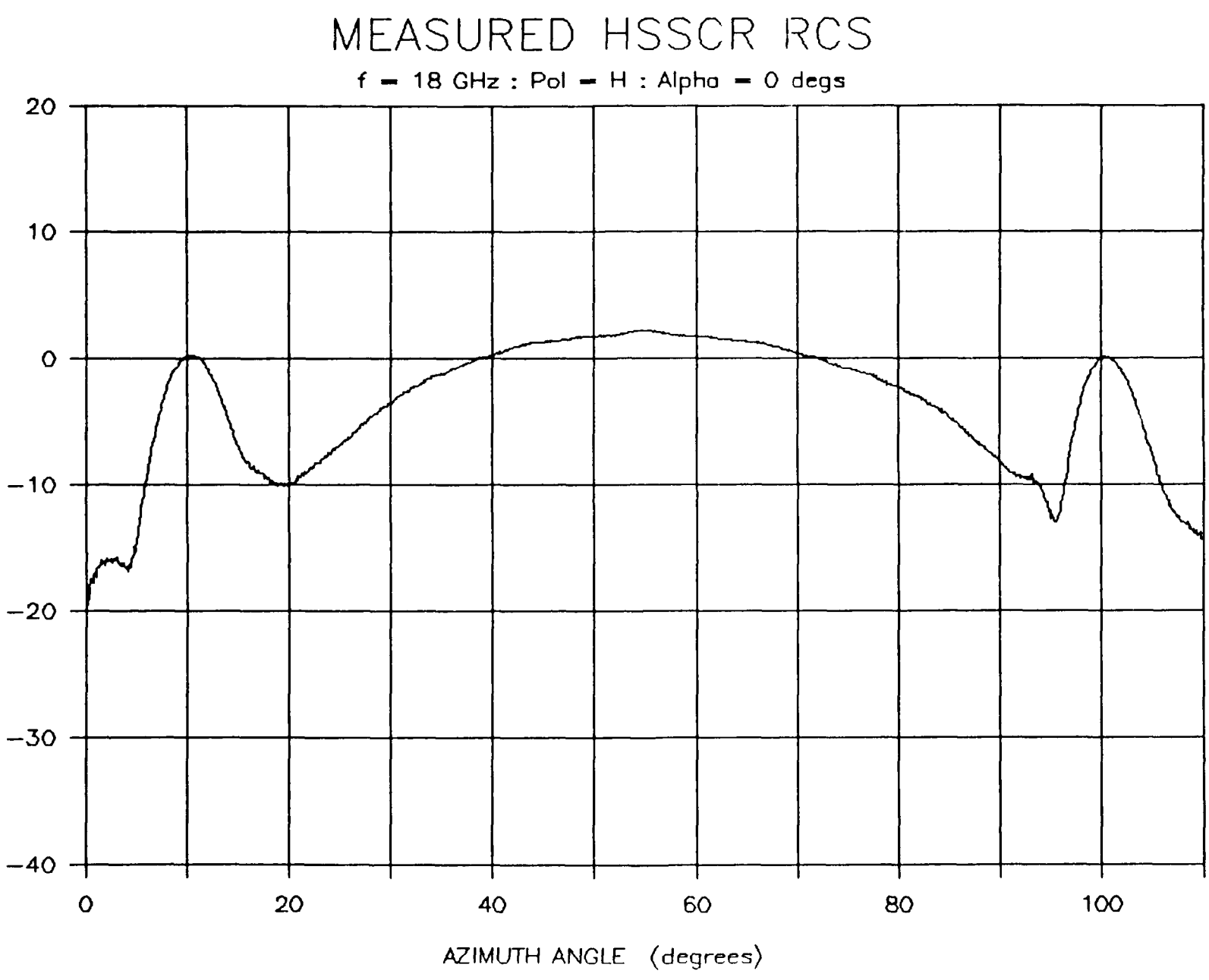

Figure B.1 Measured RCS: HSSCR, Great Circle Cut, 18 GHz, Alpha of 0 degs, Horz Pol

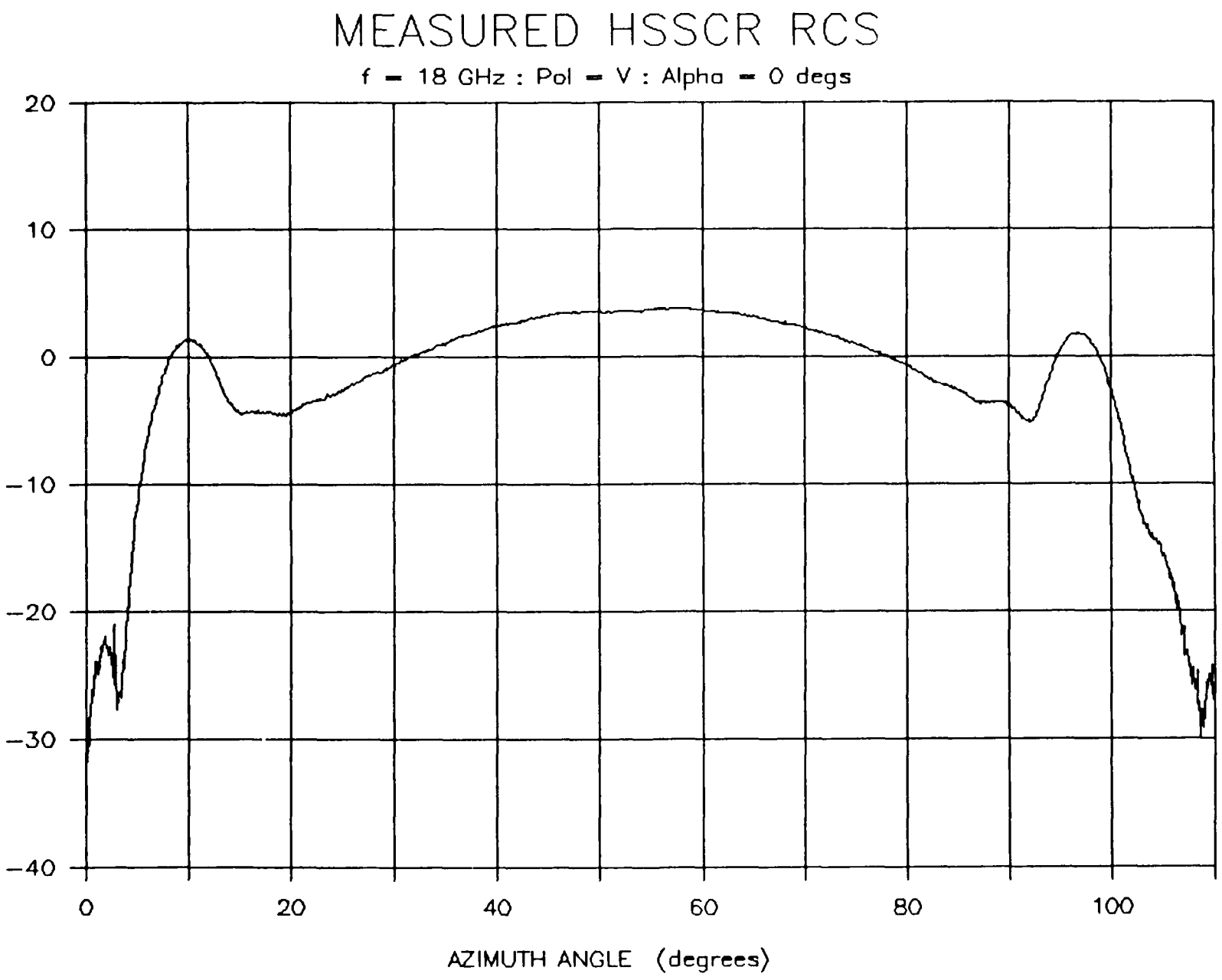

Figure B.2 Measured RCS: HSSCR, Great Circle Cut, 18 GHz, Alpha of 0 degs, Vert Pol

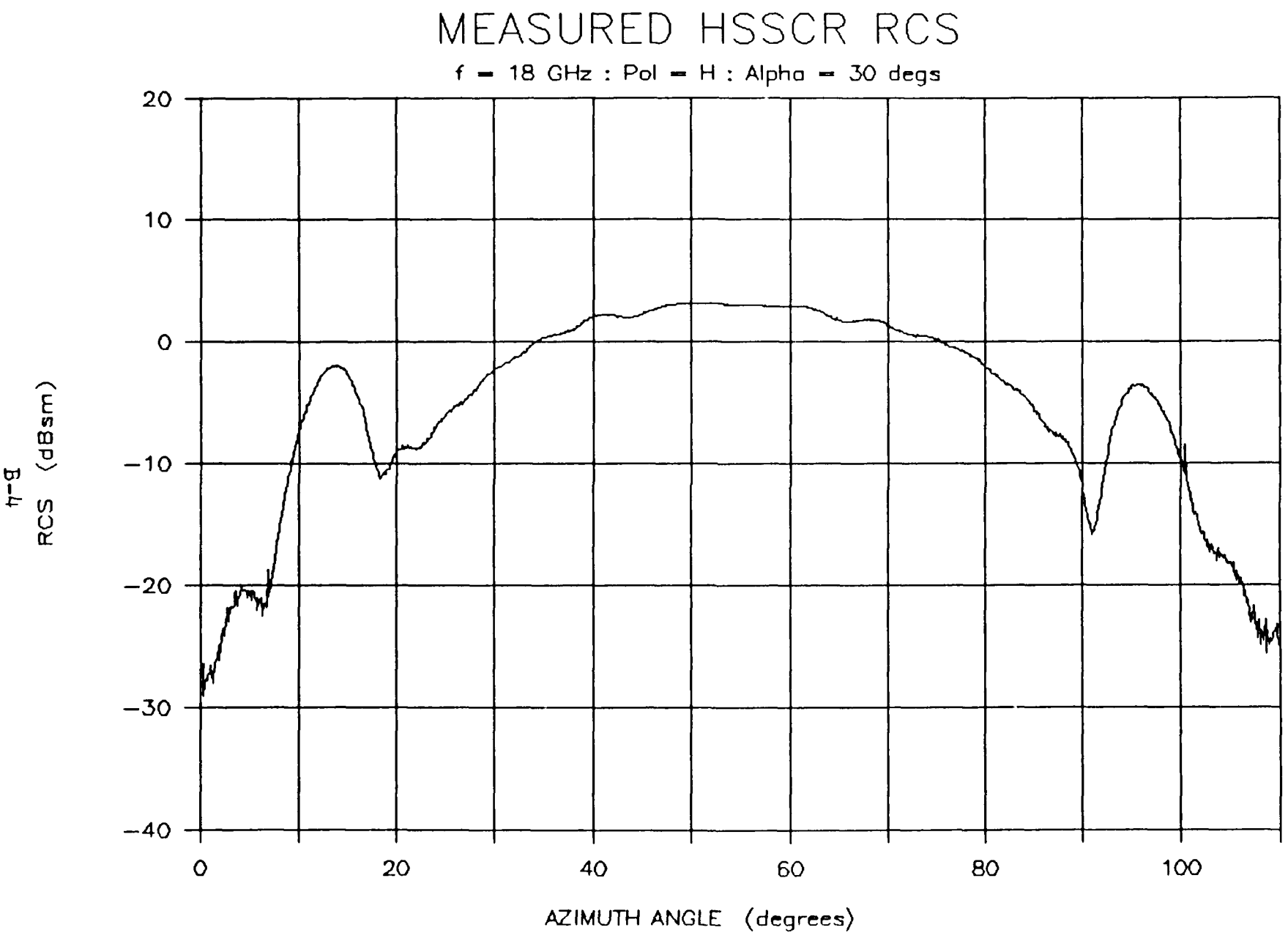

Figure B.3 Measured RCS: HSSCR, Great Circle Cut, 18 GHz, Alpha of 30 degs, Horz Pol

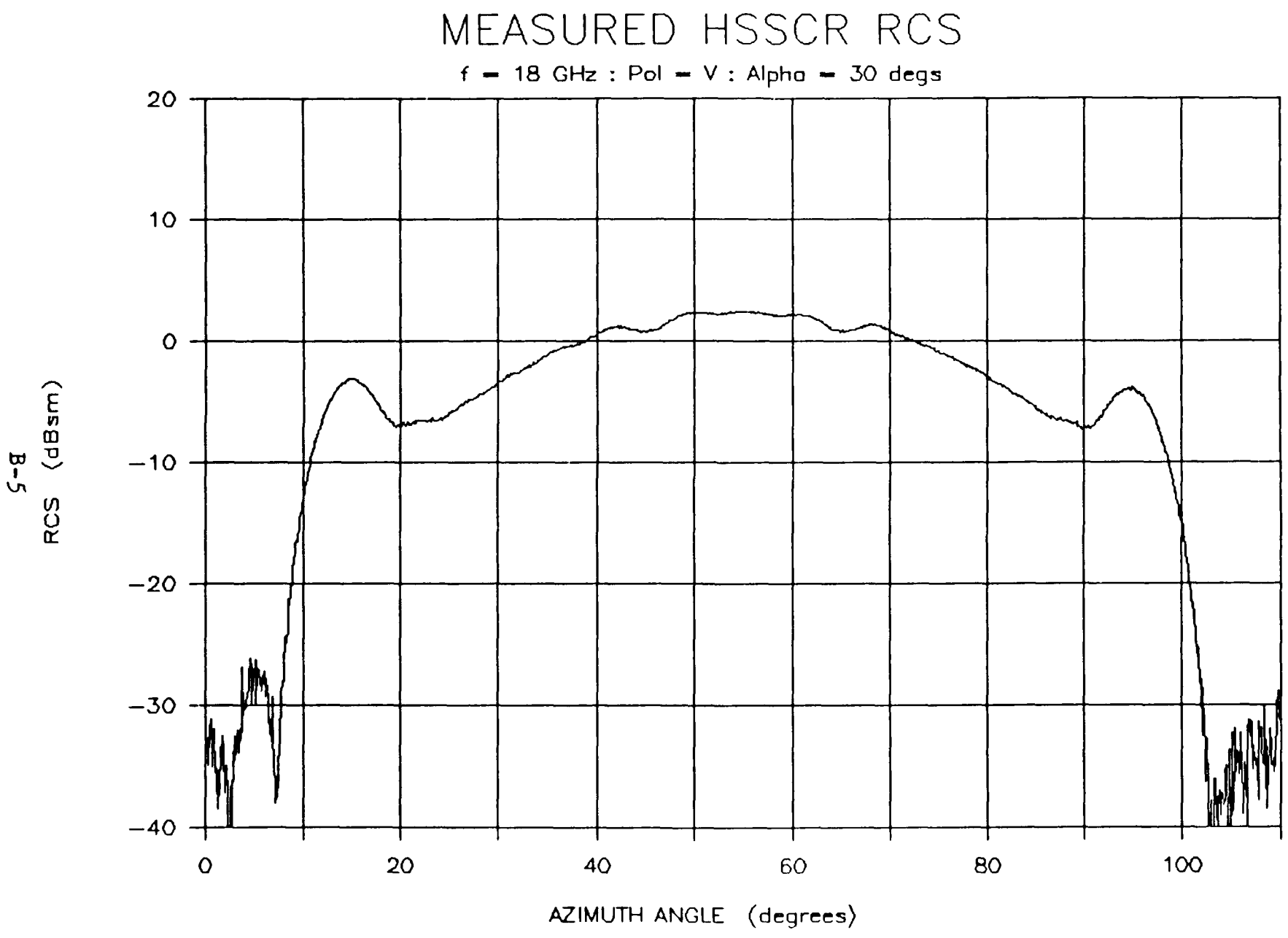

Figure B.4 Measured RCS: HSSCR, Great Circle Cut, 18 GHz, Alpha of 30 degs, Vert Pol

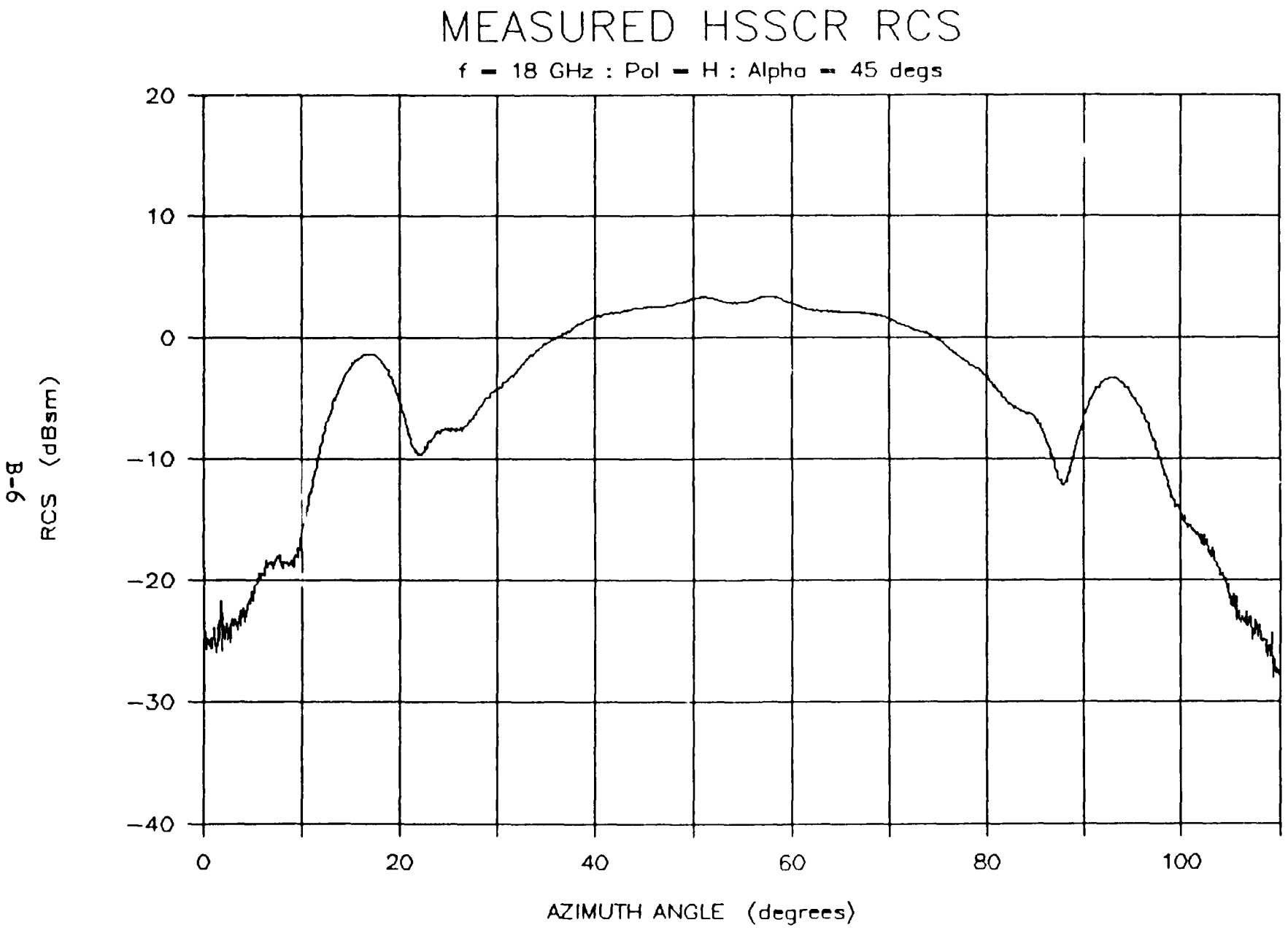

Figure B.5 Measured RCS: HSSCR, Great Circle Cut, 18 GHz, Alpha of 45 degs, Horz Pol

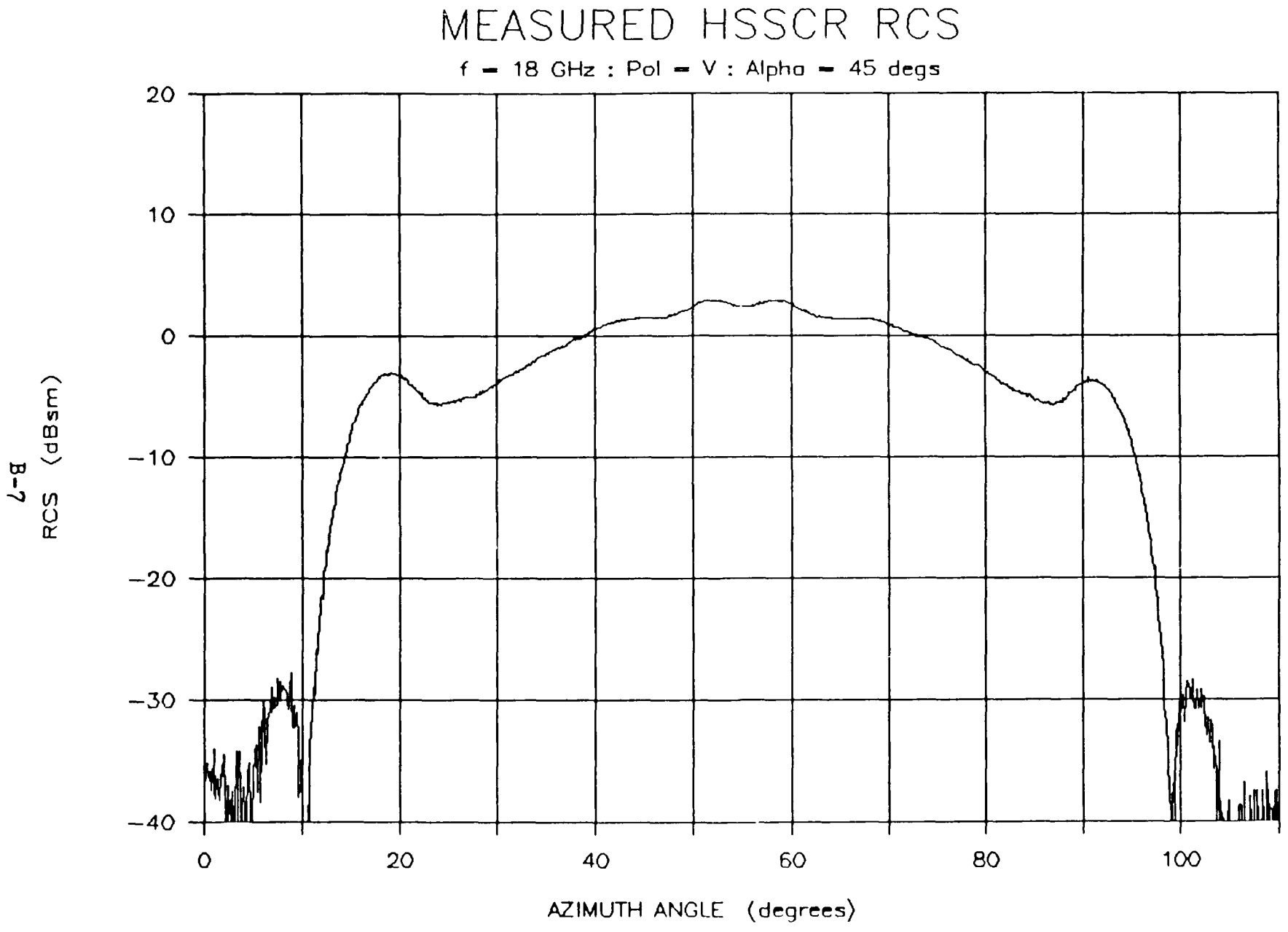

Figure B.6 Measured RCS: HSSCR, Great Circle Cut, 18 GHz, Alpha of 45 degs, Vert Pol

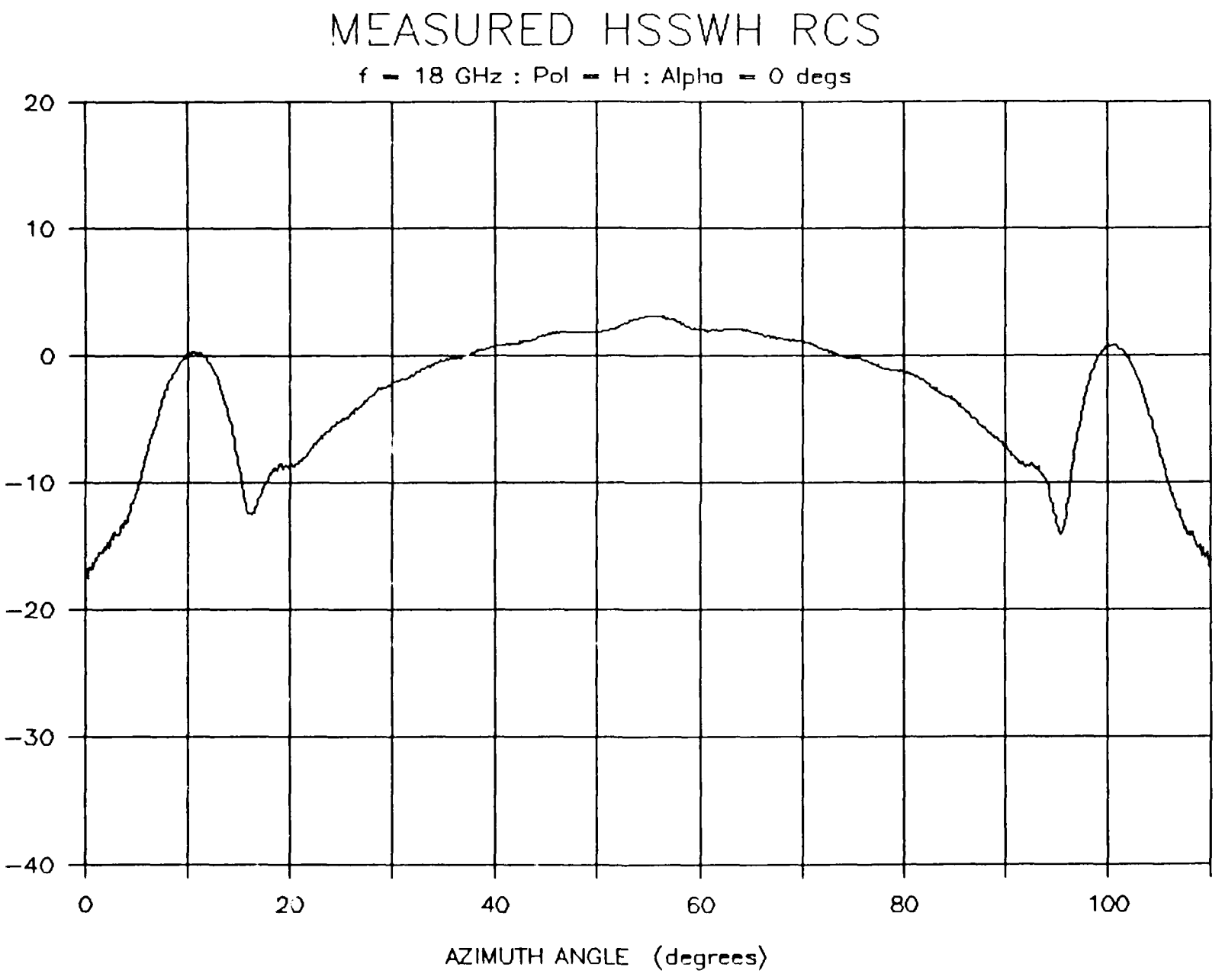

Figure B.7 Measured RCS: HSSWH, Great Circle Cut, 18 GHz, Alpha of 0 degs, Horz Pol

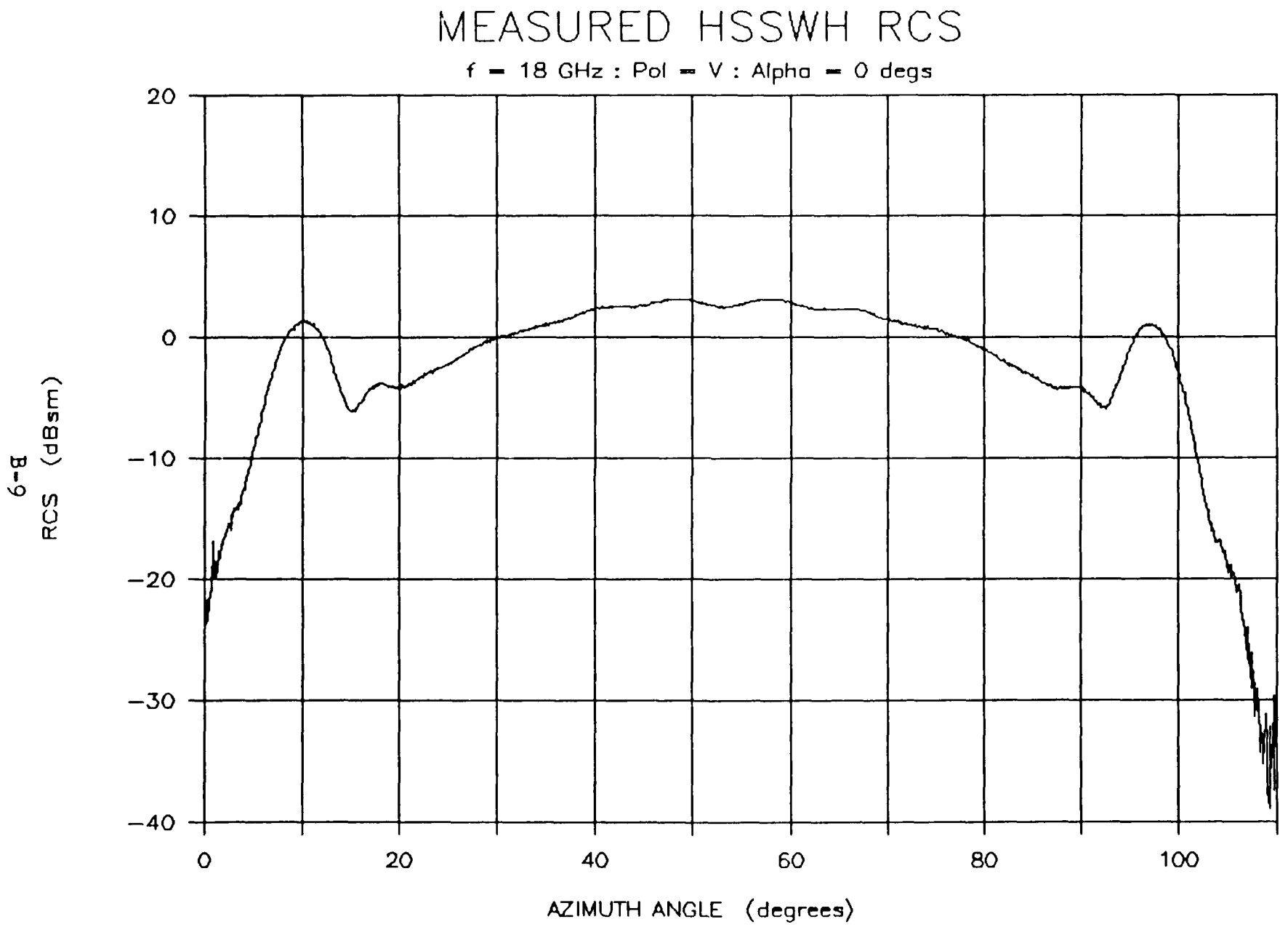

Figure B.8 Measured RCS: HSSWH, Great Circle Cut, 18 Ghz, Alpha of 0 degs, Vert Pol

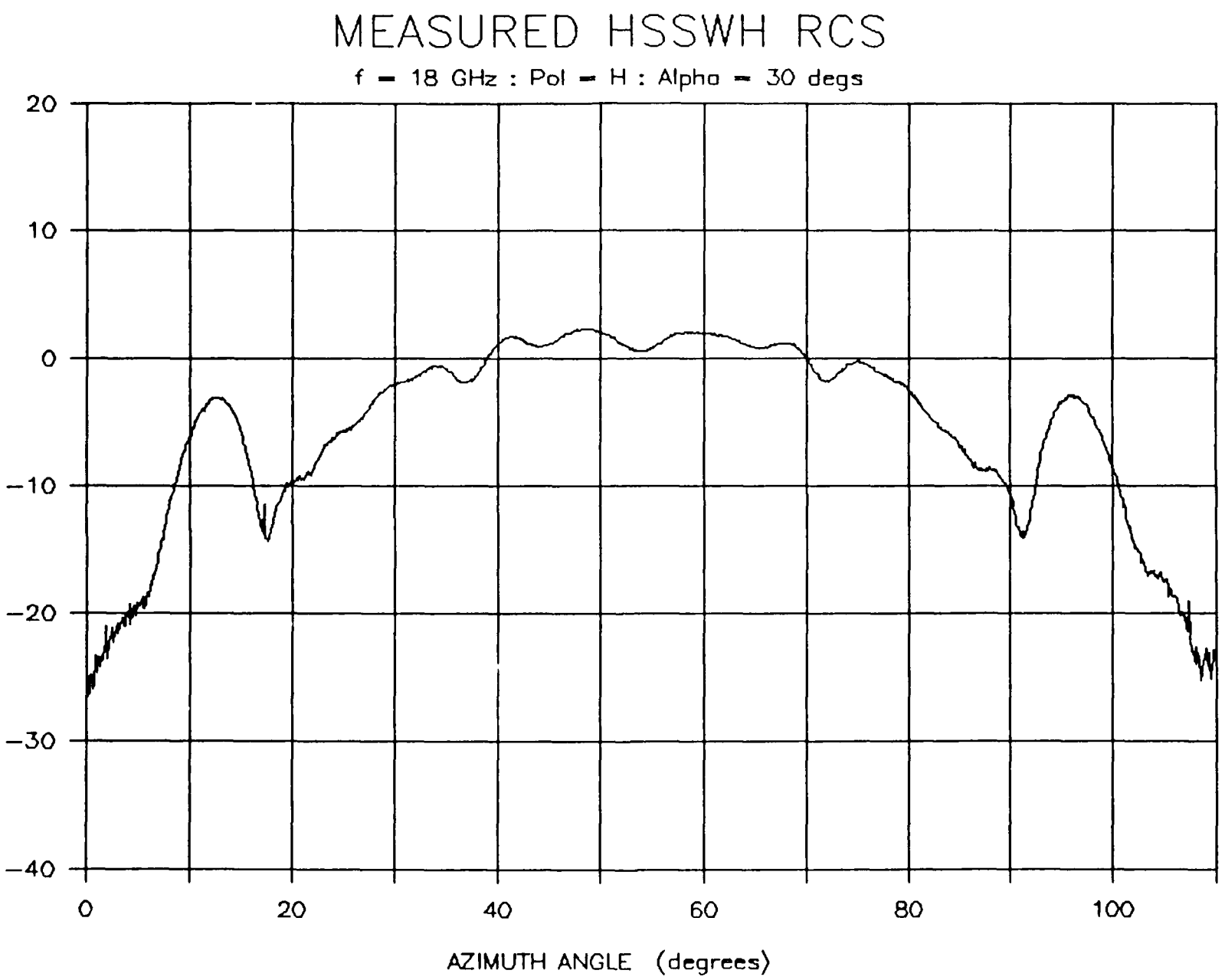

Figure B.9 Measured RCS: HSSWH, Great Circle Cut, 18 Ghz, Alpha of 30 degs, Horz Pol

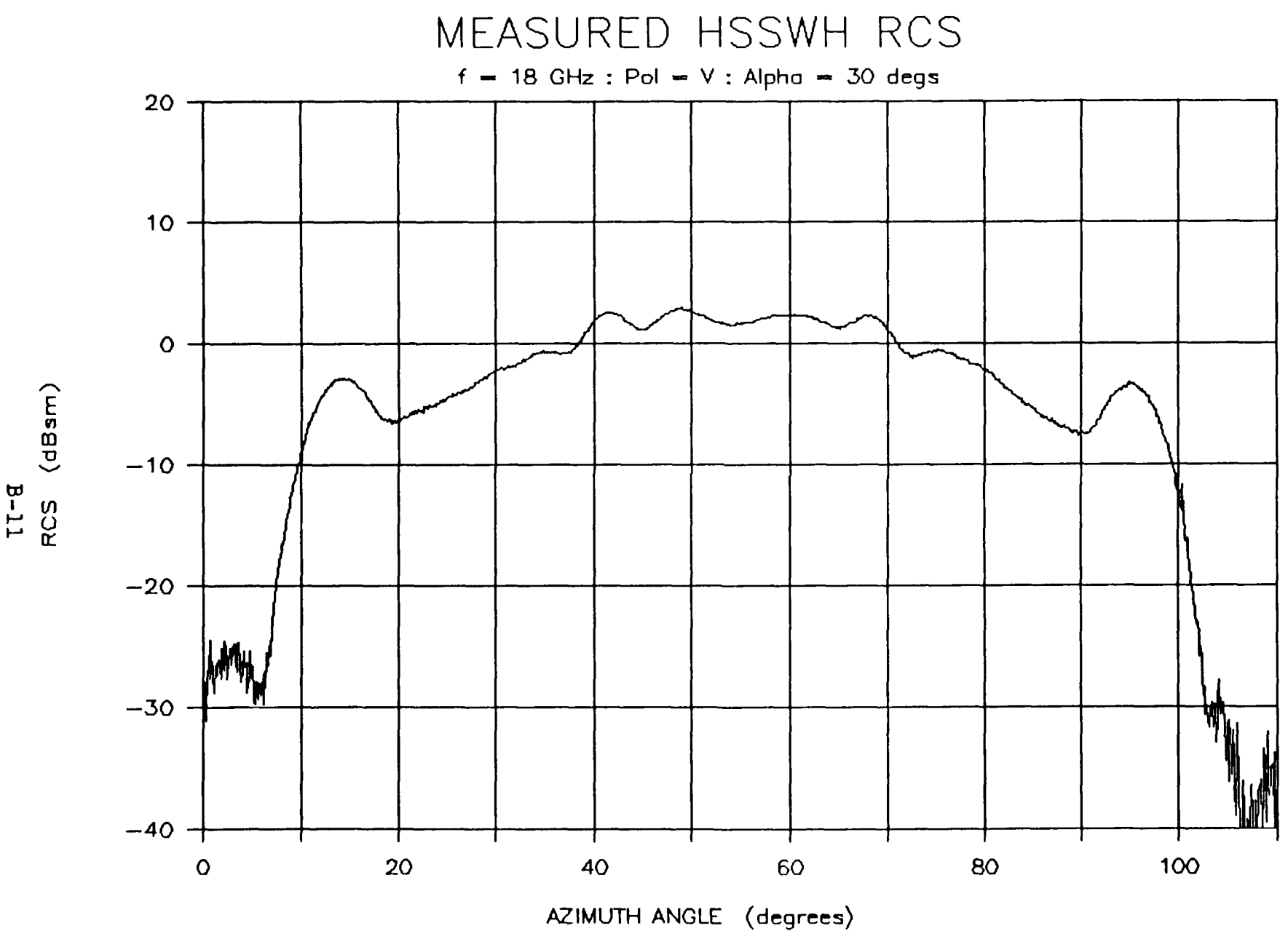

Figure B.10 Measured RCS: HSSWH, Great Circle Cut, 18 GHz, Alpha of 30 degs, Vert Pol

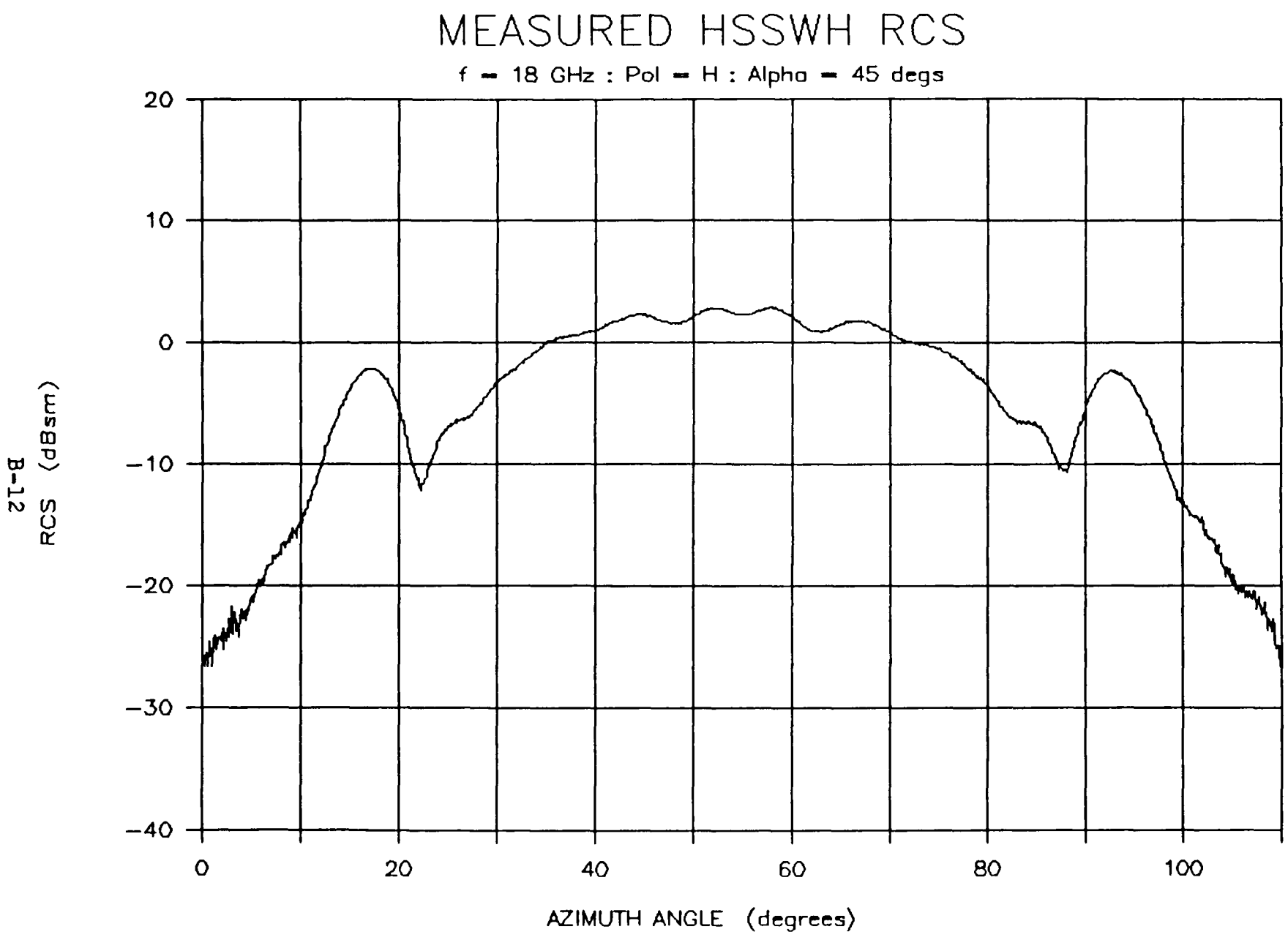

Figure B.11 Measured RCS: HSSWH, Great Circle Cut, 18 GHz, Alpha of 45 degs, Horz Pol

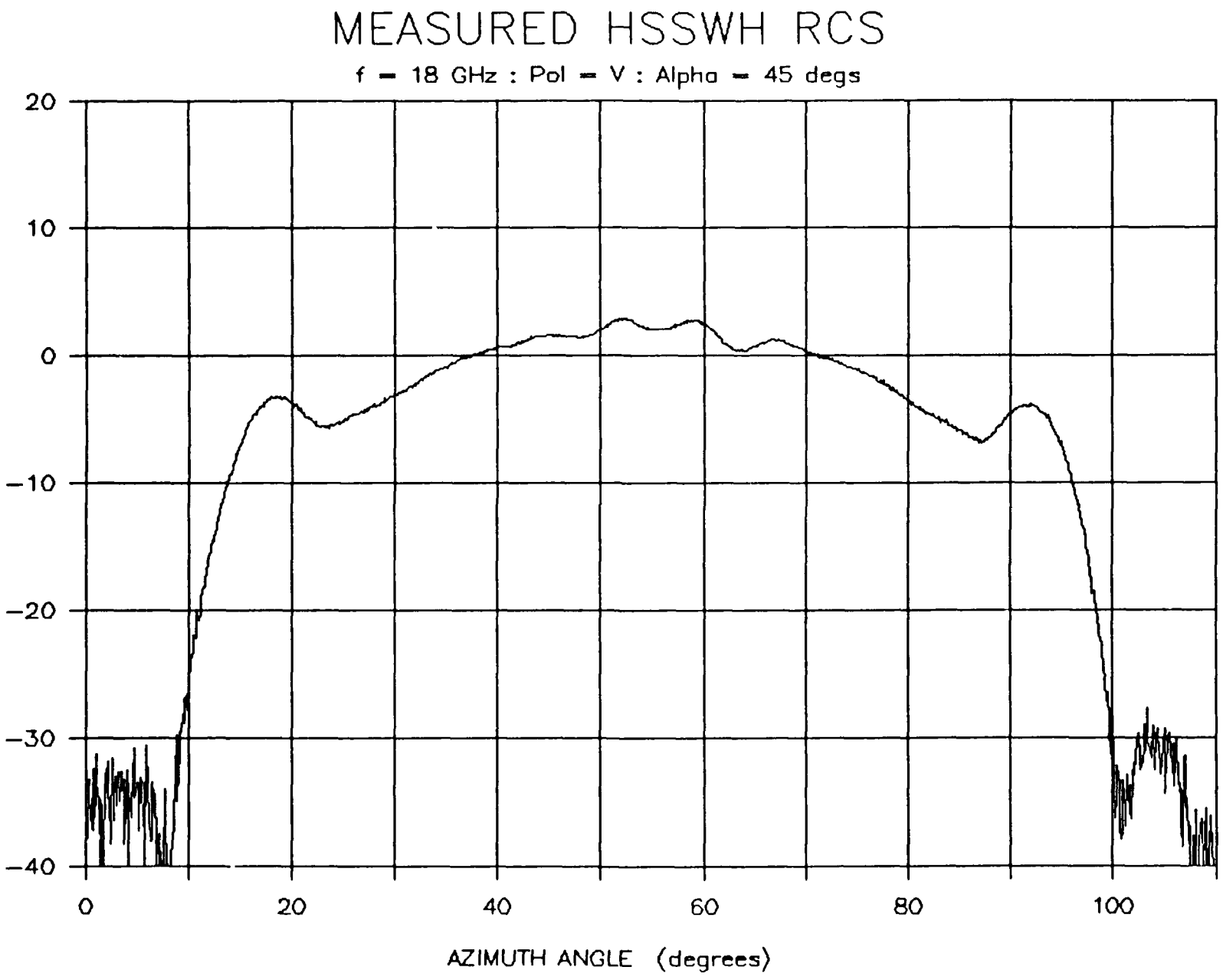

Figure B.12 Measured RCS: HSSWH, Great Circle Cut, 18 GHz, Alpha of 45 degs, Vert Pol

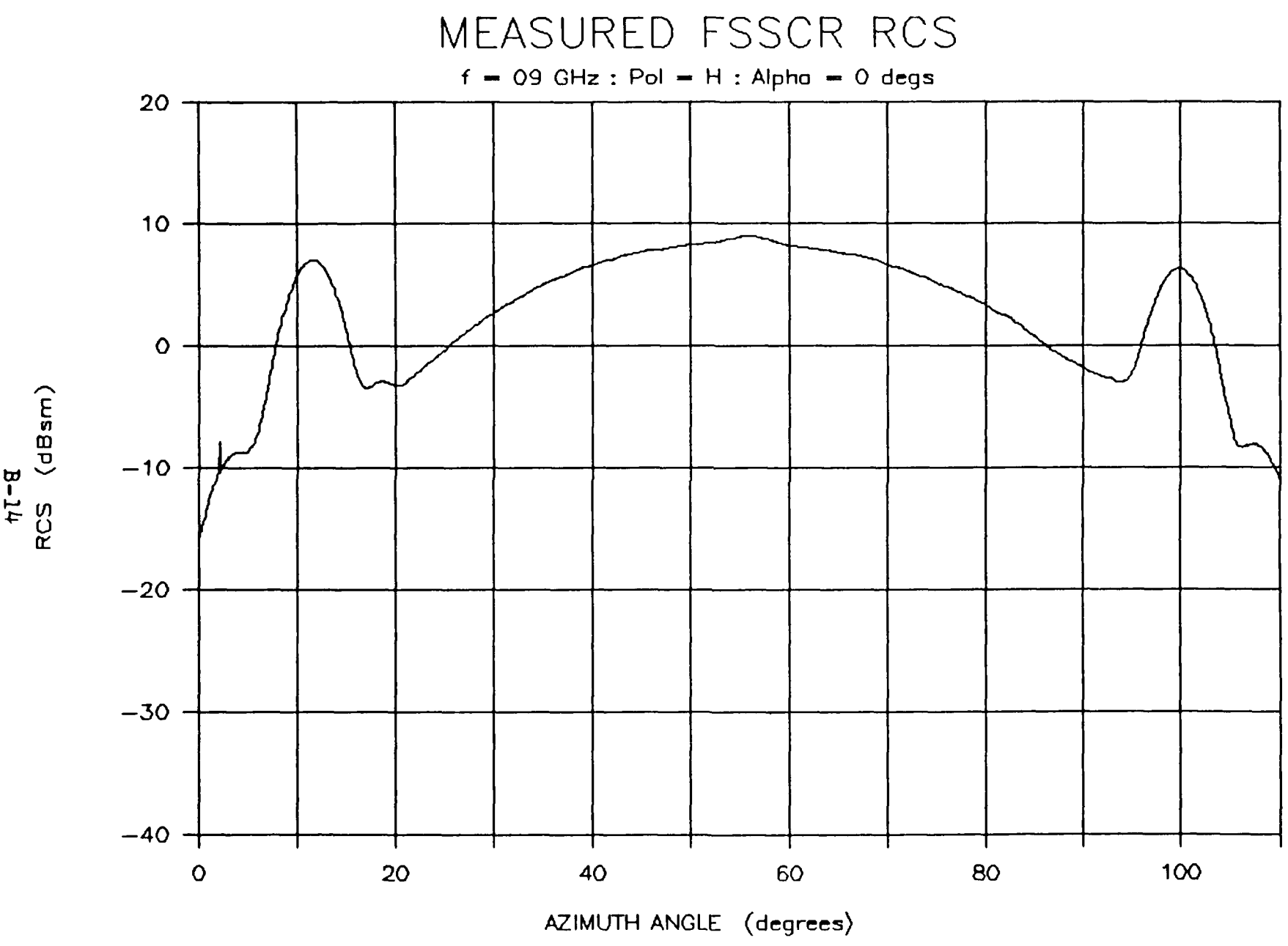

Figure B.13 Measured RCS: FSSCR, Great Circle Cut, 9 GHz, Alpha of 0 degs, Horz Pol

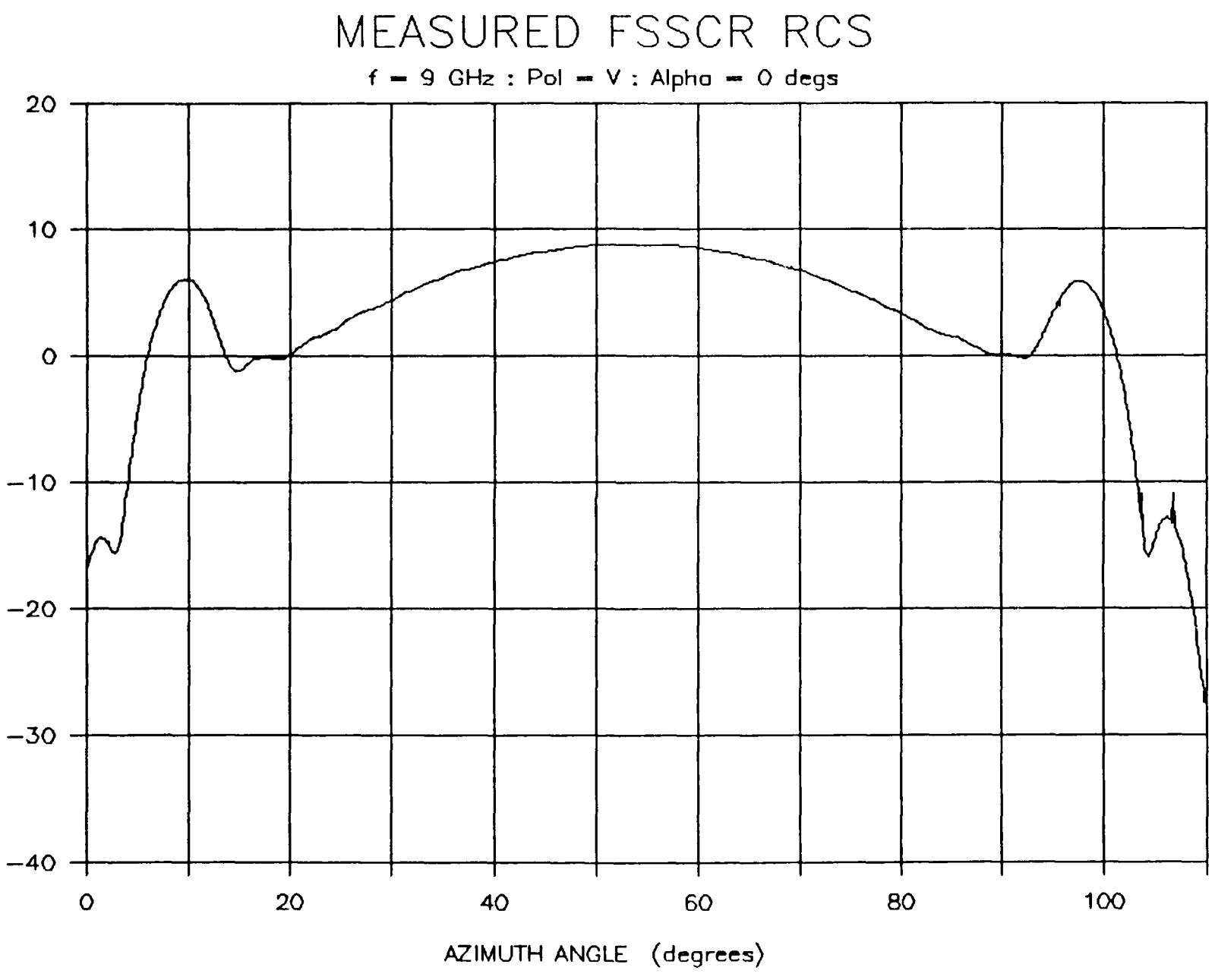

Figure B.14 Measured RCS: FSSCR, Great Circle Cut, 9 GHz, Alpha of 0 degs, Vert Pol

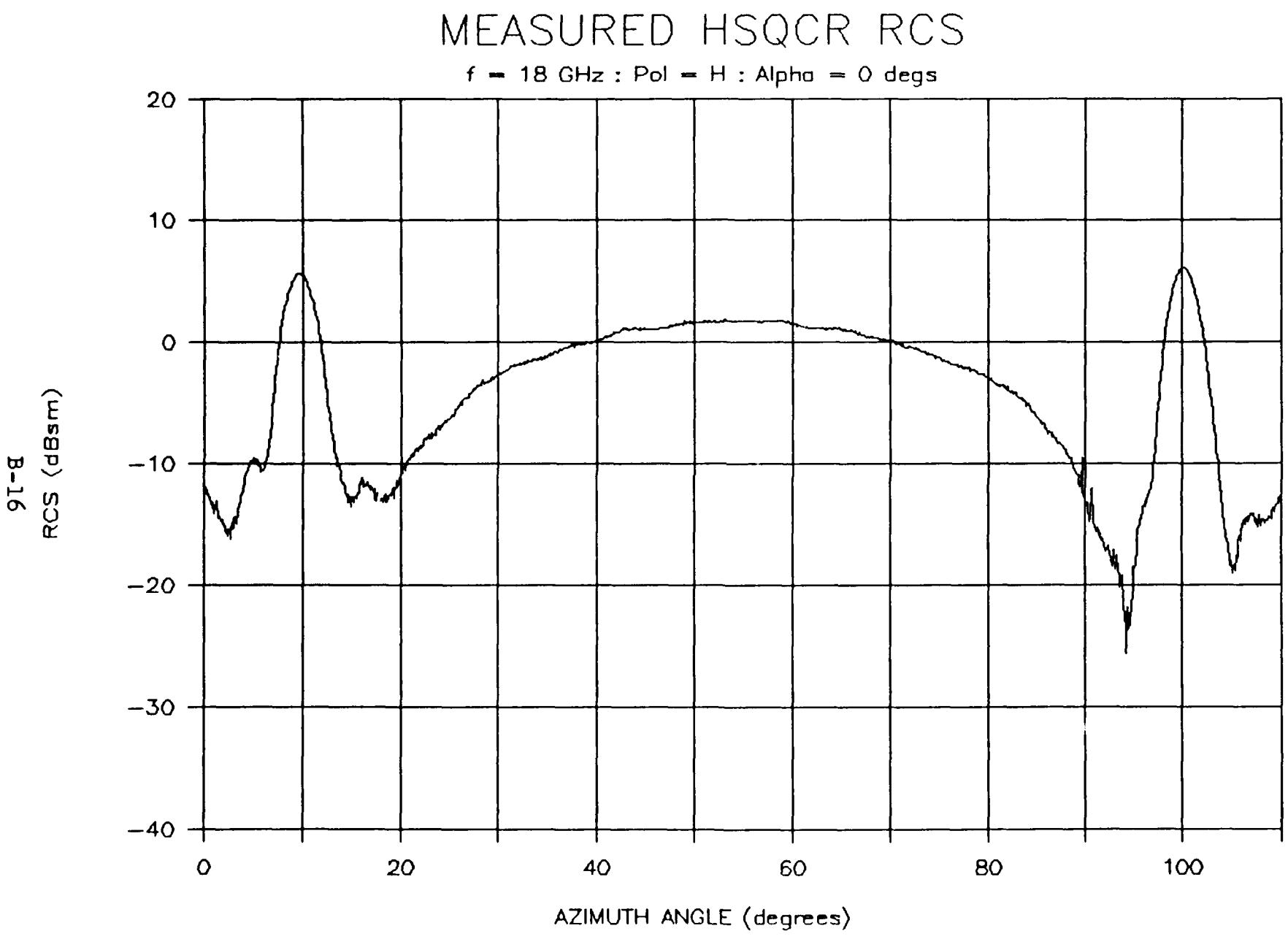

Figure B.15 Measured RCS: HSQCR, Great Circle Cut, 18 GHz, Alpha of 0 degs, Horz Pol

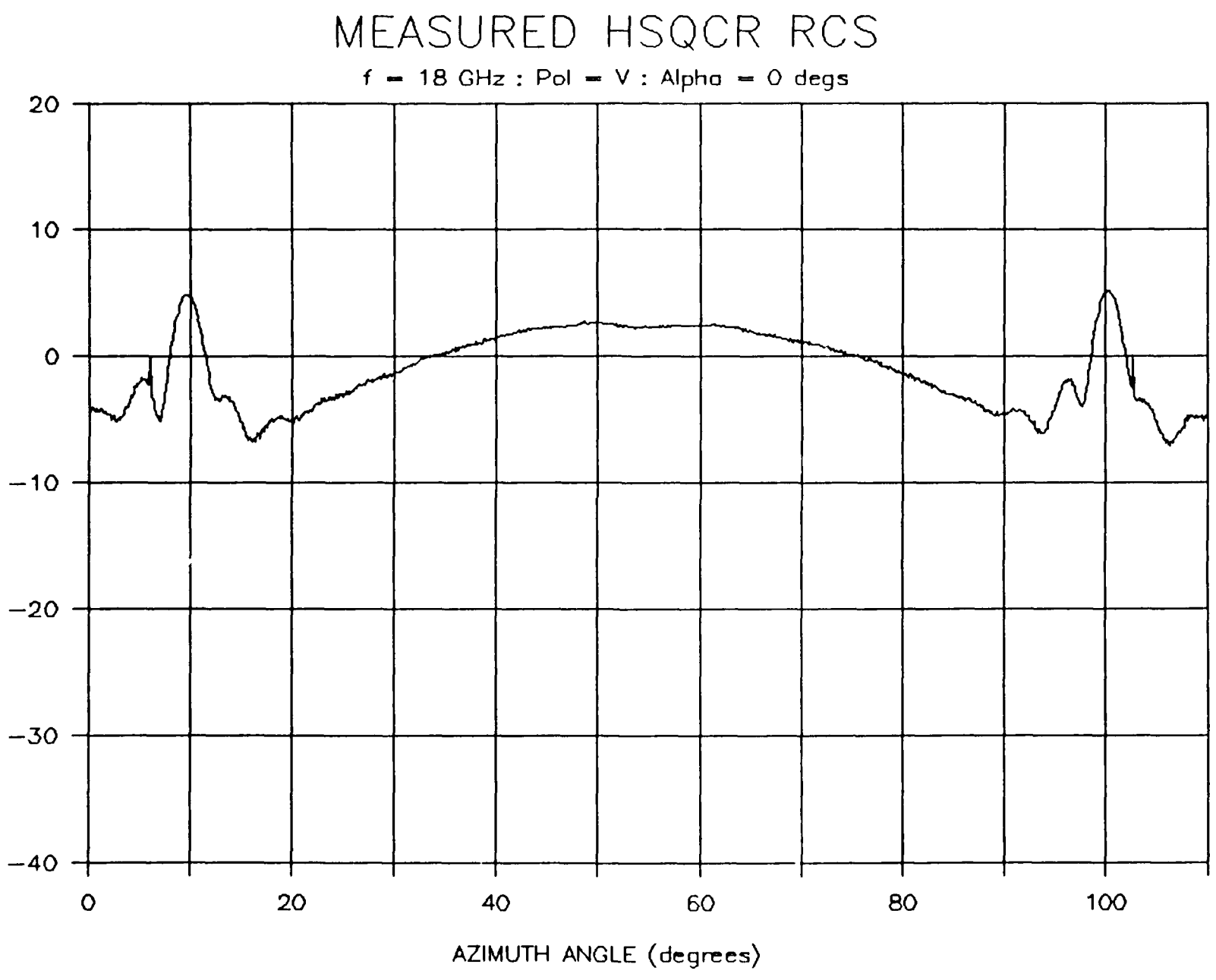

Figure B.16 Measured RCS: HSQCR, Great Circle Cut, 18 GHz, Alpha of 0 degs, Vert Pol

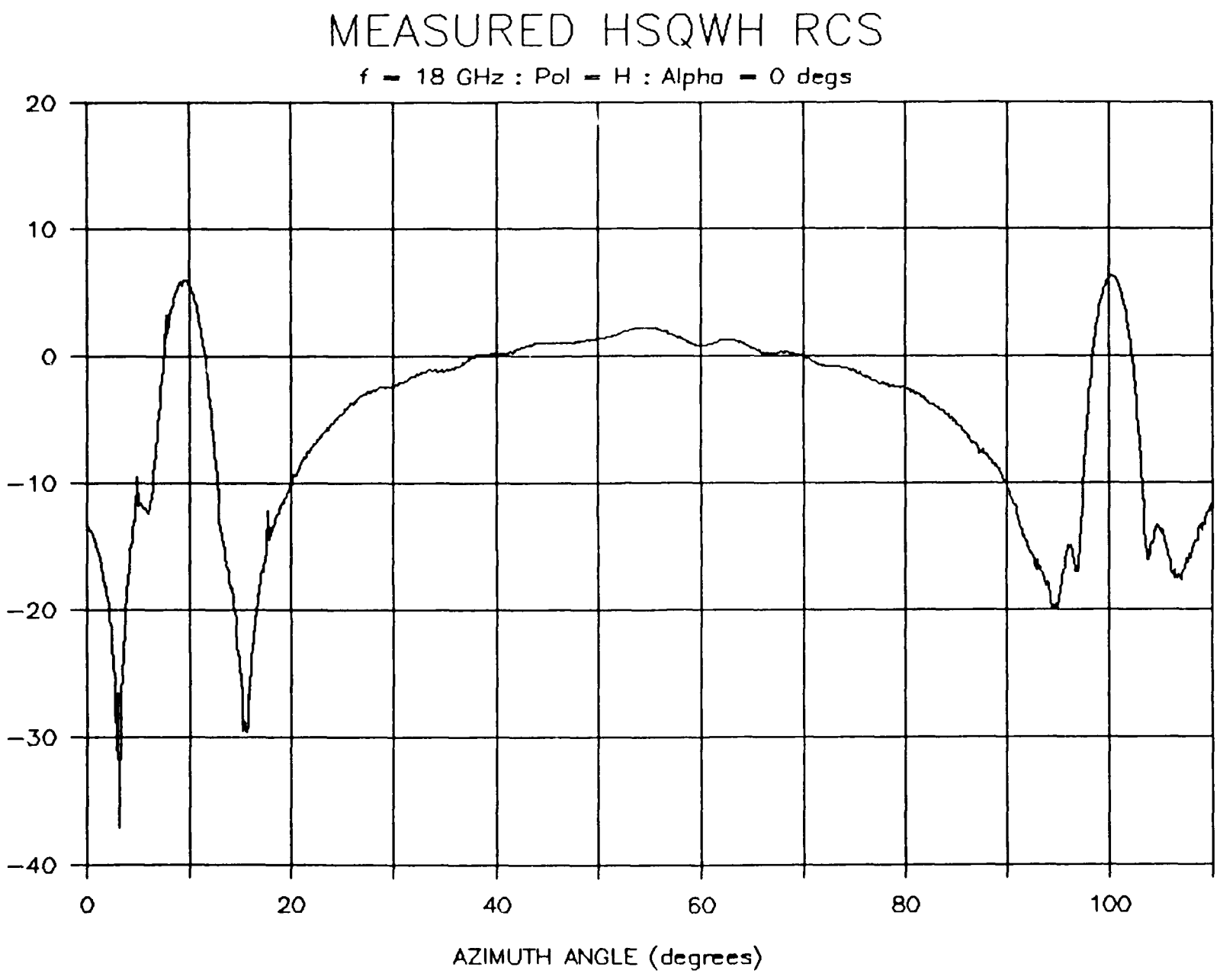

Figure B.17 Measured RCS: HSQWH, Great Circle Cut, 18 GHz, Alpha of 0 degs, Horz Pol

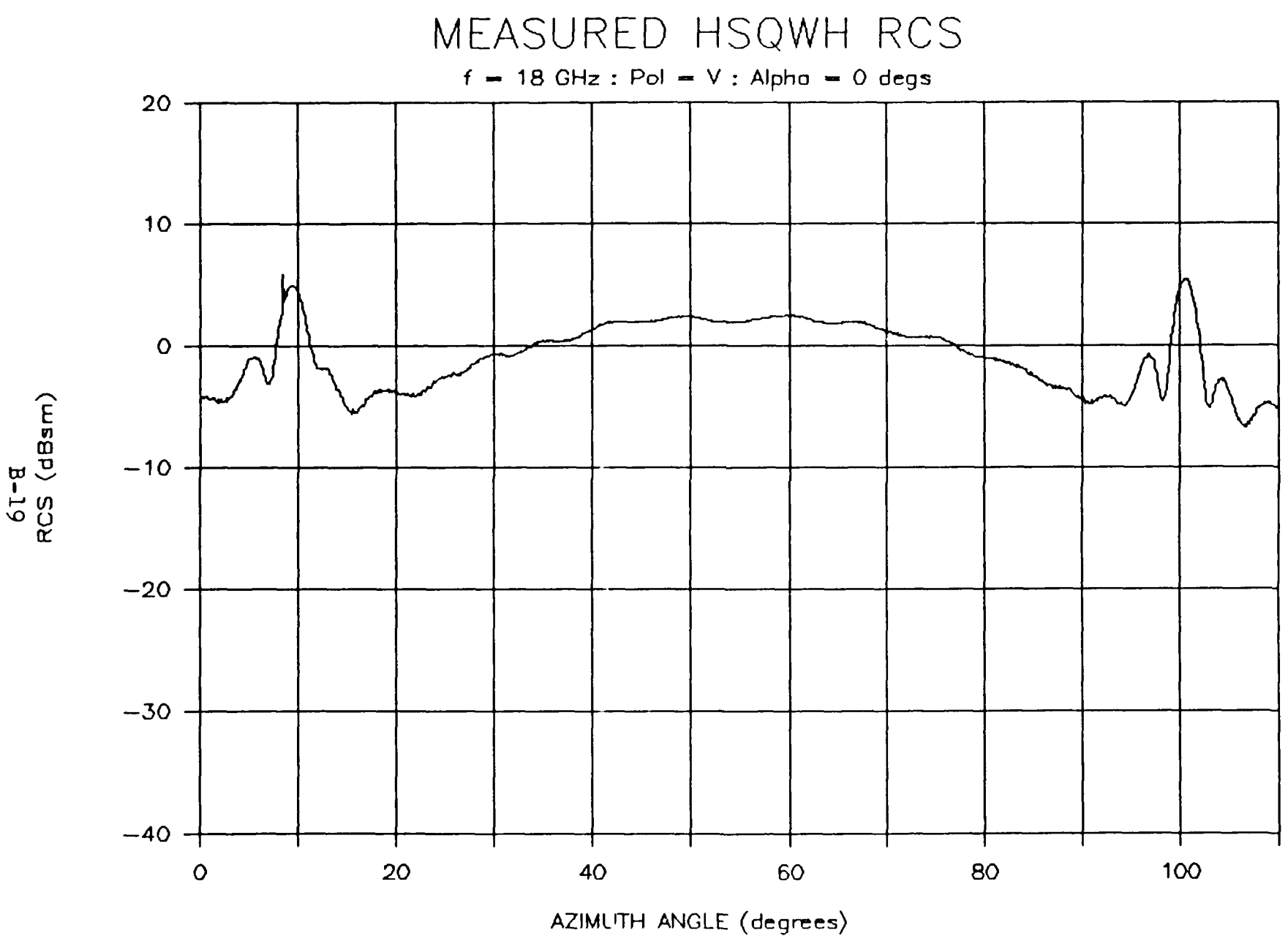

Figure B.18 Measured RCS: HSQWH, Great Circle Cut, 18 GHz, Alpha of 0 degs, Vert Pol

APPENDIX C: Single Corner Reflector Conical Cut RCS Measurement Results

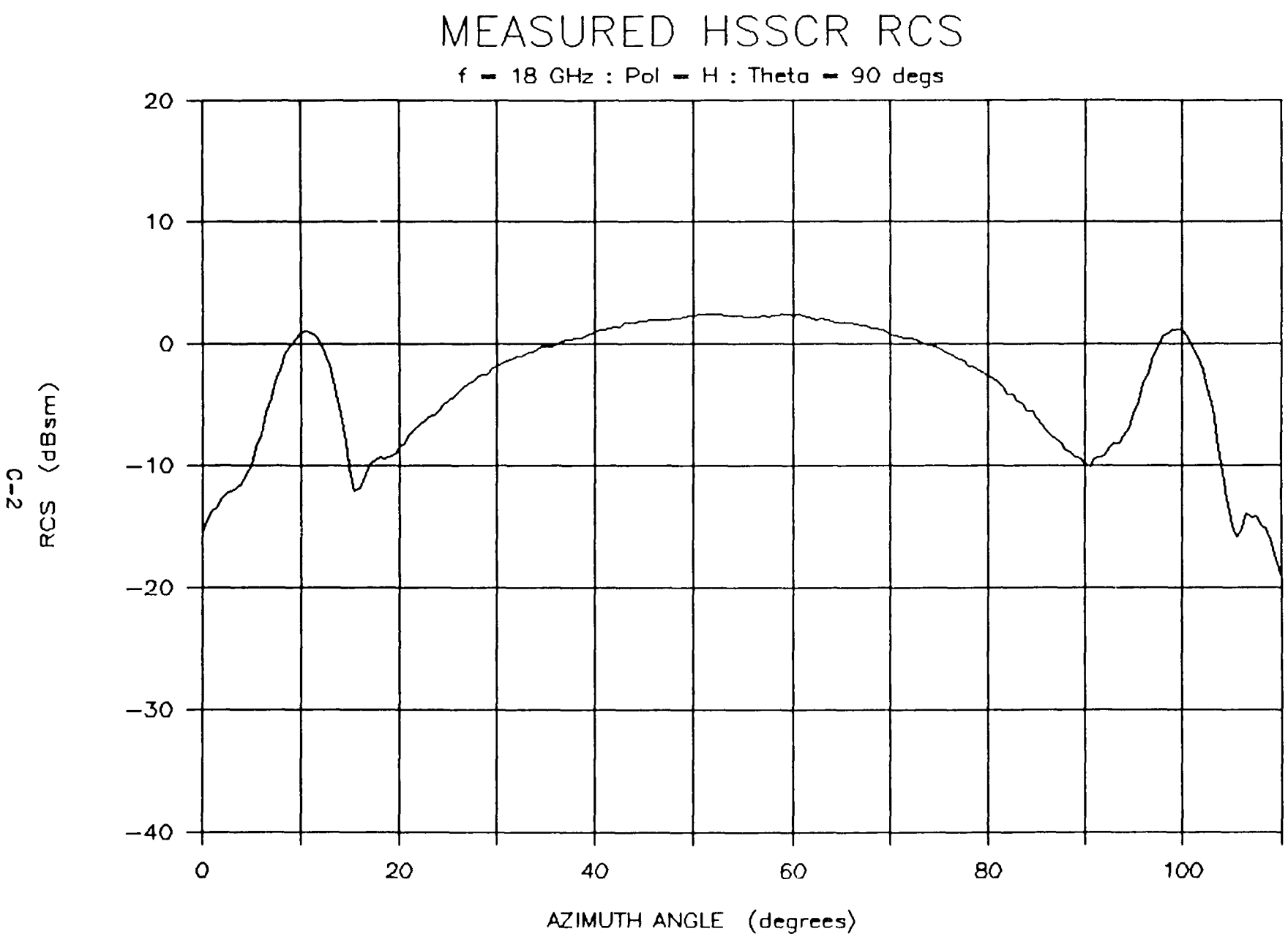

Figure C.1 Measured RCS: HSSCR, Conical Cut, 18 GHz, Theta of 90 degs, Horz Pol

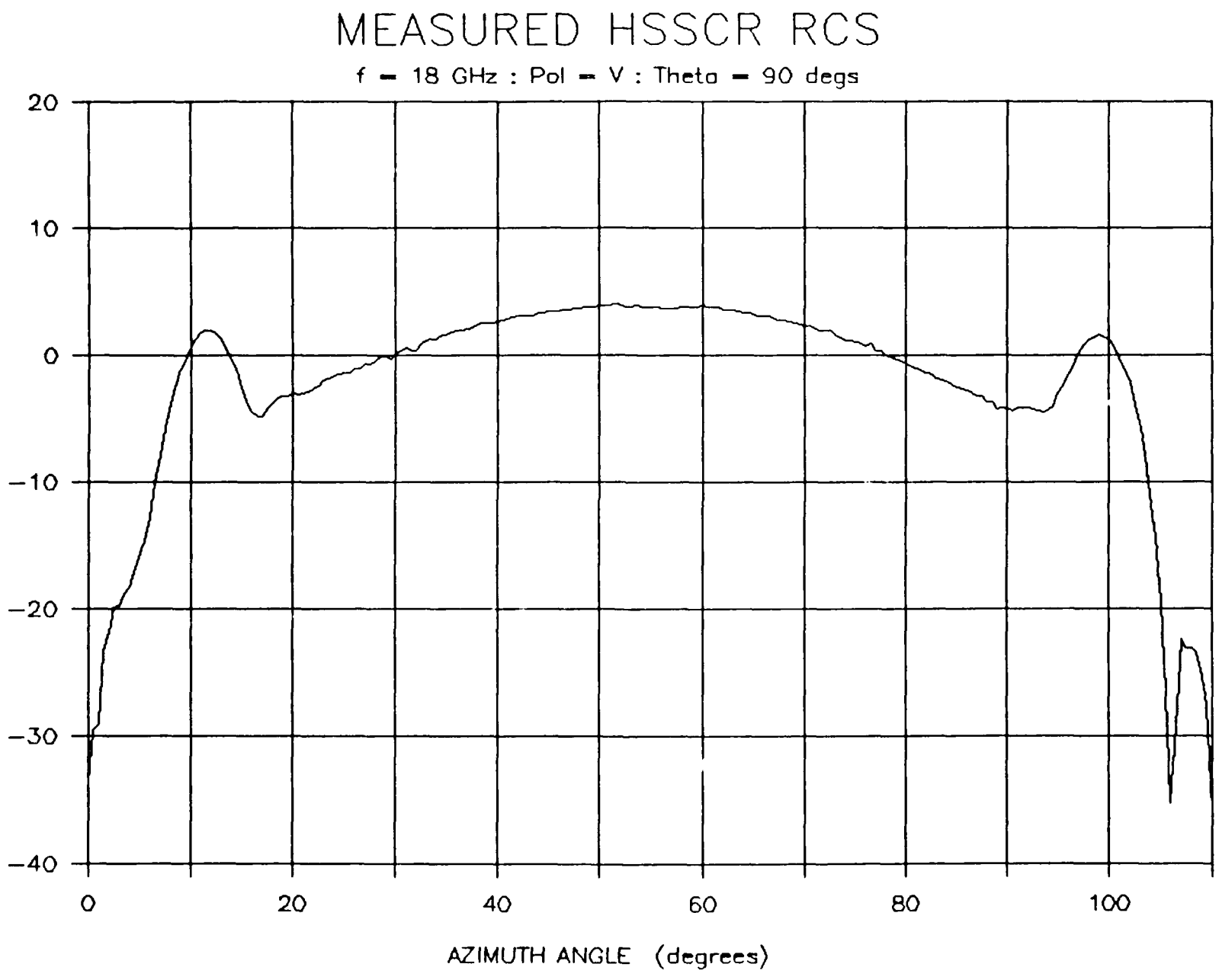

Figure C.2 Measured RCS: HSSCR, Conical Cut, 18 GHz, Theta of 90 degs, Vert Pol

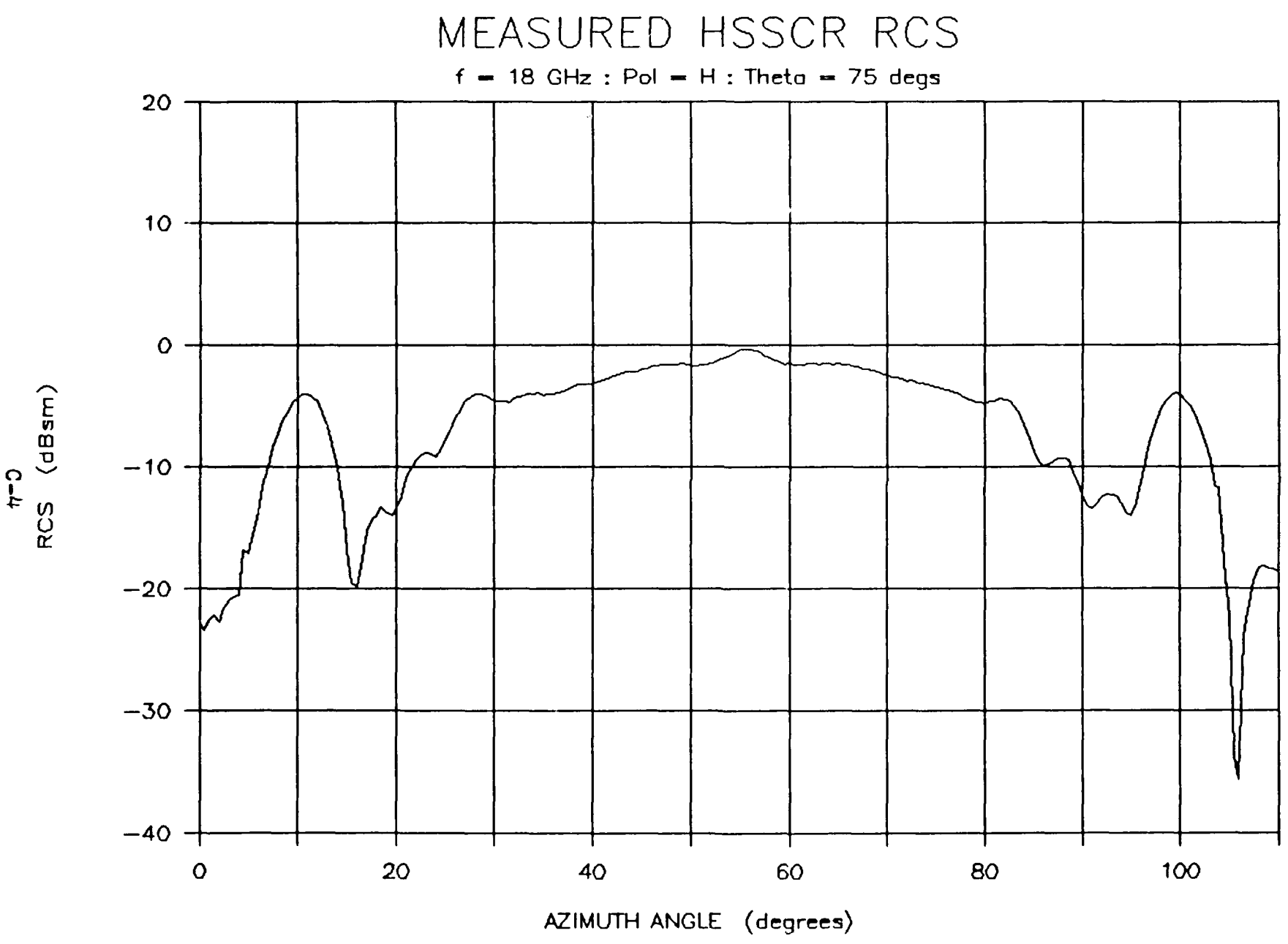

Figure C.3 Measured RCS: HSSCR, Conical Cut, 18 GHz, Theta of 75 degs, Horz Pol

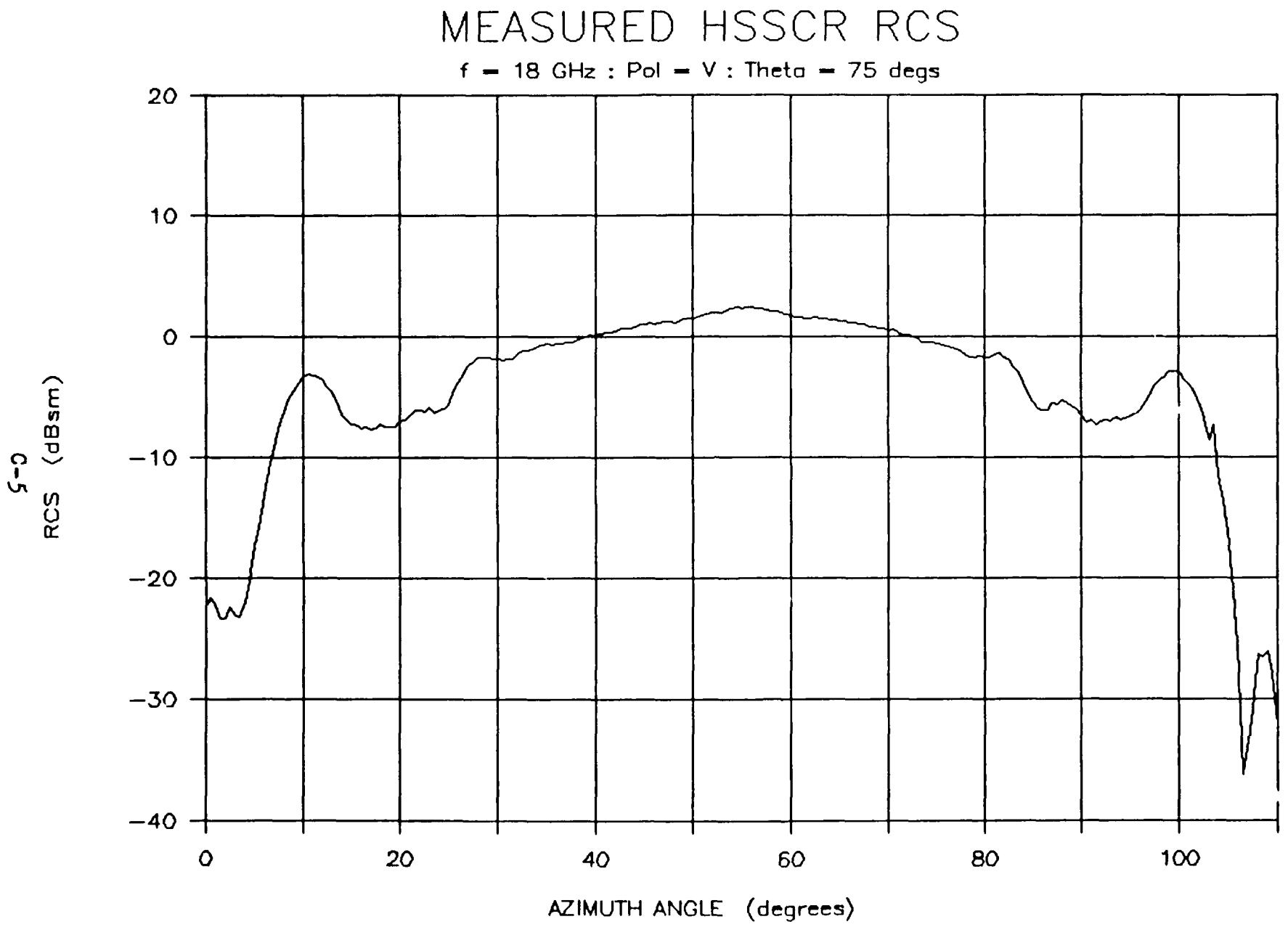

Figure C.4 Measured RCS: HSSCR, Conical Cut, 18 GHz, Theta of 75 degs, Vert Pol

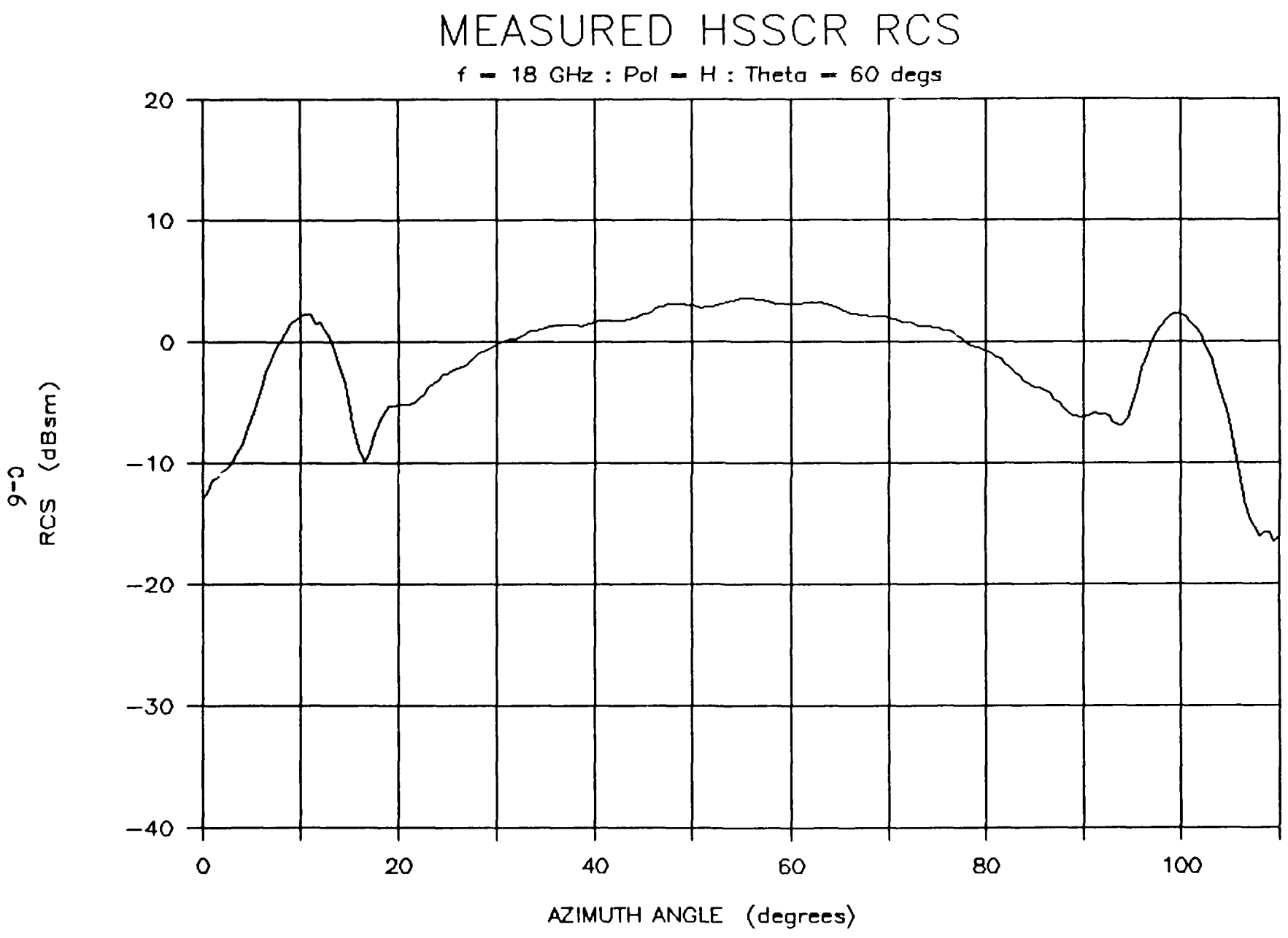

Figure C.5 Measured RCS: HSSCR, Conical Cut, 18 GHz, Theta of 60 degs, Horz Pol

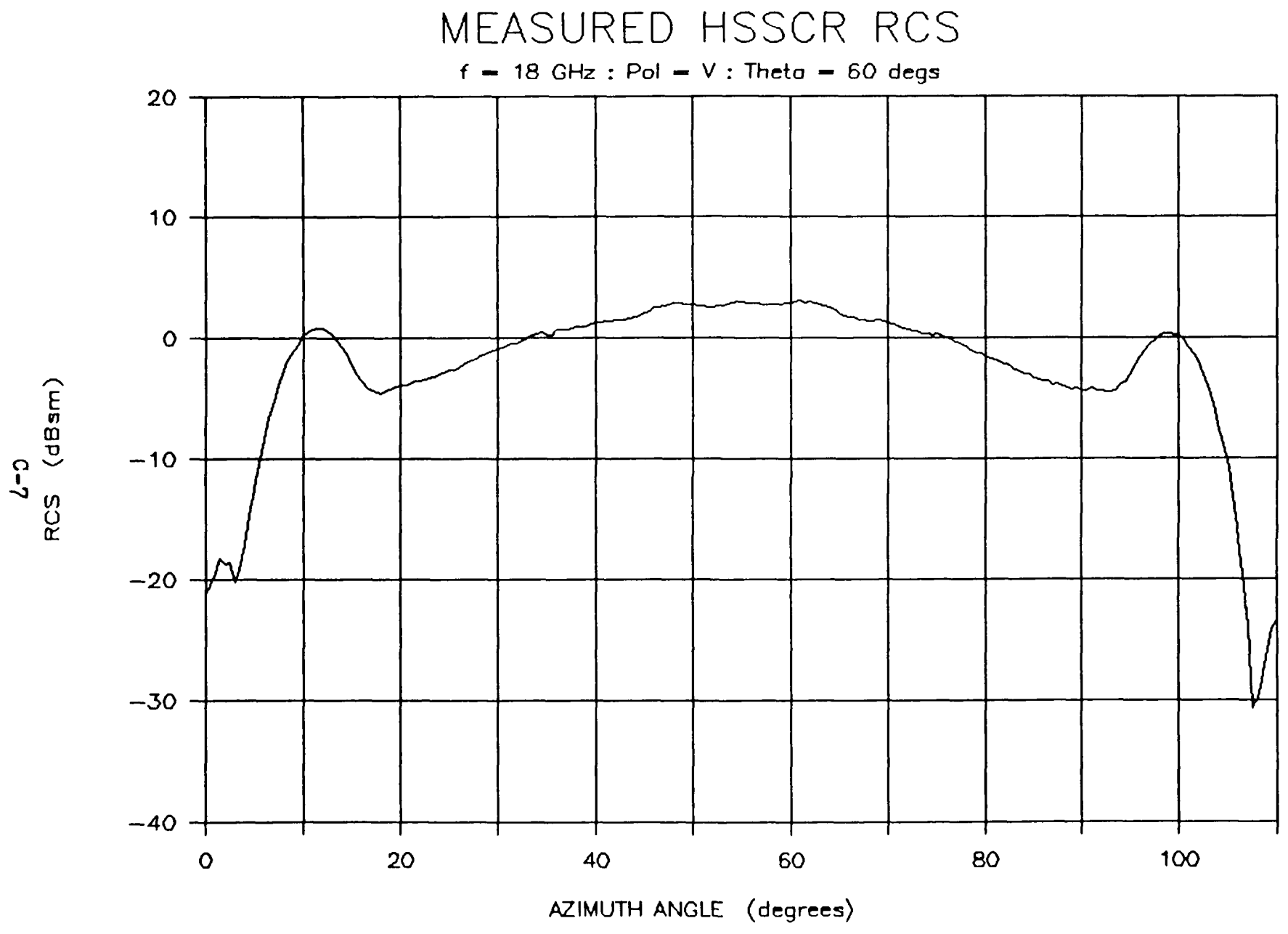

Figure C.6 Measured RCS: HSSCR, Conical Cut, 18 GHz, Theta of 60 degs, Vert Pol

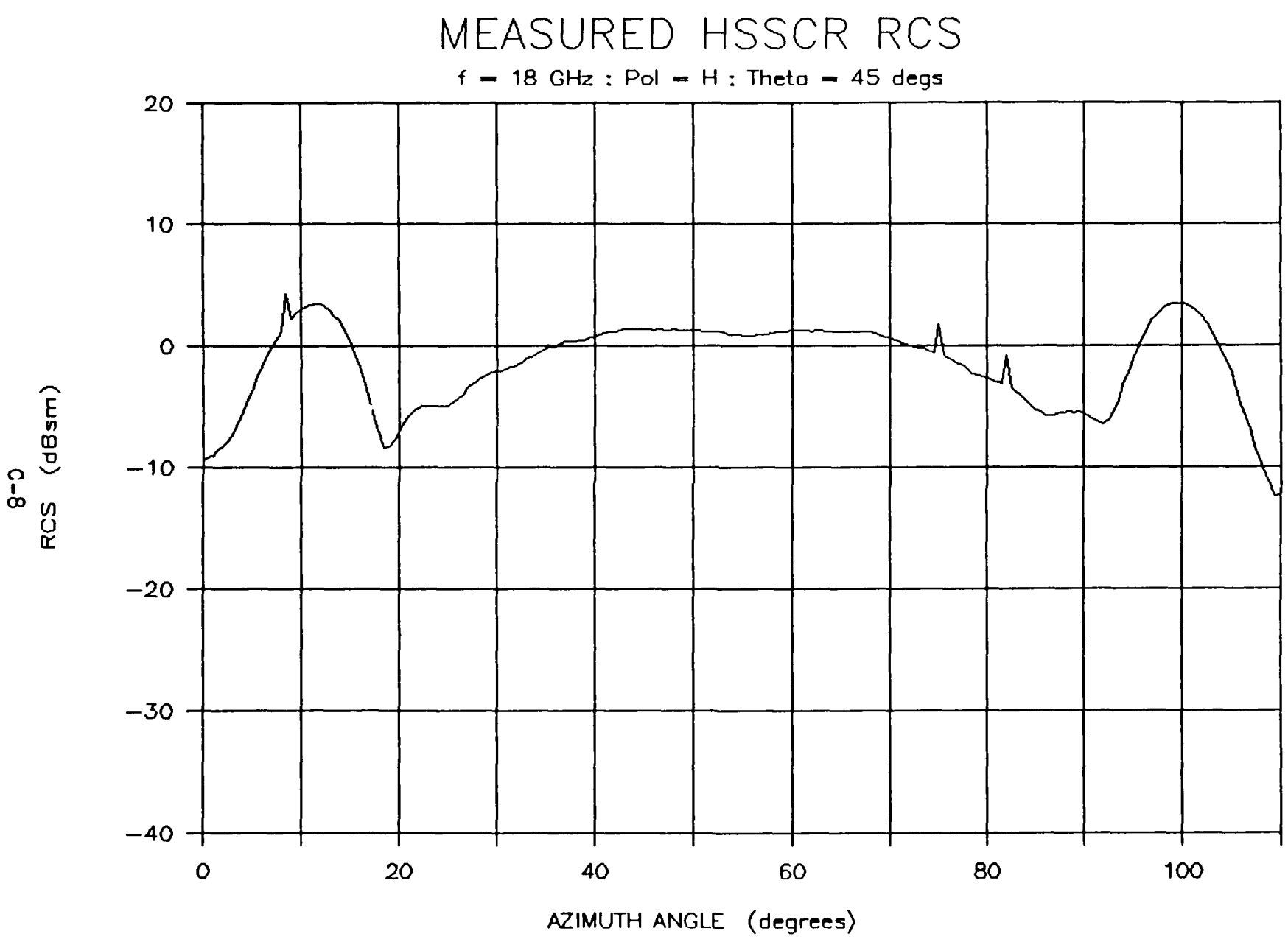

Figure C.7 Measured RCS: HSSCR, Conical Cut, 18 GHz, Theta of 45 degs, Horz Pol

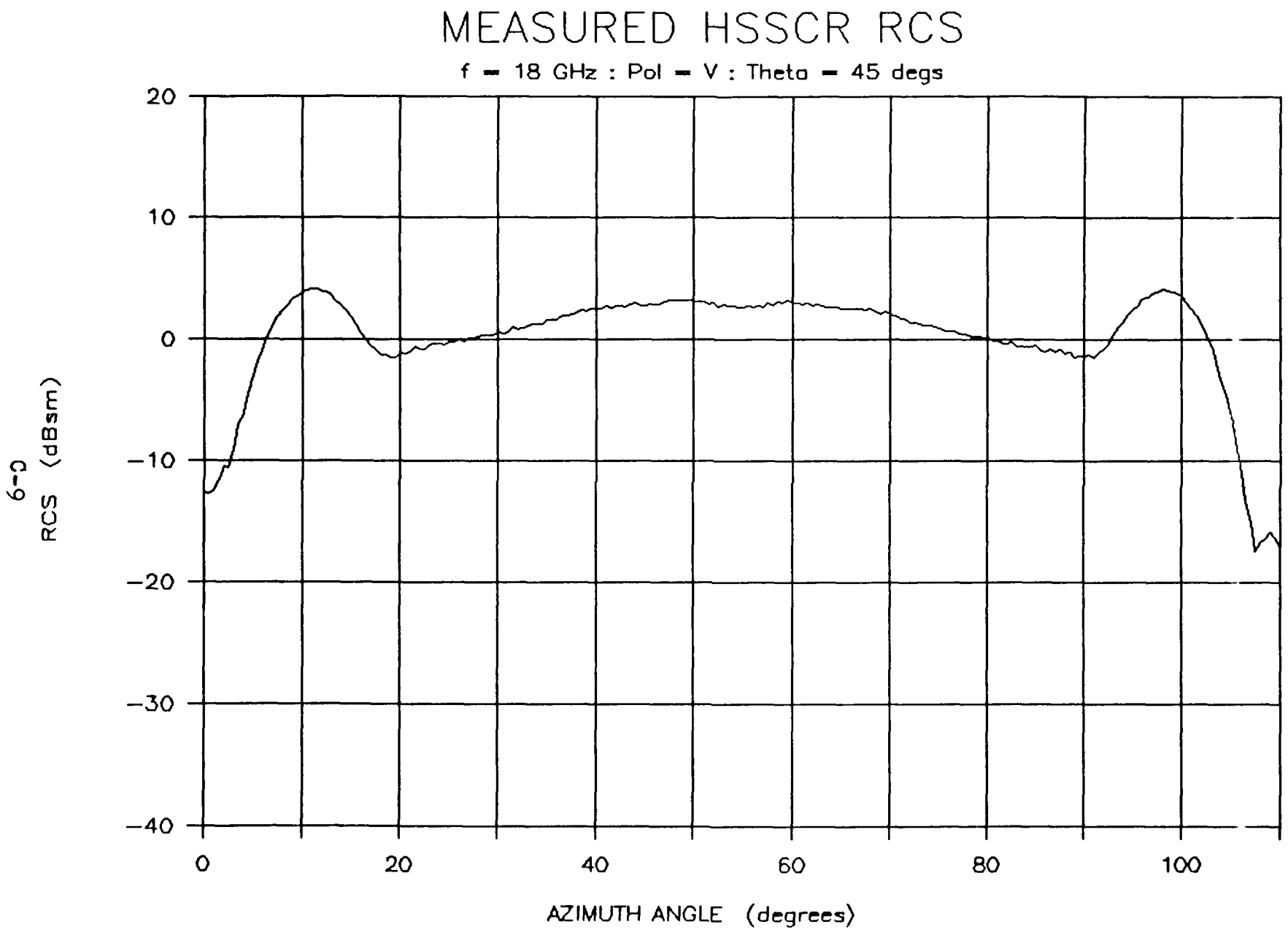

Figure C.8 Measured RCS: HSSCR, Conical Cut, 18 GHz, Theta of 45 degs, Vert Pol

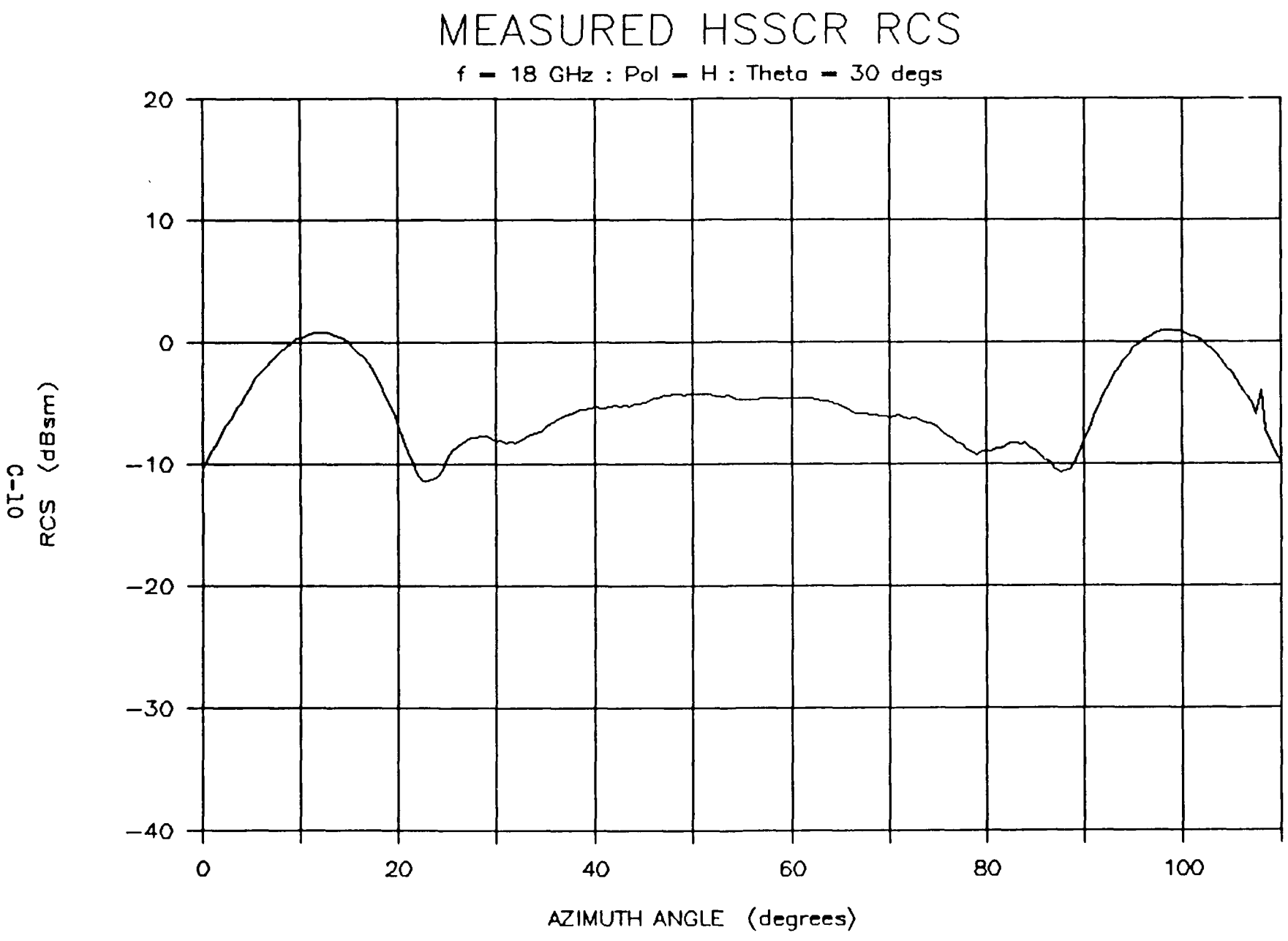

Figure C.9 Measured RCS: HSSCR, Conical Cut, 18 GHz, Theta of 30 degs, Horz Pol

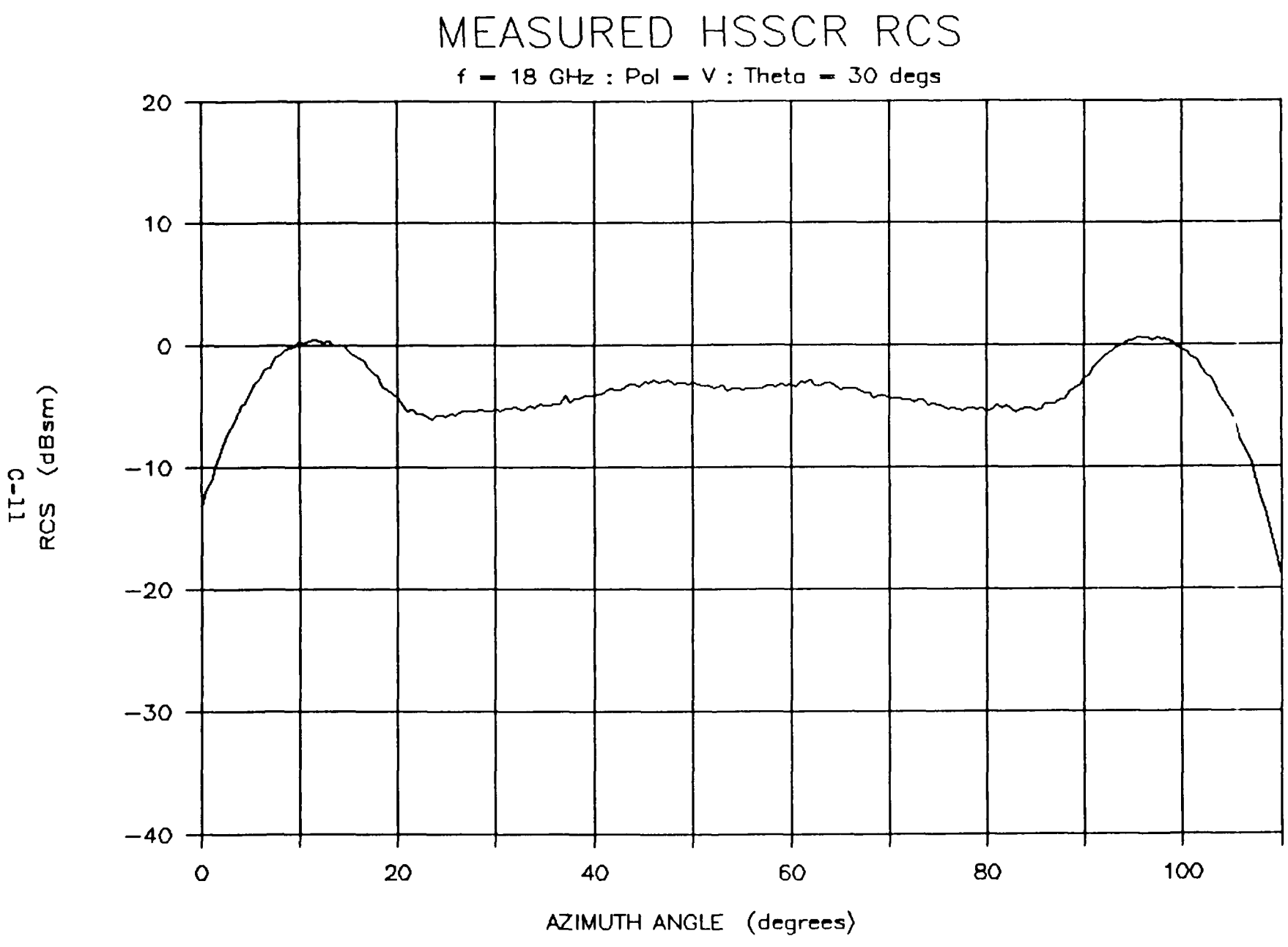

Figure C.10 Measured RCS: HSSCR, Conical Cut, 18 GHz, Theta of 30 degs, Vert Pol

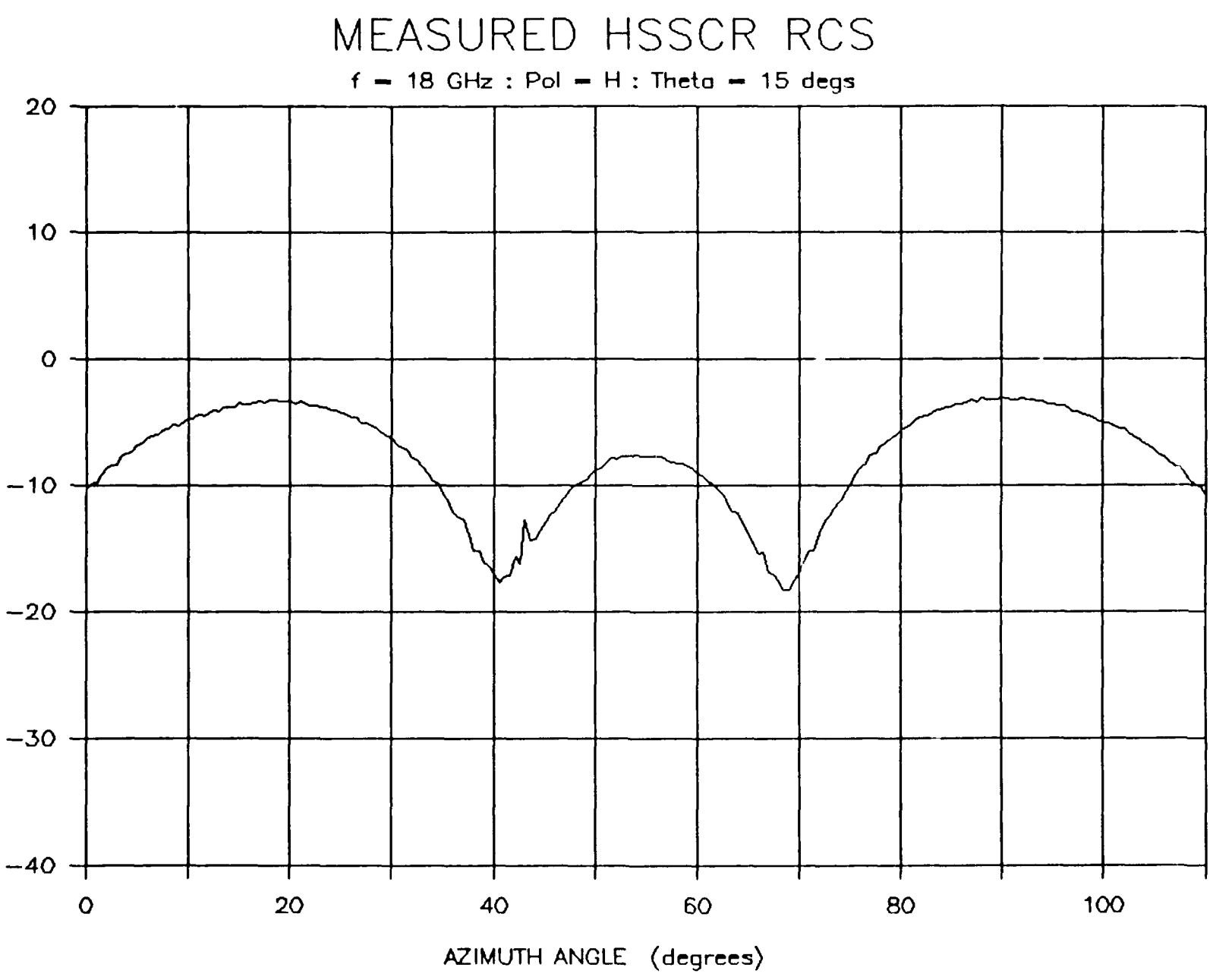

Figure C.11 Measured RCS: HSSCR, Conical Cut, 18 GHz, Theta of 15 degs, Horz Pol

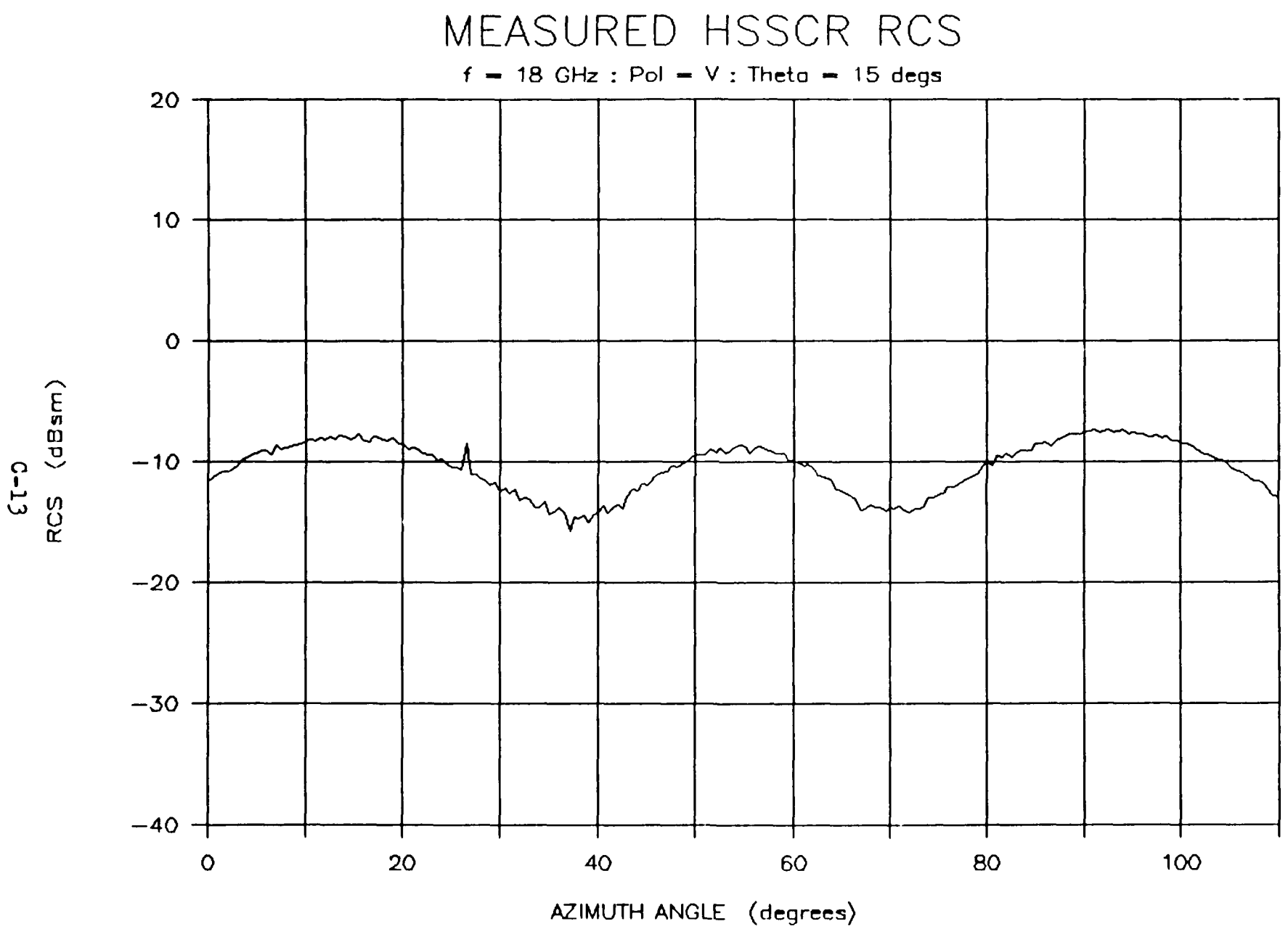

Figure C.12 Measured RCS: HSSCR, Conical Cut, 18 GHz, Theta of 15 degs, Vert Pol

APPENDIX D: Eight Corner Reflector Array Conical Cut RCS Measurement Results

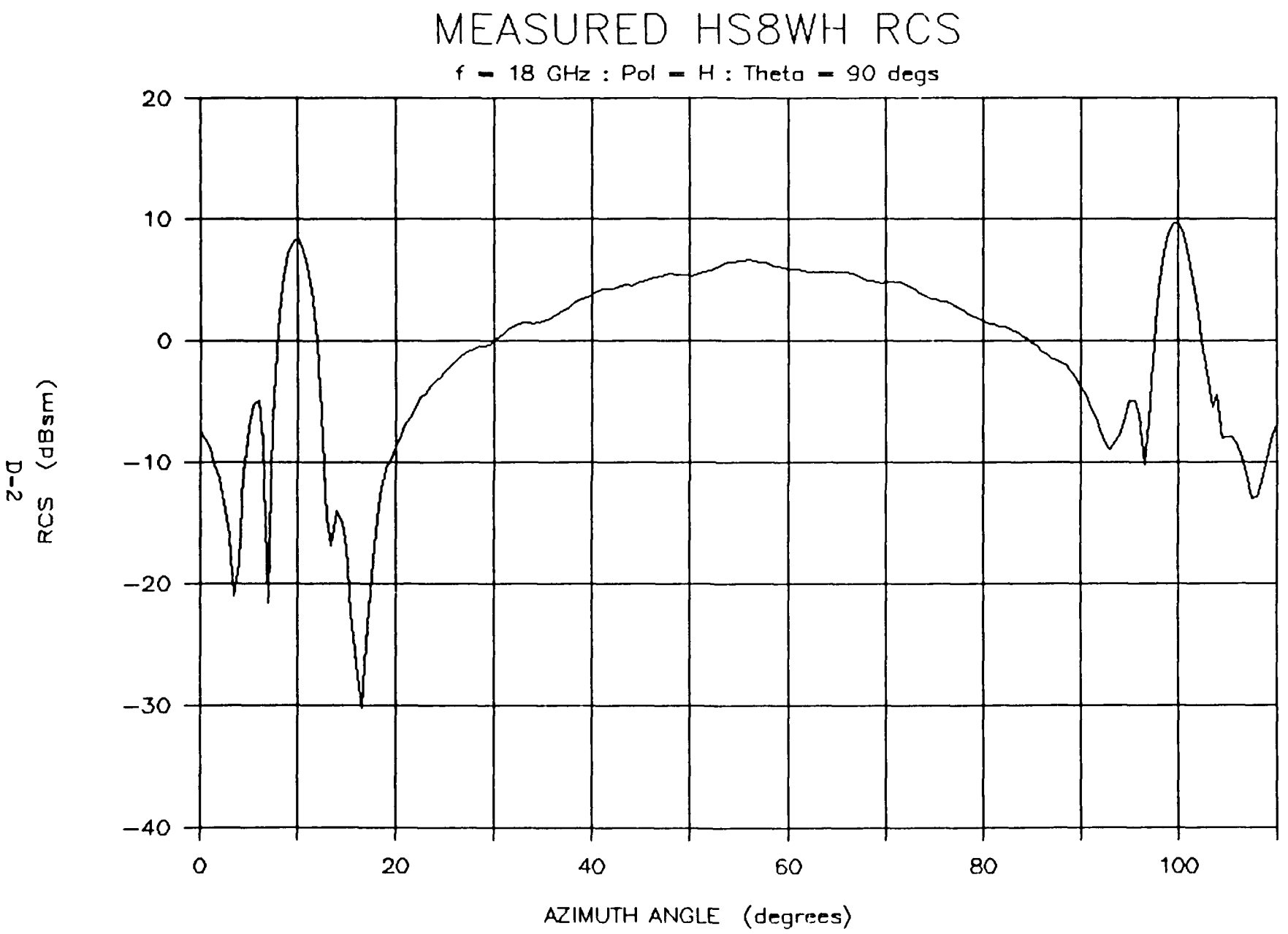

Figure D.1 Measured RCS: HS8WH, Conical Cut, 18 GHz, Theta of 90 degs, Horz Pol

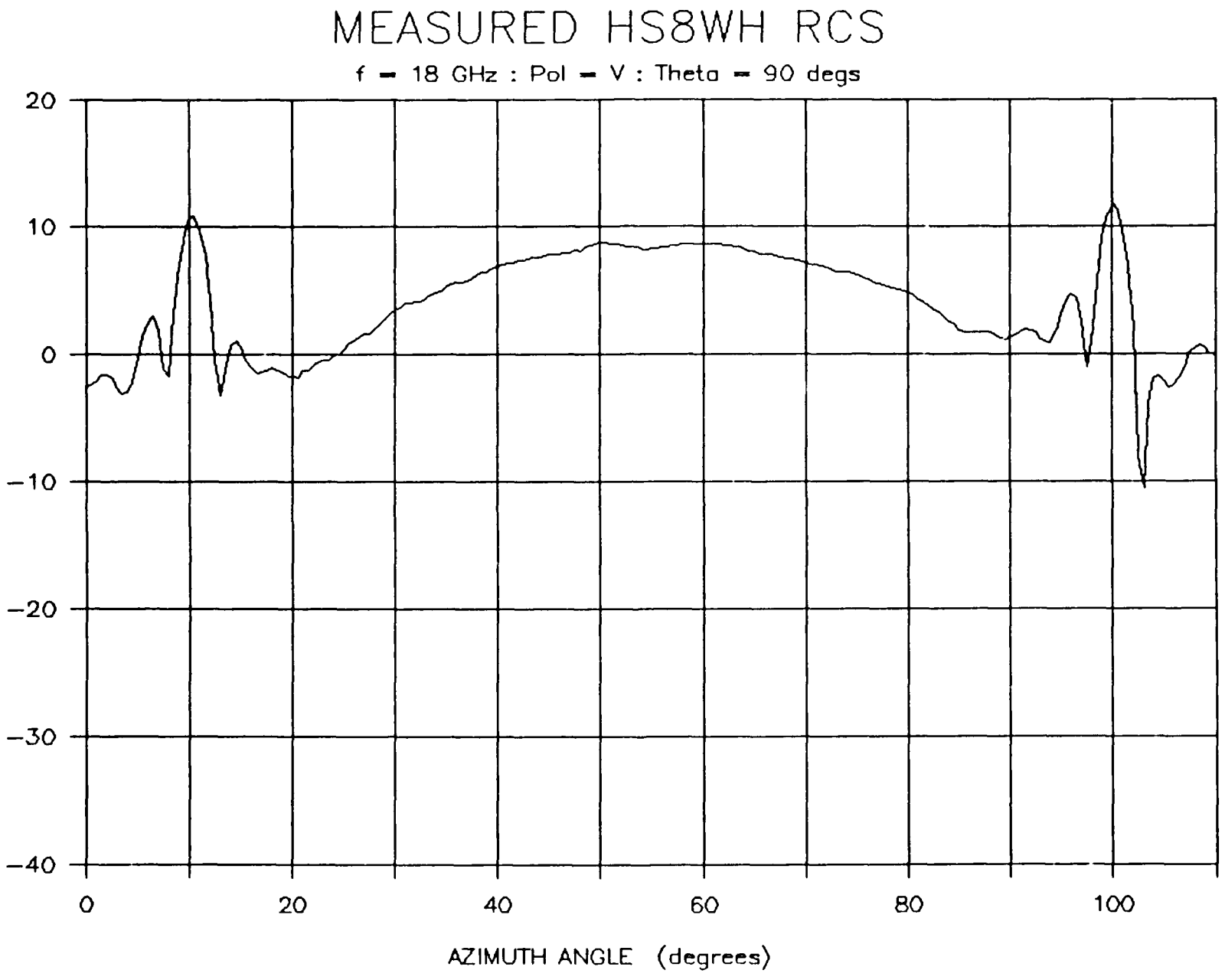

Figure D.2 Measured RCS: HS8WH, Conical Cut, 18 GHz, Theta of 90 degs, Vert Pol

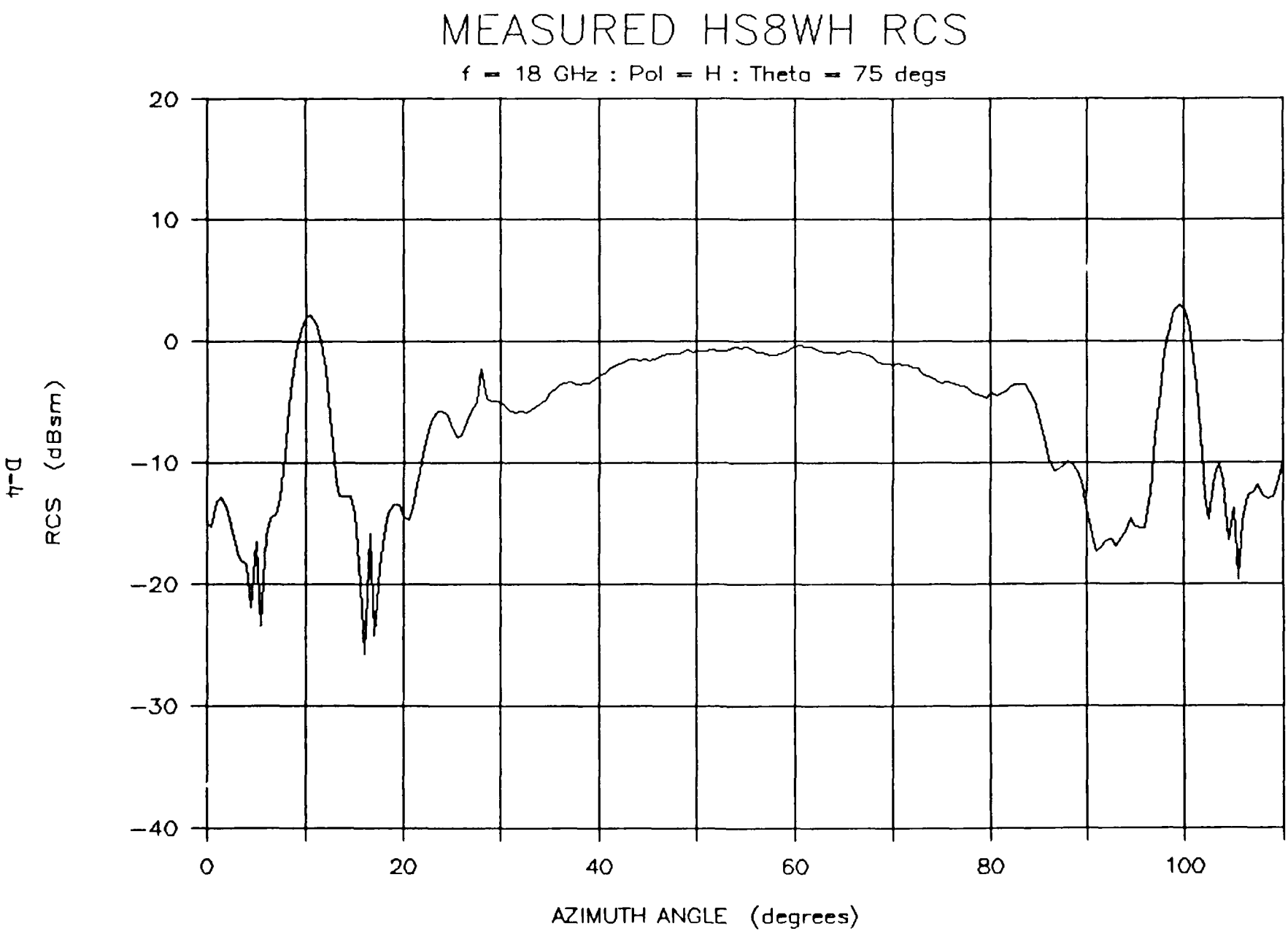

Figure D.3 Measured RCS: HS8WH, Conical Cut, 18 GHz, Theta of 75 degs, Horz Pol

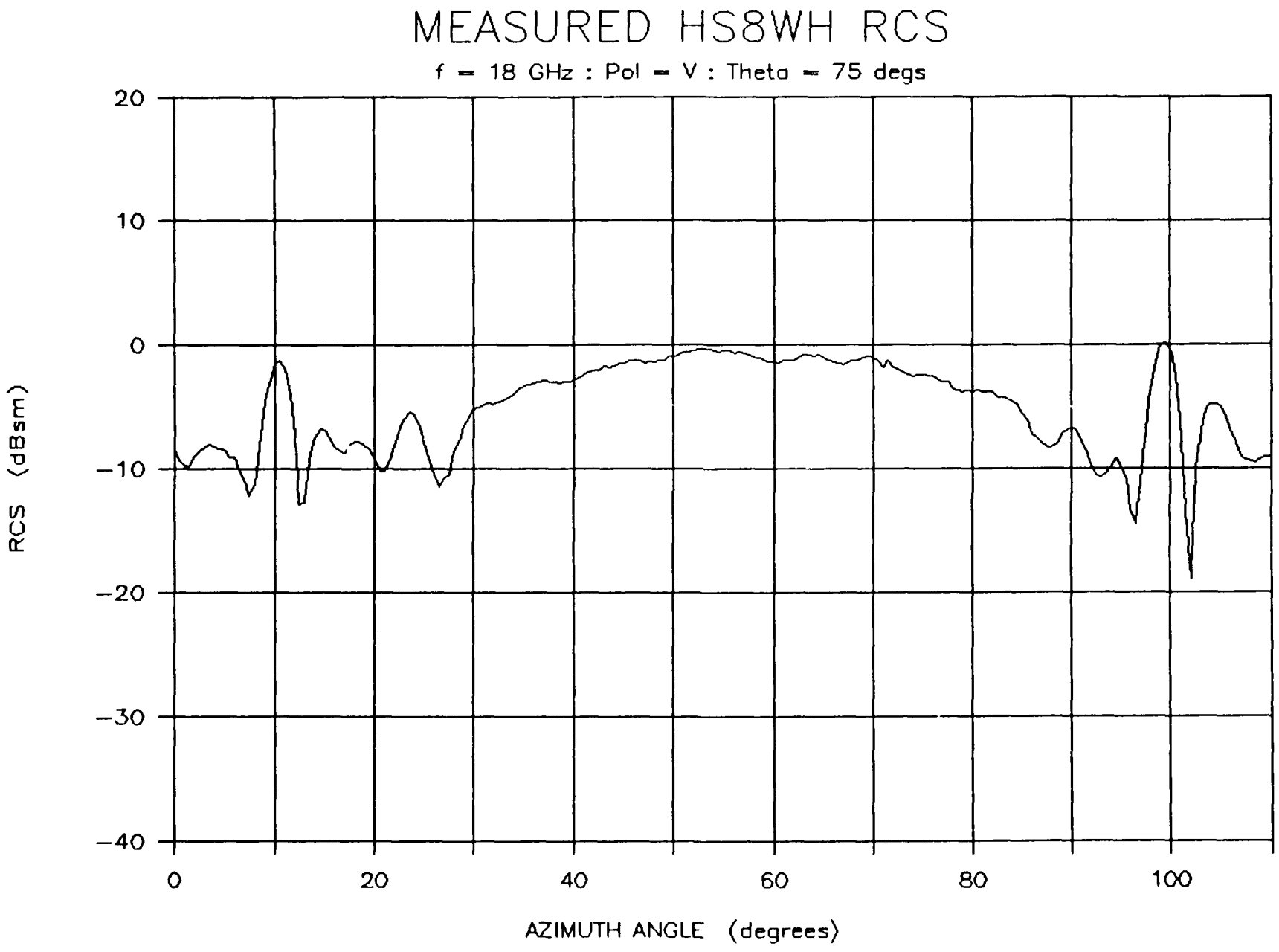

Figure D.4 Measured RCS: HS8WH, Conical Cut, 18 GHz, Theta of 75 degs, Vert Pol

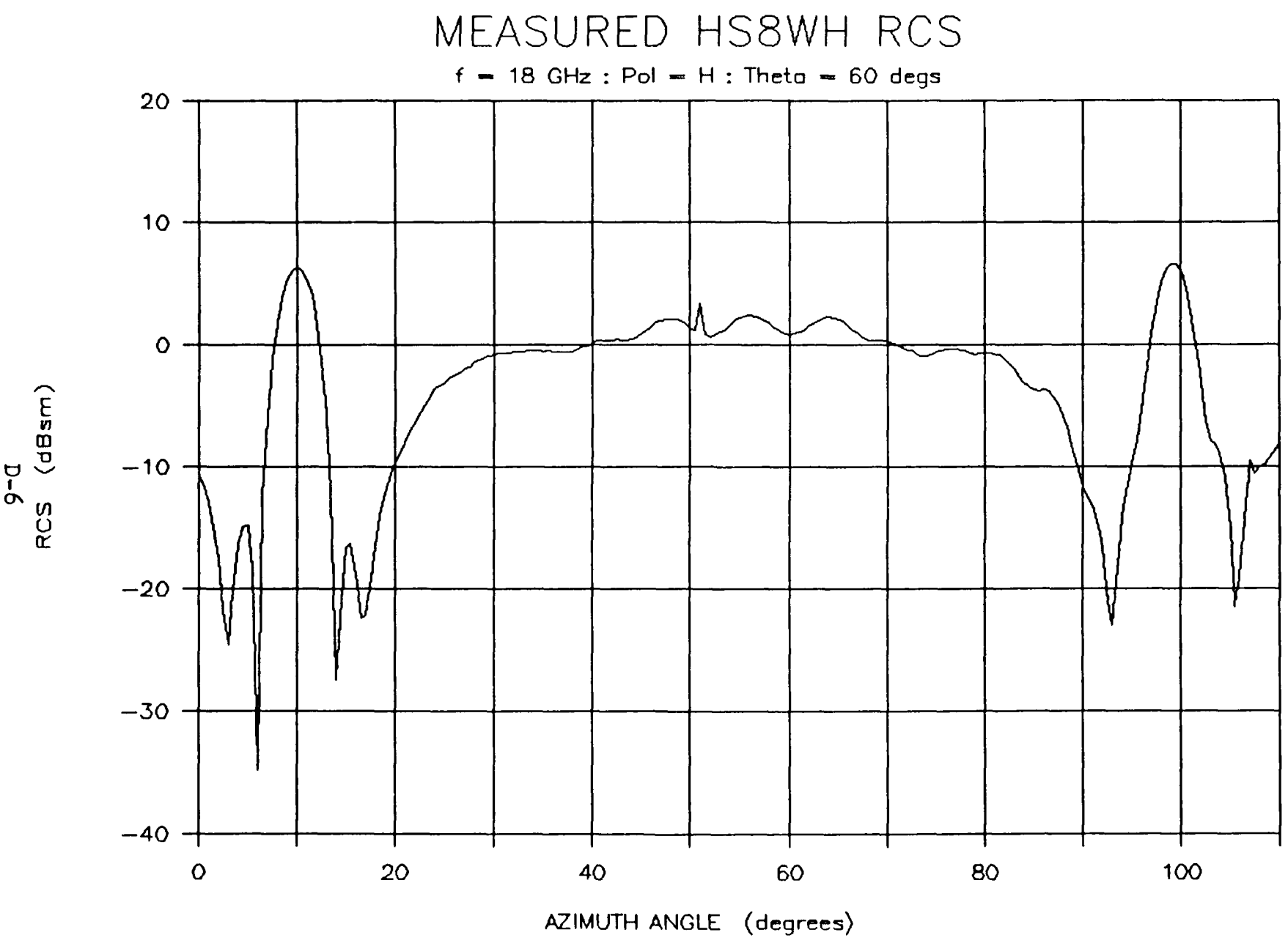

Figure D.5 Measured RCS: HS8WH, Conical Cut, 18 GHz, Theta of 60 degs, Horz Pol

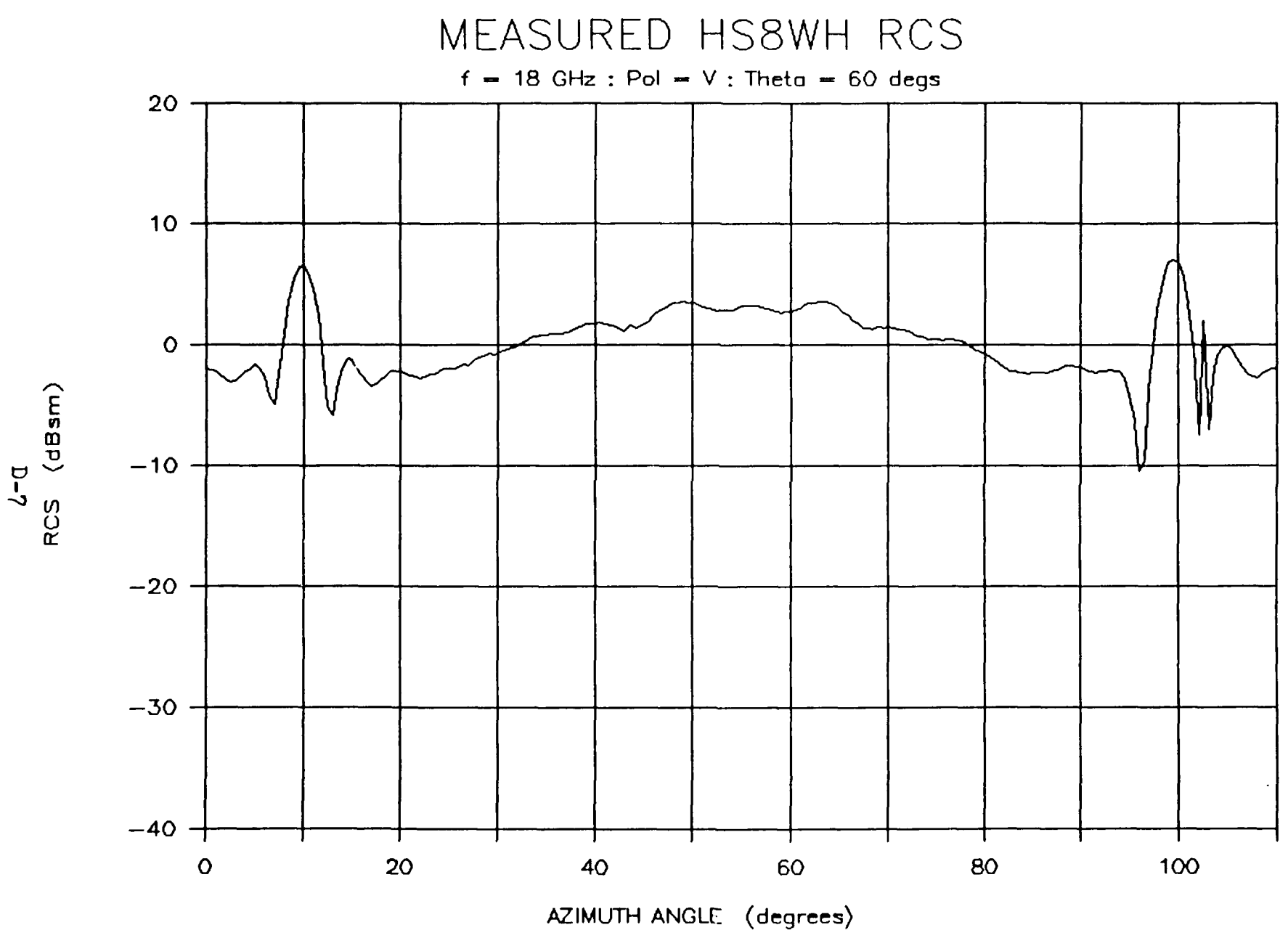

Figure D.6 Measured RCS: HS8WH, Conical Cut, 18 GHz, Theta of 60 degs, Vert Pol

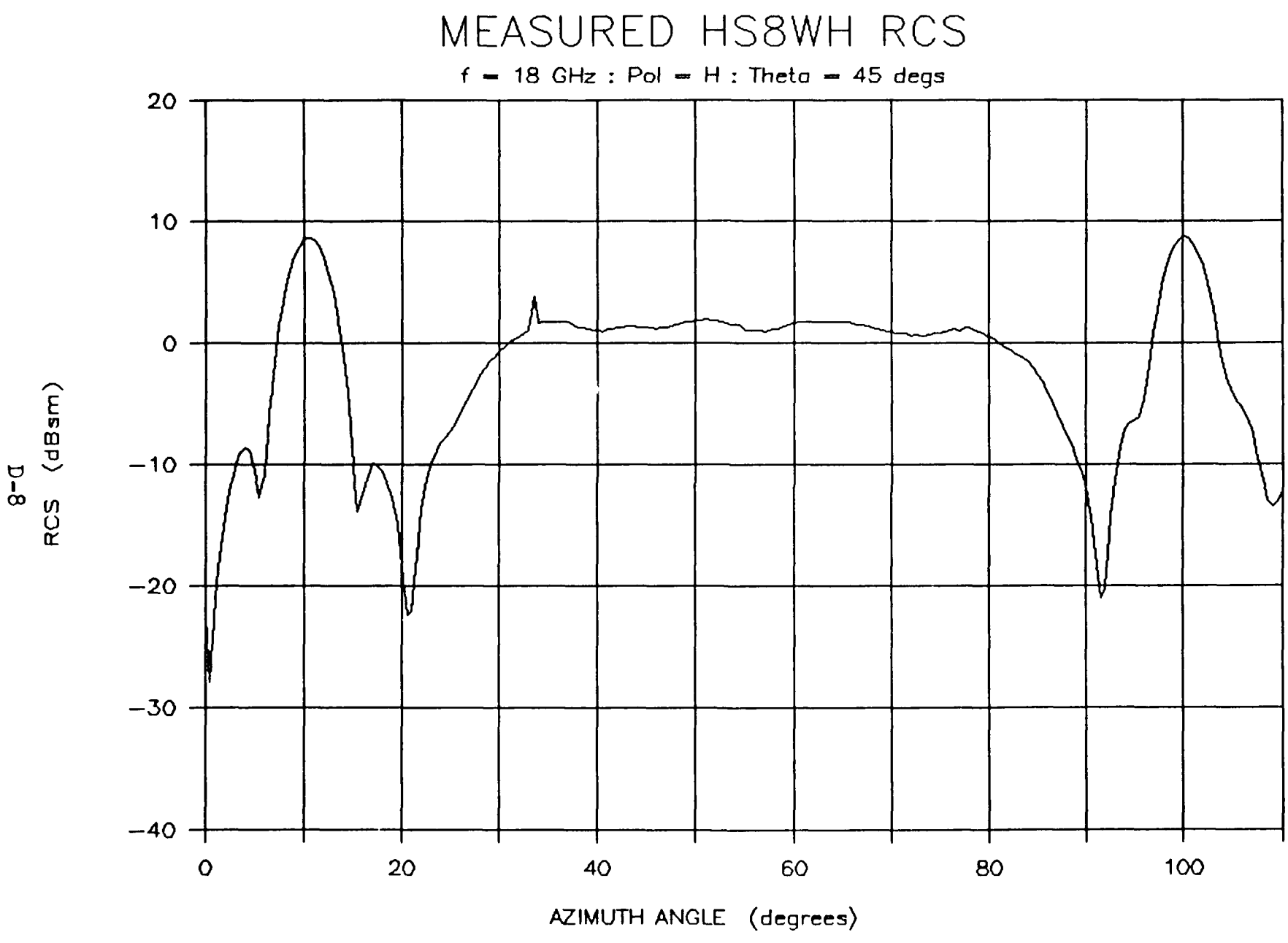

Figure D.7 Measured RCS: HS8WH, Conical Cut, 18 GHz, Theta of 45 degs, Horz Pol

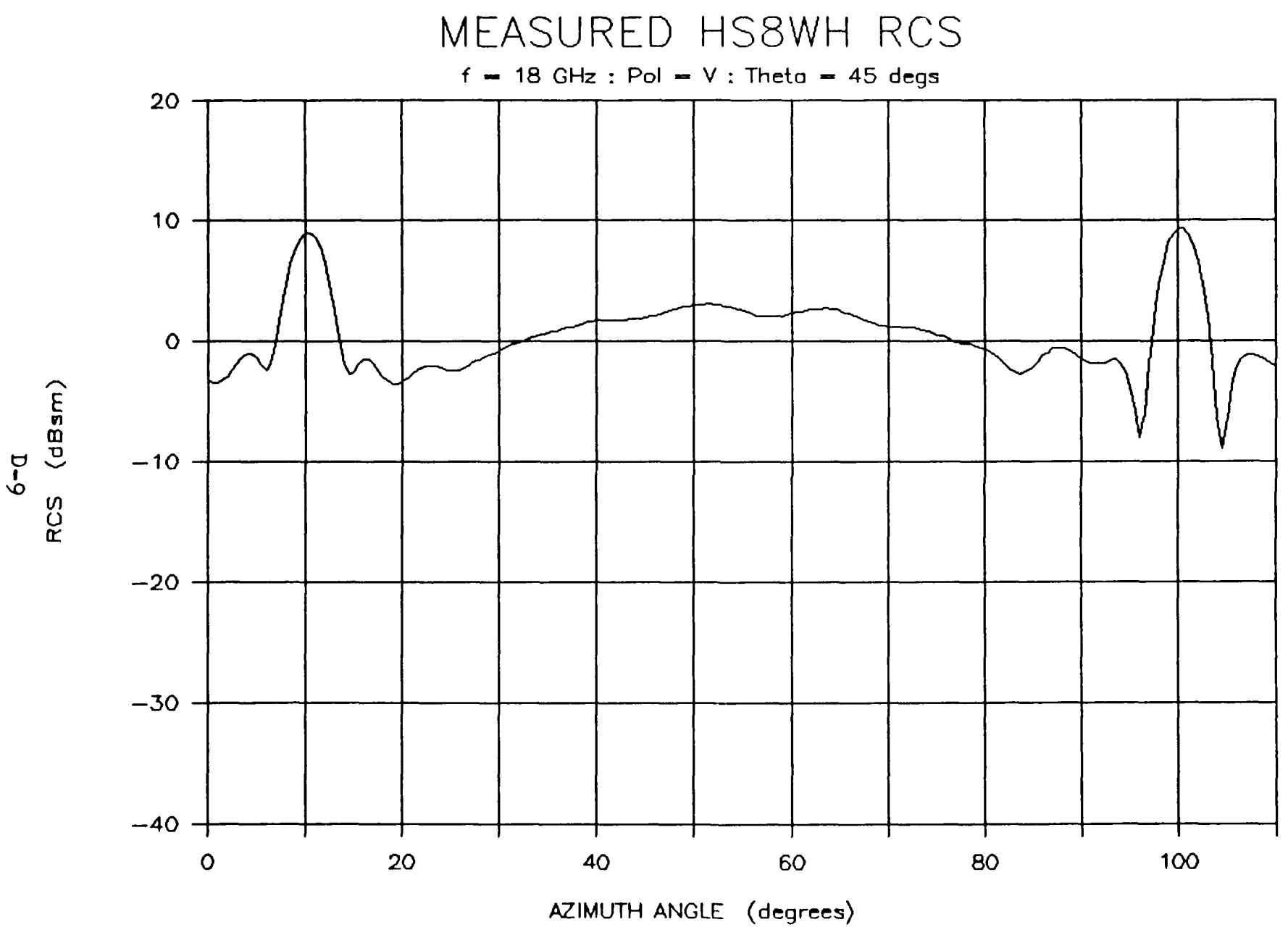

Figure D.8 Measured RCS: HS8WH, Conical Cut, 18 GHz, Theta of 45 degs, Vert Pol

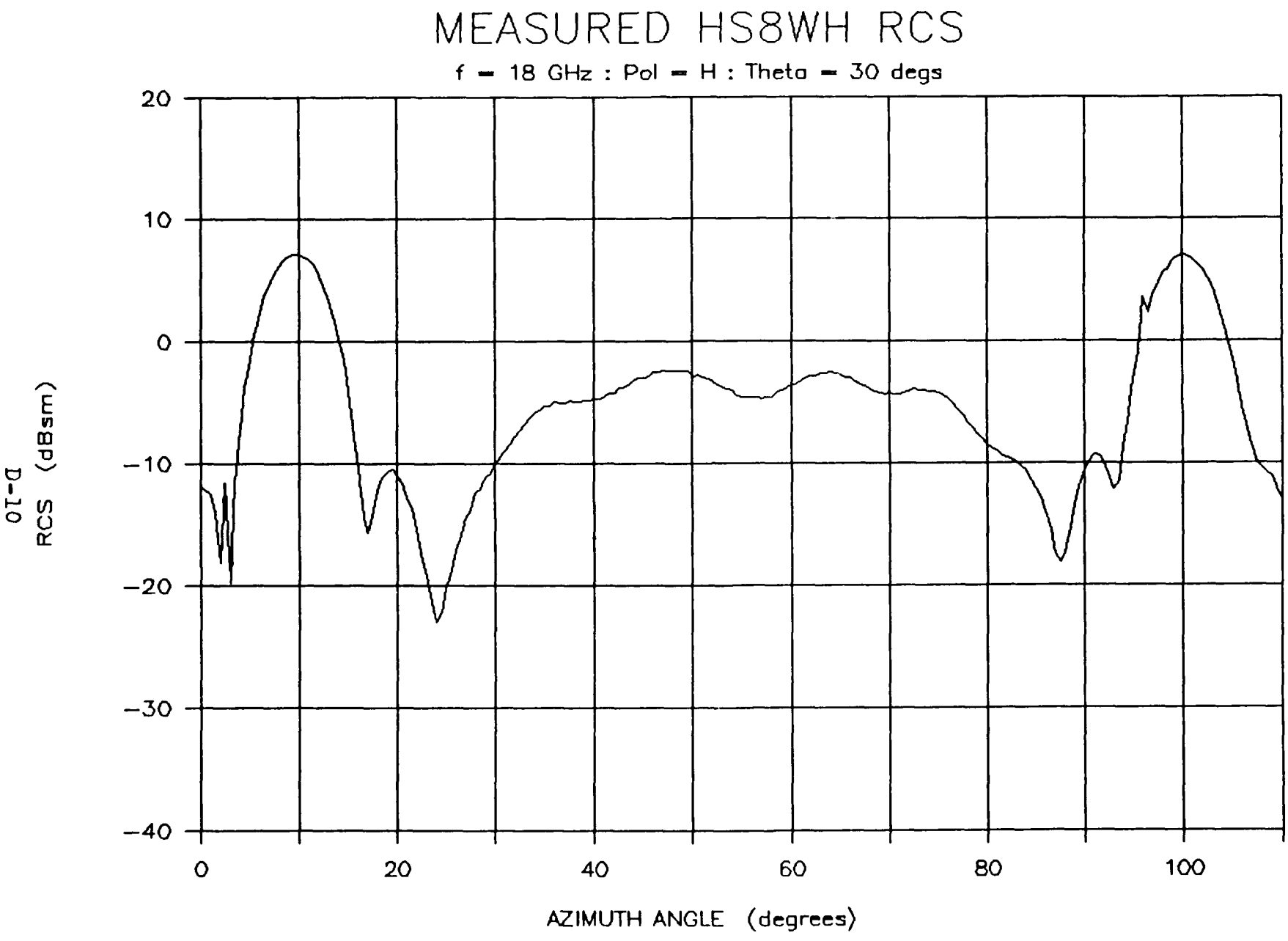

Figure D.9 Measured RCS: HS8WH, Conical Cut, 18 GHz, Theta of 30 degs, Horz Pol

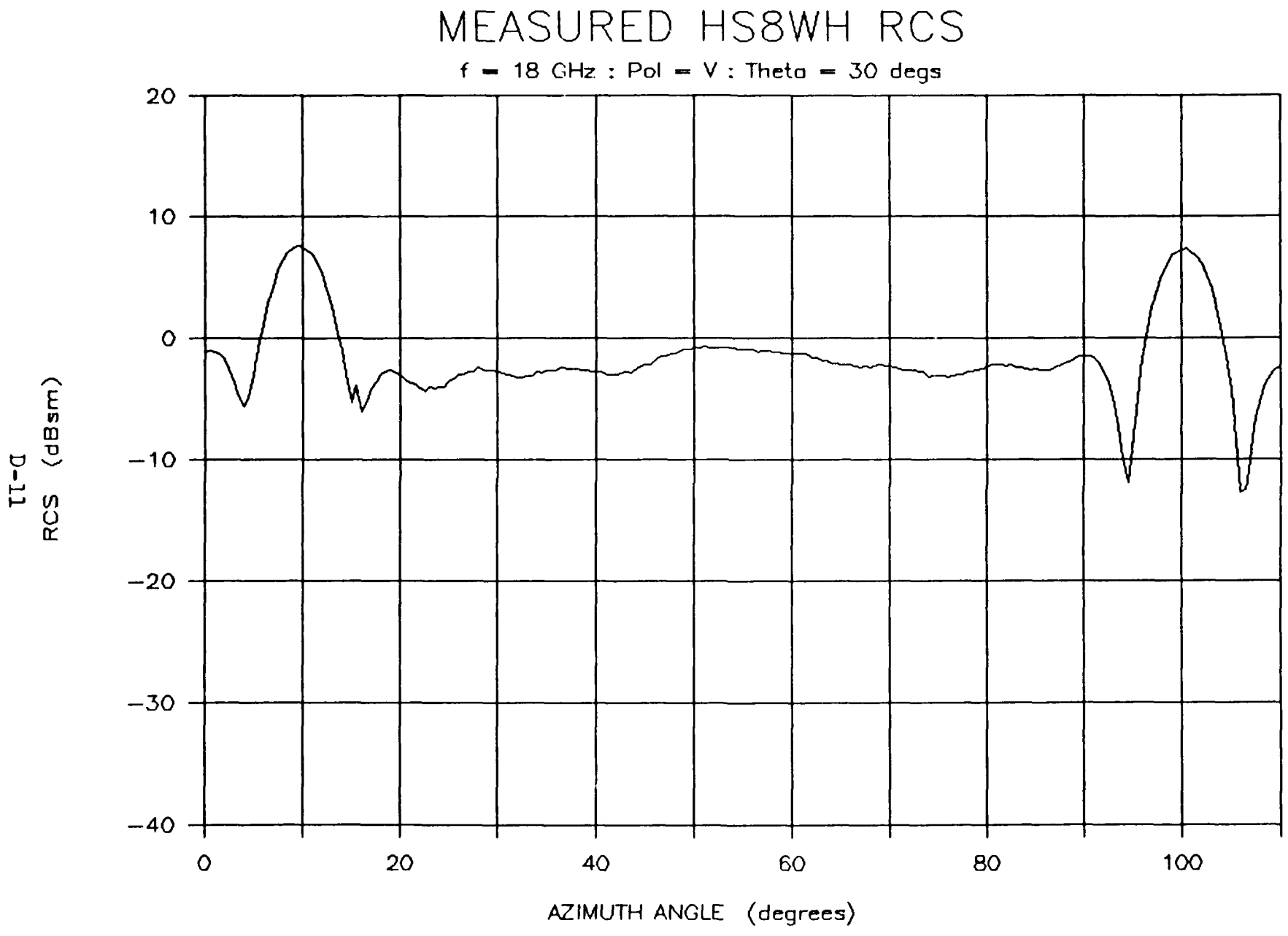

Figure D.10 Measured RCS: HS8WH, Conical Cut, 18 GHz, Theta of 30 degs, Vert Pol

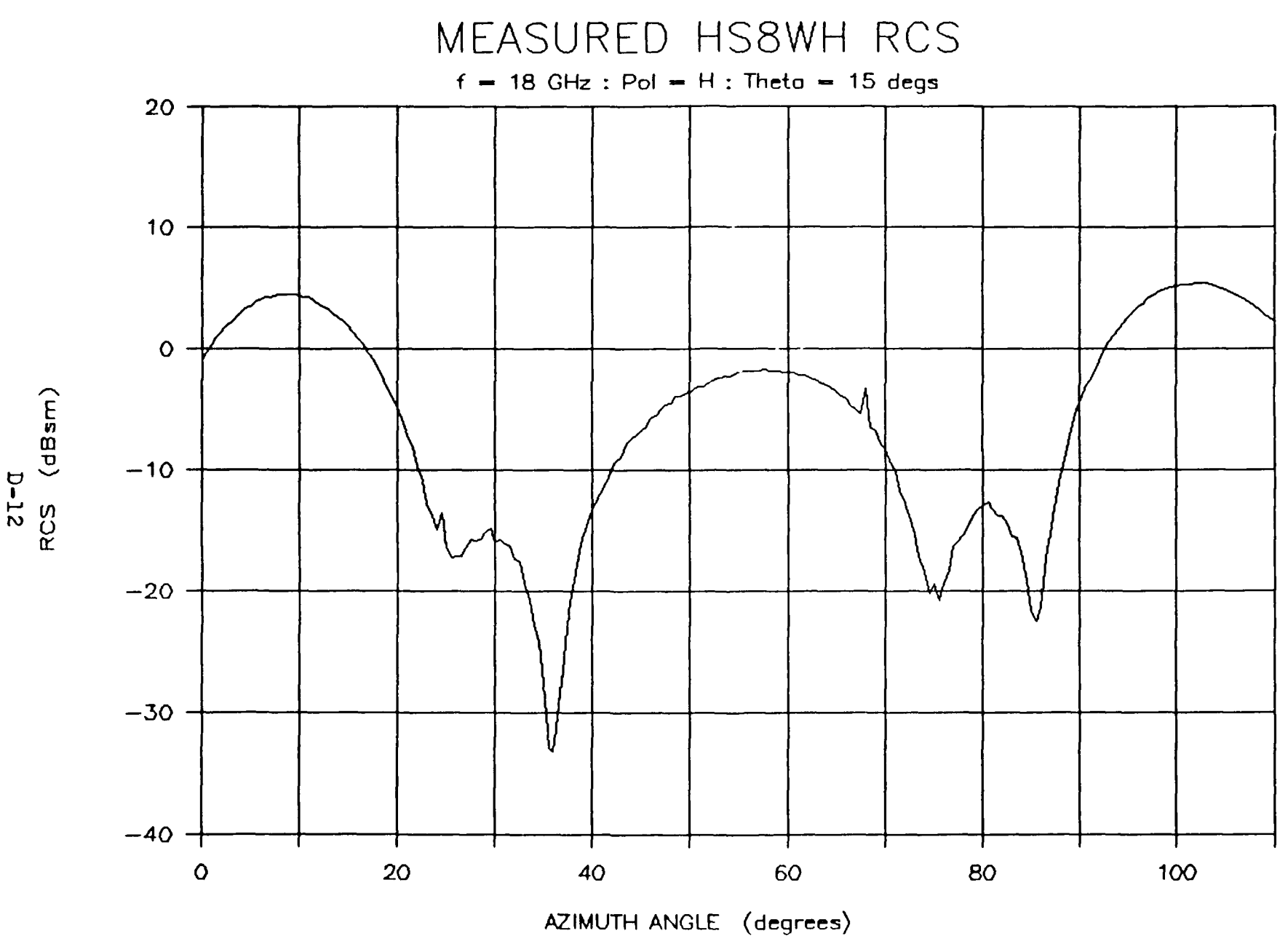

Figure D.11 Measured RCS: HS8WH, Conical Cut, 18 GHz, Theta of 15 degs, Horz Pol

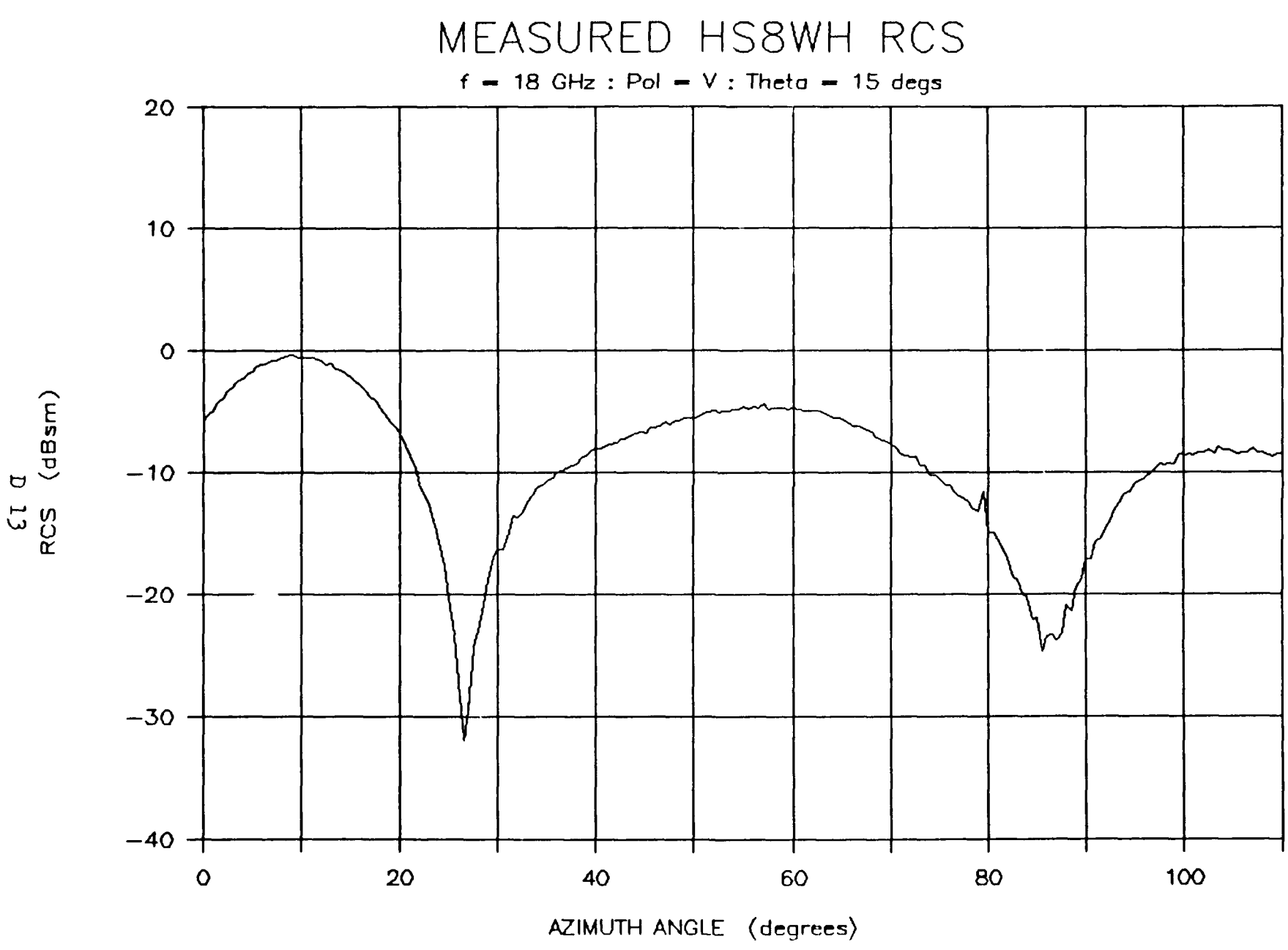

Figure D.12 Measured RCS: HS8WH, Conical Cut, 18 GHz, Theta of 15 degs, Vert Pol

APPENDIX E: Geodesic Array Conical Cut RCS Measurement Results

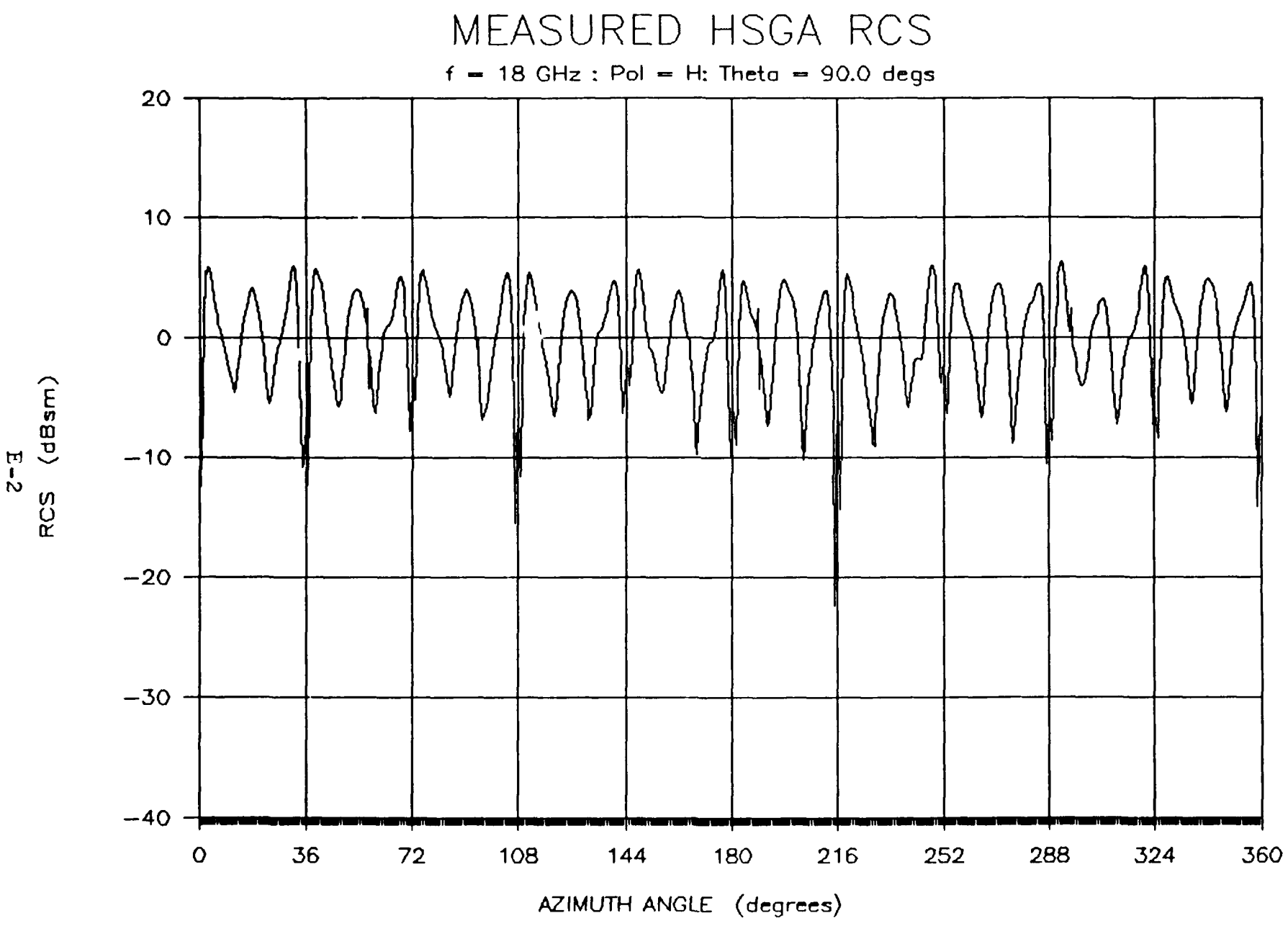

Figure E.1 Measured RCS: HSGA, Conical Cut, 18 GHz, Theta of 90.0 degs, Horz Pol

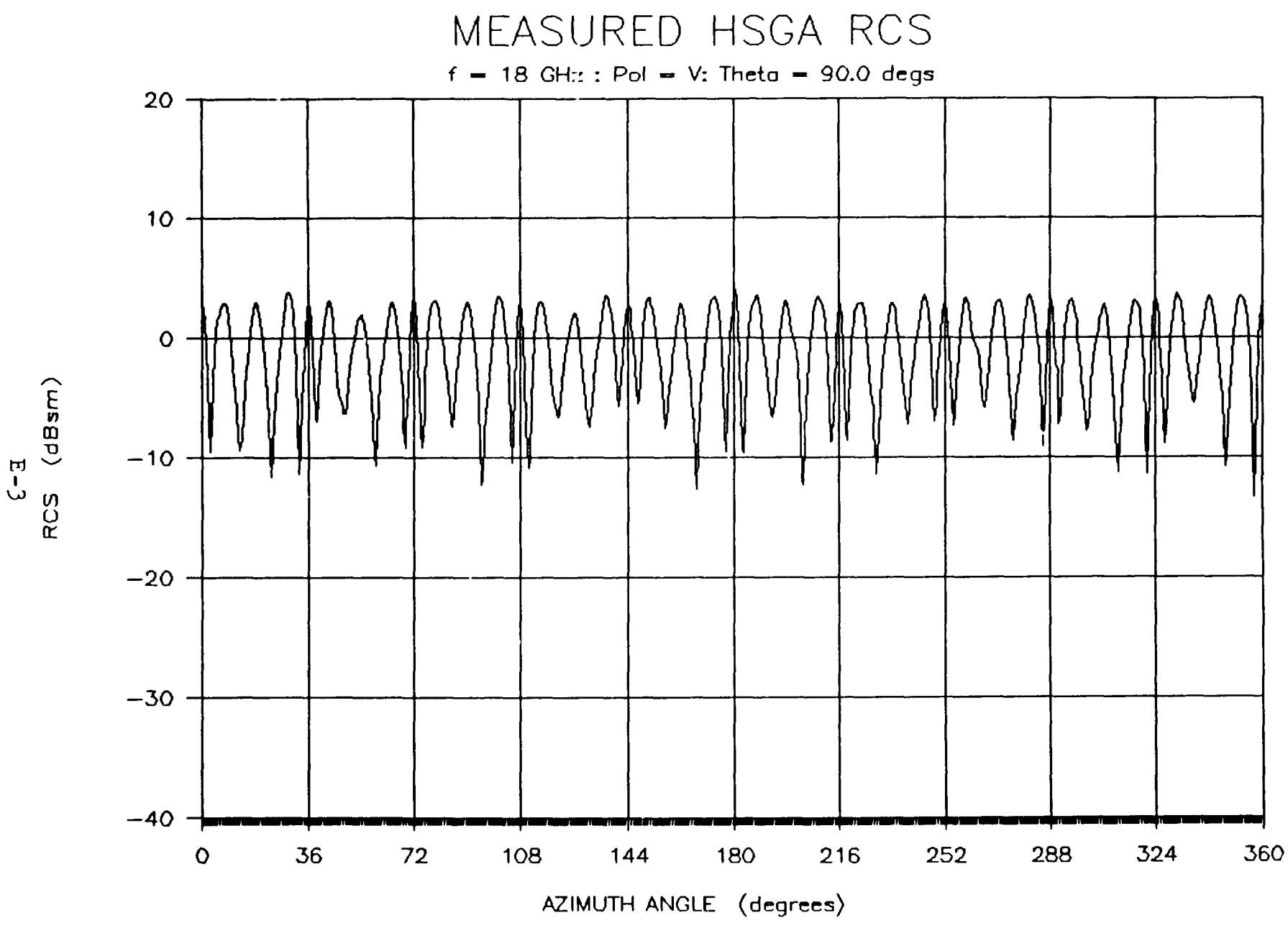

Figure E.2 Measured RCS: HSGA, Conical Cut, 18 GHz, Theta of 90.0 degs, Vert Pol

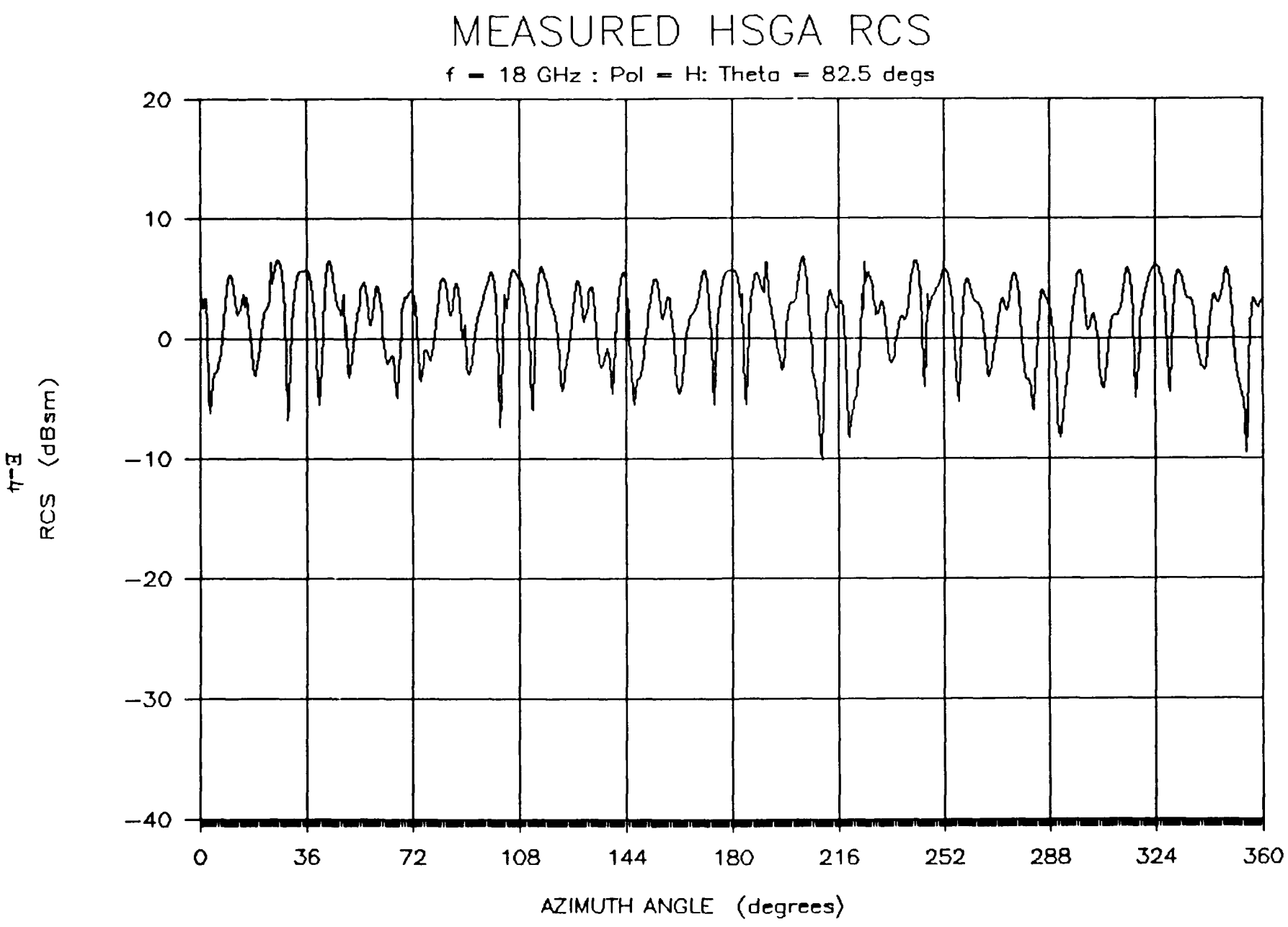

Figure E.3 Measured RCS: HSGA, Conical Cut, 18 GHz, Theta of 82.5 degs, Horz Pol

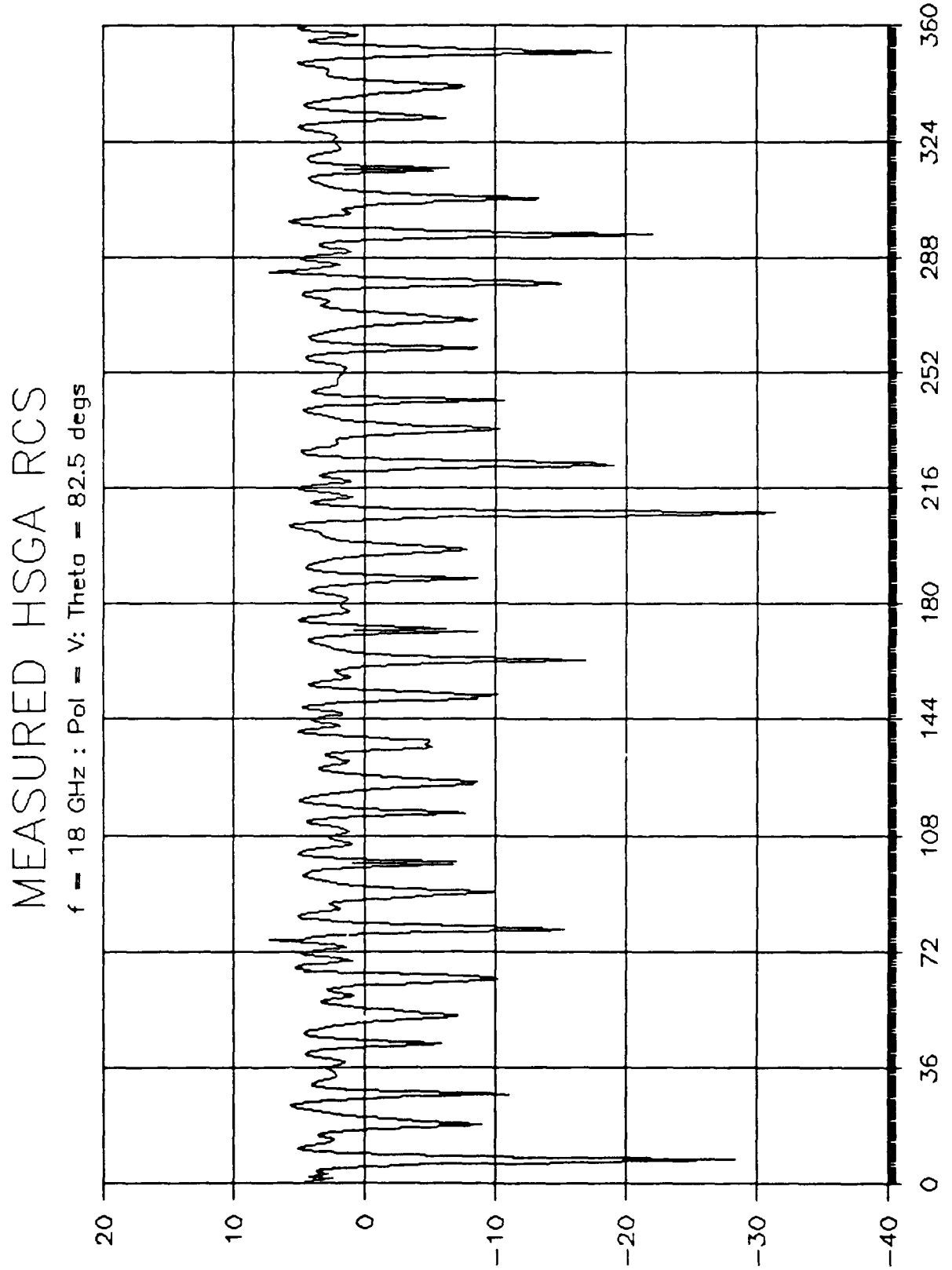

Figure E.4 Measured RCS: HSGA, Conical Cut, 18 GHz, Theta of 82.5 degs, Vert Pol

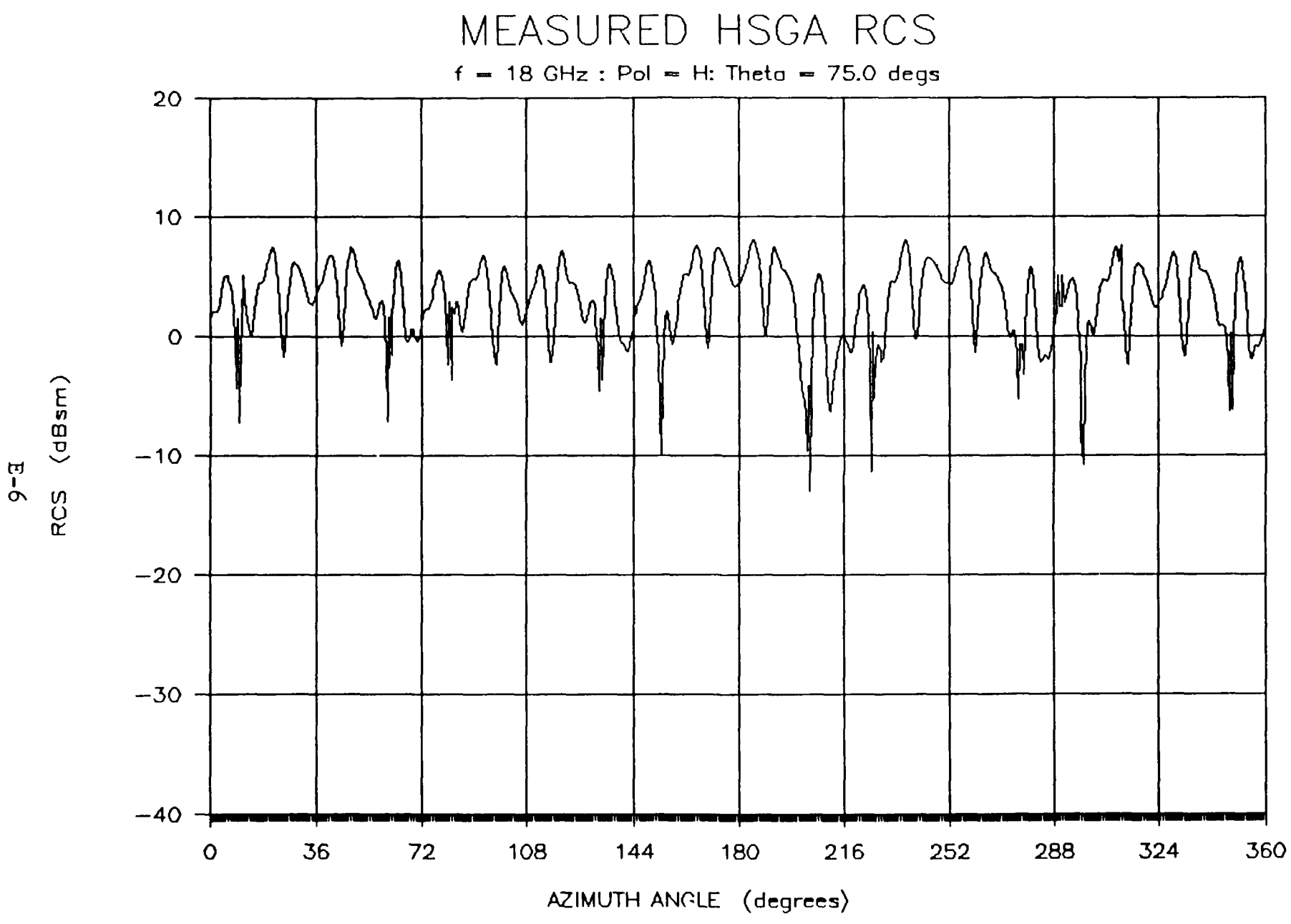

Figure E.5 Measured RCS: HSGA, Conical Cut, 18 GHz, Theta of 75.0 degs, Horz Pol

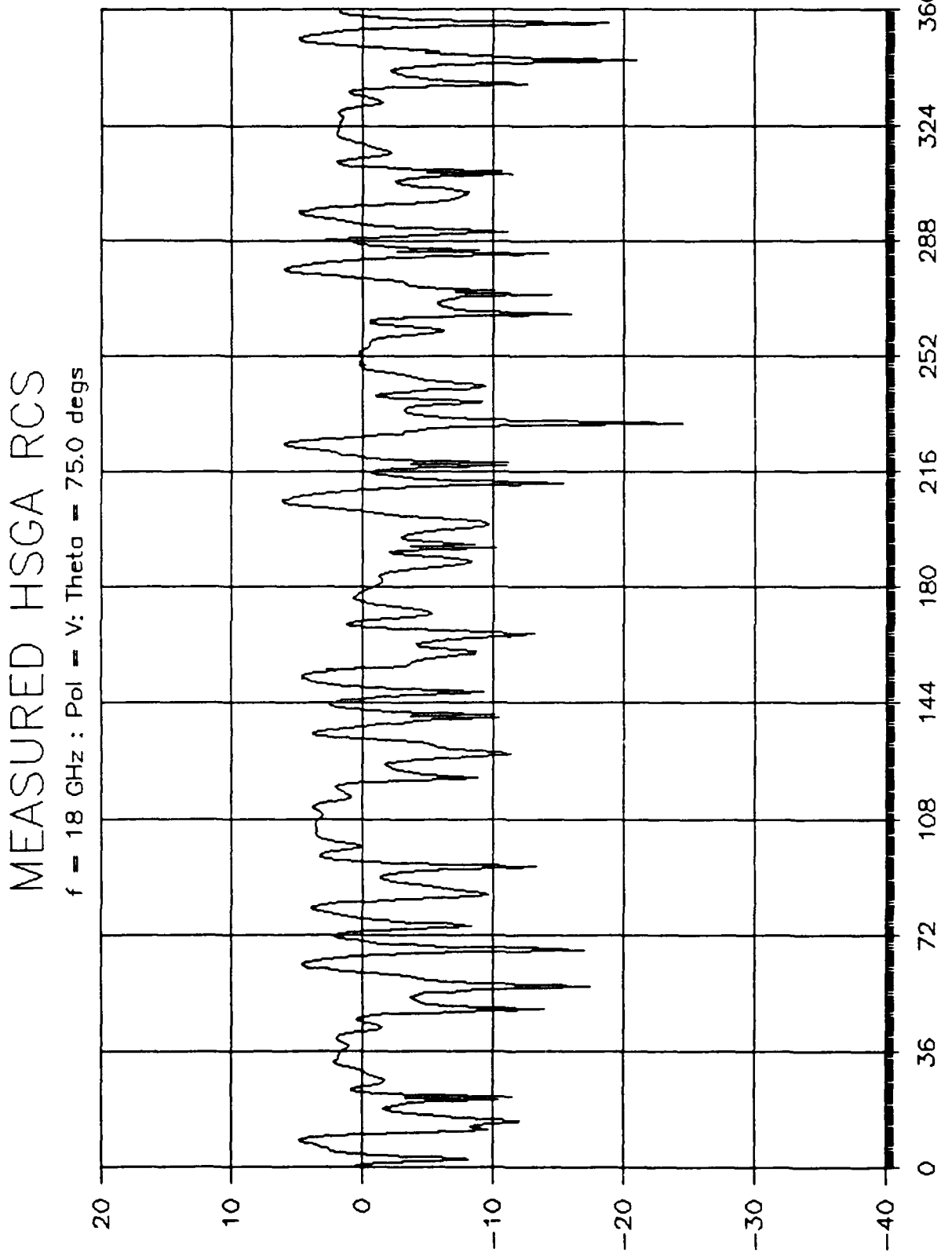

Figure E.6 Measured RCS: HSGA, Conical Cut, 18 GHz, Theta of 75.0 degs, Vert Pol

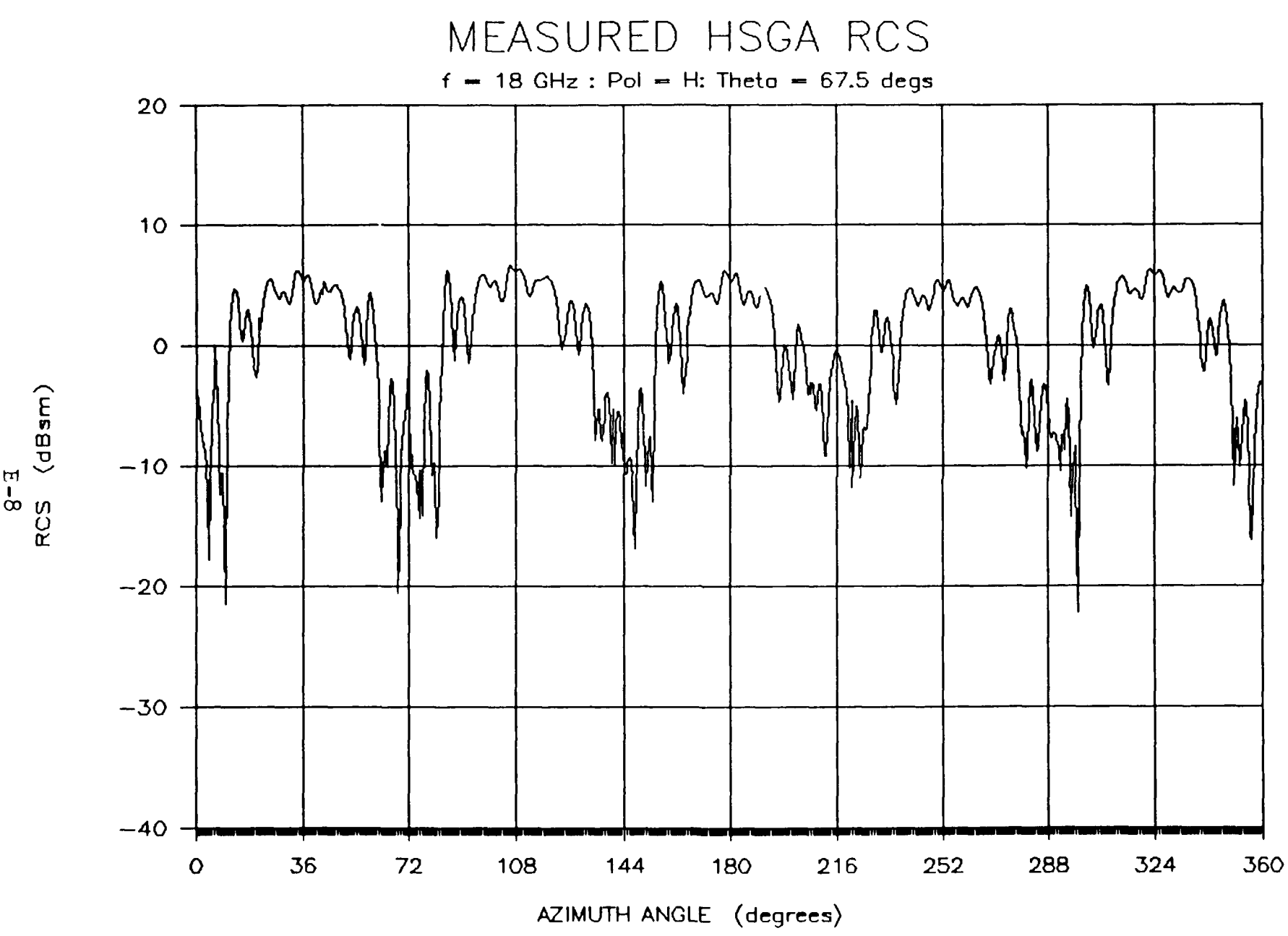

Figure E.7 Measured RCS: HSGA, Conical Cut, 18 GHz, Theta of 67.5 degs, Horz Pol

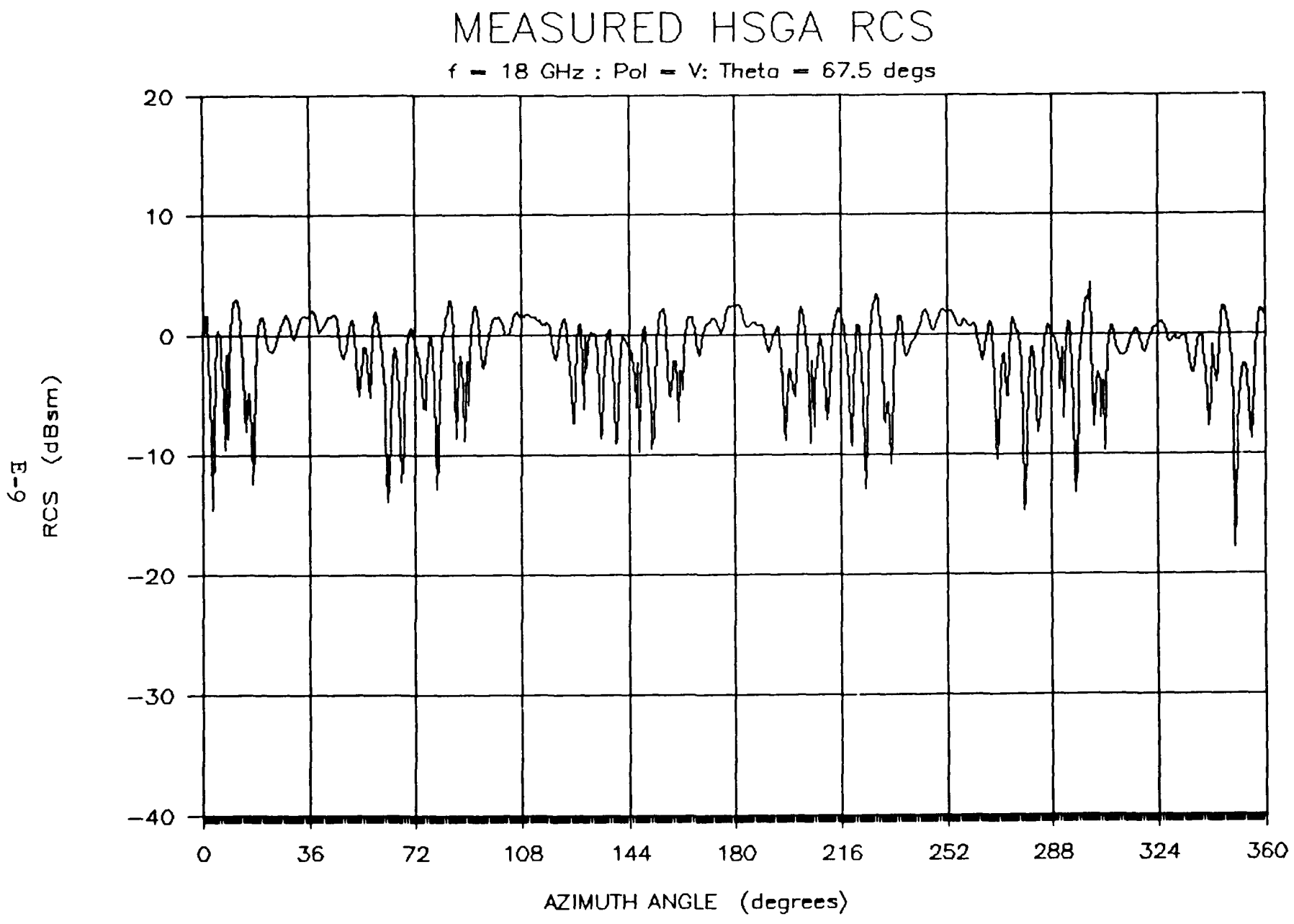

Figure E.8 Measured RCS: HSGA, Conical Cut, 18 GHz, Theta of 67.5 degs, Vert Pol

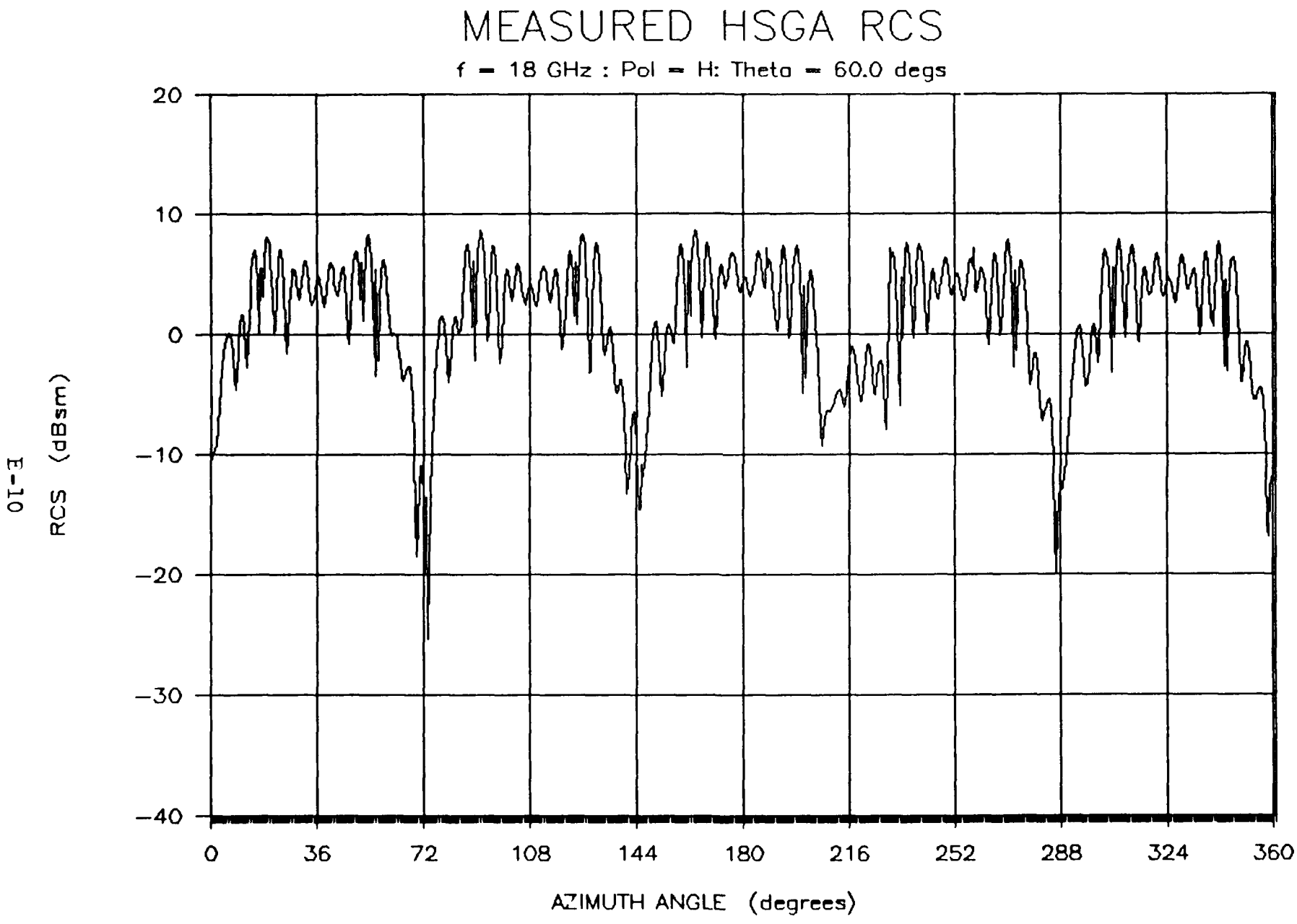

Figure E.9 Measured RCS: HSGA, Conical Cut, 18 GHz, Theta of 60.0 degs, Horz Pol

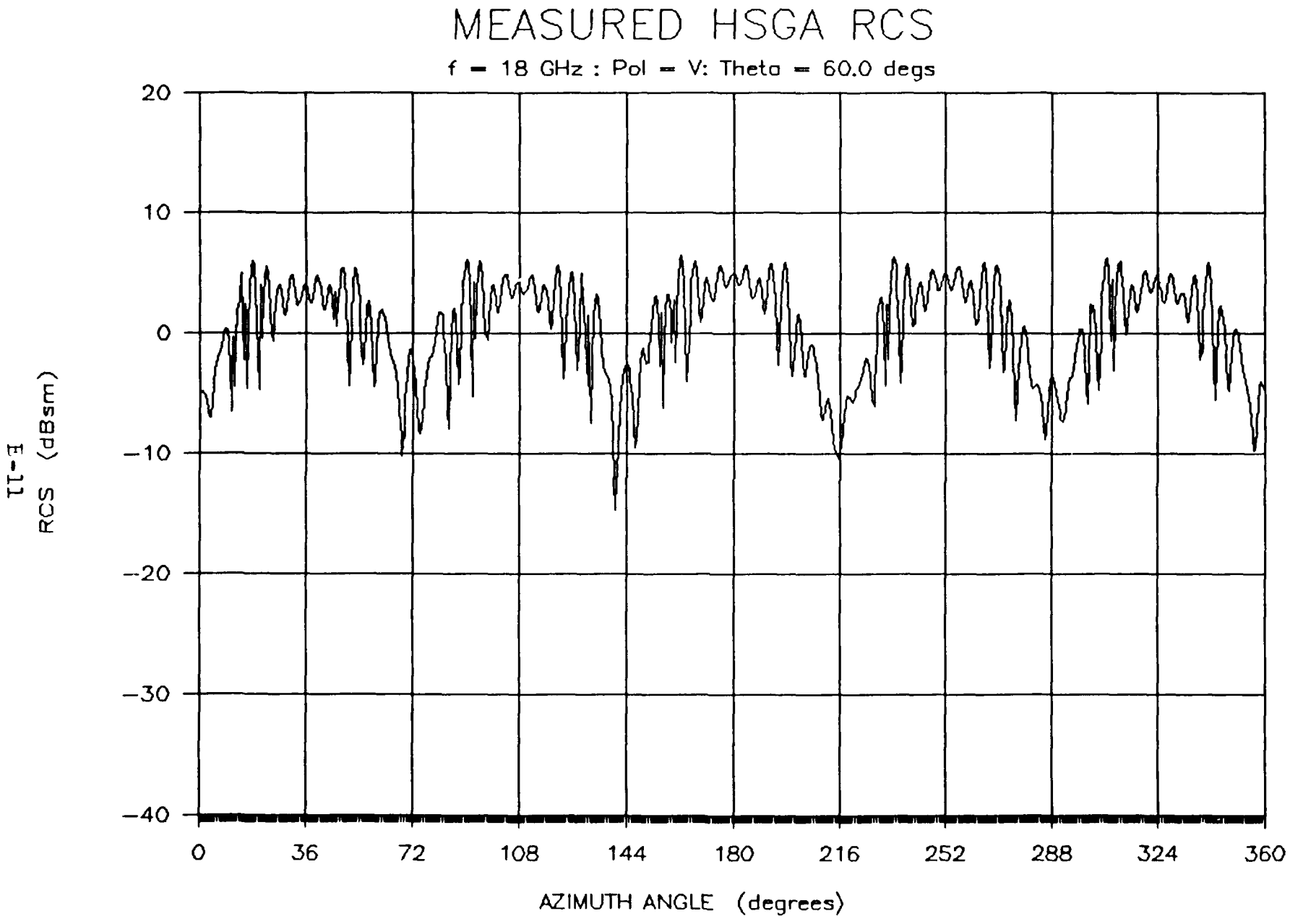

Figure E.10 Measured RCS: HSGA, Conical Cut, 18 GHz, Theta of 60.0 degs, Vert Pol

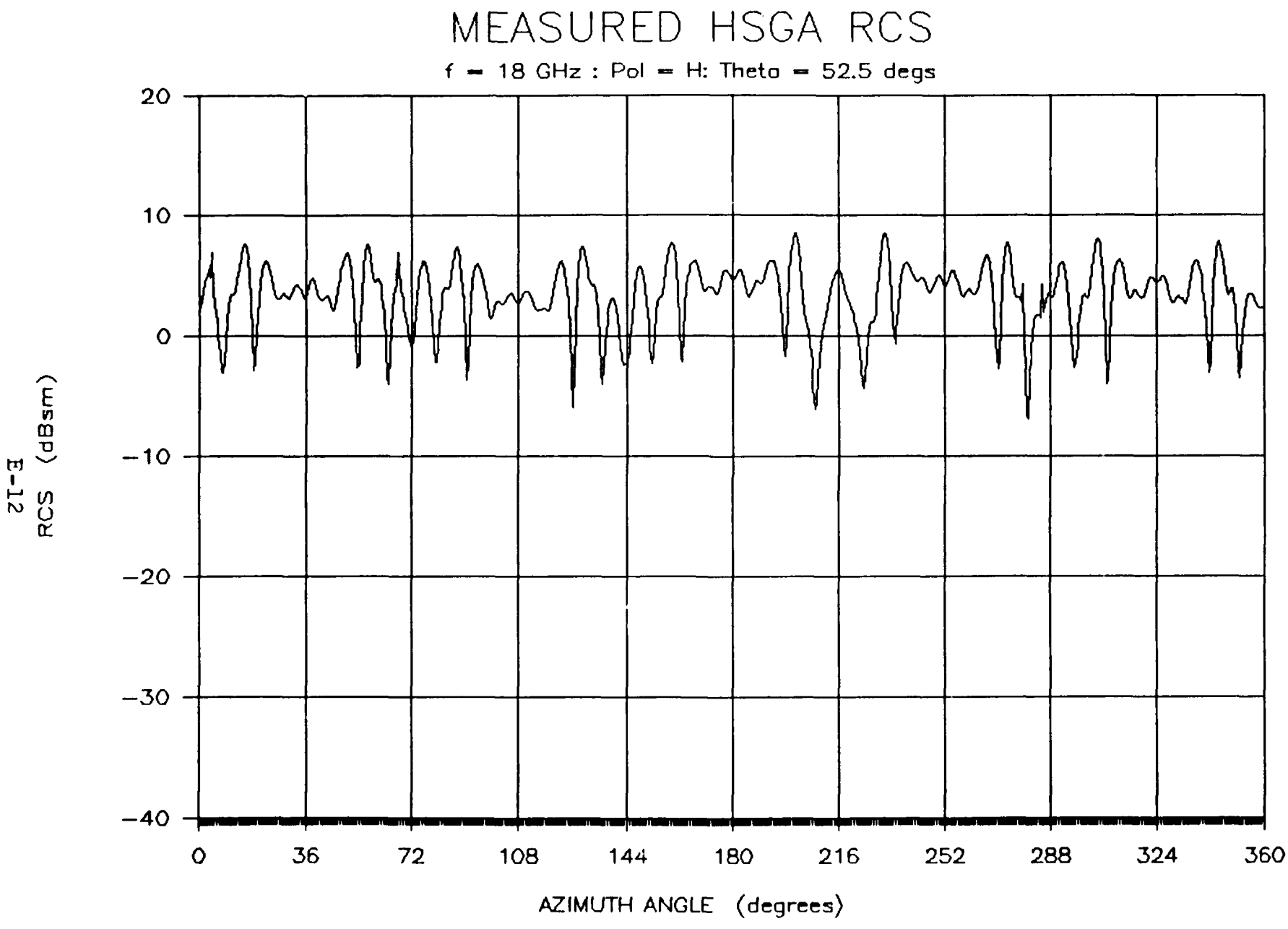

Figure E.11 Measured RCS: HSGA, Conical Cut, 18 GHz, Theta of 52.5 degs, Horz Pol

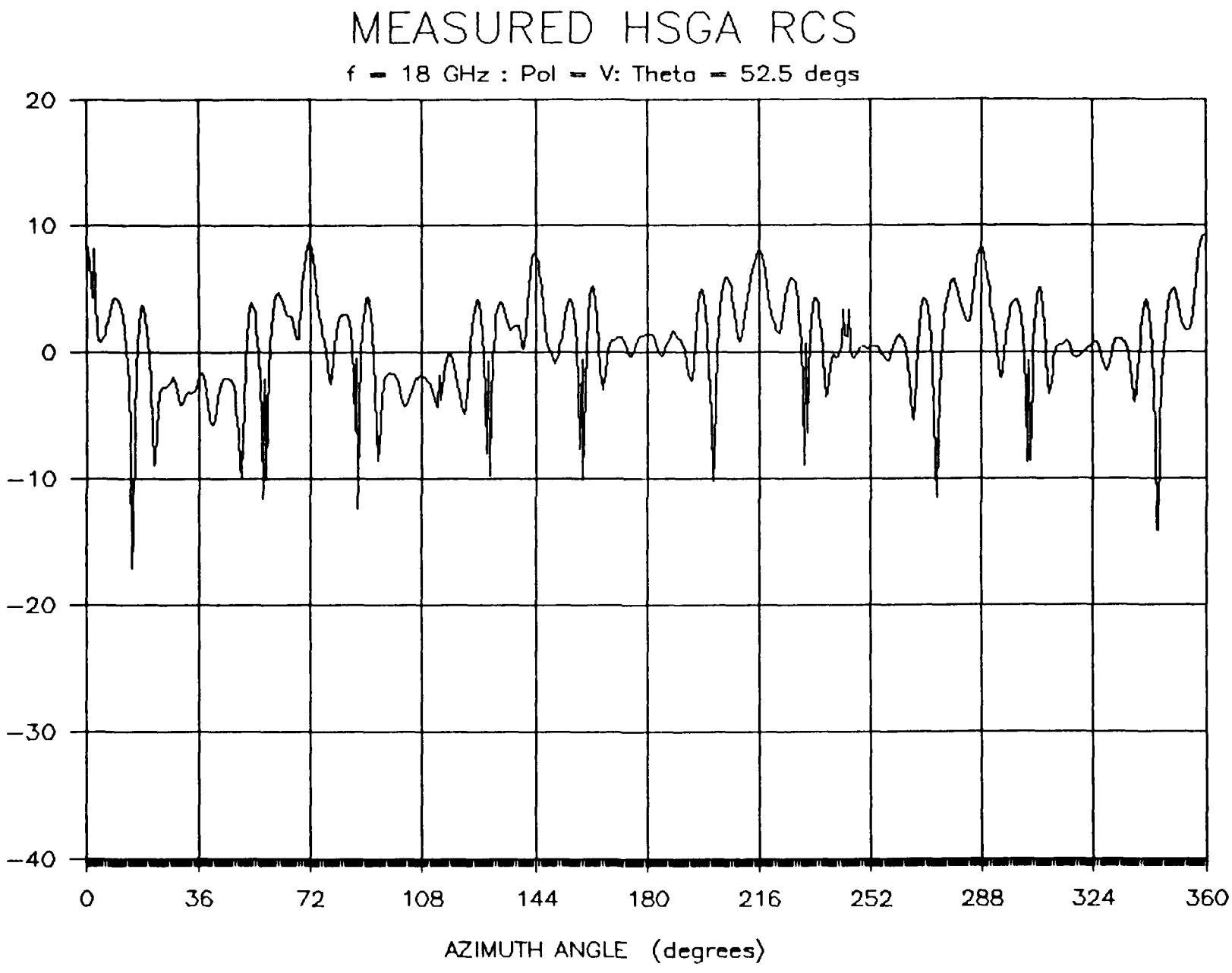

Figure E.12 Measured RCS: HSGA, Conical Cut, 18 GHz, Theta of 52.5 degs, Vert Pol

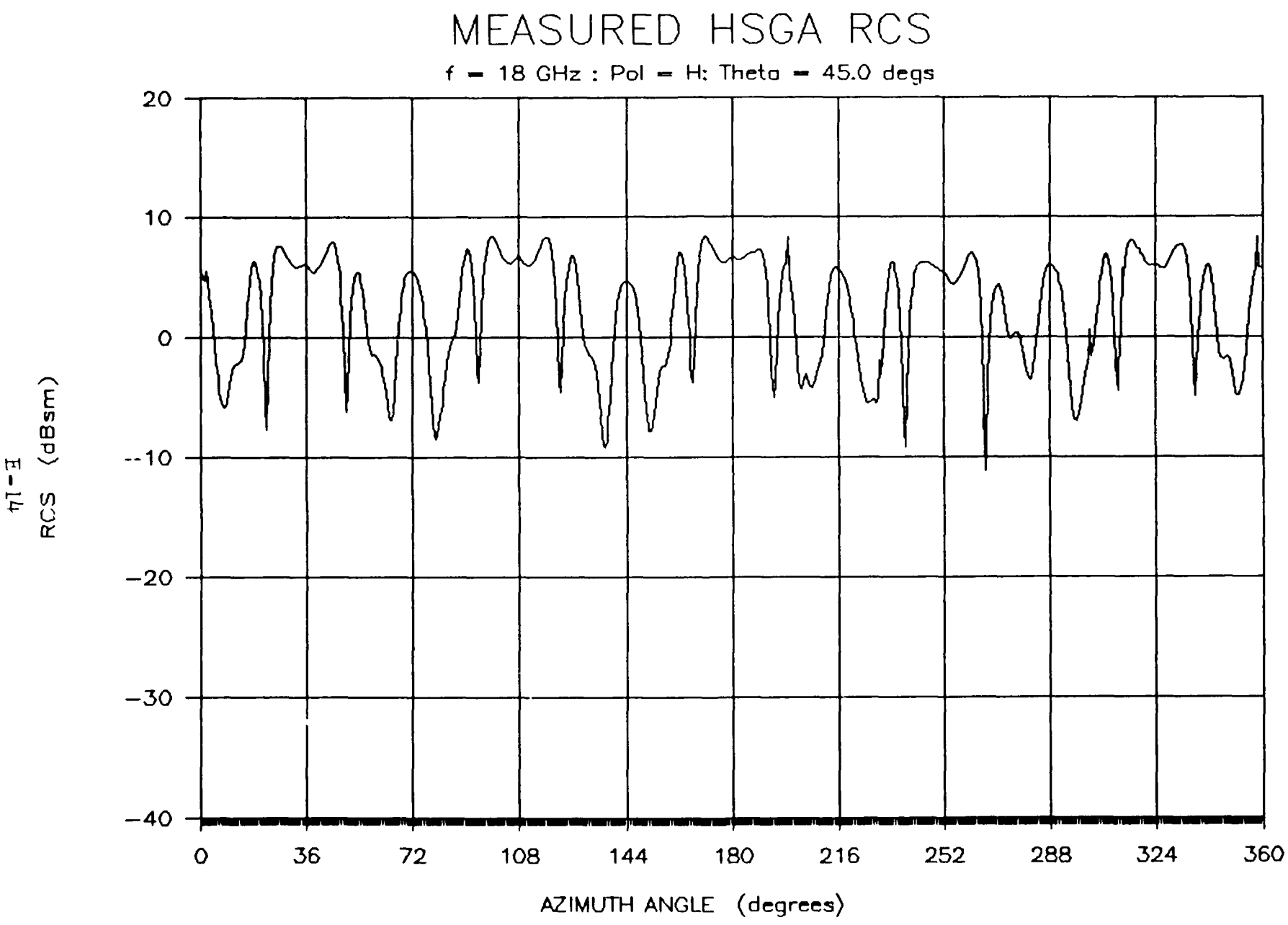

Figure E.13 Measured RCS: HSGA, Conical Cut, 18 GHz, Theta of 45.0 degs, Horz Pol

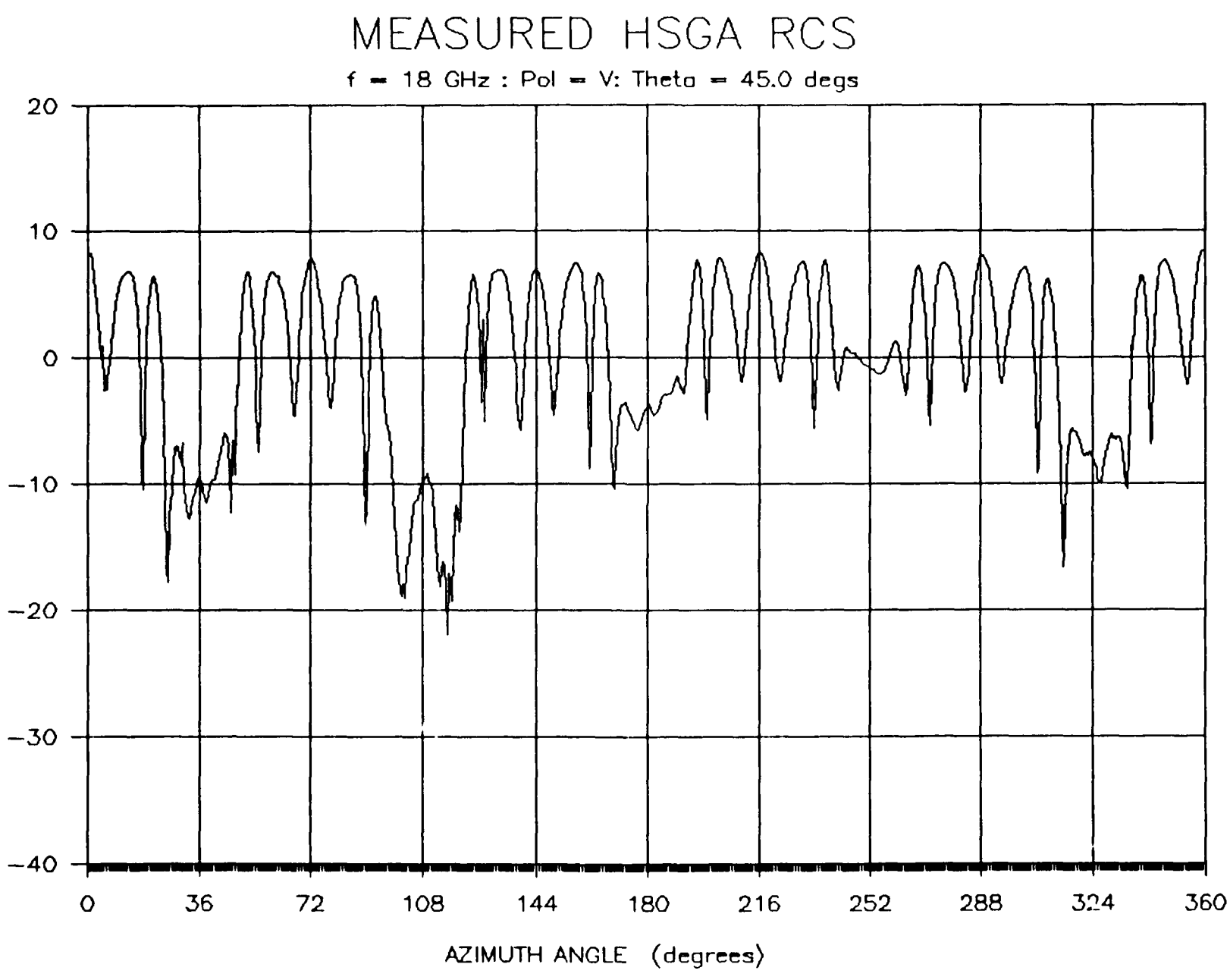

Figure E.14 Measured RCS: HSGA, Conical Cut, 18 GHz, Theta of 45.0 degs, Vert Pol

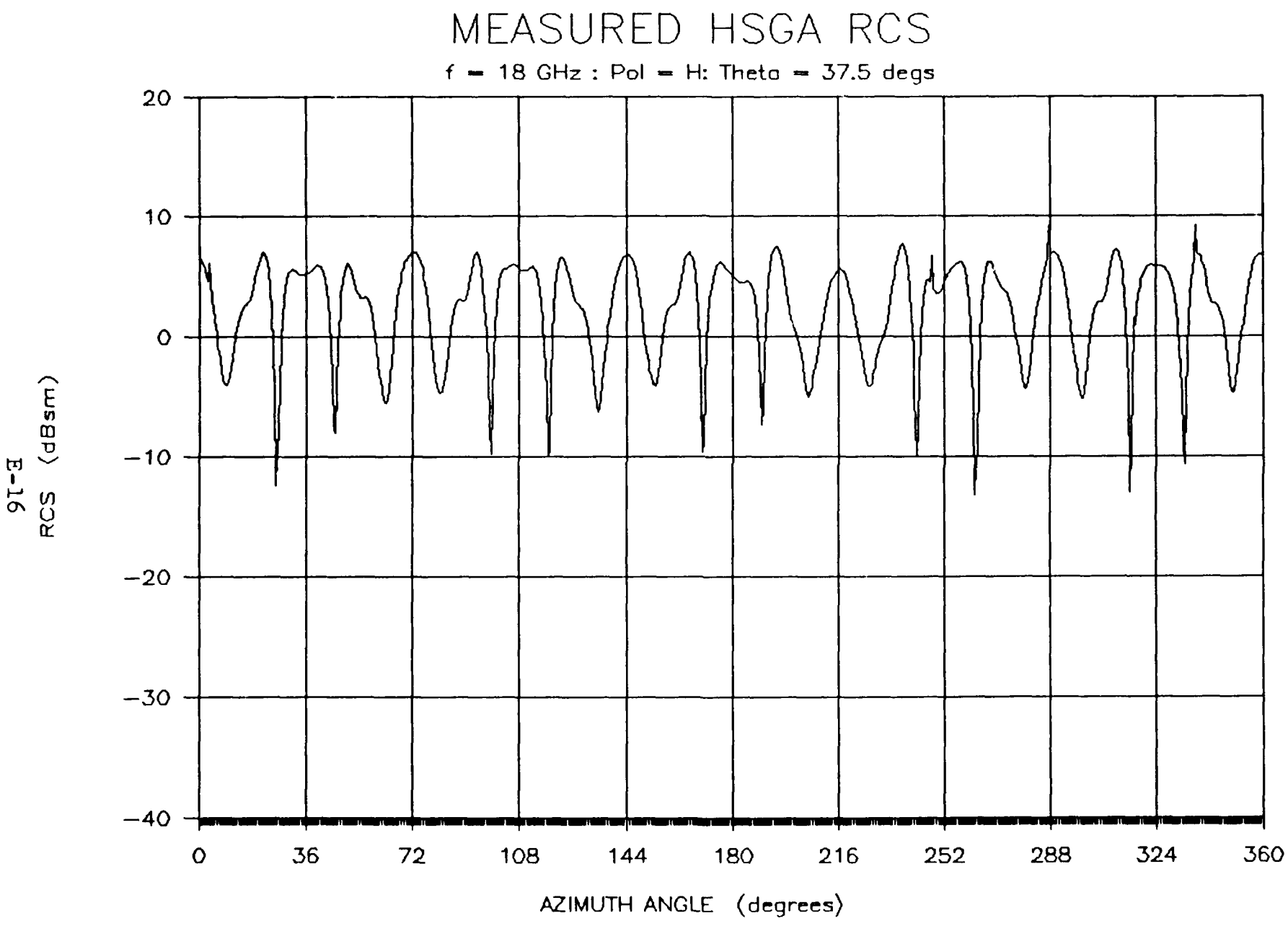

Figure E.15 Measured RCS: HSGA, Conical Cut, 18 GHz, Theta of 37.5 degs, Horz Pol

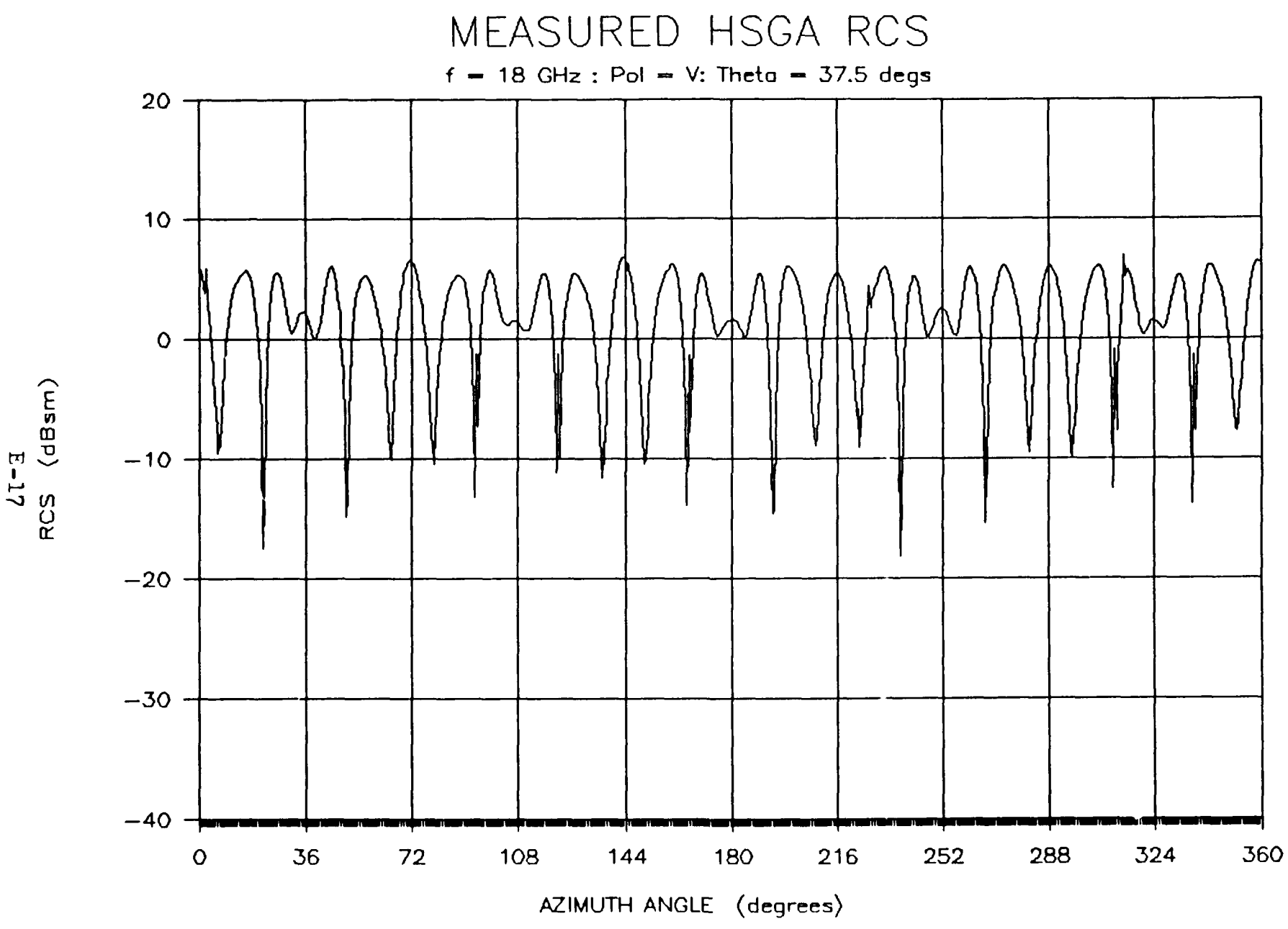

Figure E.16 Measured RCS: HSGA, Conical Cut, 18 GHz, Theta of 37.5 degs, Vert Pol

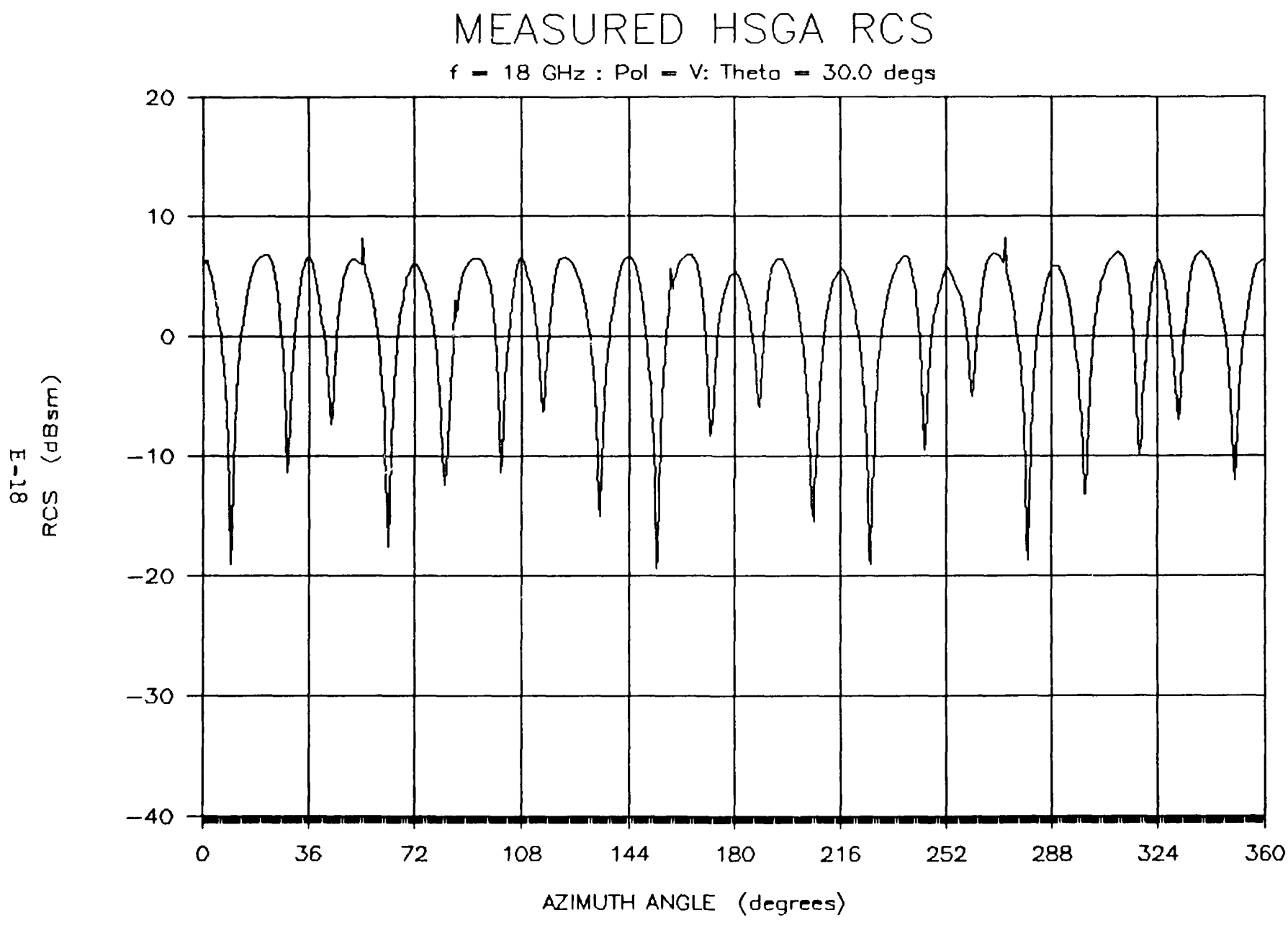

Figure E.18 Measured RCS: HSGA, Conical Cut, 18 GHz, Theta of 30.0 degs, Vert Pol

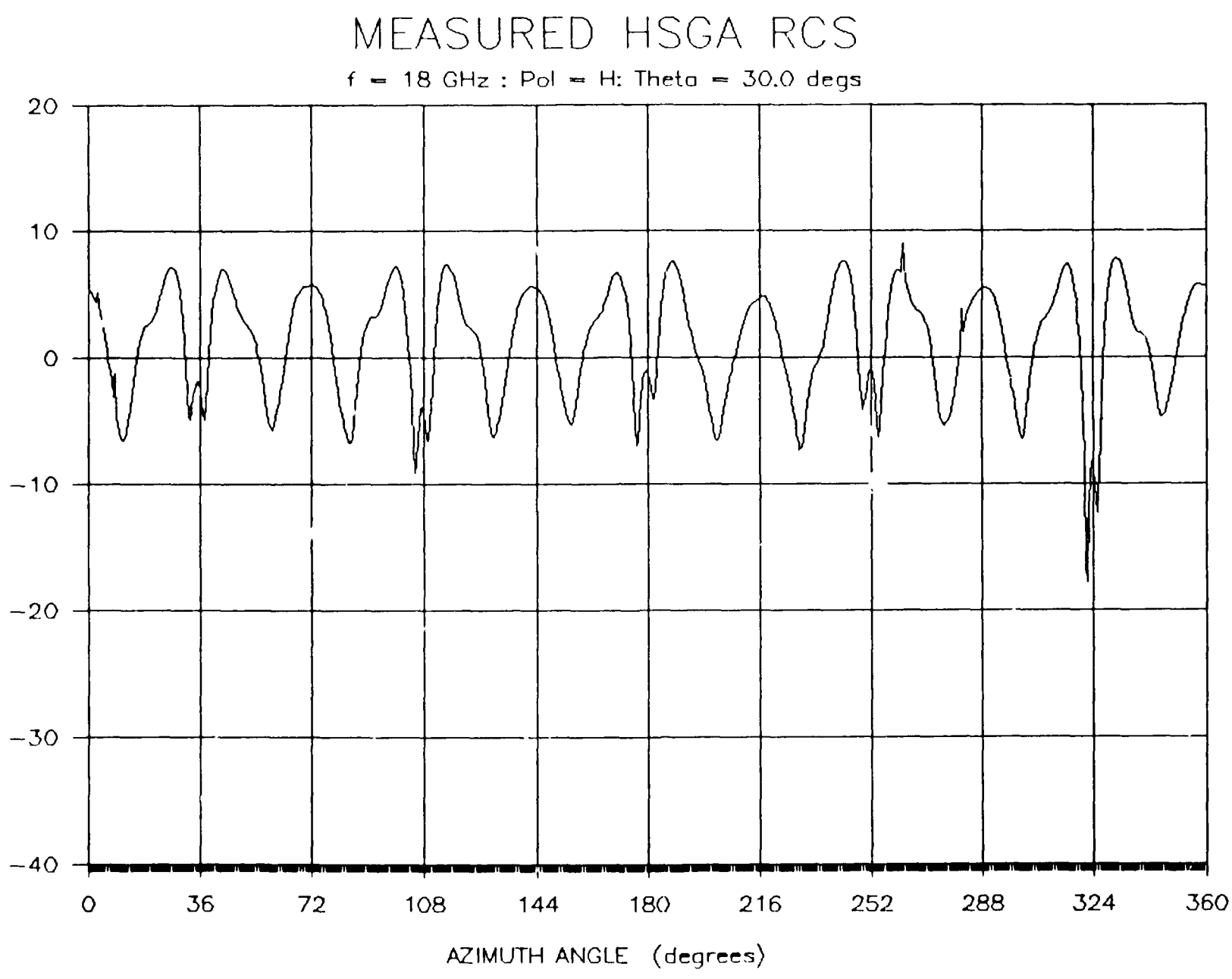

Figure E.17 Measured RCS: HSGA, Conical Cut, 18 GHz, Theta of 30.0 degs, Horz Pol

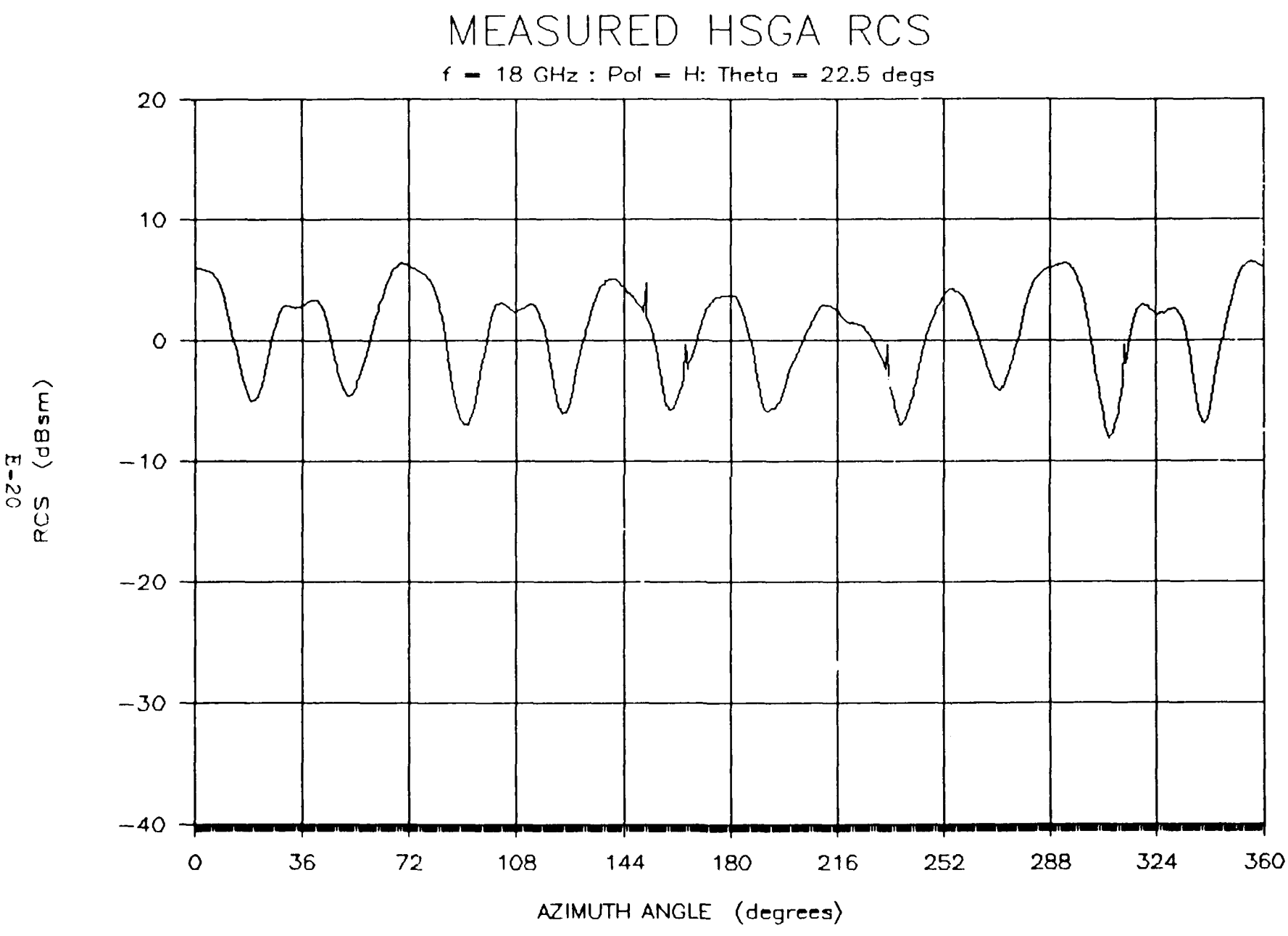

Figure E.19 Measured RCS: HSGA, Conical Cut, 18 GHz, Theta of 22.5 degs, Horz Pol

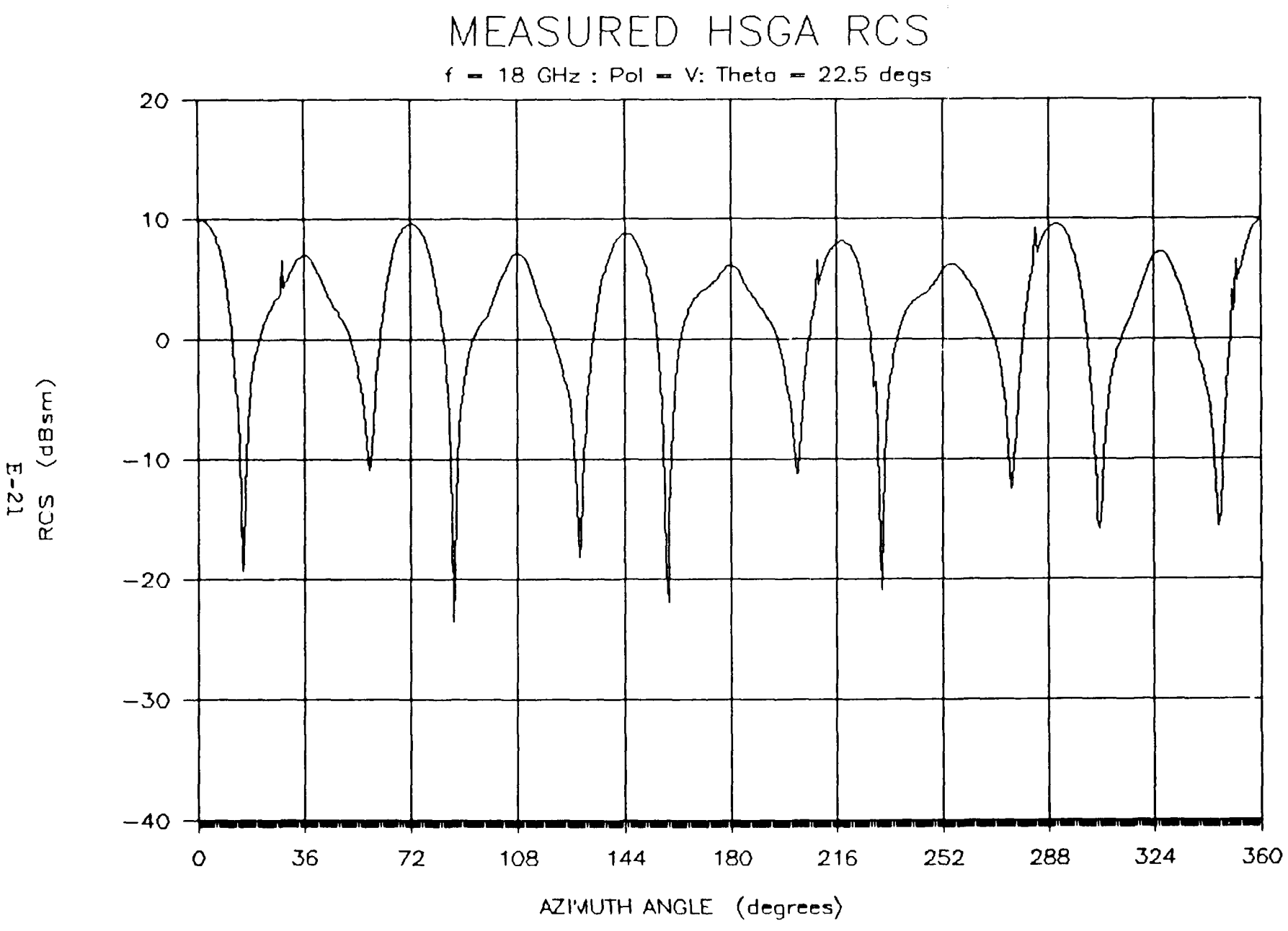

Figure E.20 Measured RCS: HSGA, Conical Cut, 18 GHz, Theta of 22.5 degs, Vert Pol

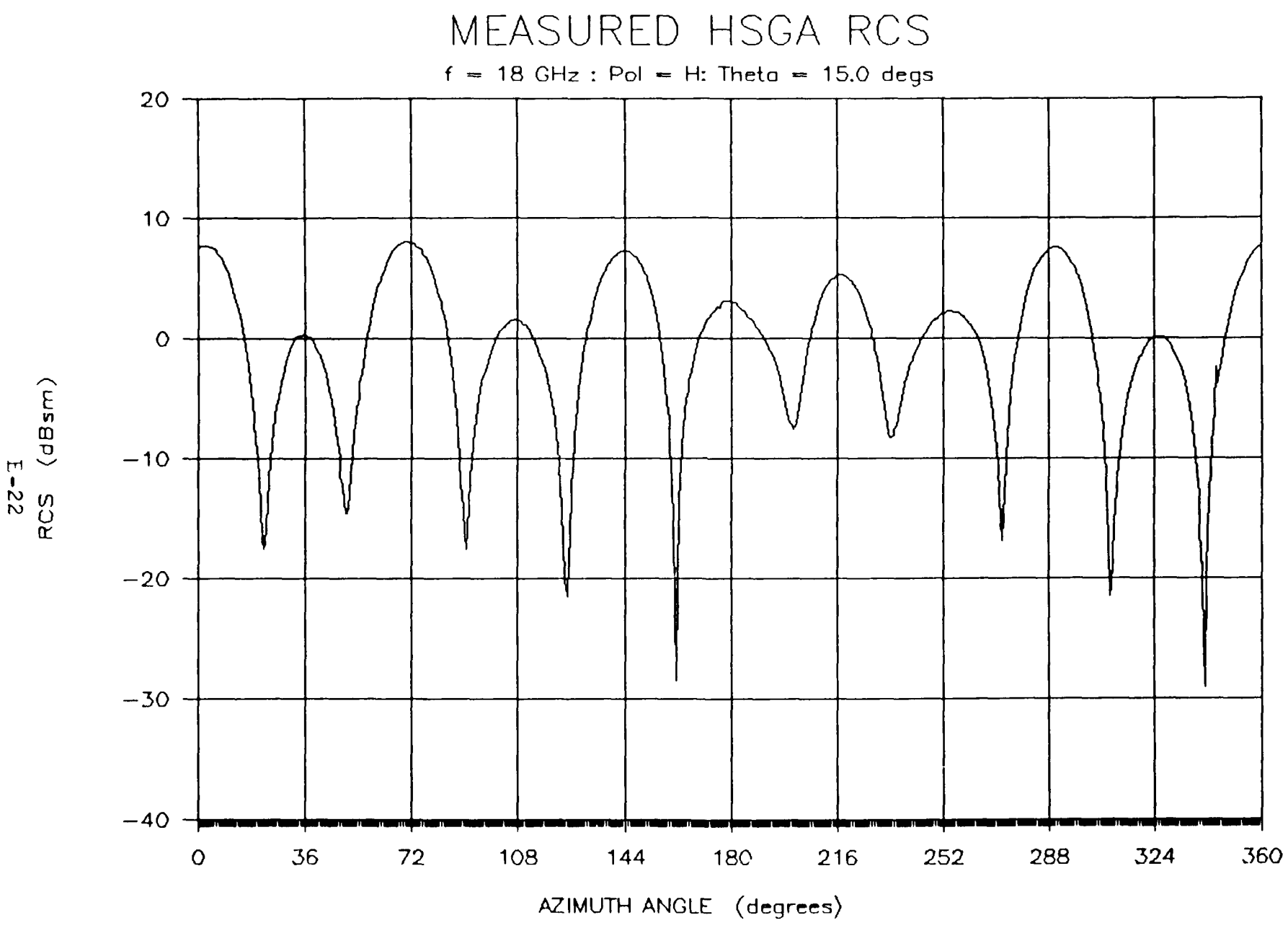

Figure E.21 Measured RCS: HSGA, Conical Cut, 18 GHz, Theta of 15.0 degs, Horz Pol

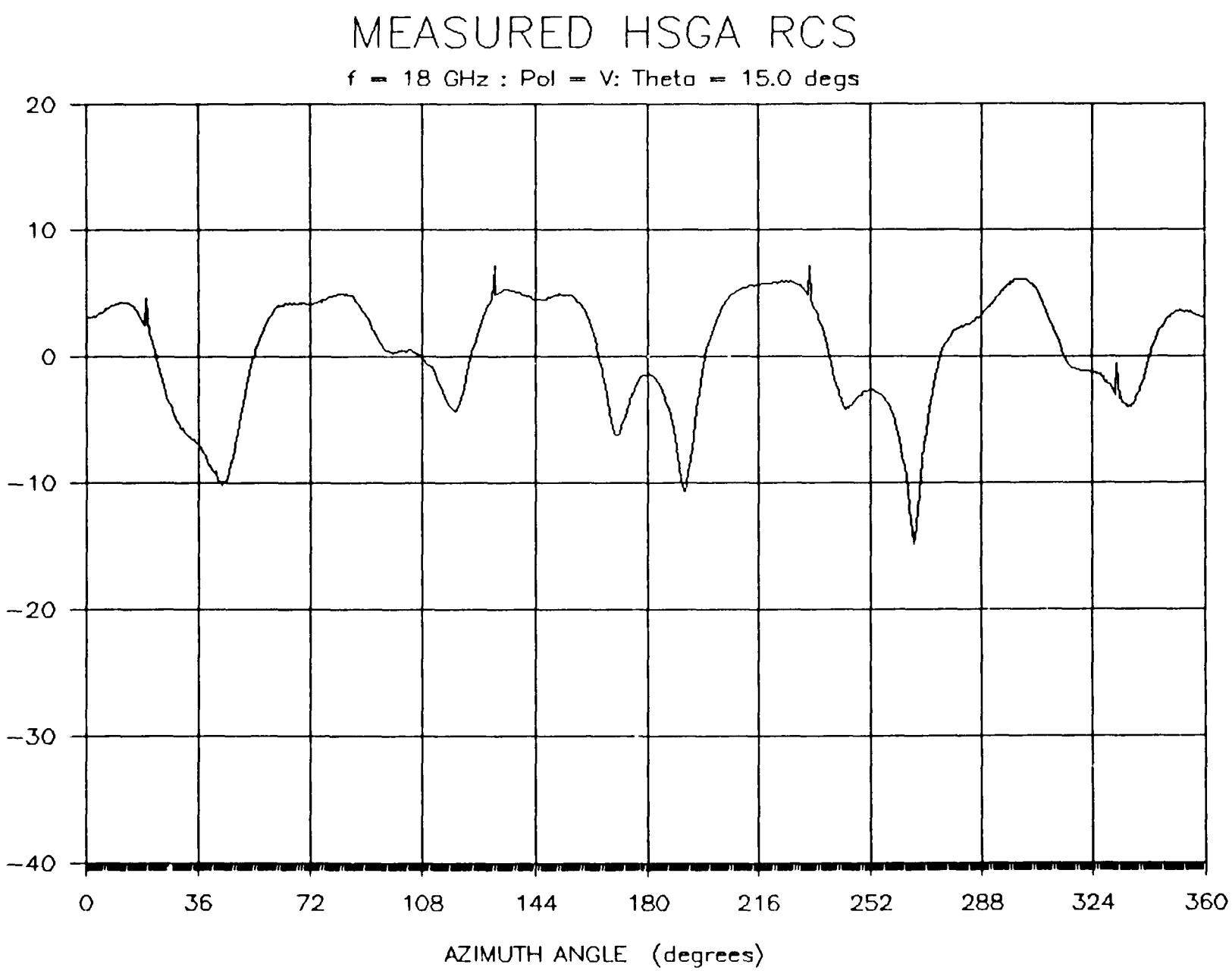

Figure E.22 Measured RCS: HSGA, Conical Cut, 18 GHz, Theta of 15.0 degs, Vert Pol

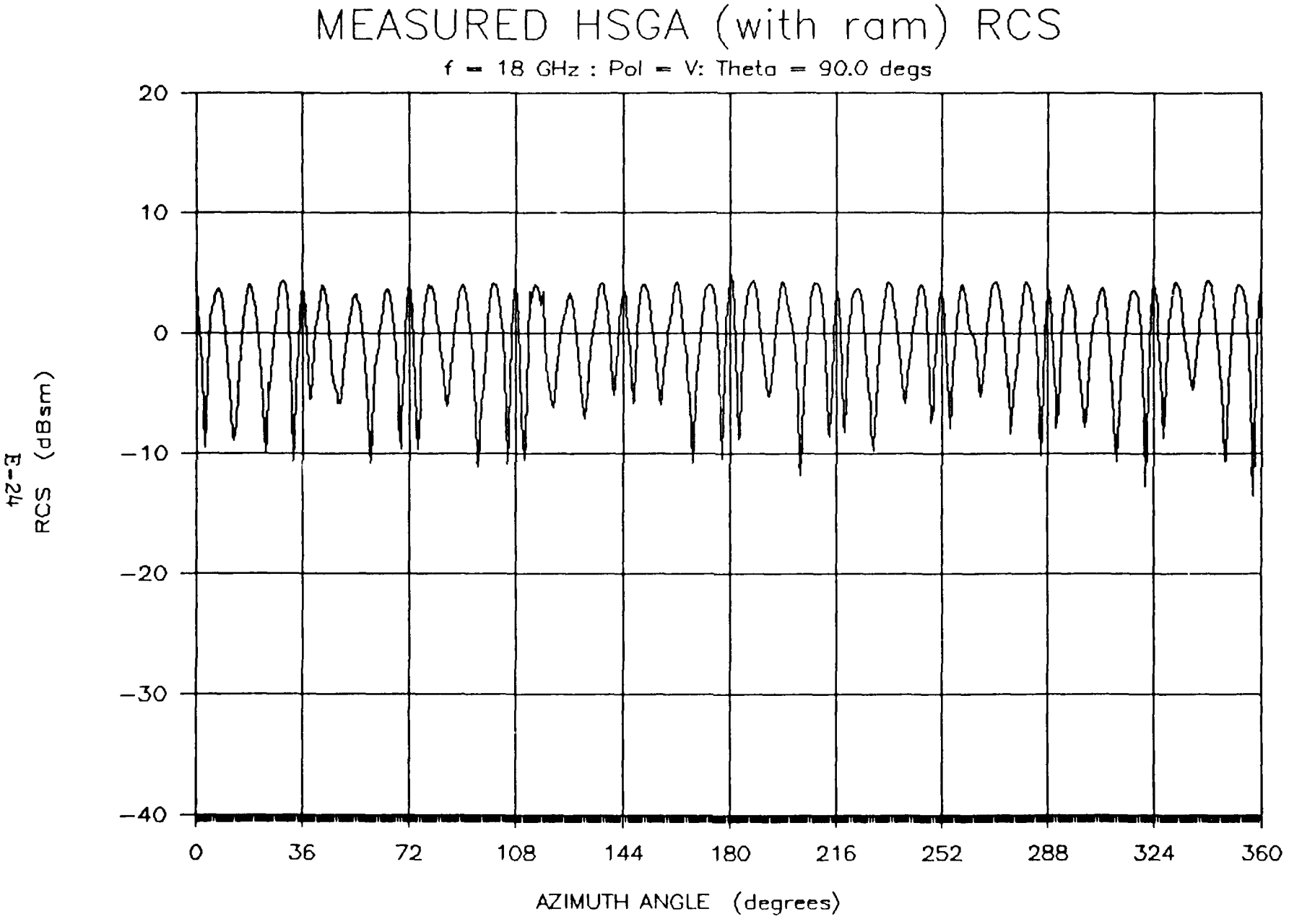

Figure E.23 Measured RCS: HSGA (with RAM), Conical Cut, 18 GHz, Theta of 90.0 degs,Vert Pol

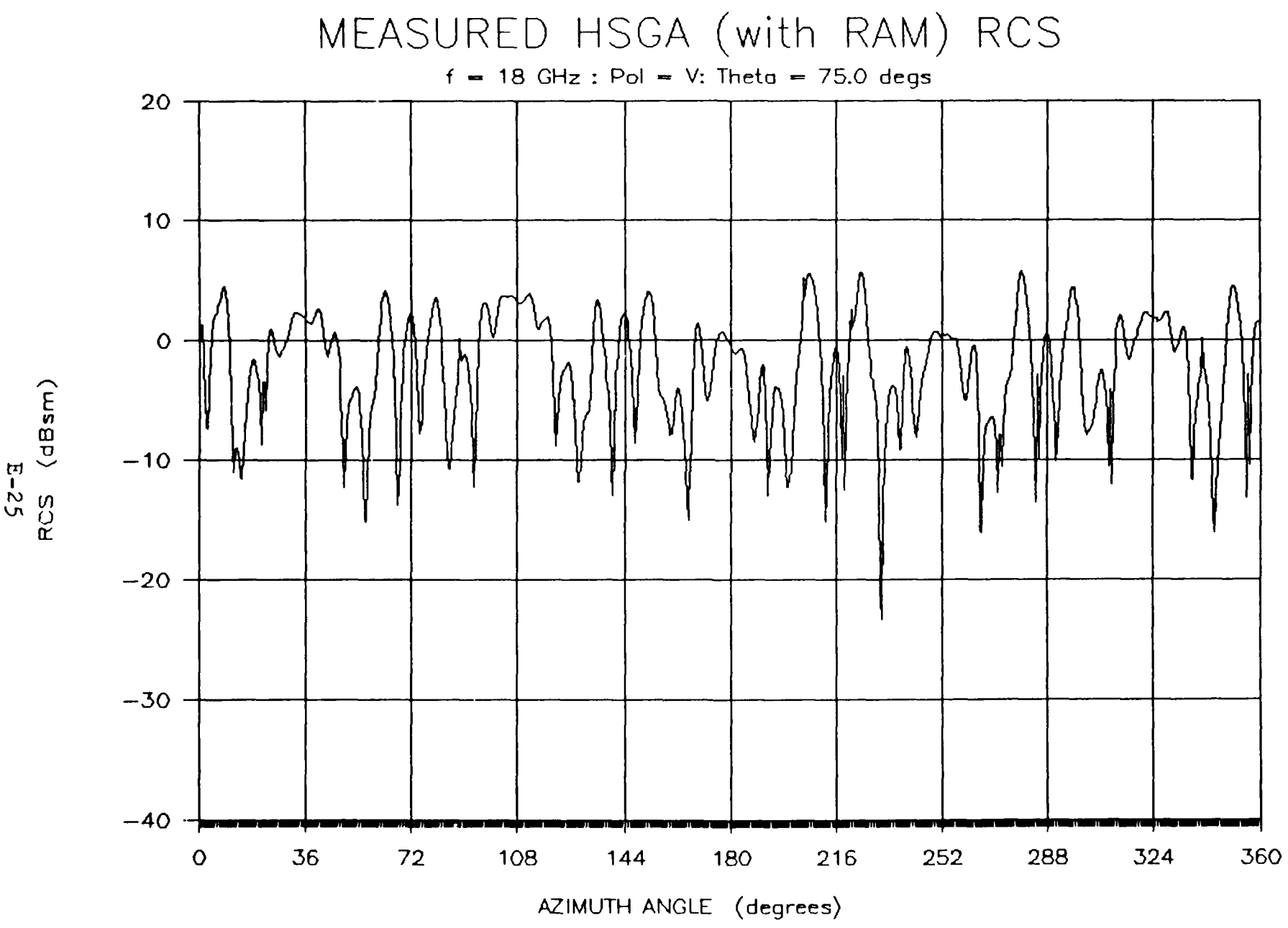

Figure E.24 Measured RCS: HSGA (with RAM), Conical Cut, 18 Ghz, Theta of 75.0 degs, Vert Pol

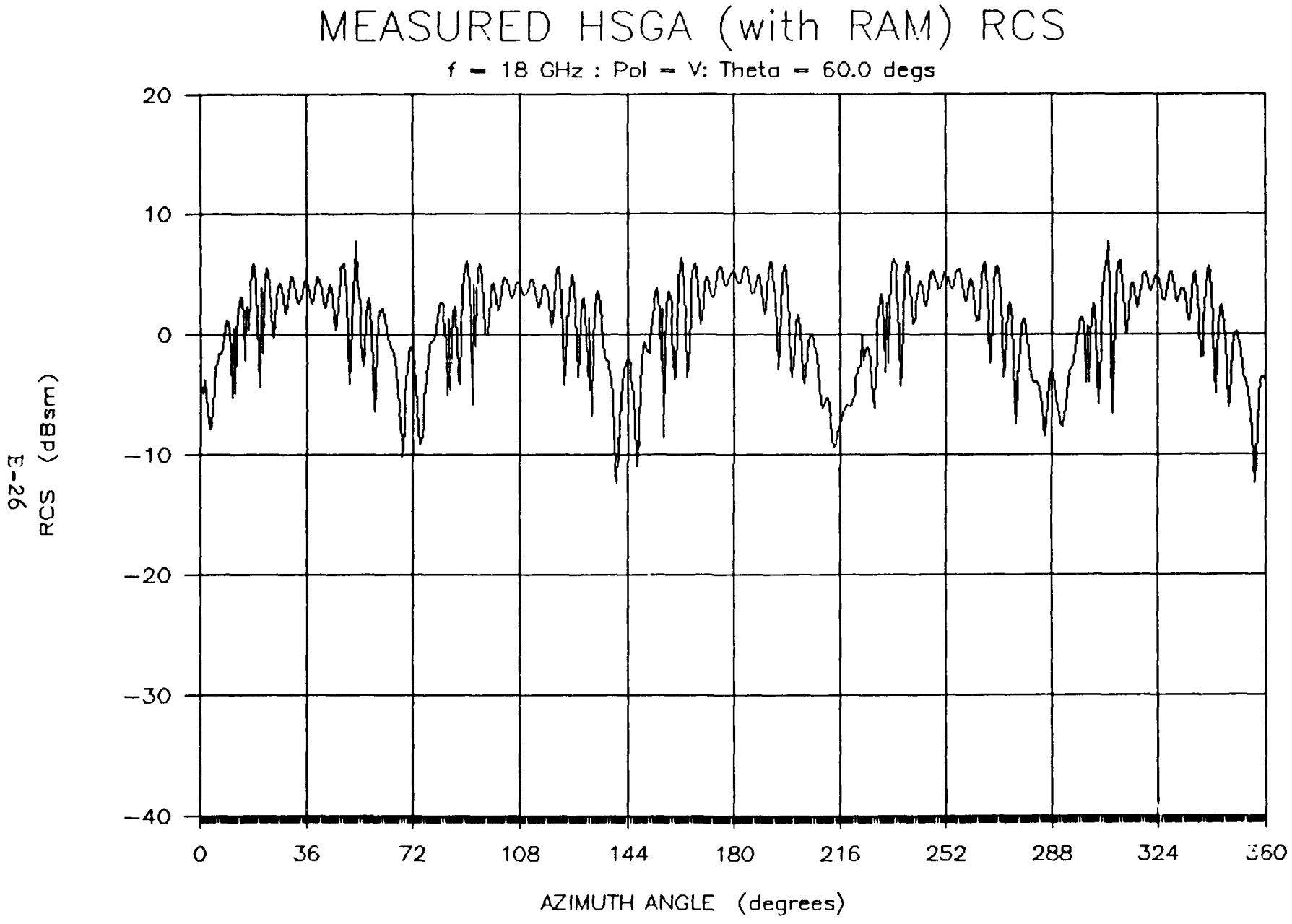

Figure E.25 Measured RCS: HSGA (with RAM), Conical Cut, 18 GHz, Theta of 60.0 degs, Vert Pol

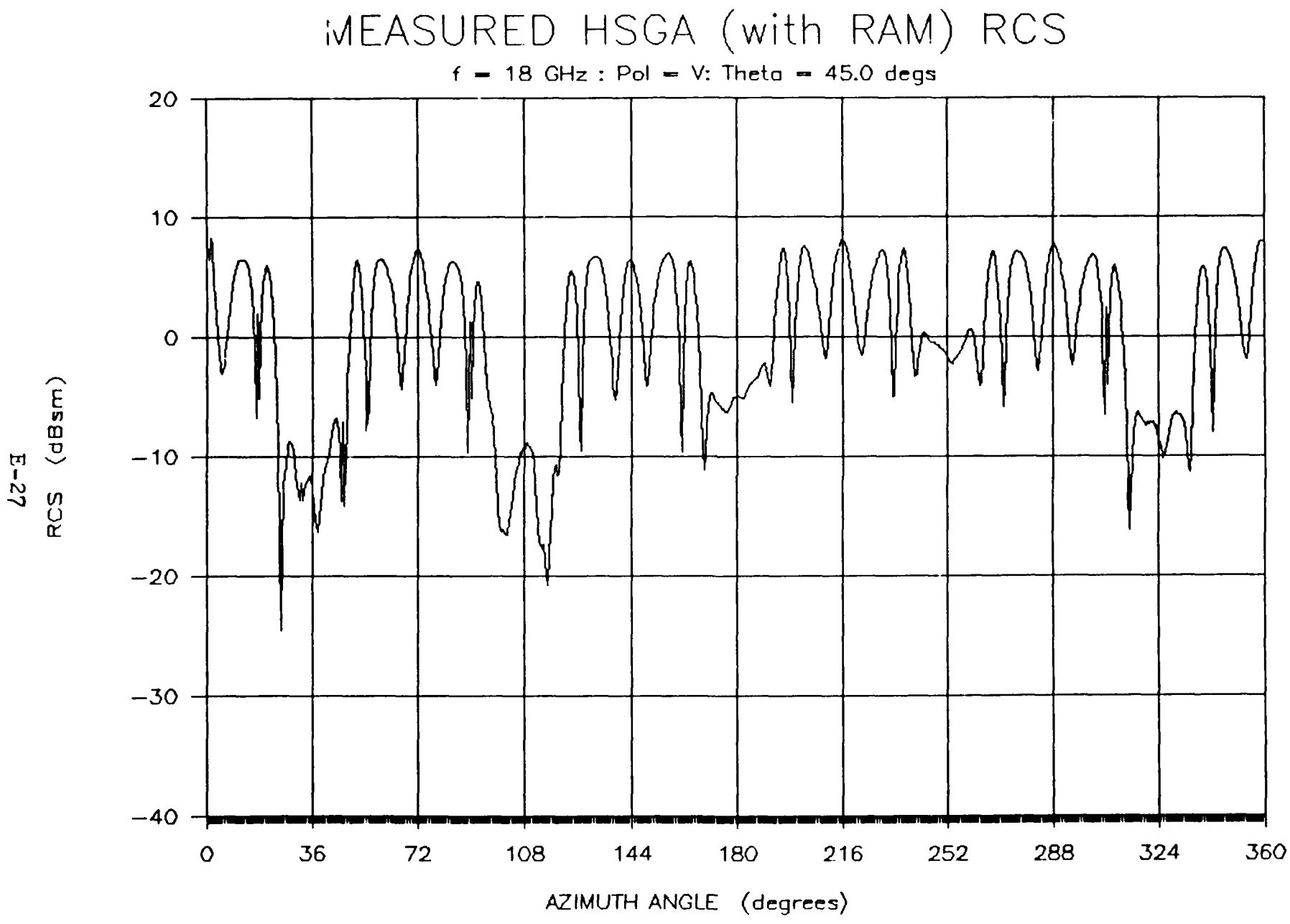

Figure E.26 Measured RCS: HSGA (with RAM), Conical Cut, 18 GHz, Theta of 45.0 degs, Vert Pol

APPENDIX F: RCS Data Distribution Plots

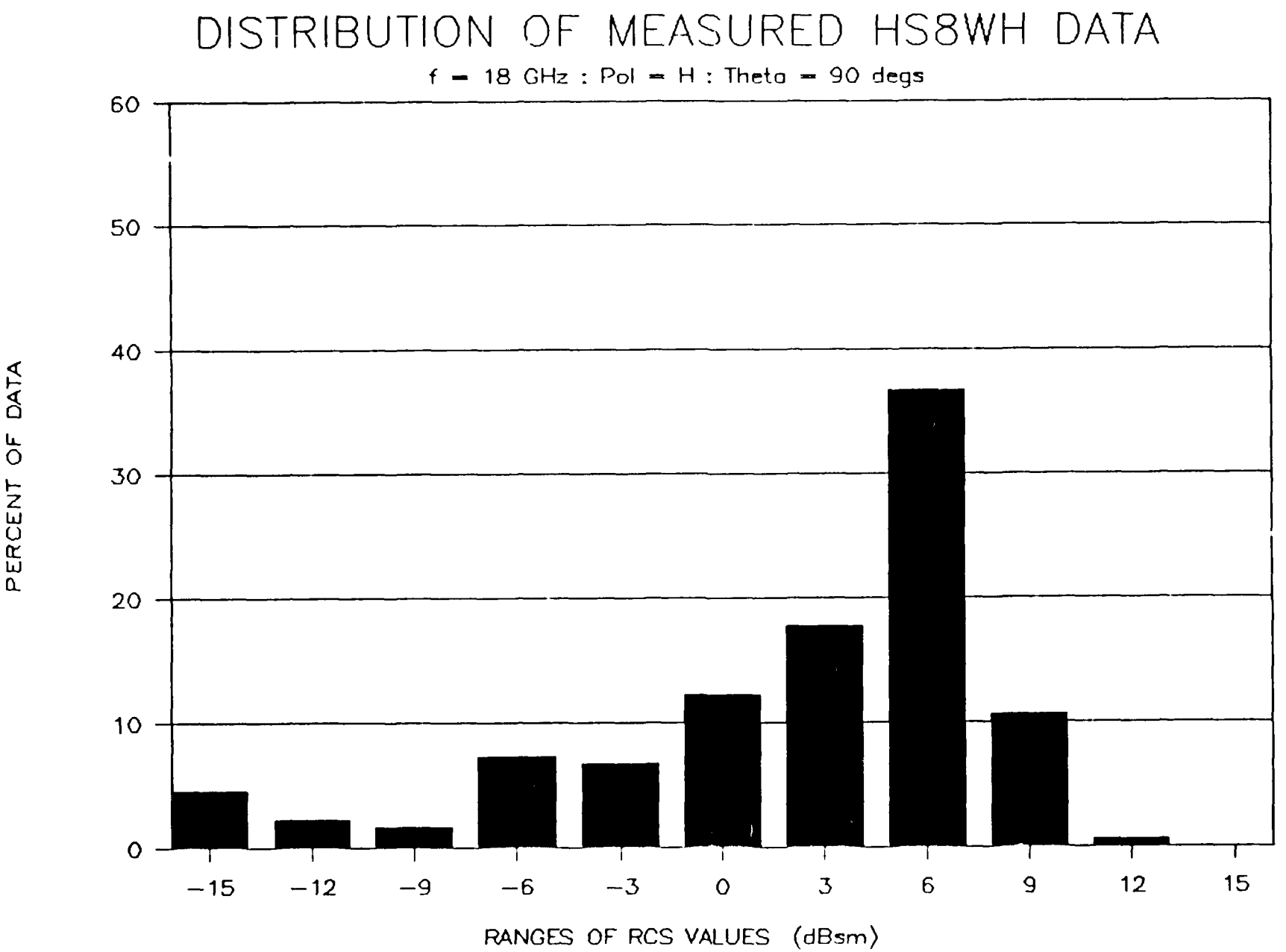

Figure F.1 Distribution of the Measured HS8WH RCS, 18 GHz, Theta of 90 degs, Horz Pol

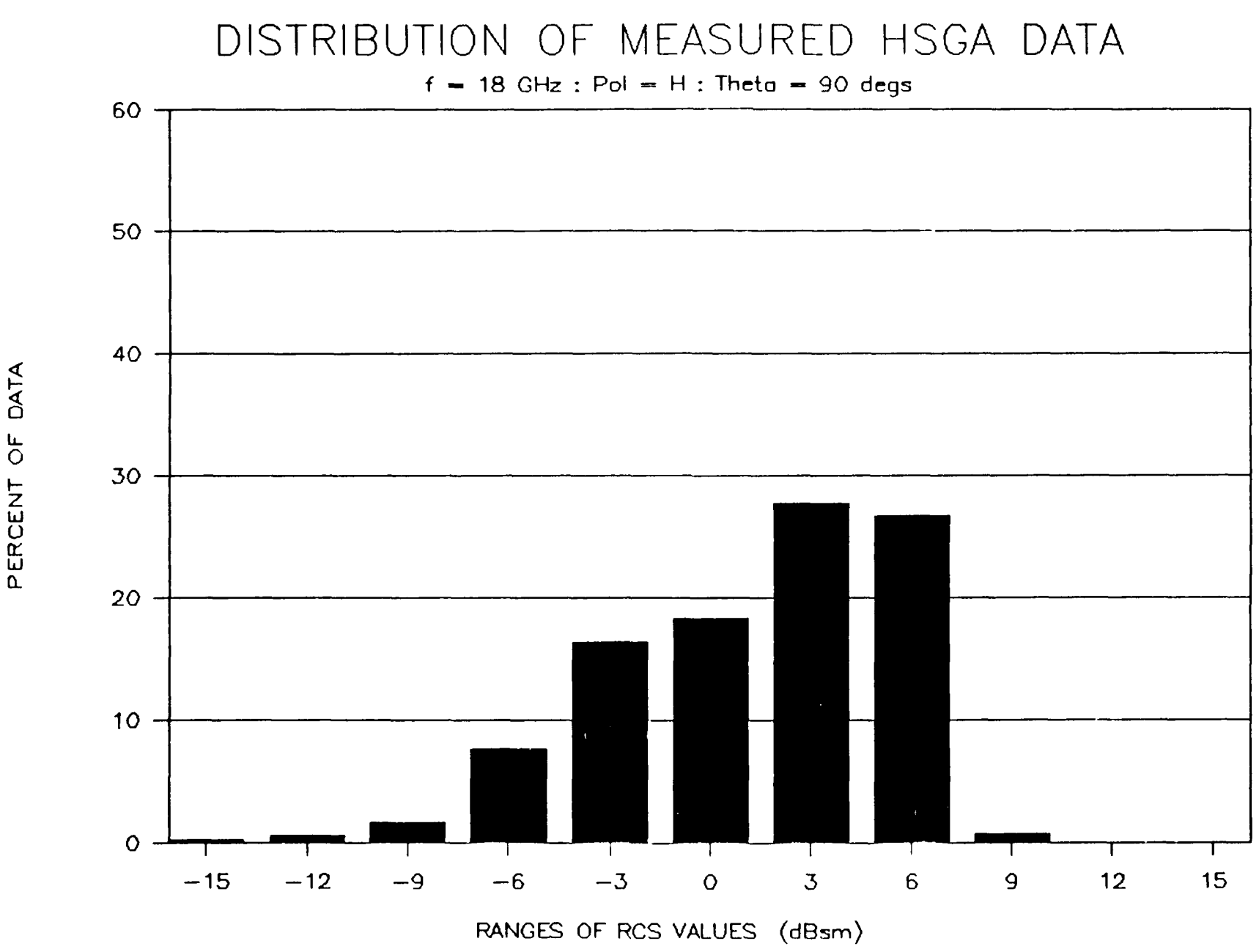

Figure F.2 Distribution of the Measured HSGA RCS, 18 GHz, Theta of 90 degs, Horz Pol

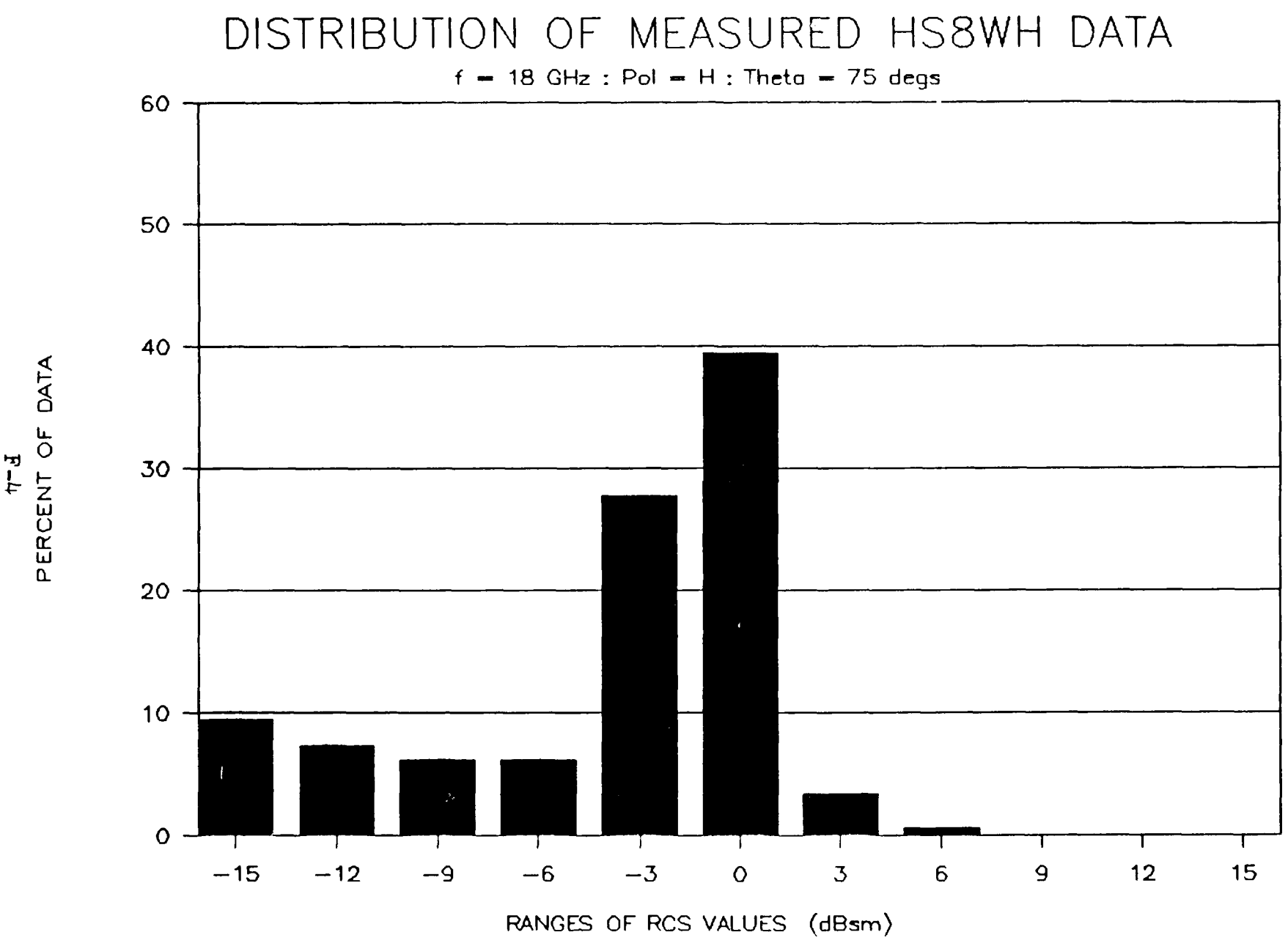

Figure F.3 Distribution of the Measured HS8WH RCS, 18 GHz, Theta of 75 degs, Horz Pol

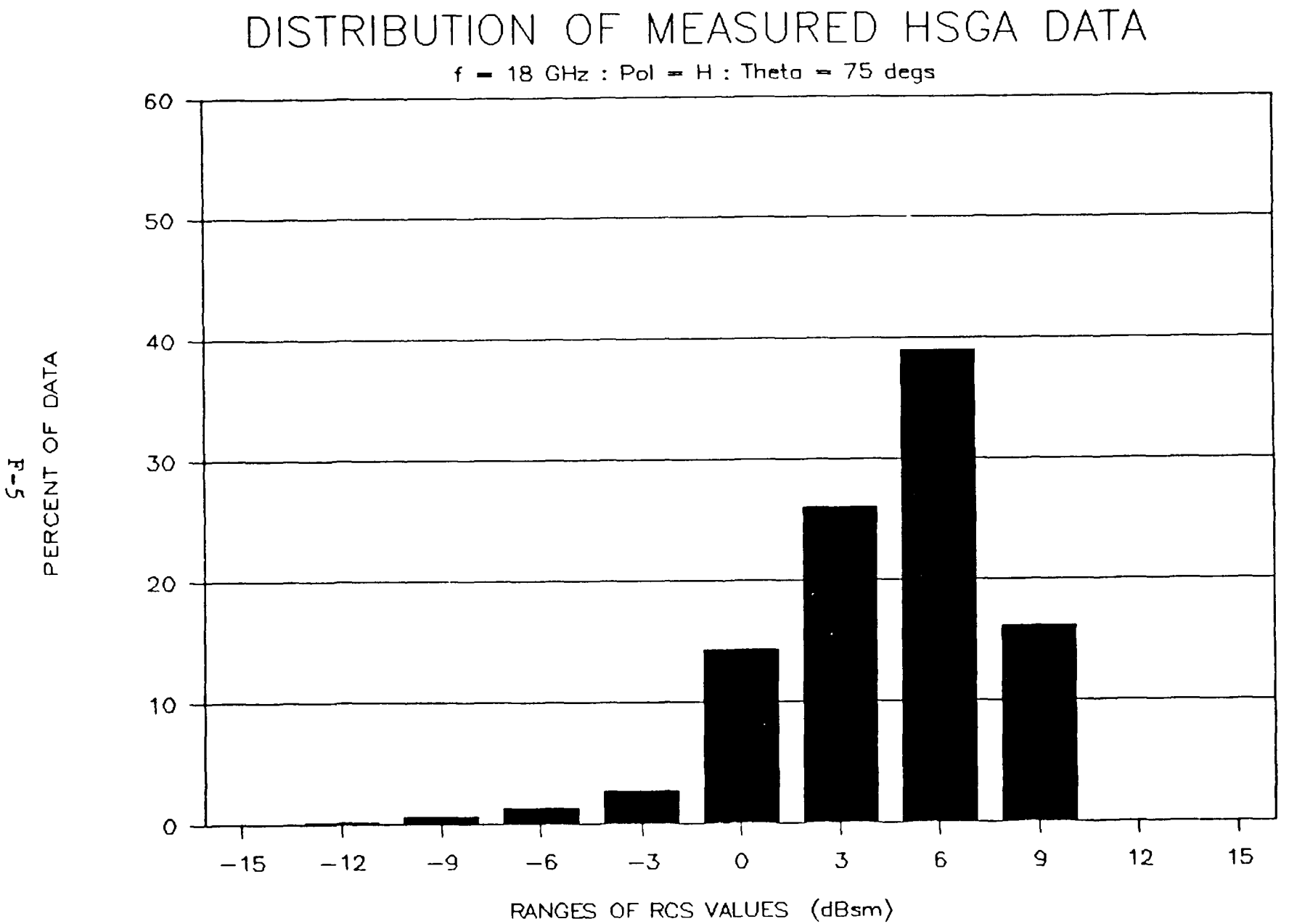

Figure F.4 Distribution of the Measured HSGA RCS, 18 GHz, Theta of 75 degs, Horz Pol

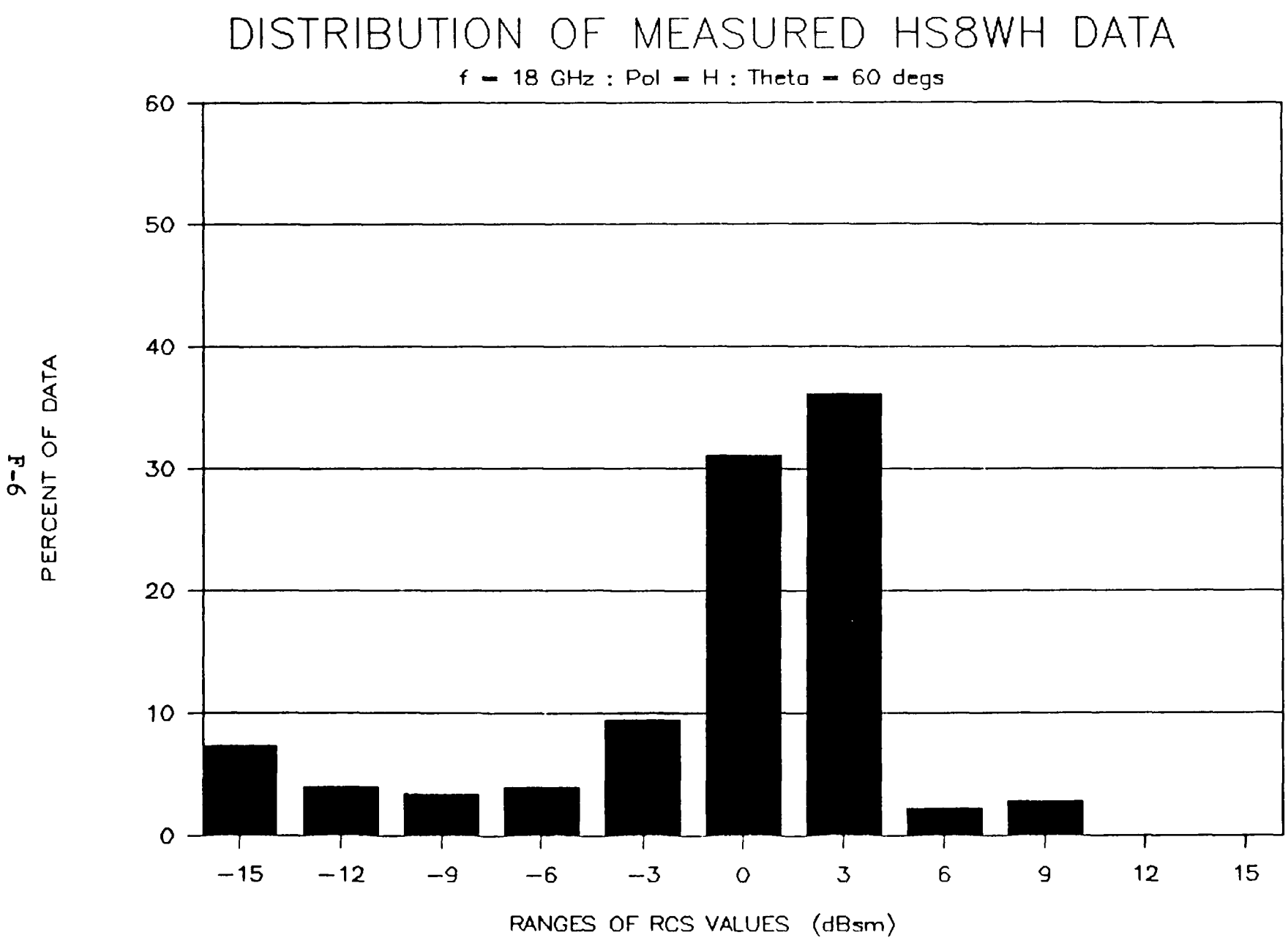

Figure F.5 Distribution of the Measured HS8WH RCS, 18 GHz, Theta of 60 degs, Horz Pol

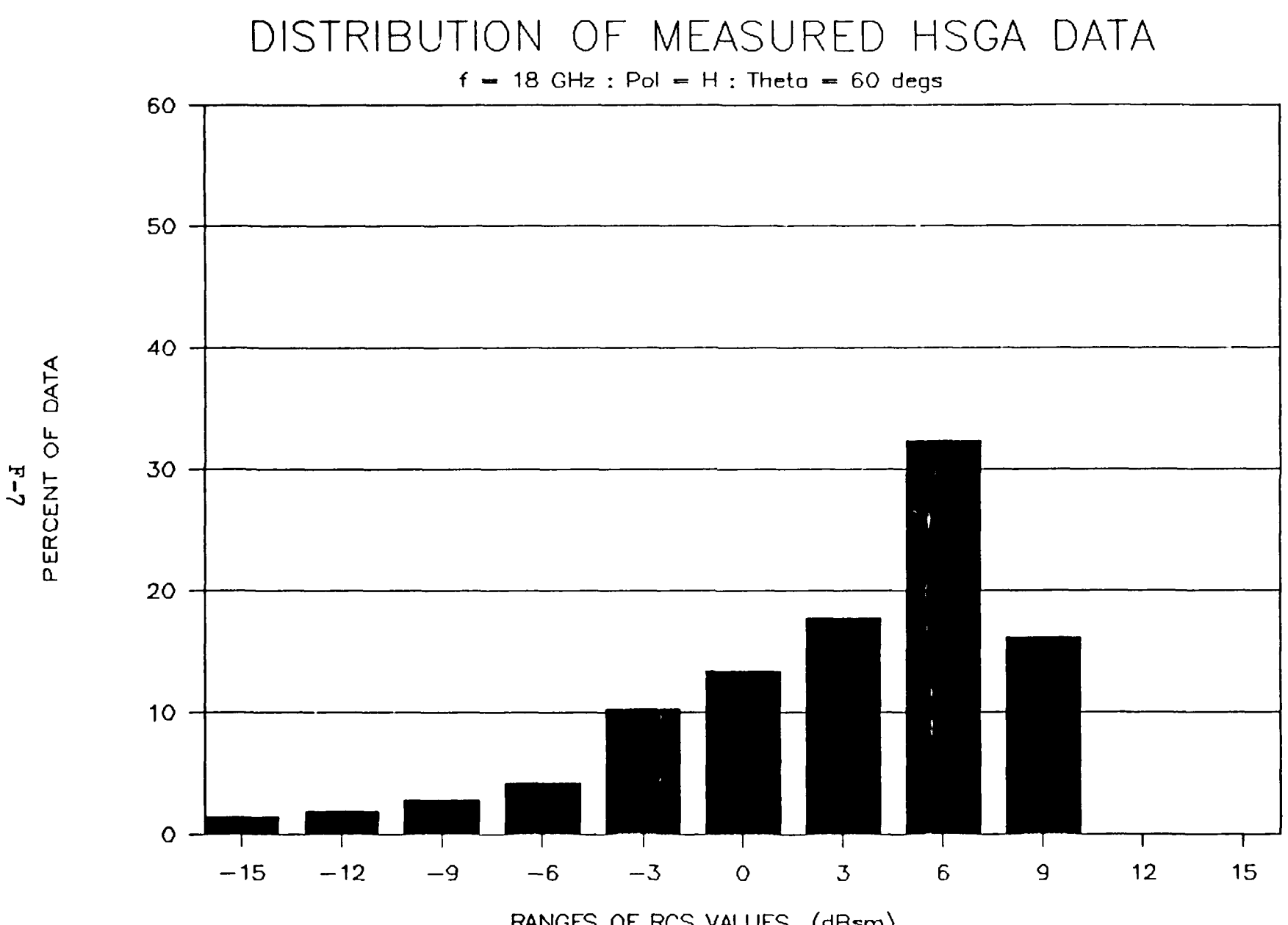

Figure F.6 Distribution of the Measured HSGA RCS, 18 GHz, Theta of 60 degs, Horz Pol

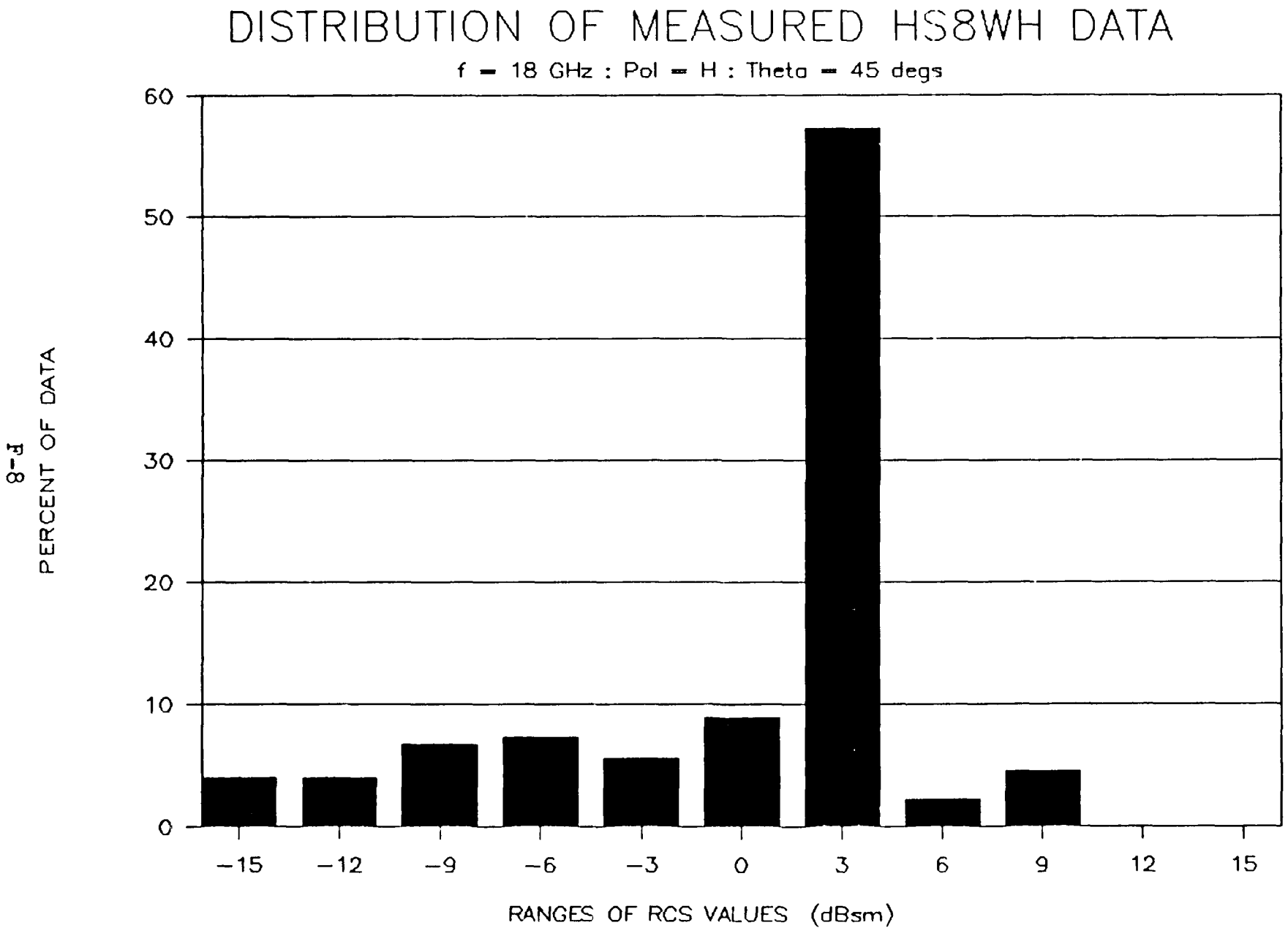

Figure F.7 Distribution of the Measured HS8WH RCS, 18 GHz, Theta of 45 degs, Horz Pol

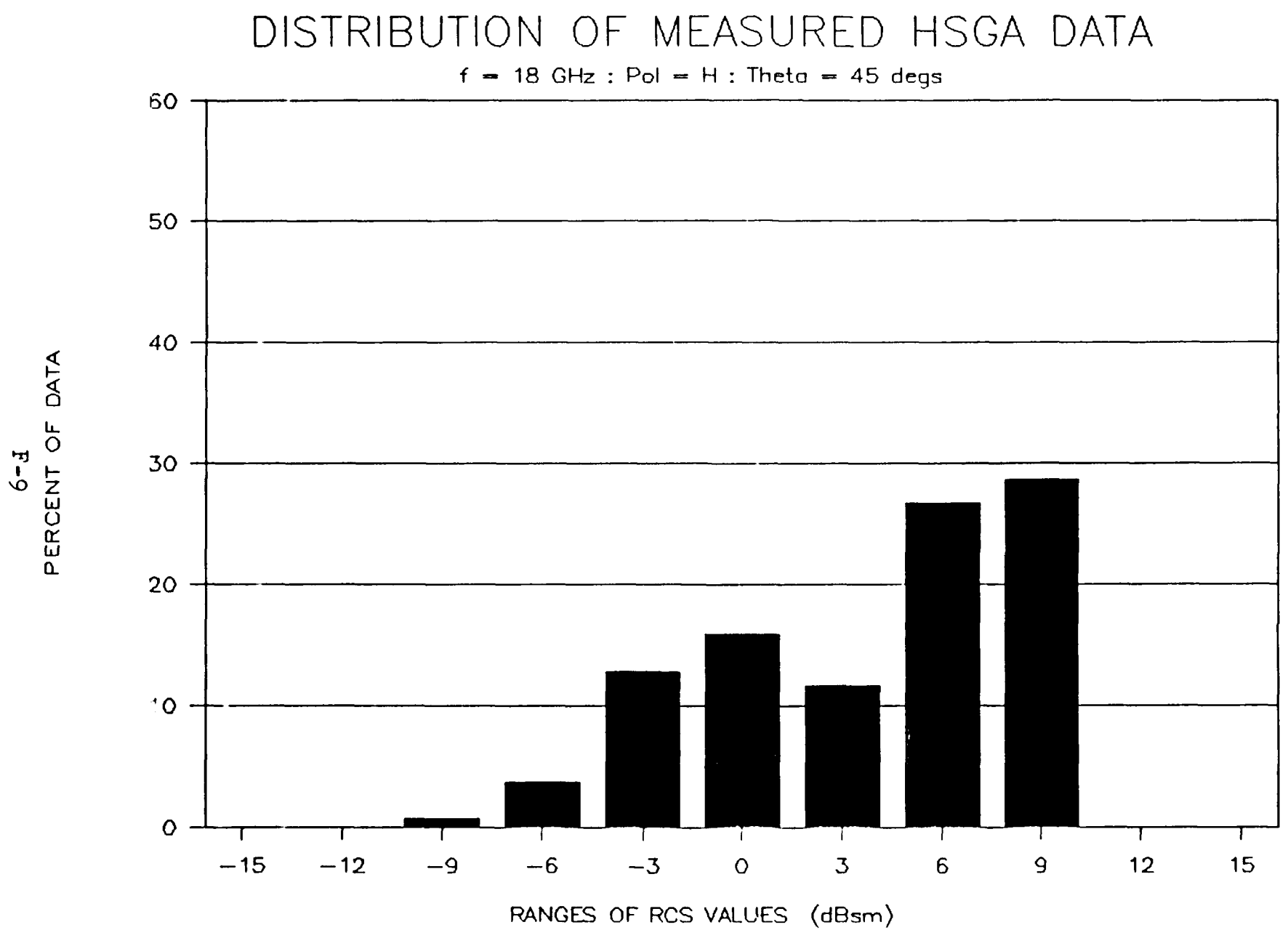

Figure F.8 Distribution of the Measured HSGA RCS, 18 GHz, Theta of 45 degs, Horz Pol

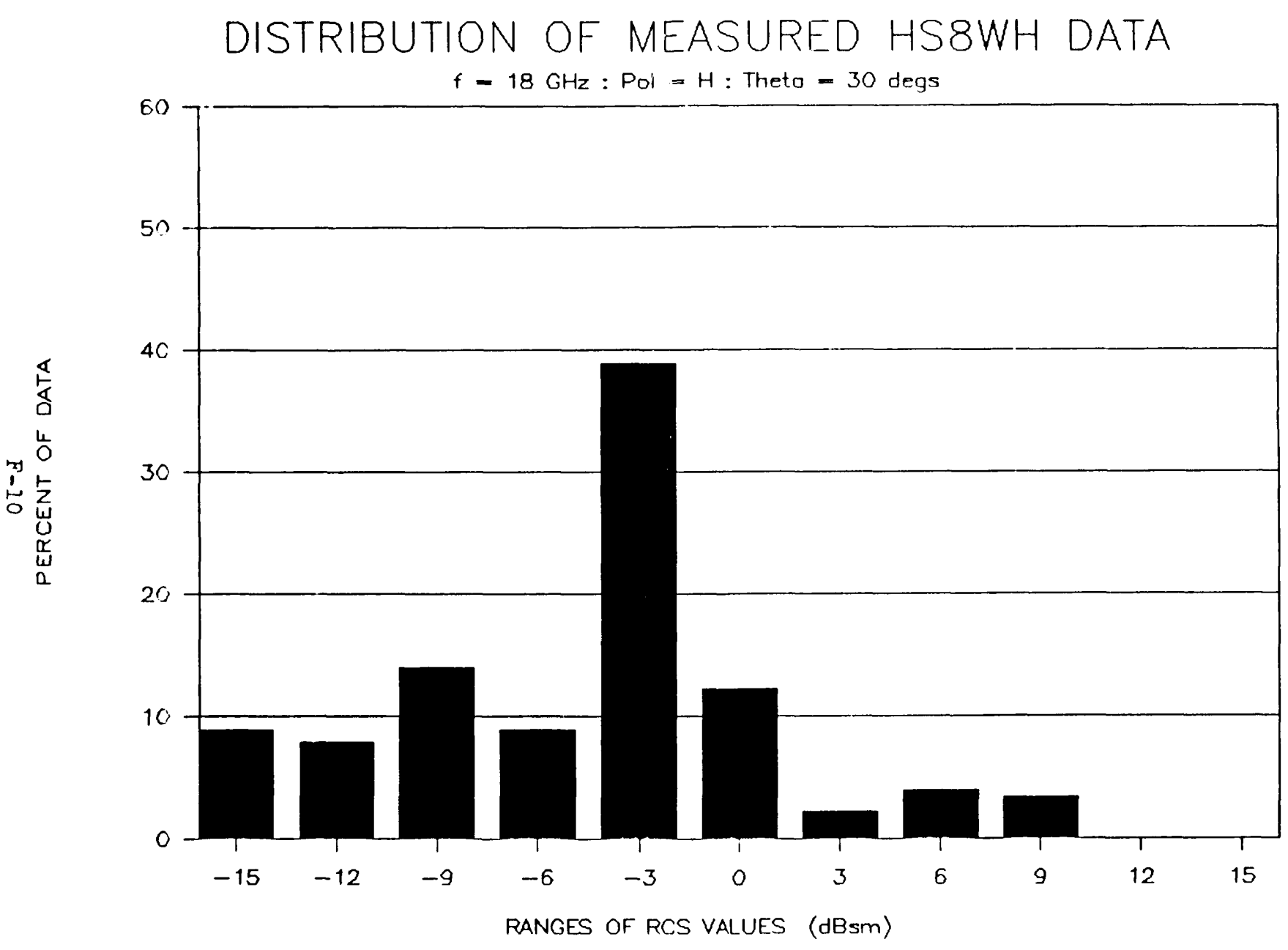

Figure F.9 Distribution of the Measured HS8WH RCS, 18 GHz, Theta of 30 degs, Horz Pol

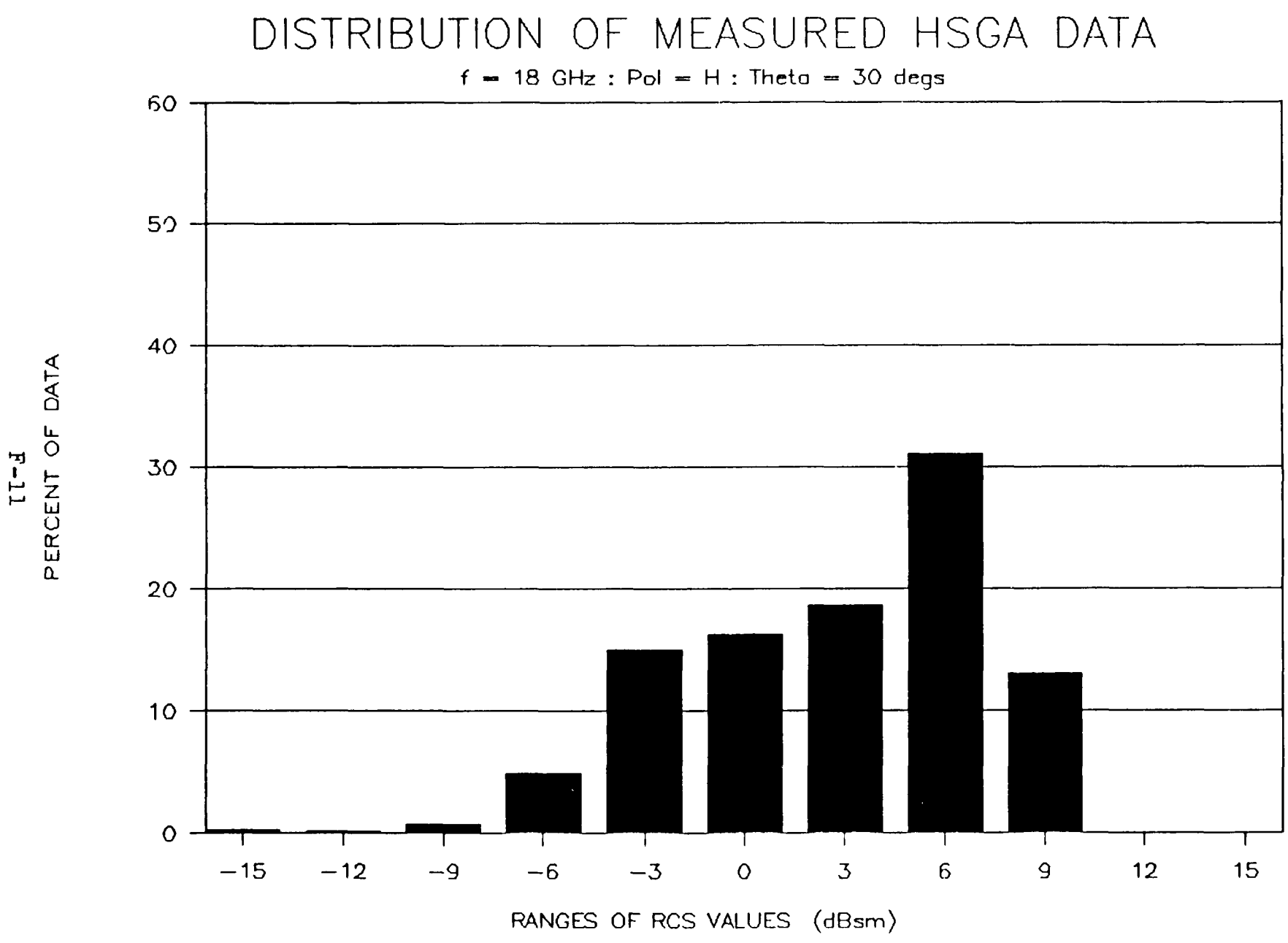

Figure F.10 Distribution of the Measured HSGA RCS, 18 GHz, Theta of 30 degs, Horz Pol

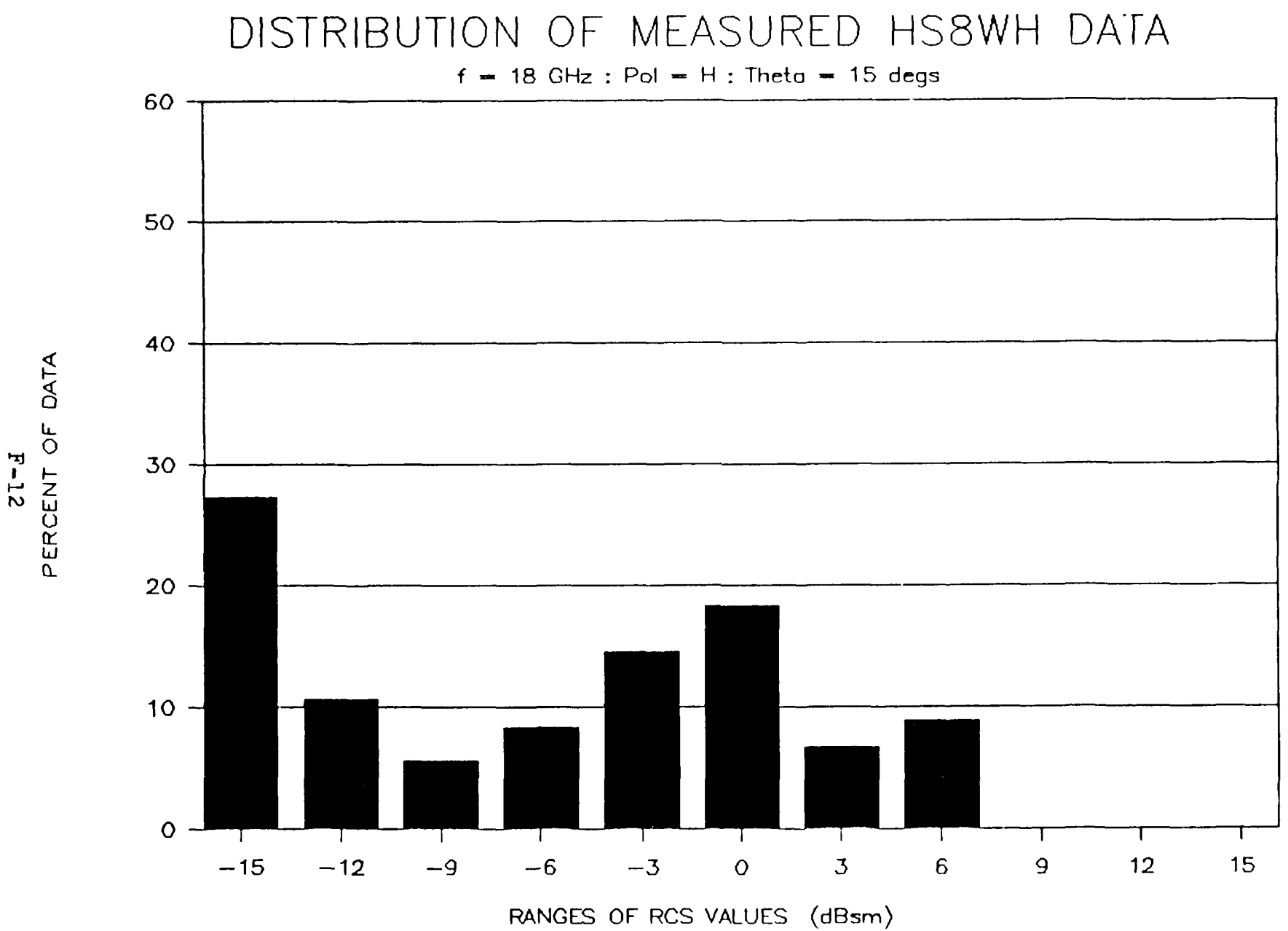

Figure F.11 Distribution of the Measured HS8WH RCS, 18 GHz, Theta of 15 degs, Horz Pol

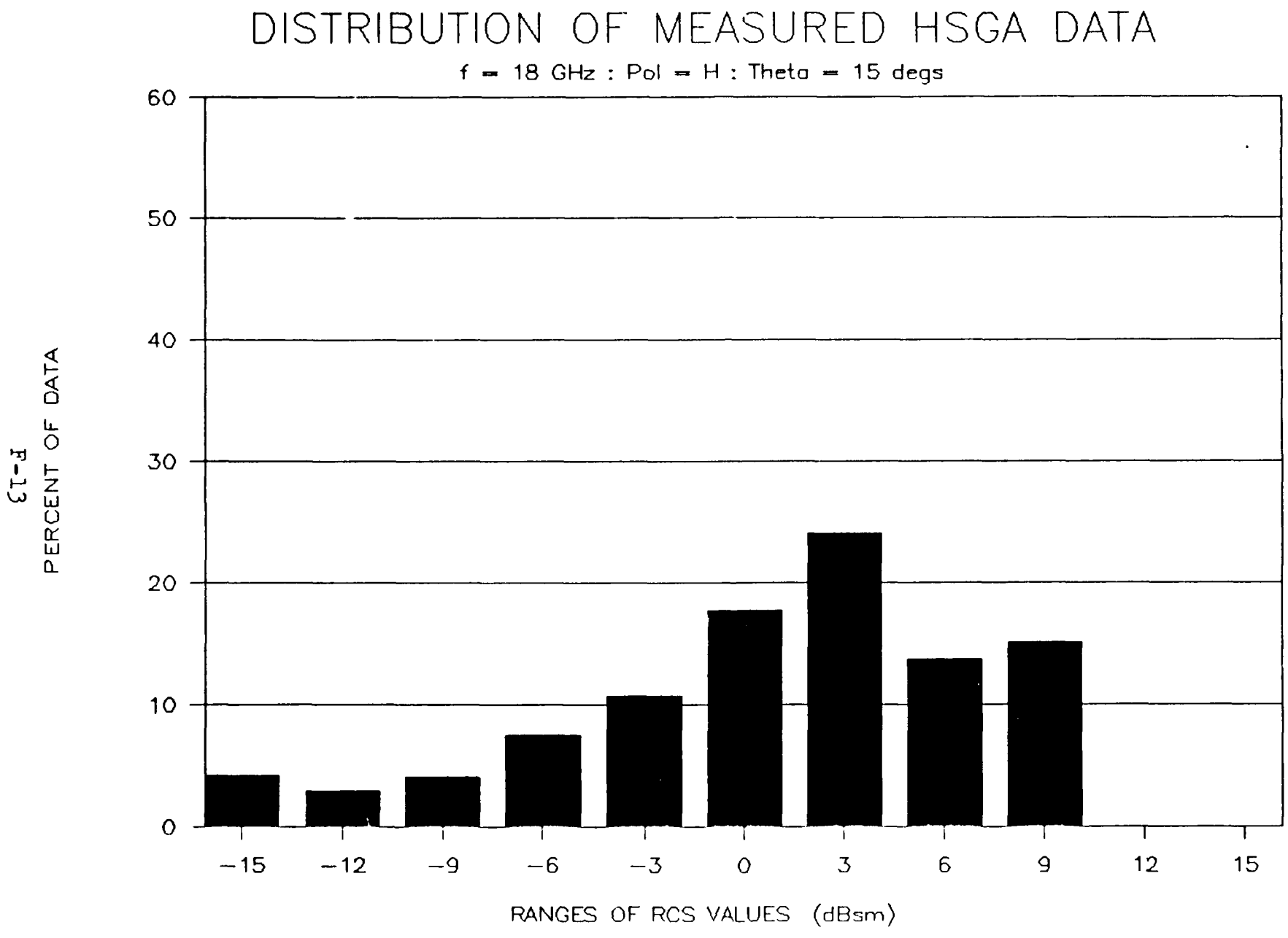

Figure F.12 Distribution of the Measured HSGA RCS, 18 GHz, Theta of 15 degs, Horz Pol

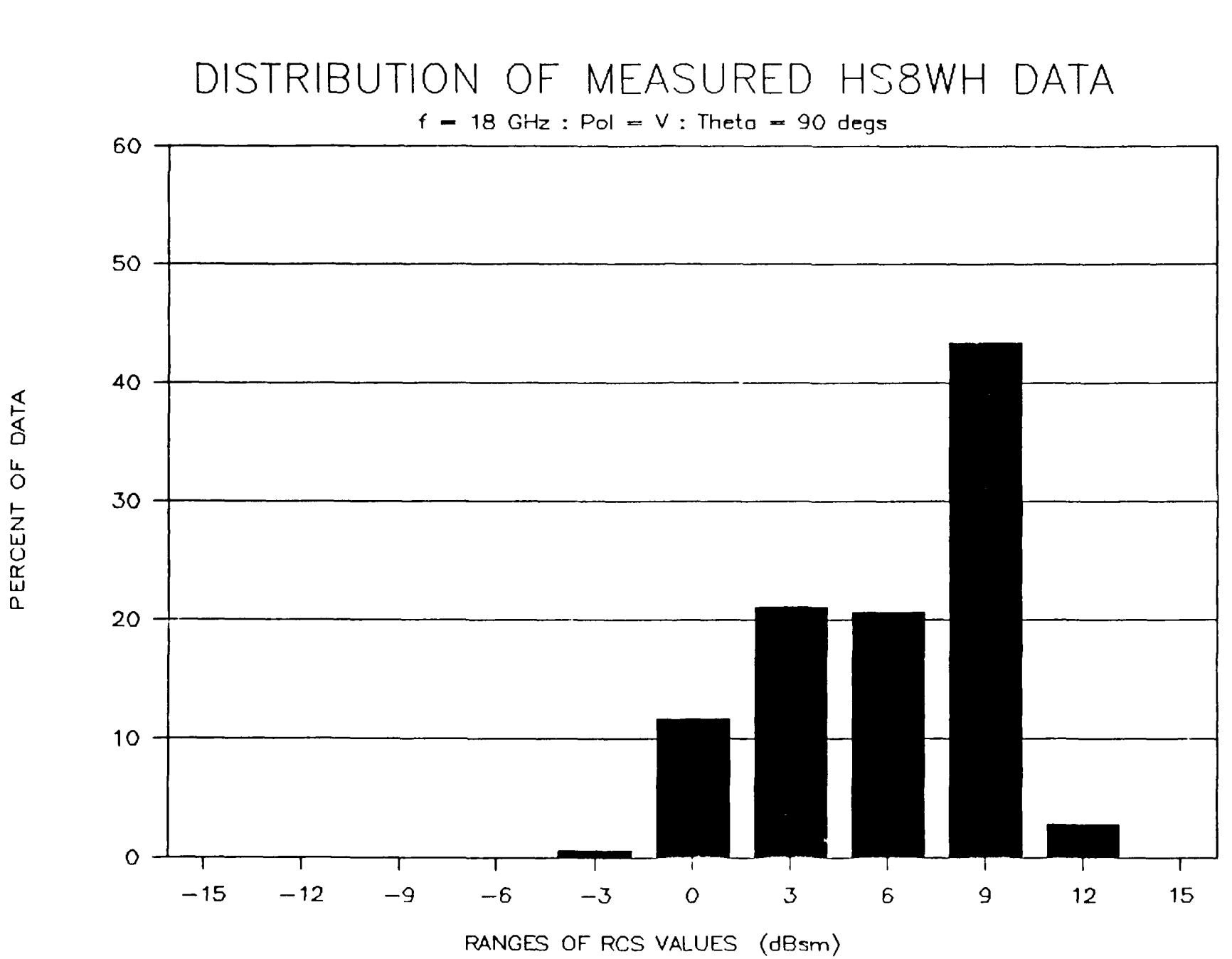

Figure F.13 Distribution of the Measured HS8WH RCS, 18 GHz, Theta of 90 degs, Vert Pol

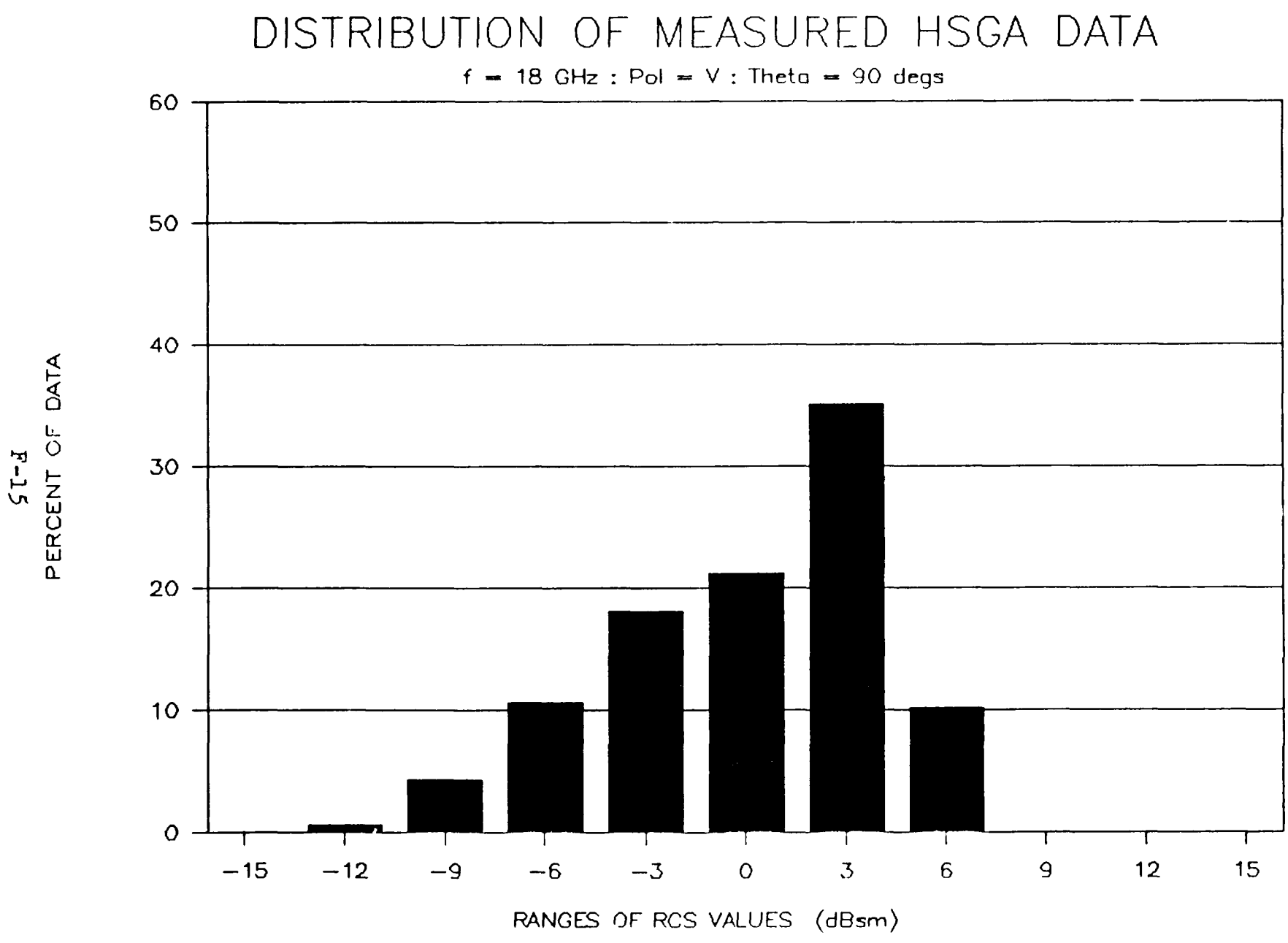

Figure F.14 Distribution of the Measured HSGA RCS, 18 GHz, Theta of 90 degs, Vert Pol

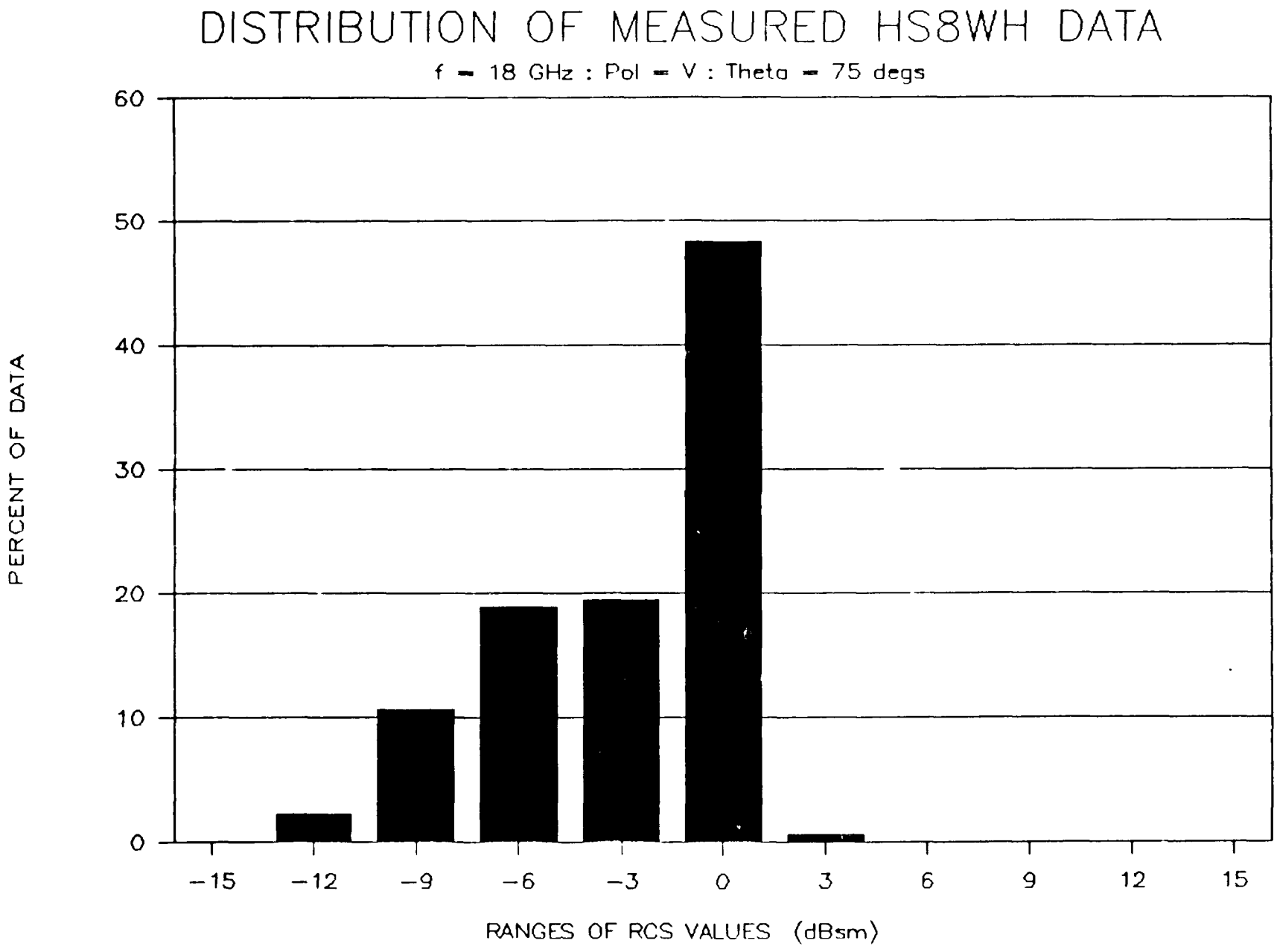

Figure F.15 Distribution of the Measured HS8WH RCS, 18 GHz, Theta of 75 degs, Vert Pol

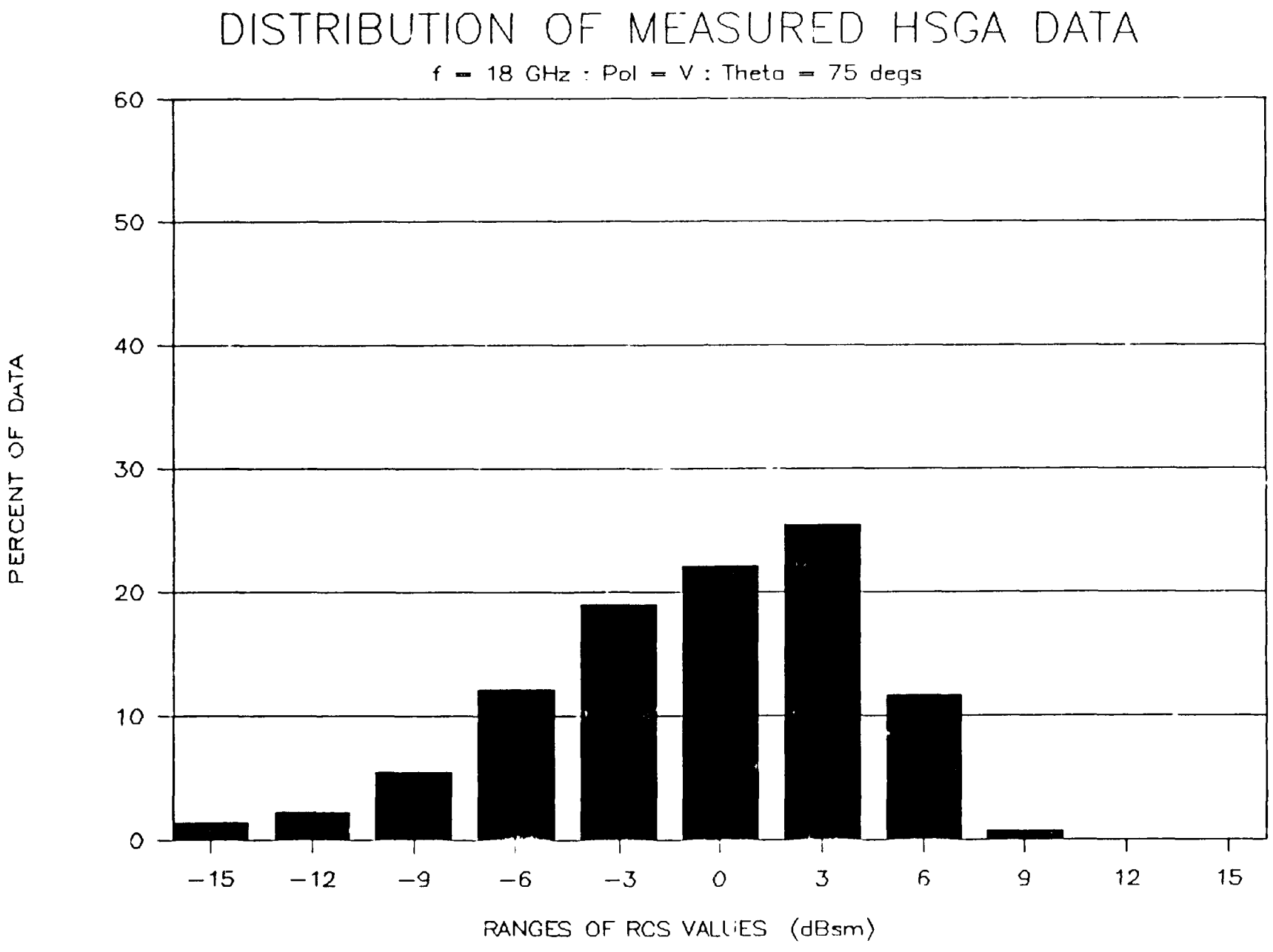

Figure F.16 Distribution of the Measured HSGA RCS, 18 GHz, Theta of 75 degs, Vert Pol

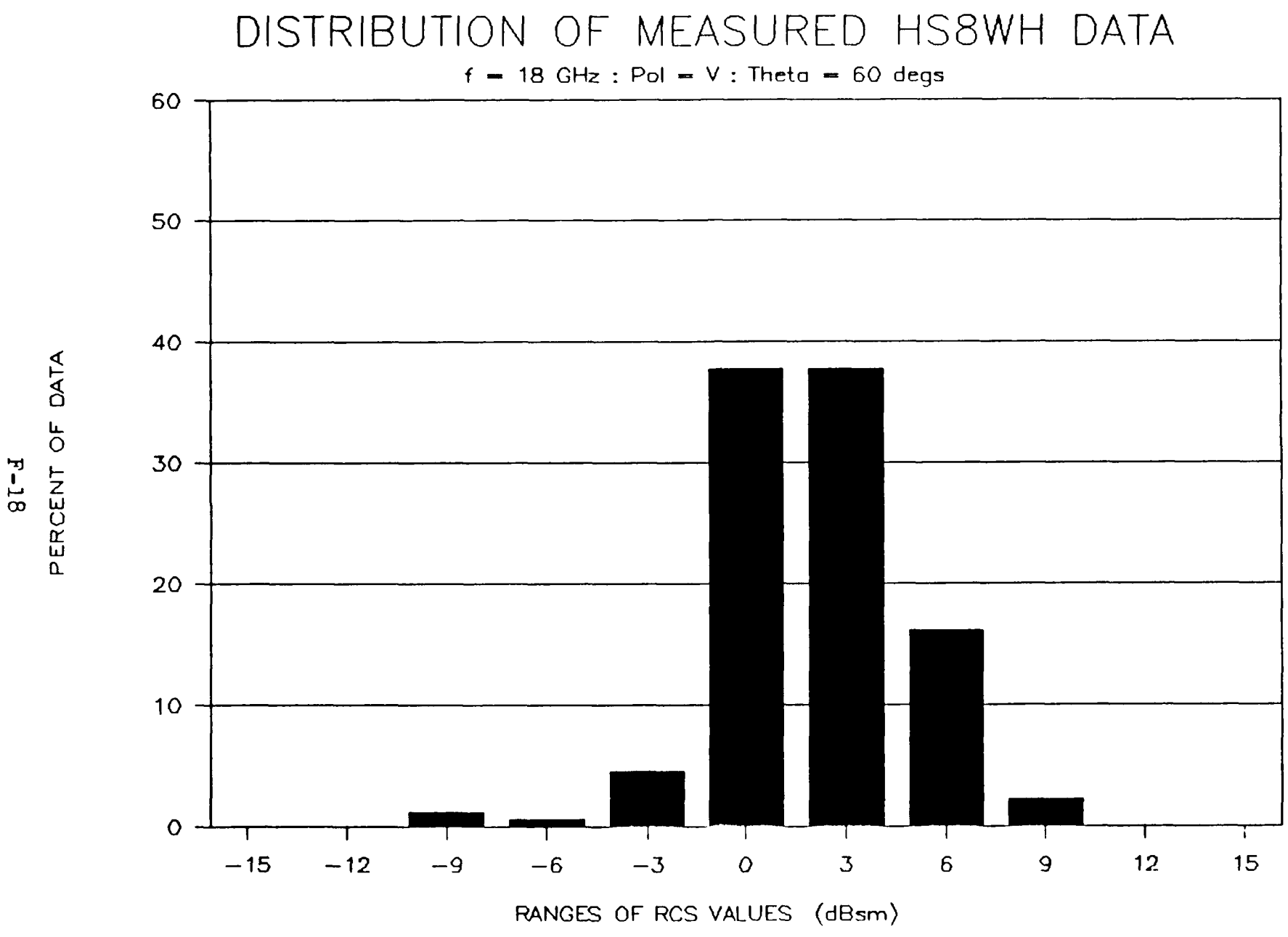

Figure F.17 Distribution of the Measured HS8WH RCS, 18 GHz, Theta of 60 degs, Vert Pol

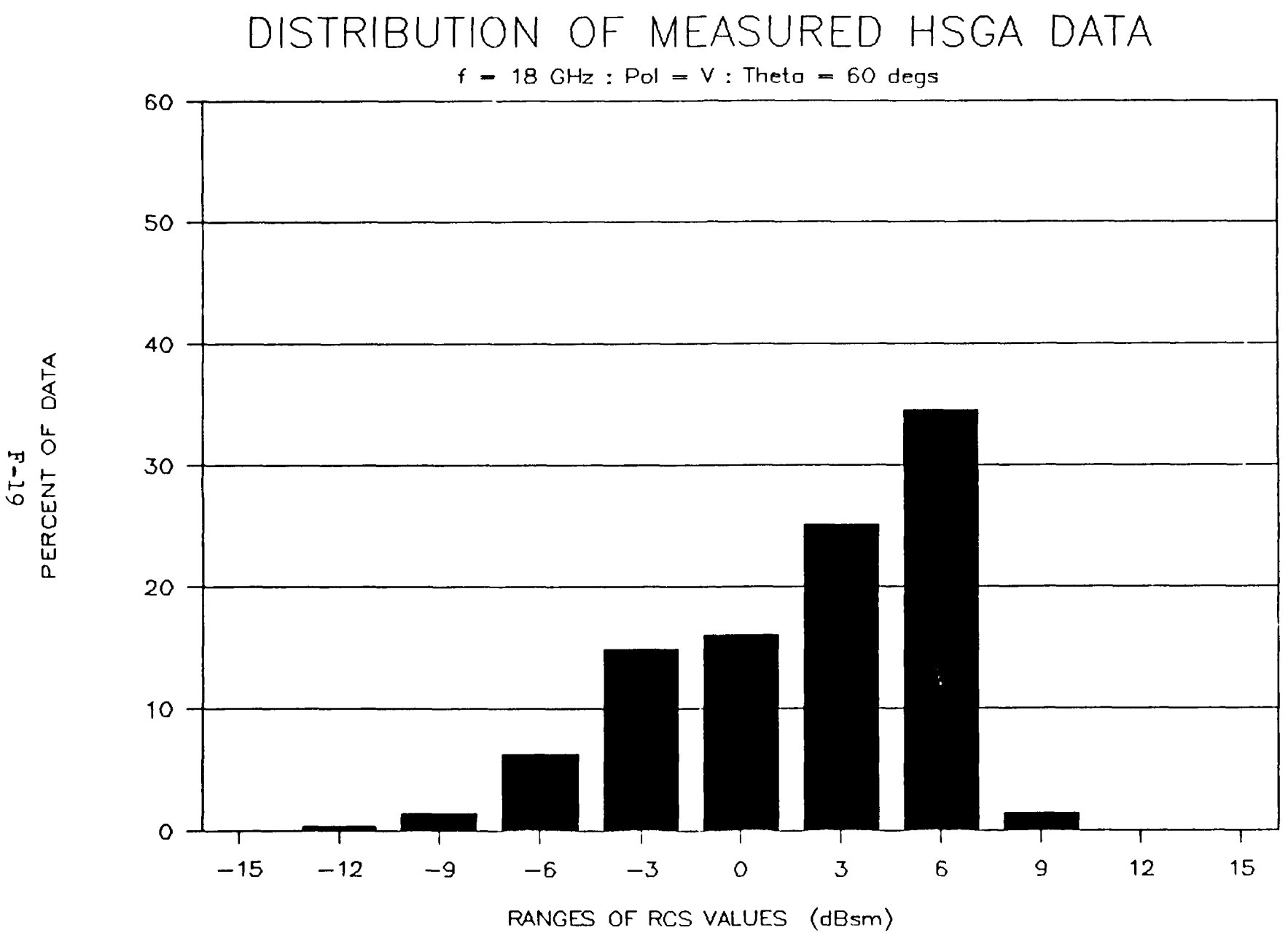

Figure F.18 Distribution of the Measured HSGA RCS, 18 GHz, Theta of 60 degs, Vert Pol

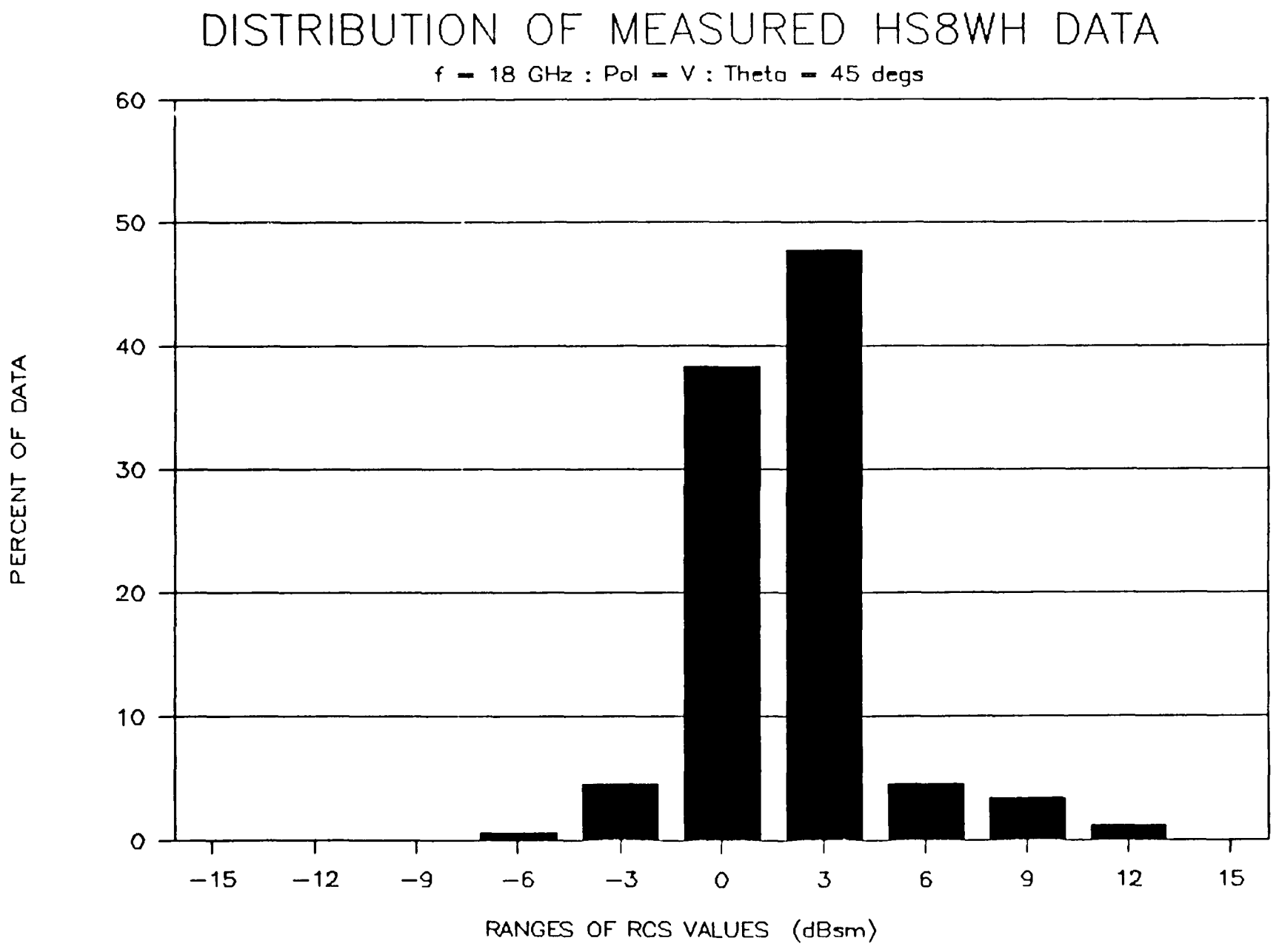

Figure F.19 Distribution of the Measured HS8WH RCS, 18 GHz, Theta of 45 degs, Vert Pol

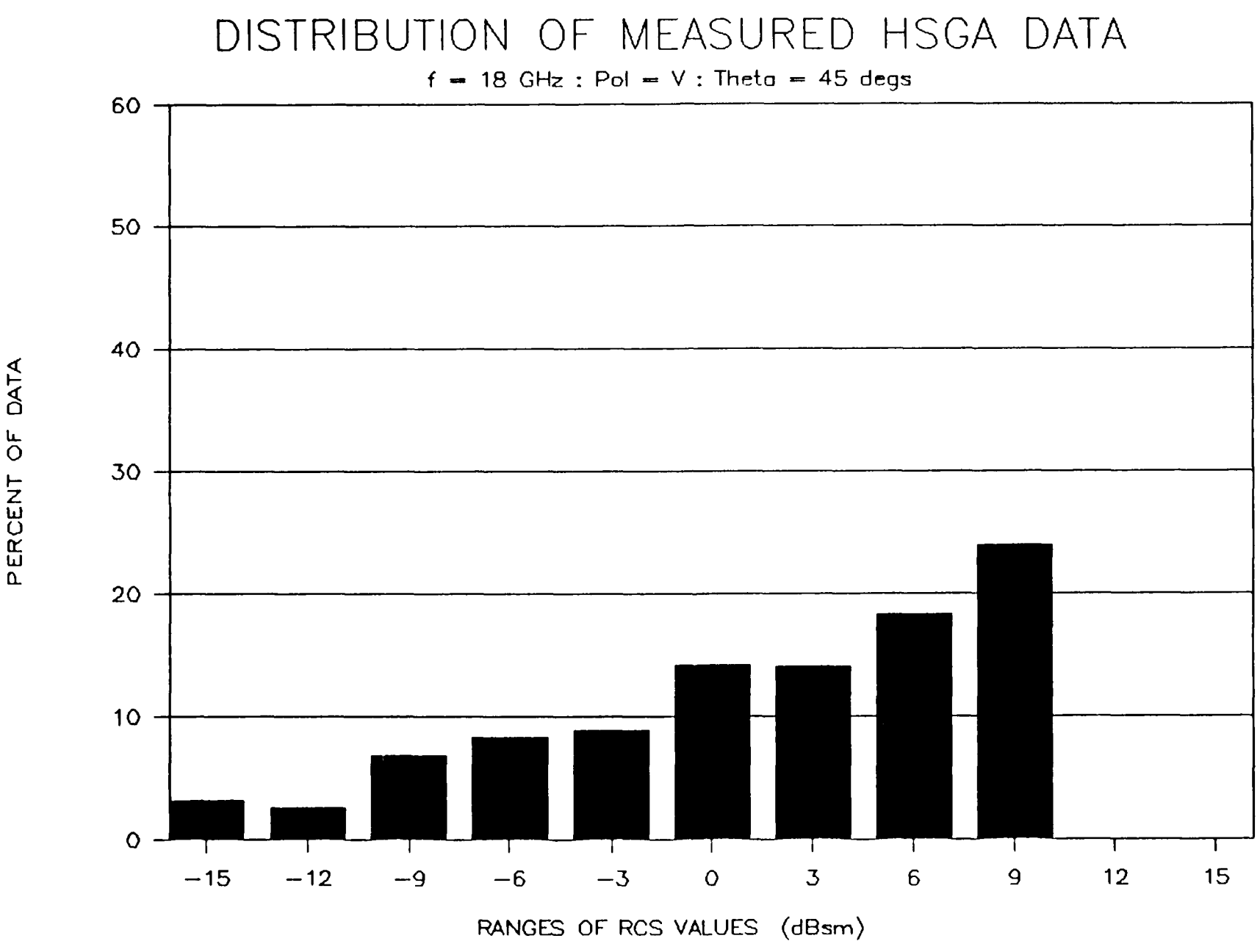

Figure F.20 Distribution of the Measured HSGA RCS, 18 GHz, Theta of 45 degs, Vert Pol

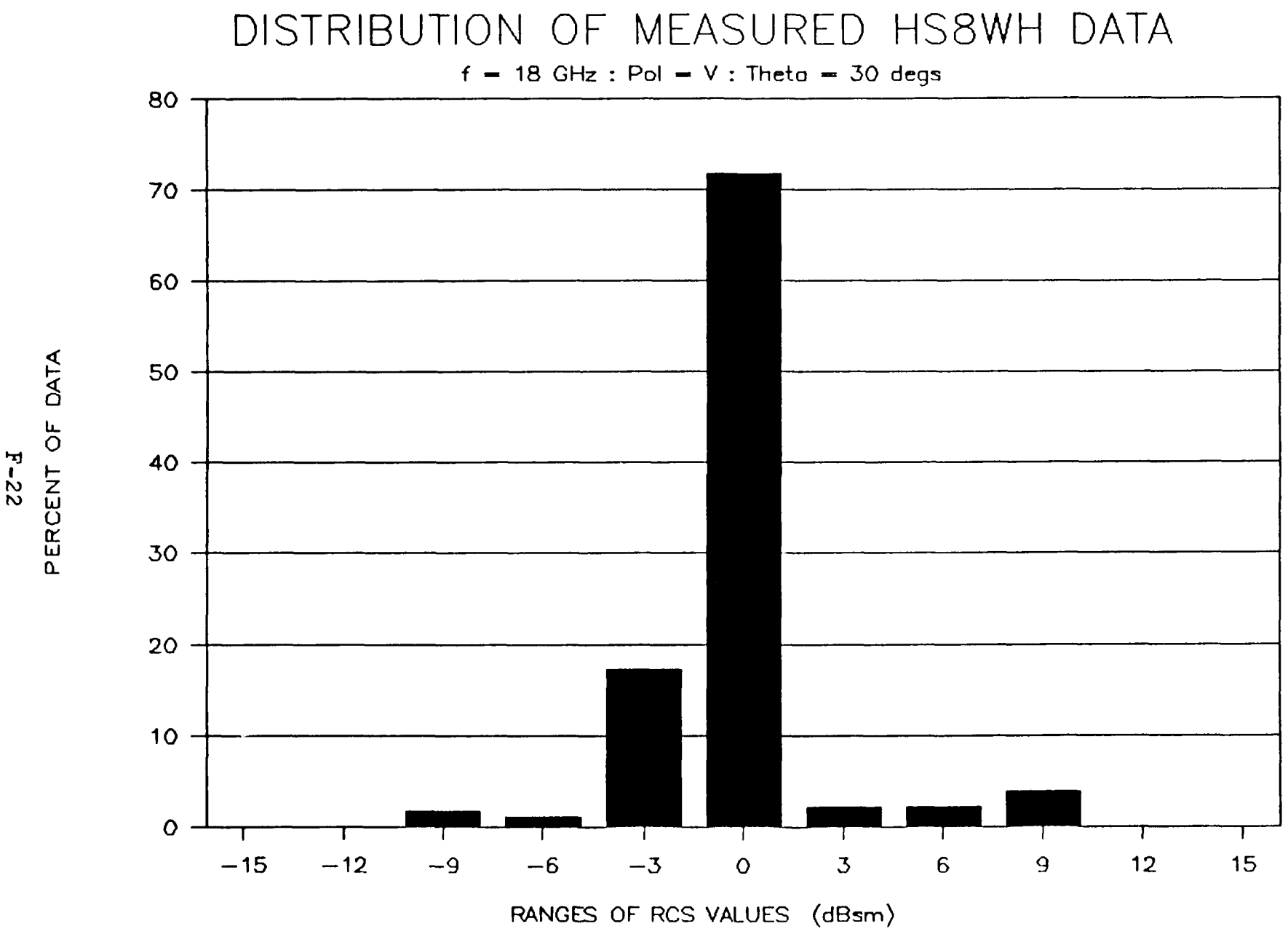

Figure F.21 Distribution of the Measured HS8WH RCS, 18 GHz, Theta of 30 degs, Vert Pol

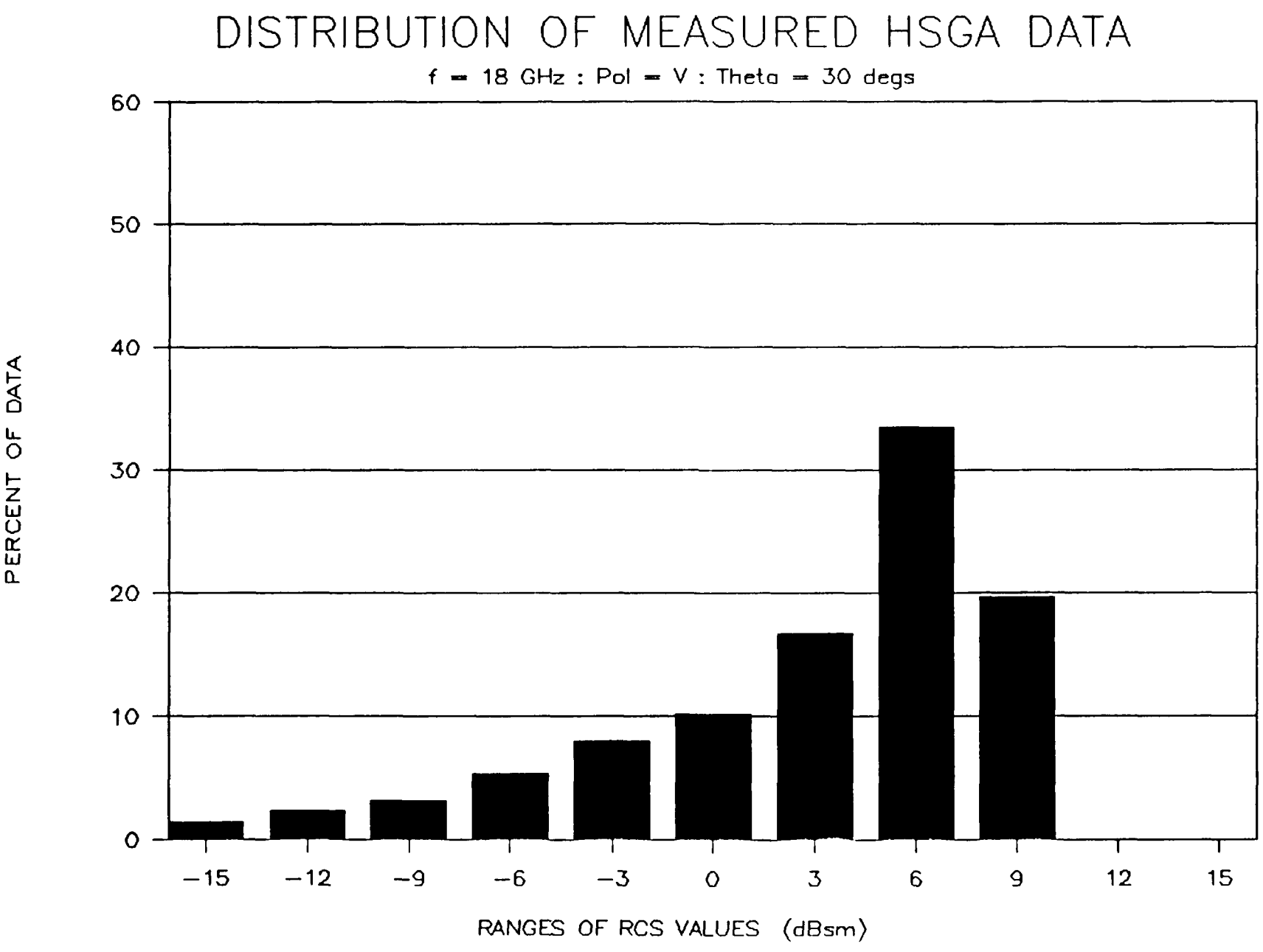

Figure F.22 Distribution of the Measured HSGA RCS, 18 GHz, Theta of 30 degs, Vert Pol

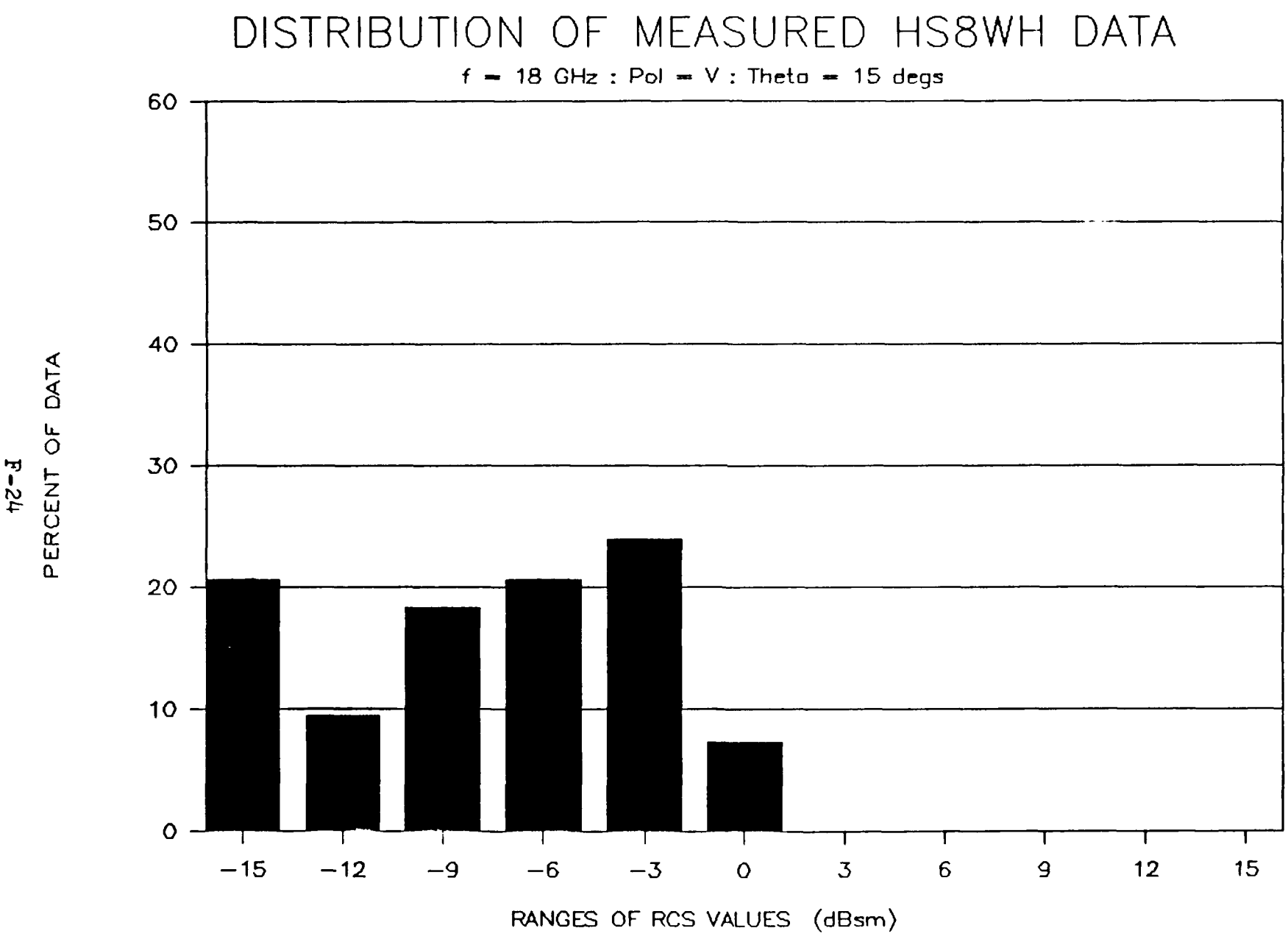

Figure F.23 Distribution of the Measured HS8WH RCS, 18 GHz, Theta of 15 degs, Vert Pol

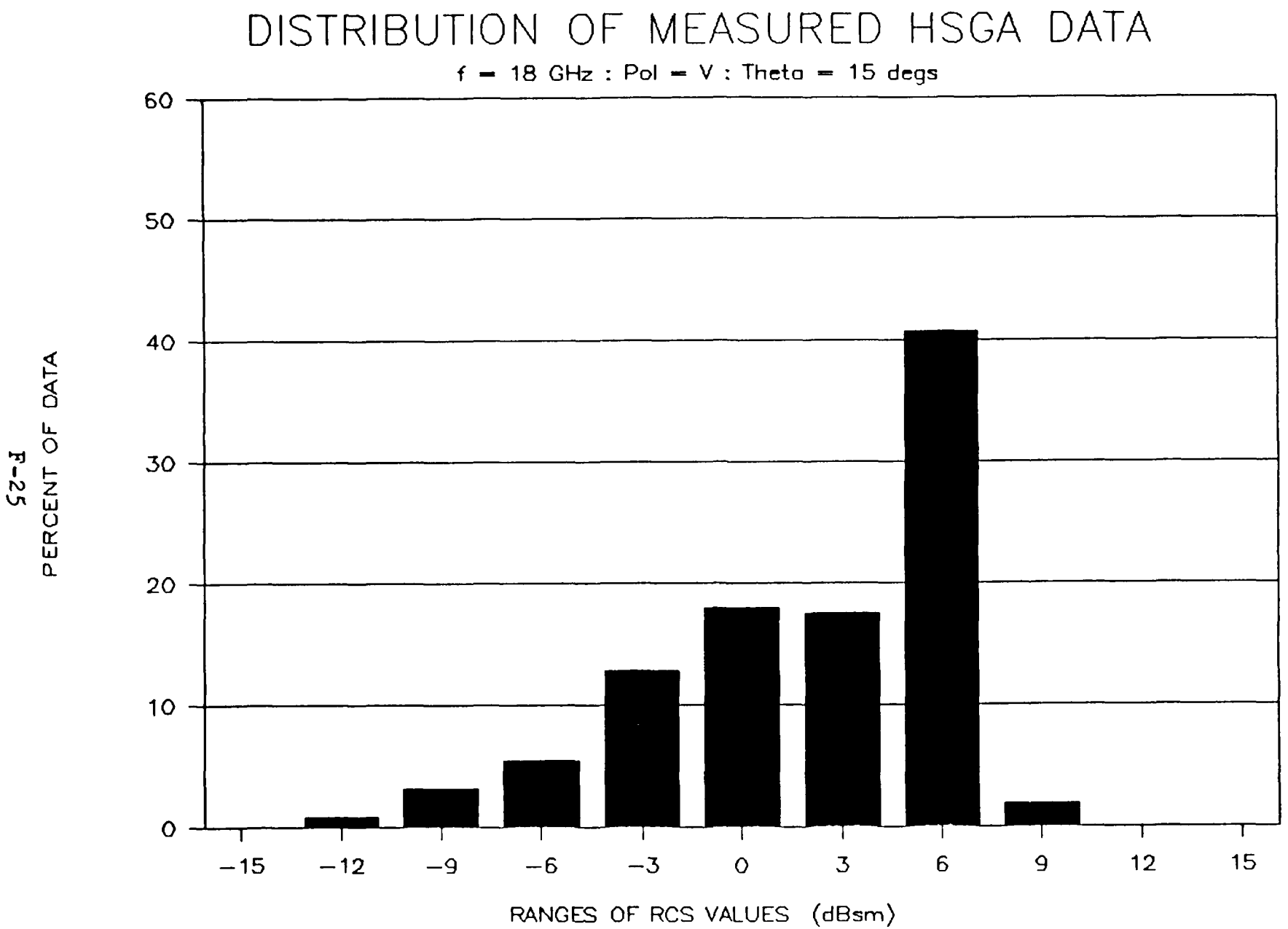

Figure F.24 Distribution of the Measured HSGA RCS, 18 GHz, Theta of 15 degs, Vert Pol

APPENDIX G: Theoretical vs Measured RCS Results

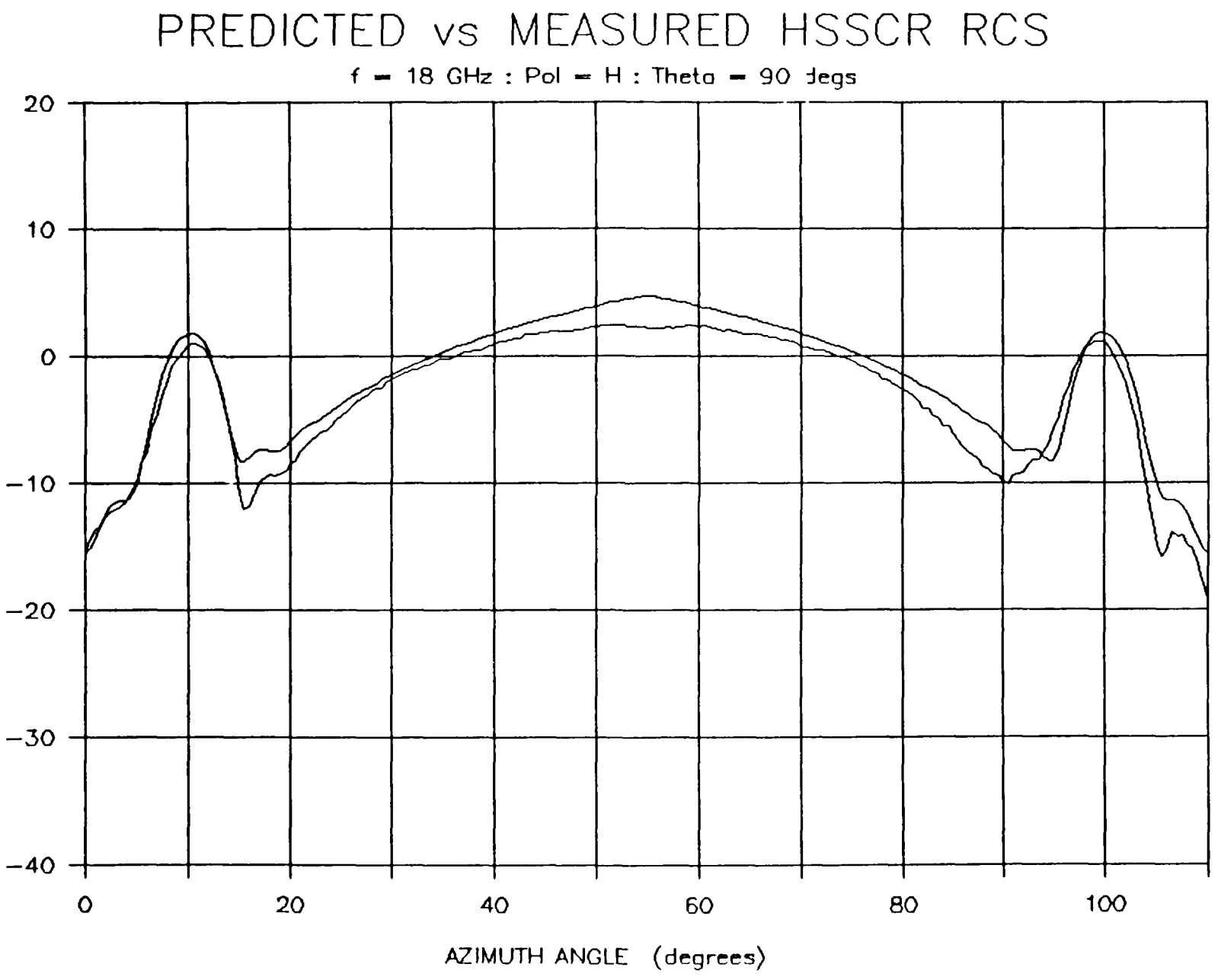

Figure G.1 Predicted vs Measured RCS: HSSCR, 18 GHz, Theta of 90 degs, Horz Pol

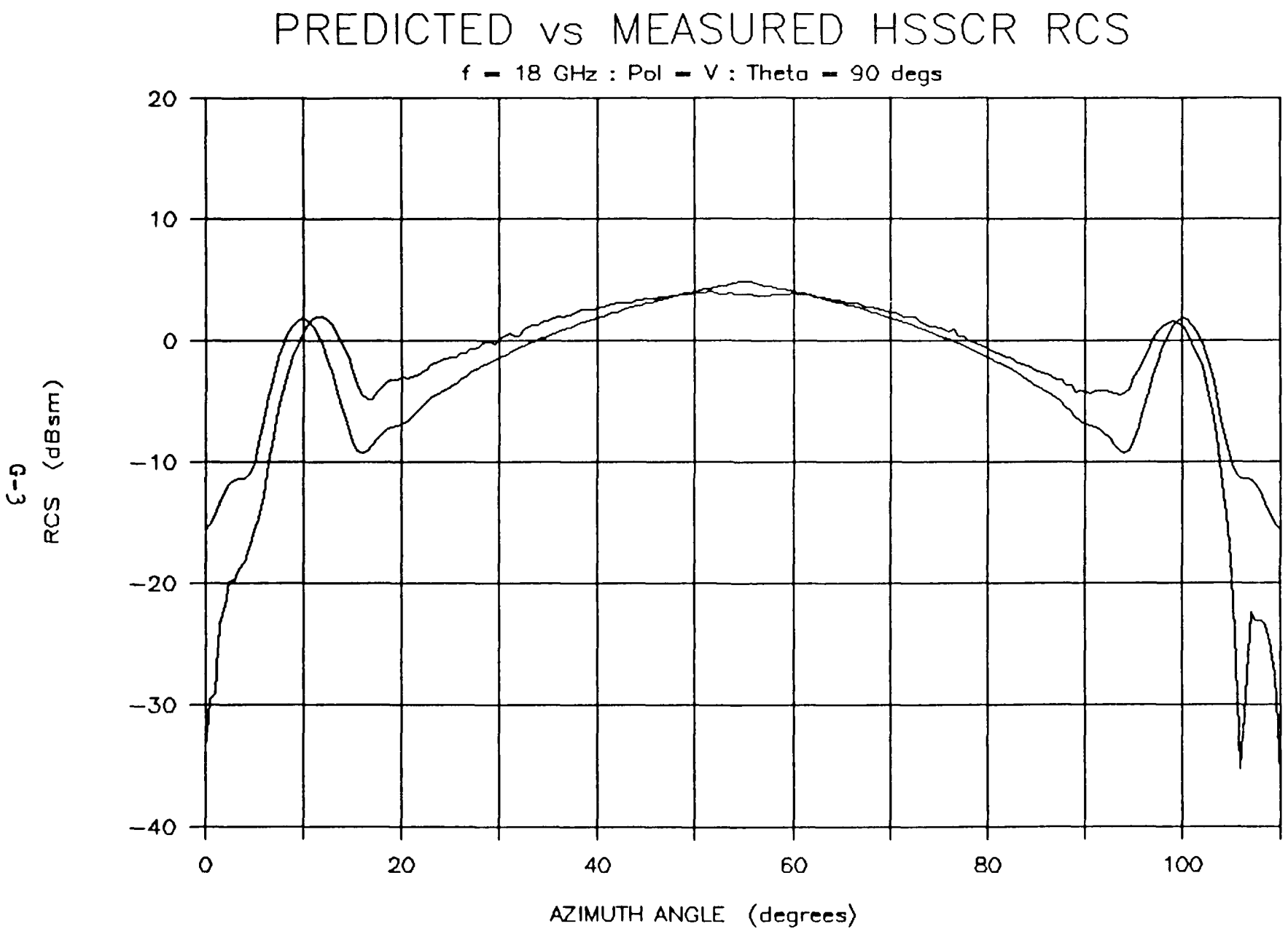

Figure G.2 Predicted vs Measured RCS: HSSCR, 18 GHz, Theta of 90 degs, Vert Pol

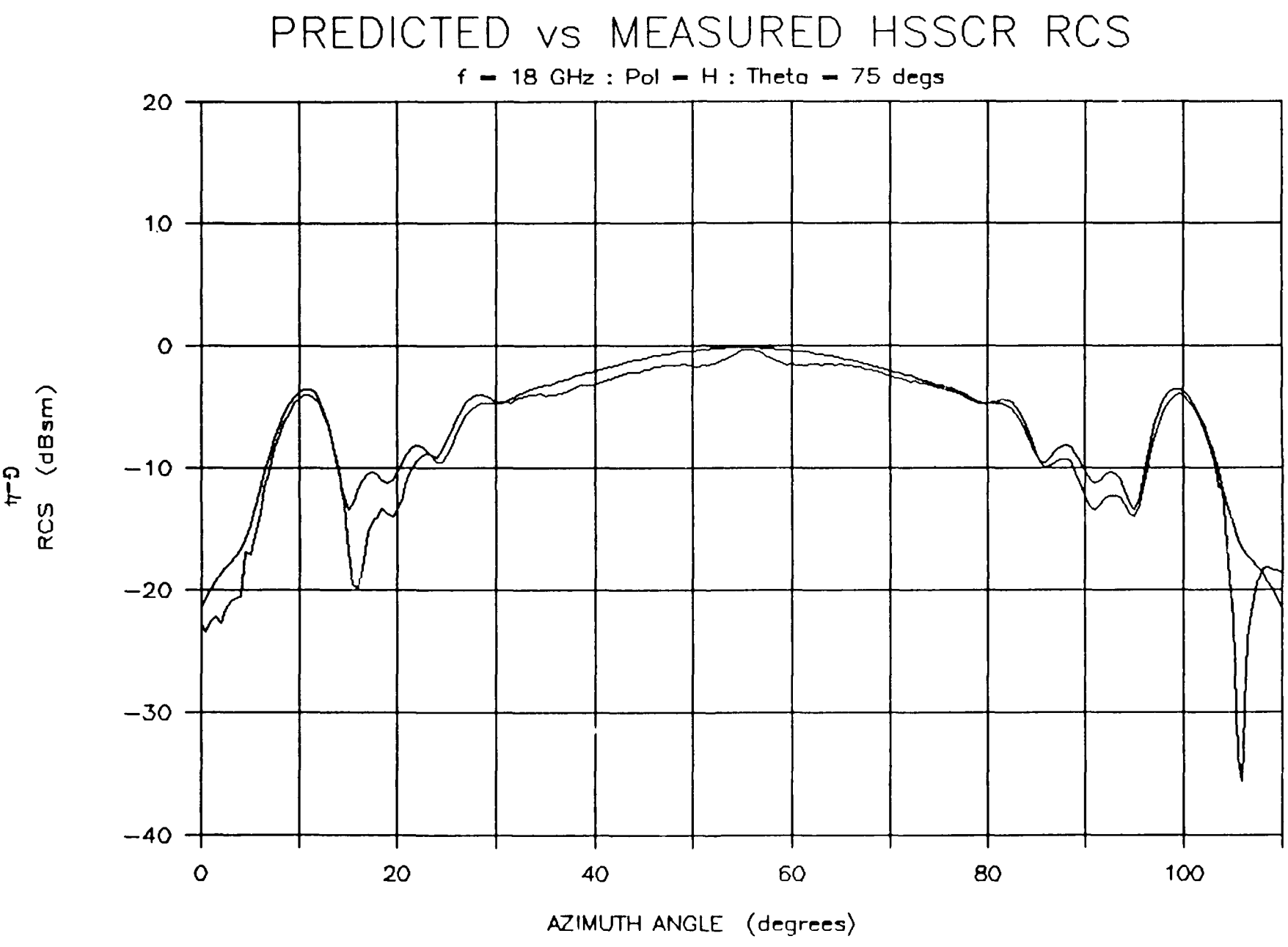

Figure G.3 Predicted vs Measured RCS: HSSCR, 18 GHz, Theta of 75 degs, Horz Pol

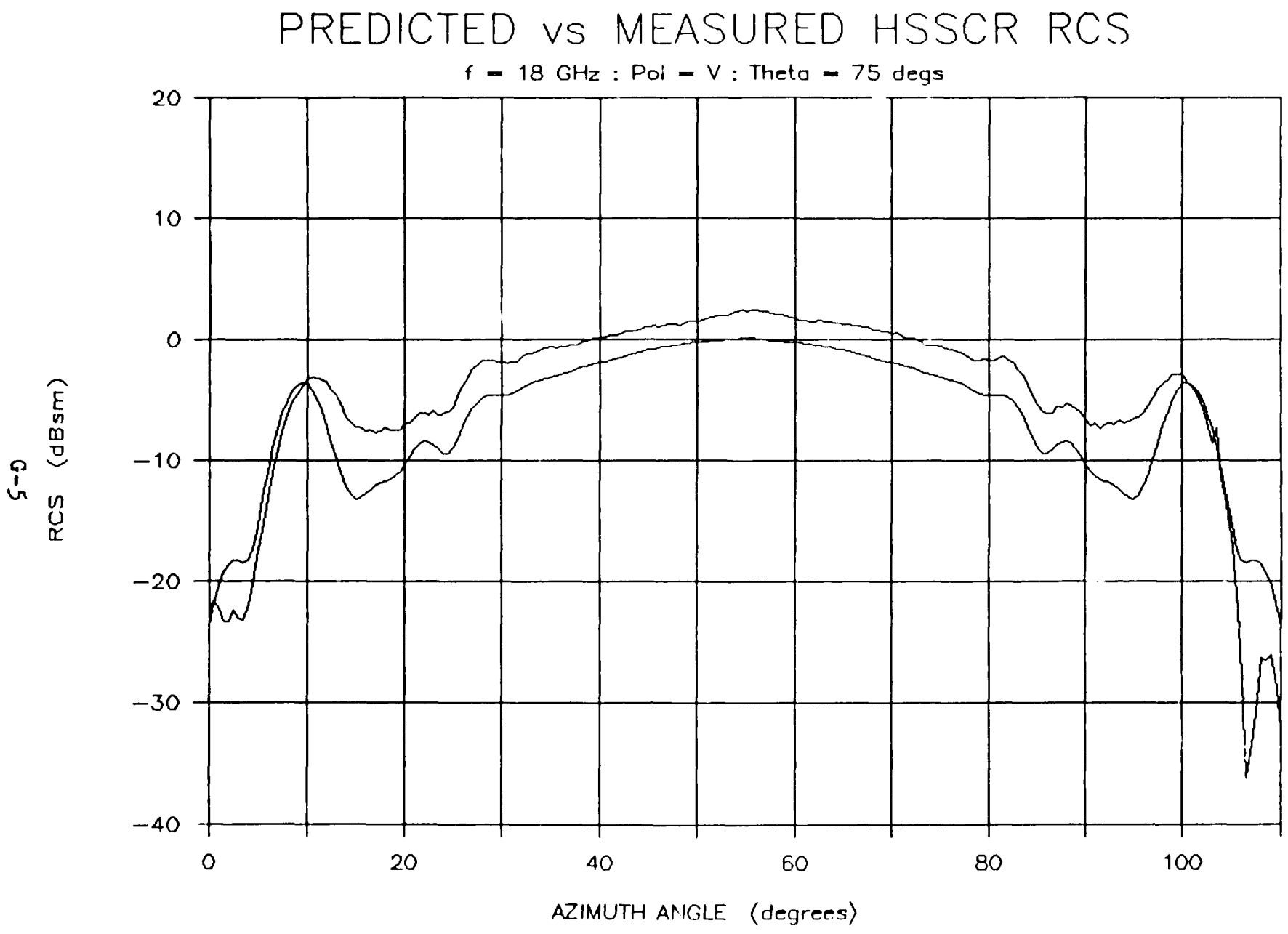

Figure G 4 Predicted vs Measured RCS: HSSCR, 18 GHz, Theta of 75 degs, Vert Pol

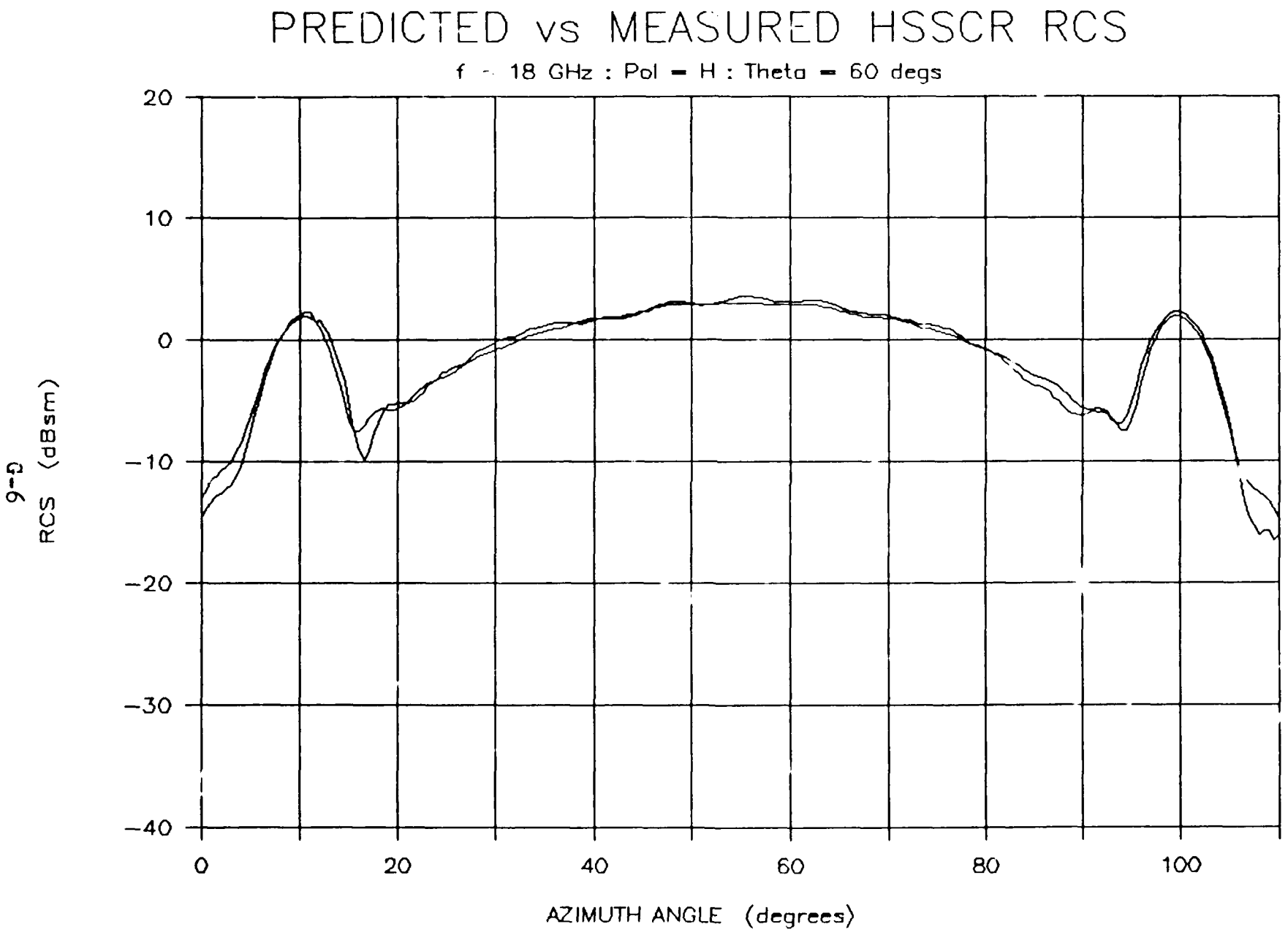

Figure G.5 Predicted vs Measured RCS: HSSCR, 18 GHz, Theta of 60 degs, Horz Pol

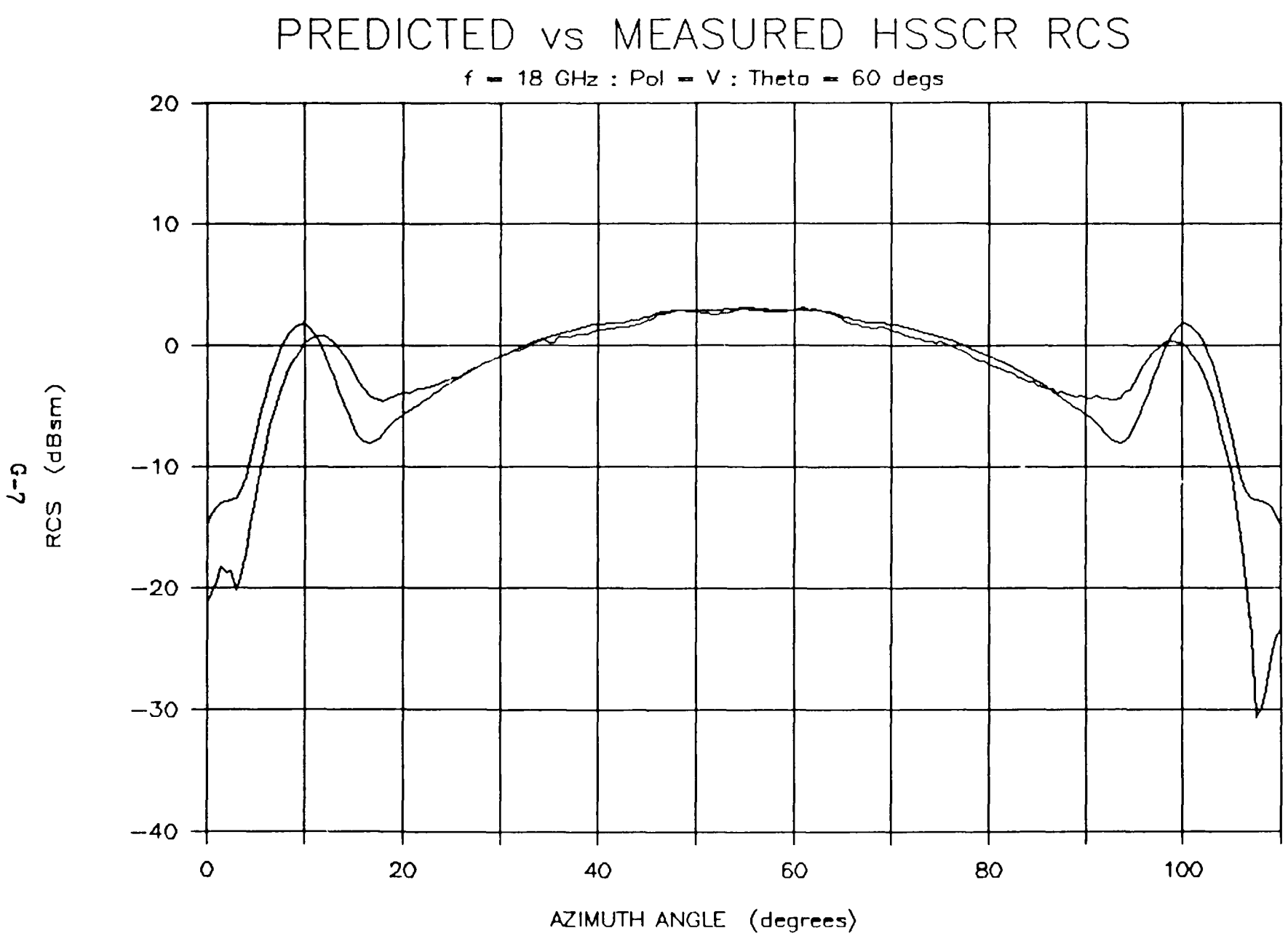

Figure G.6 Predicted vs Measured RCS, HSSCR, 18 GHz, Theta of 60 degs, Vert Pol

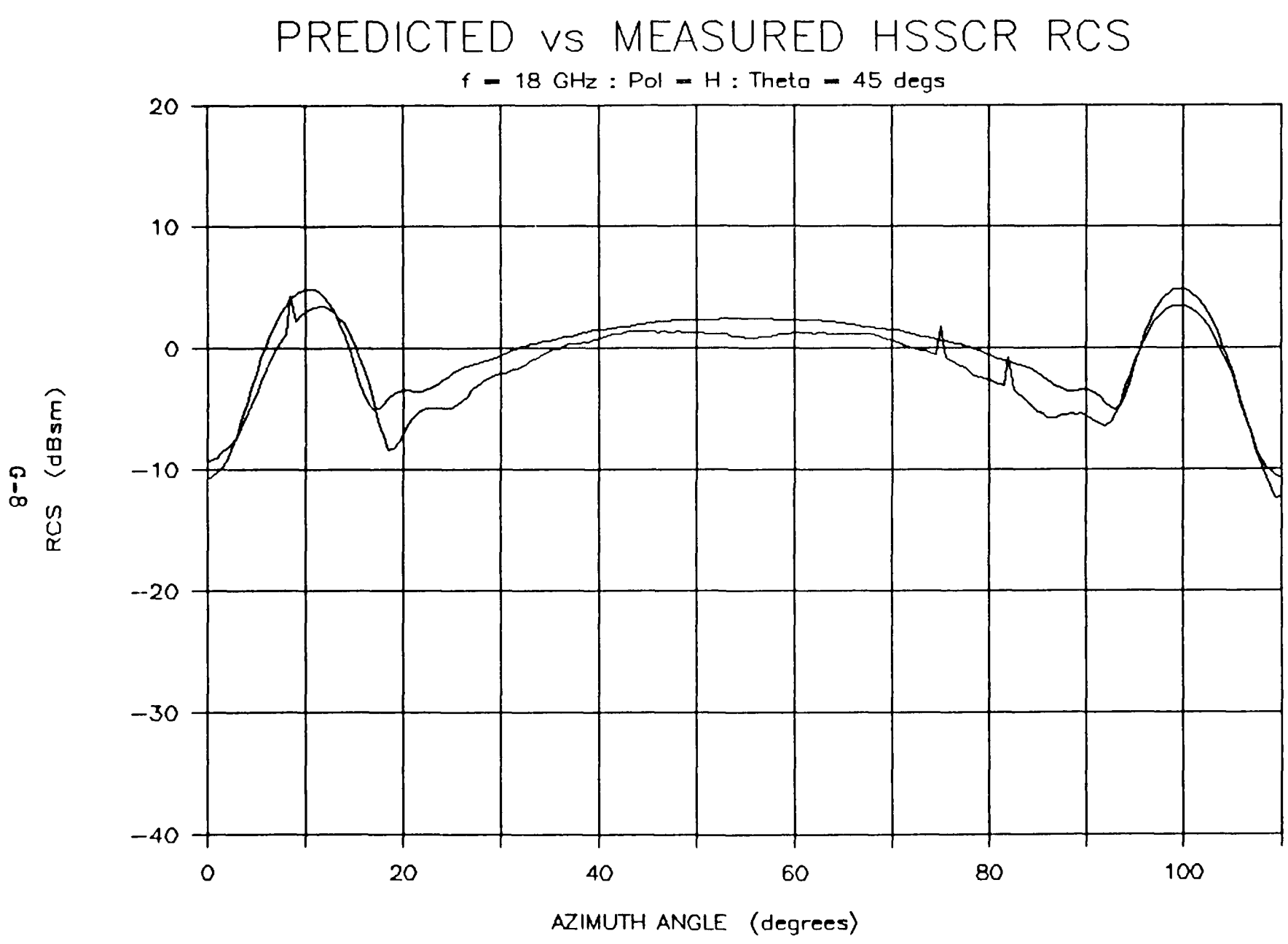

Figure G.7 Predicted vs Measured RCS: HSSCR, 18 GHz, Theta of 45 degs, Horz Pol

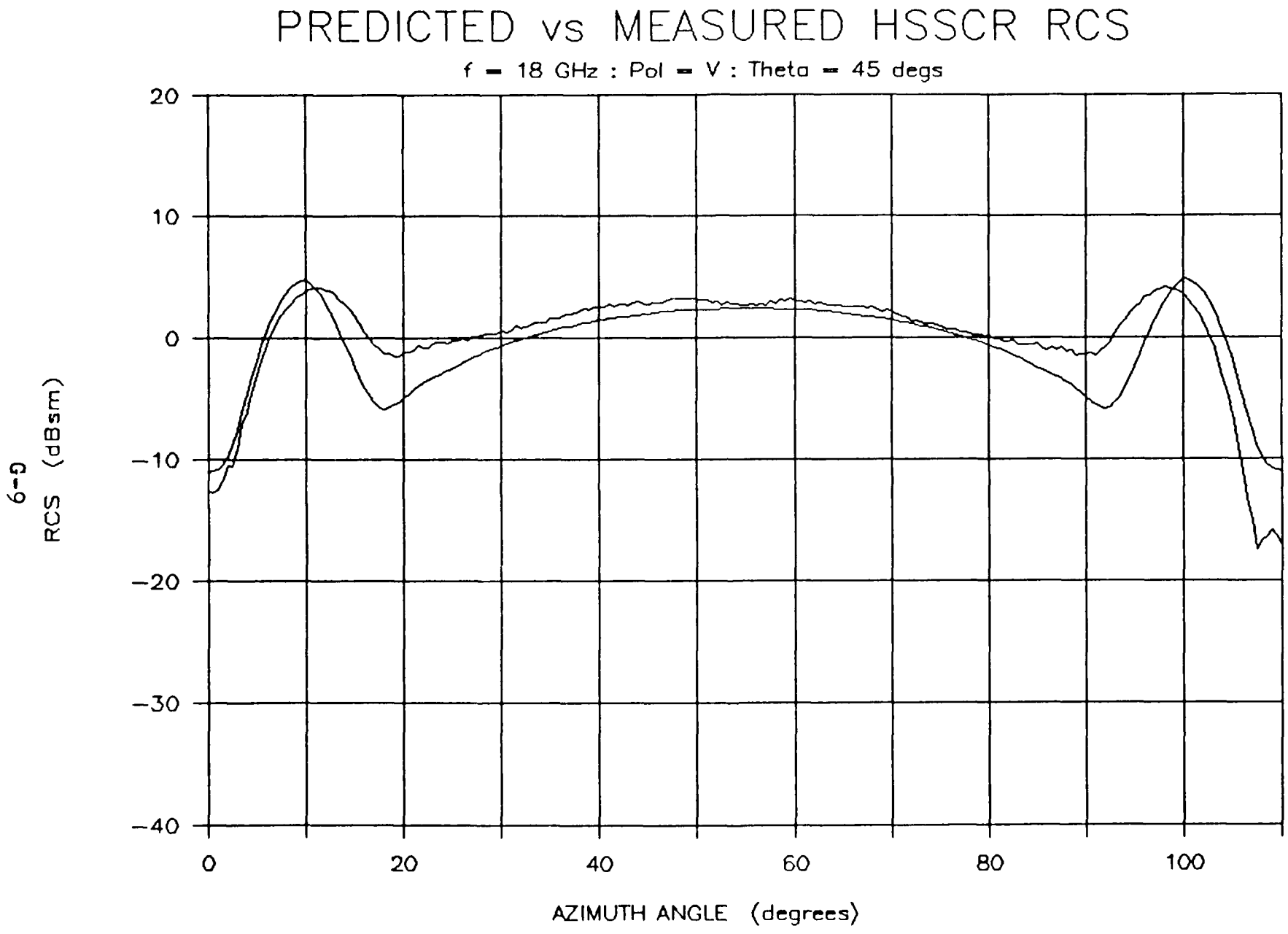

Figure G.8 Predicted vs Measured RCS: HSSCR, 18 GHz, Theta of 45 degs, Vert Pol

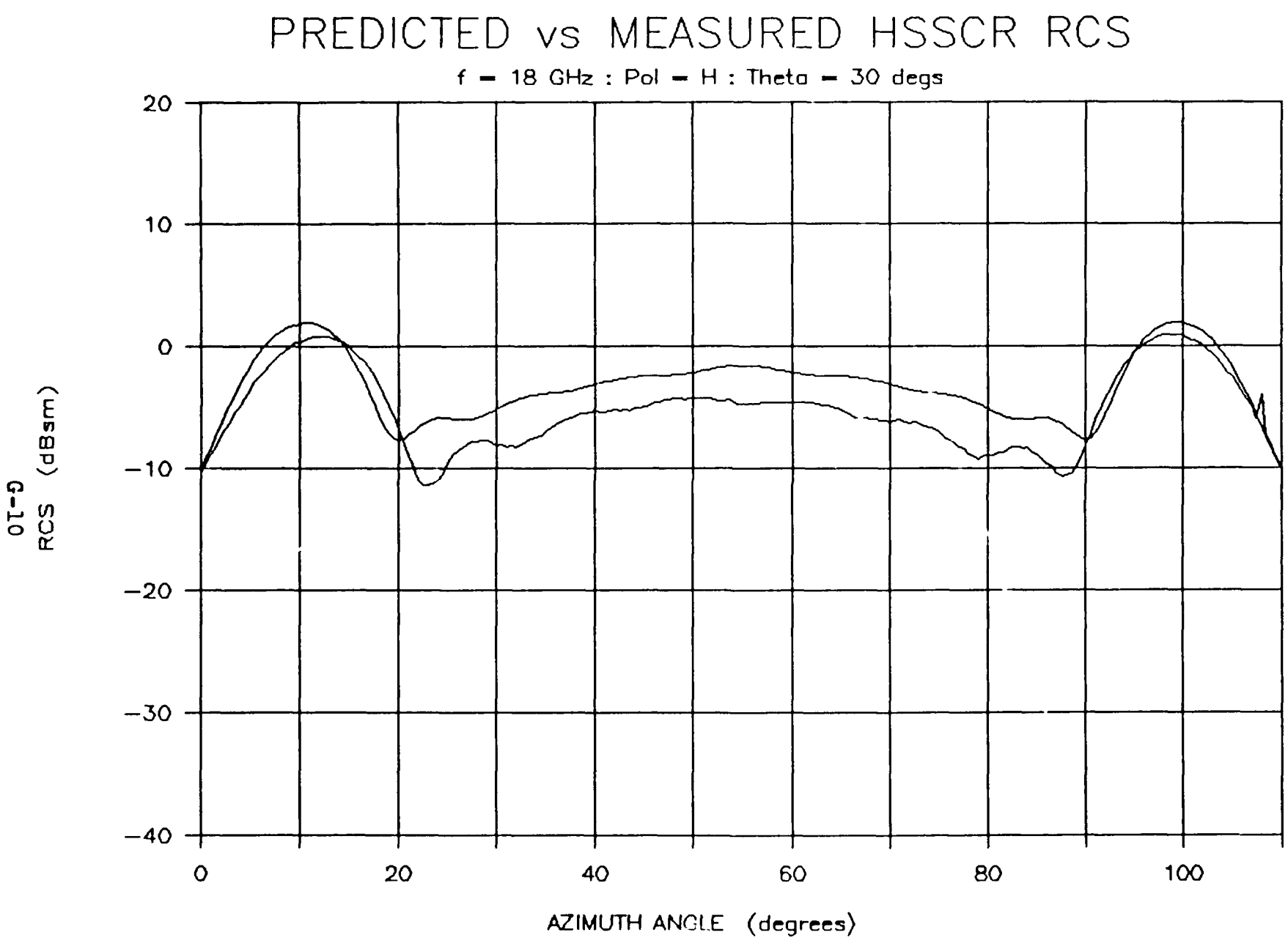

Figure G.9 Predicted vs Measured RCS: HSSCR, 18 GHz, Theta of 30 degs, Horz Pol

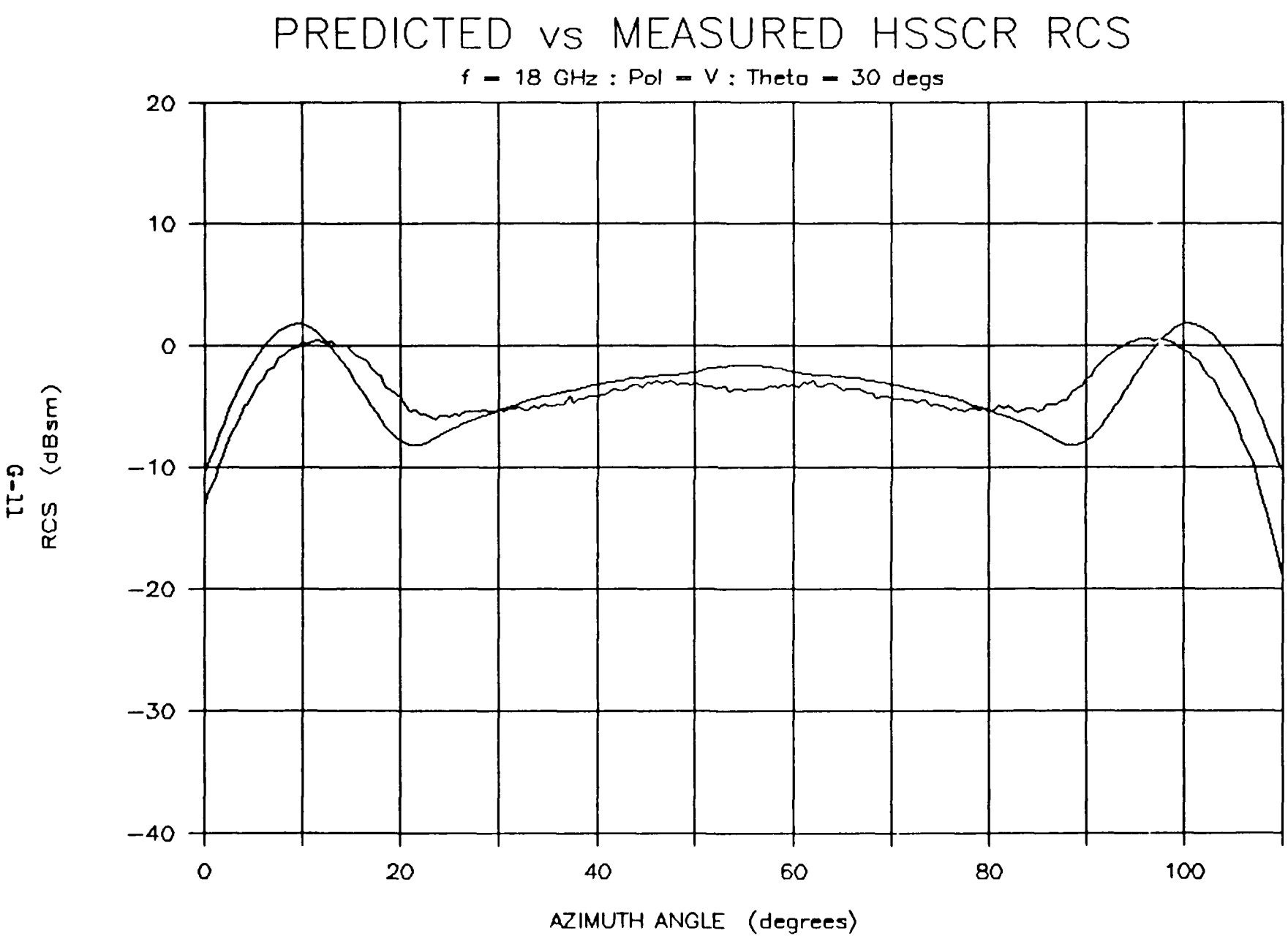

Figure G.10 Predicted vs Measured RCS: HSSCR, 18 GHz, Theta of 30 degs, Vert Pol

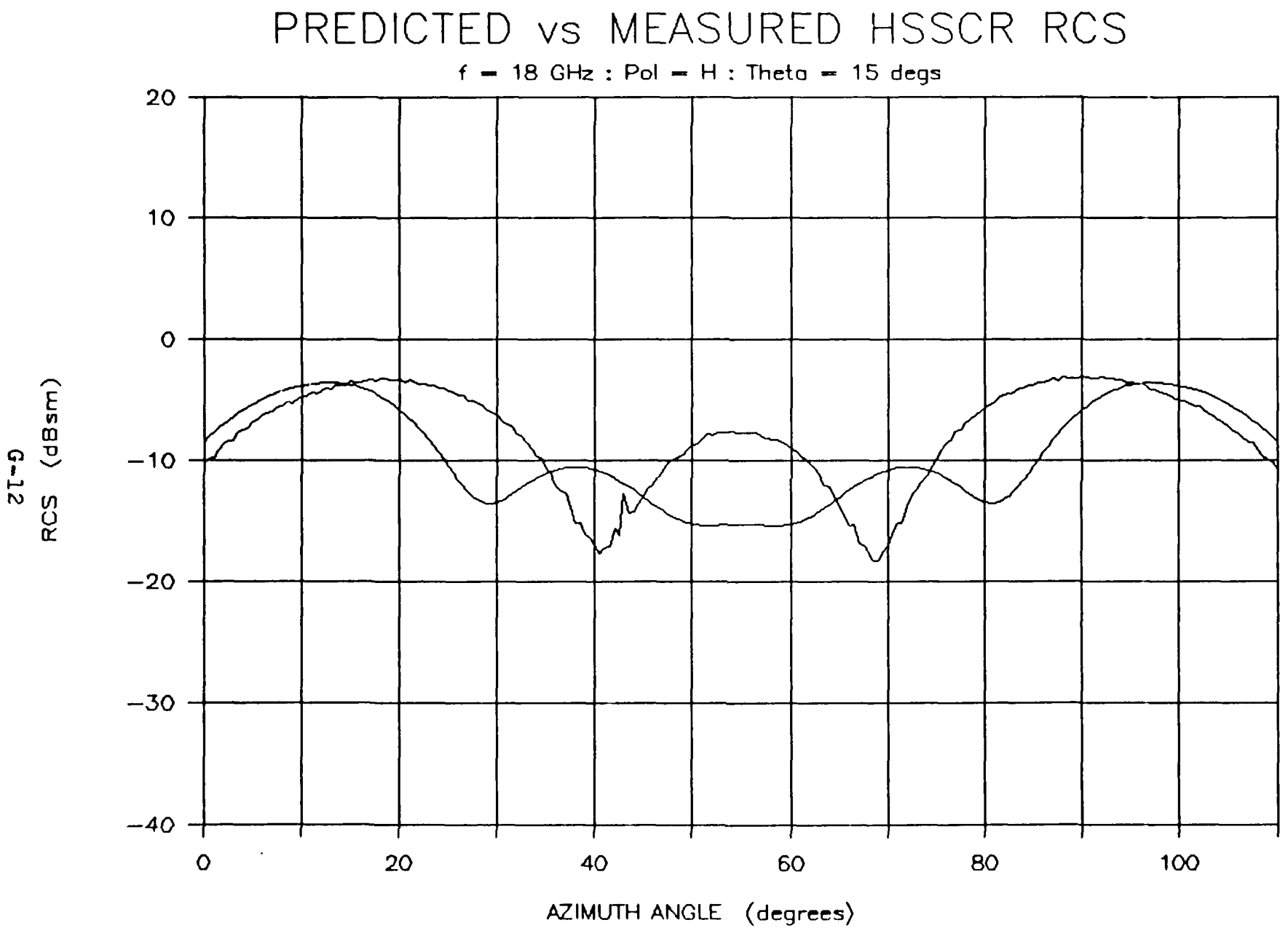

Figure G.11 Predicted vs Measured RCS: HSSCR, 18 GHz, Theta of 15 degs, Horz Pol

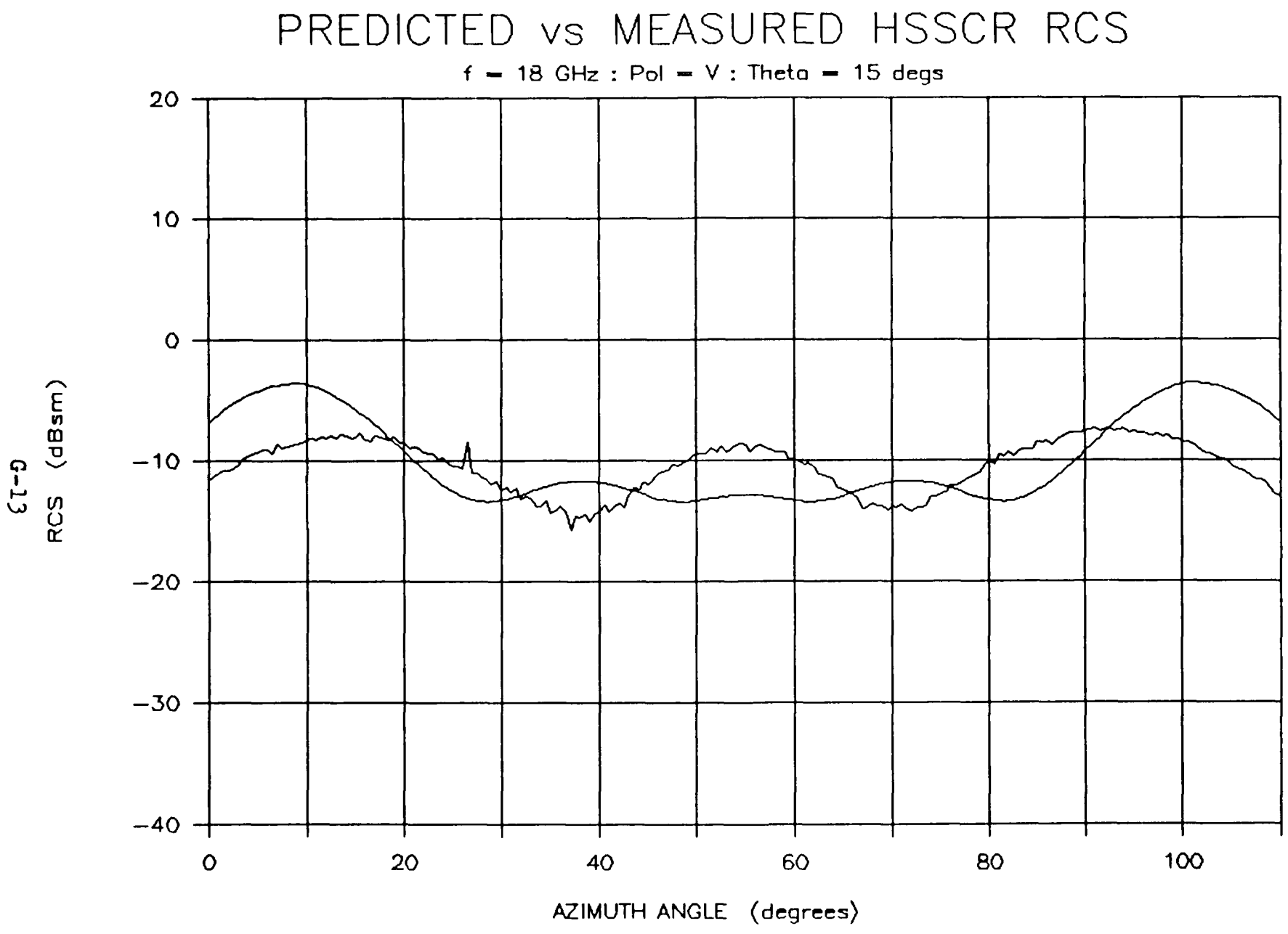

Figure G.12 Predicted vs Measured RCS: HSSCR, 18 GHz, Theta of 15 degs, Vert Pol

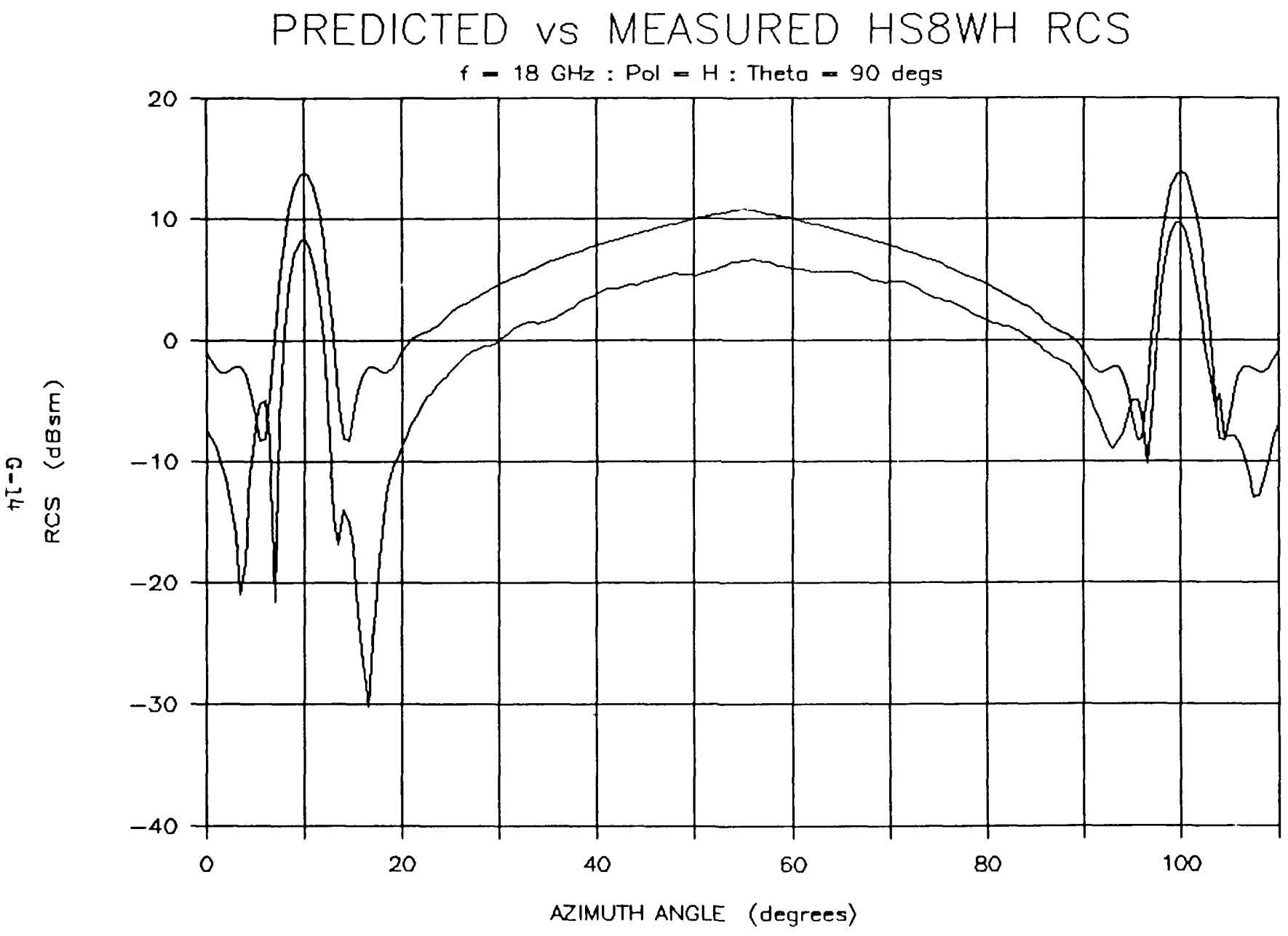

Figure G.13 Predicted vs Measured RCS: HS8WH, 18 GHz, Theta of 90 degs, Horz Pol

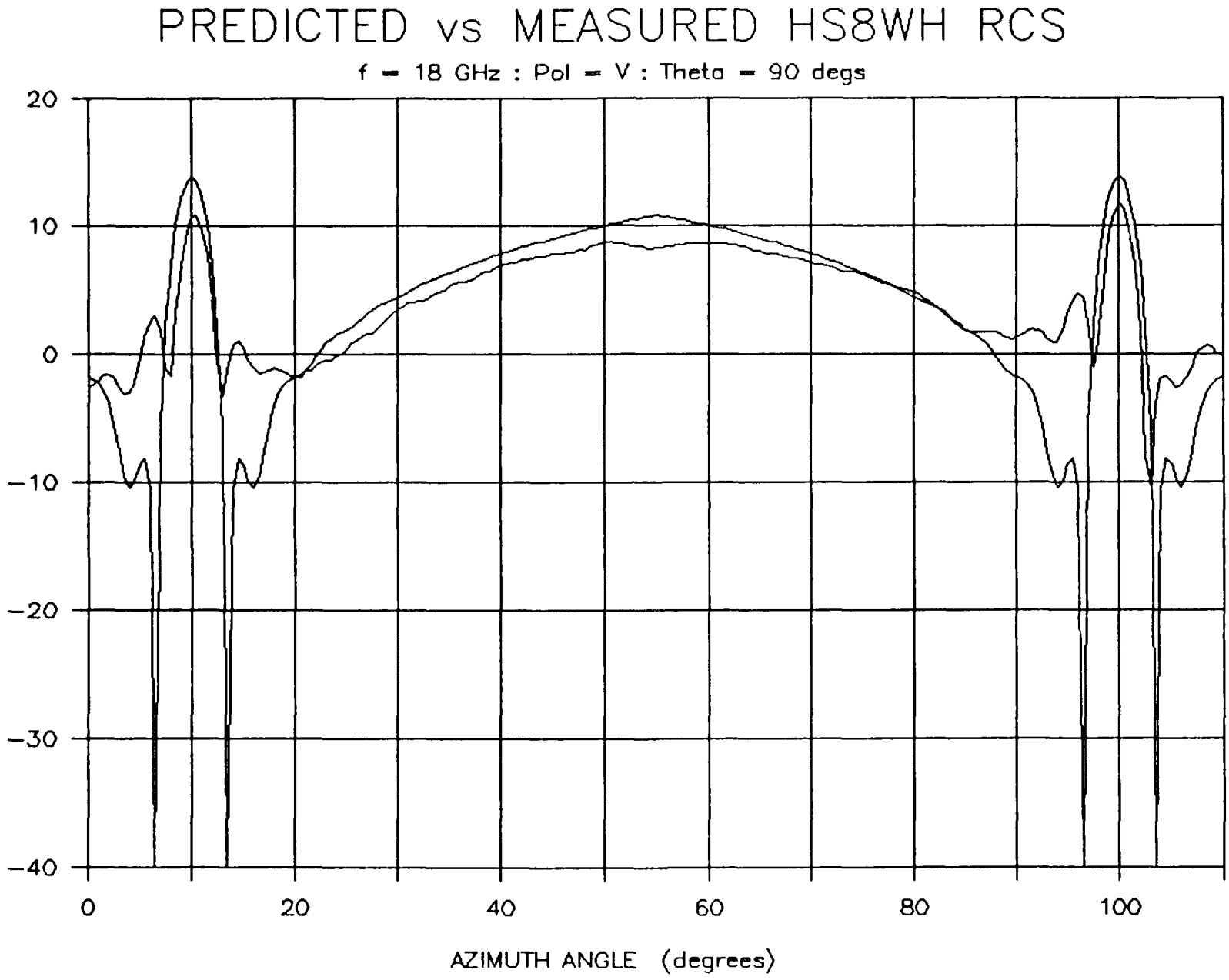

Figure G.14 Predicted vs Measured RCS: HS8WH, 18 GHz, Theta of 90 degs, Vert Pol

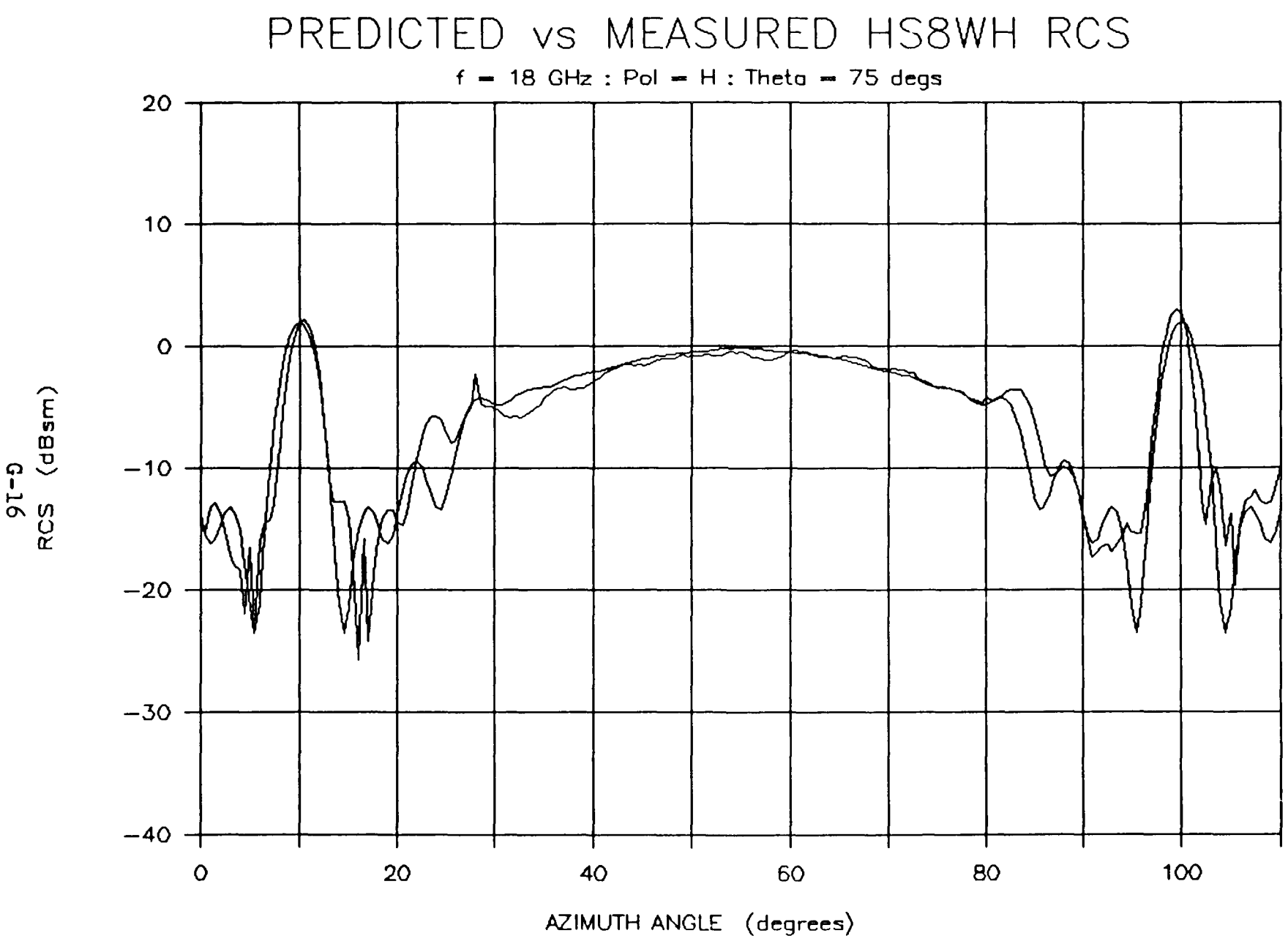

Figure G.15 Predicted vs Measured RCS: HS8WH, 18 GHz, Theta of 75 degs, Horz Pol

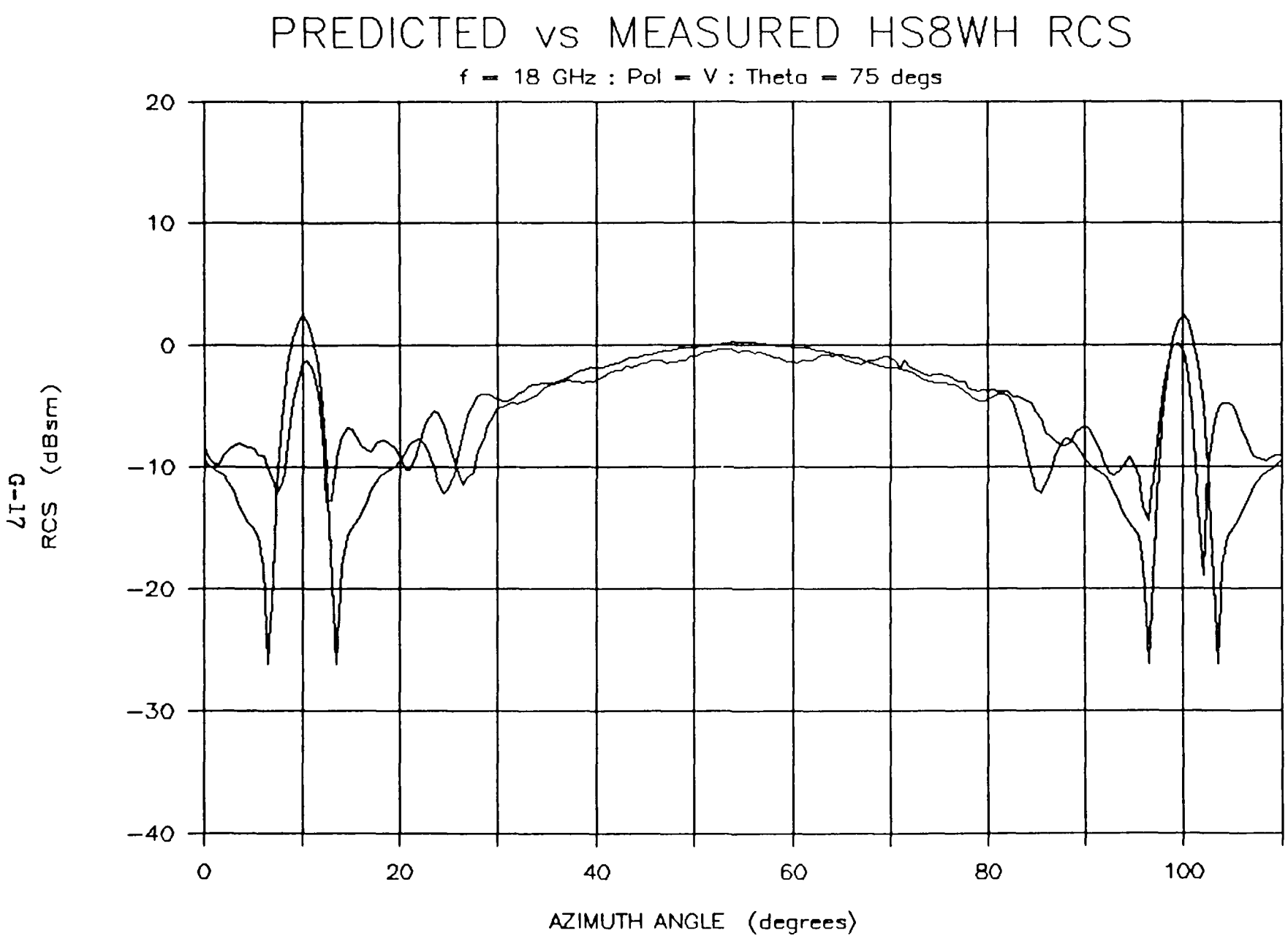

Figure G.16 Predicted vs Measured RCS: HS8WH, 18 GHz, Theta of 75 degs, Vert Pol

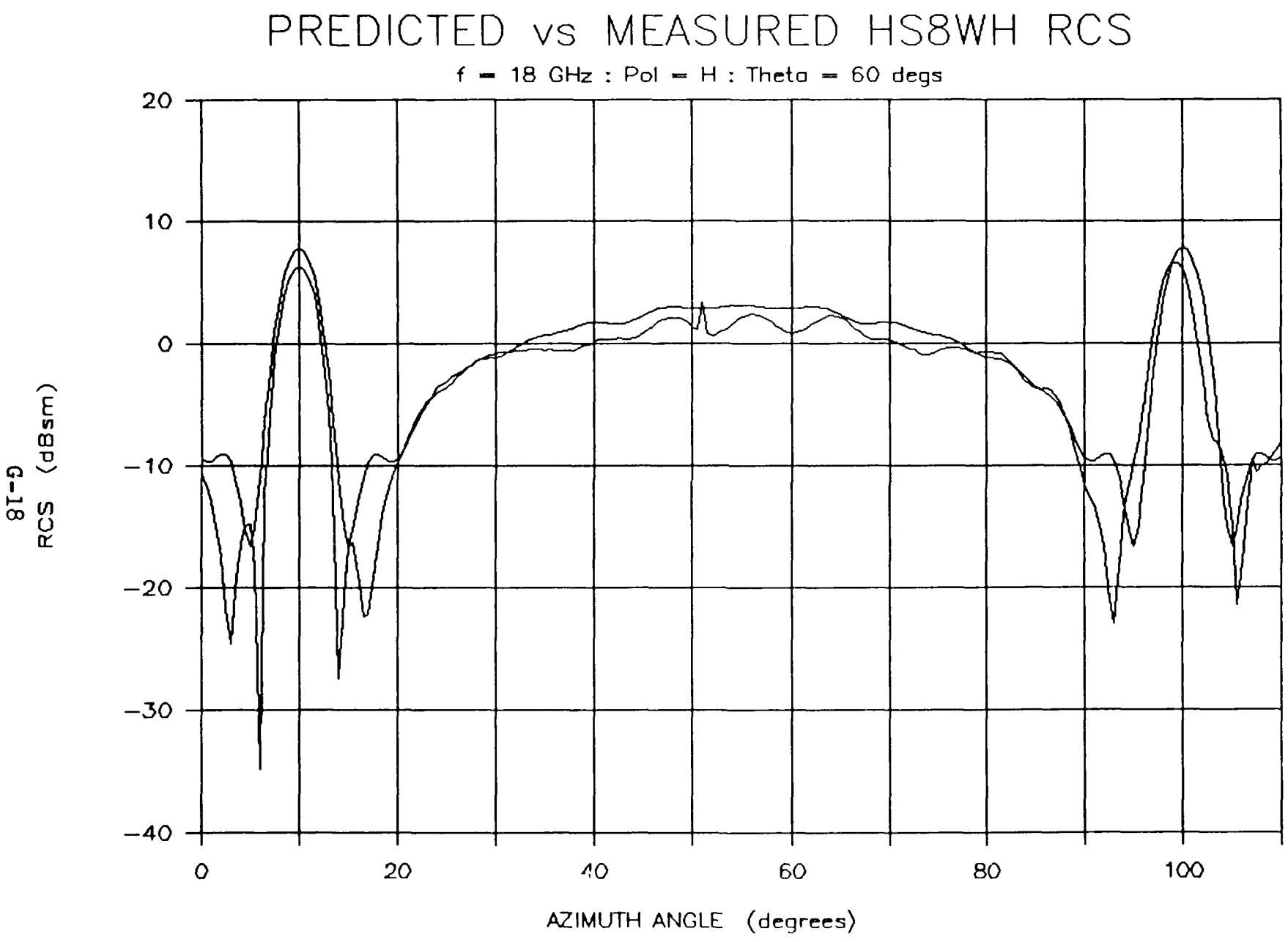

Figure G.17 Predicted vs Measured RCS: HS8WH, 18 GHz, Theta of 60 degs, Horz Pol

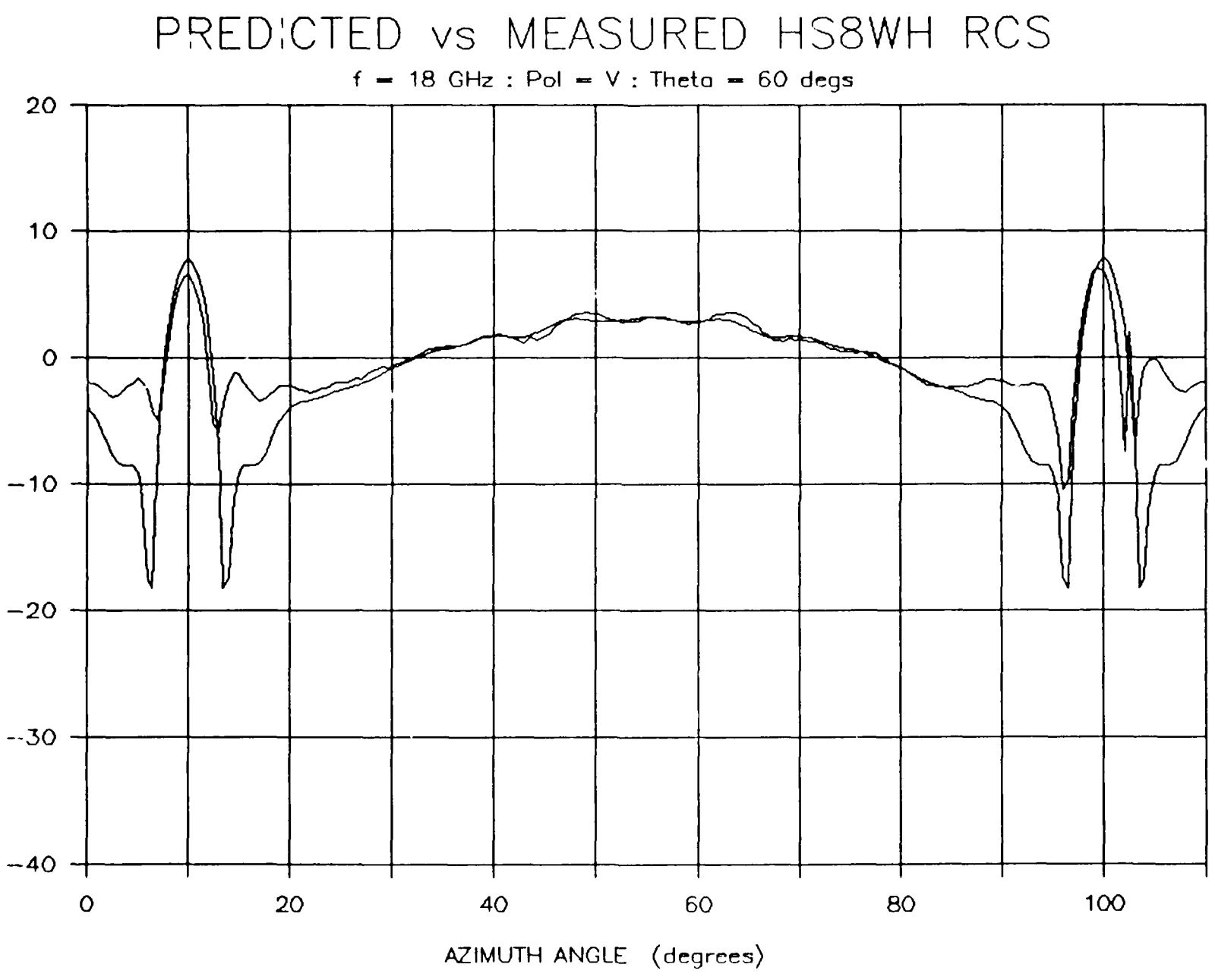

Figure G.18 Predicted vs Measured RCS: HS8WH, 18 GHz, Theta of 60 degs, Vert Pol

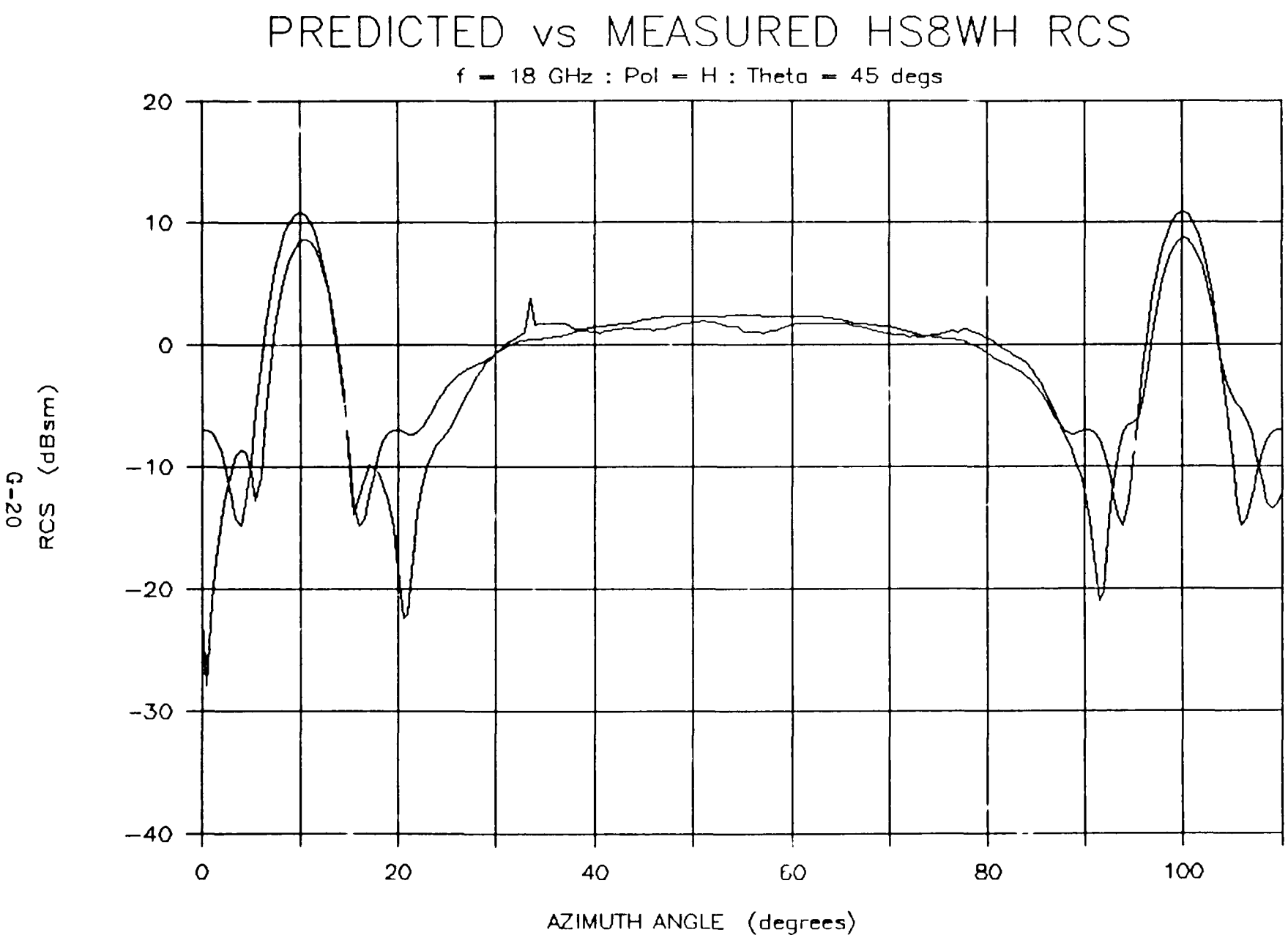

Figure G.19 Predicted vs Measured RCS: HS8WH, 18 GHz, Theta of 45 degs, Horz Pol

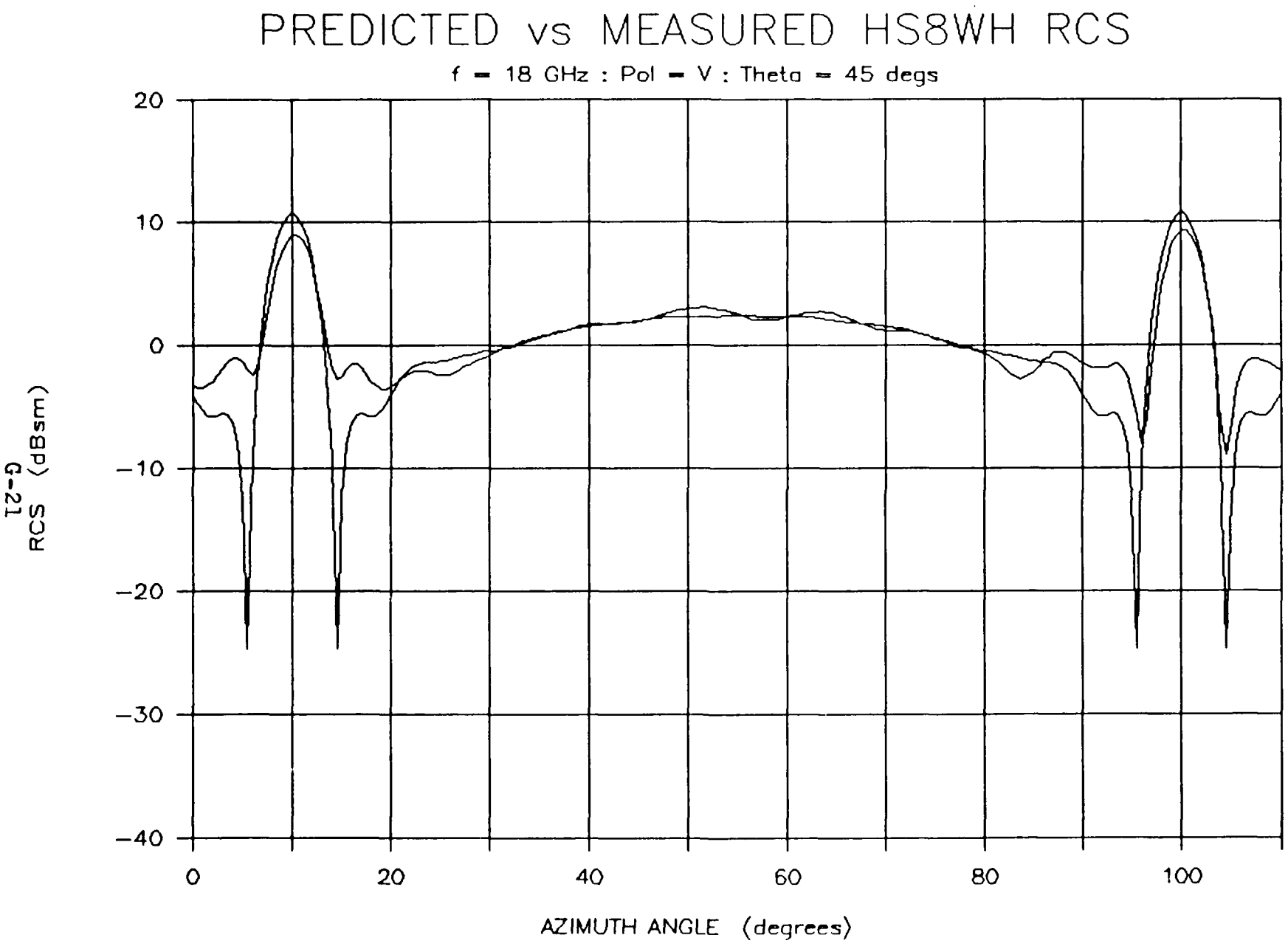

Figure G.20 Predicted vs Measured RCS: HS8WH, 18 GHz, Theta of 45 degs, Vert Pol

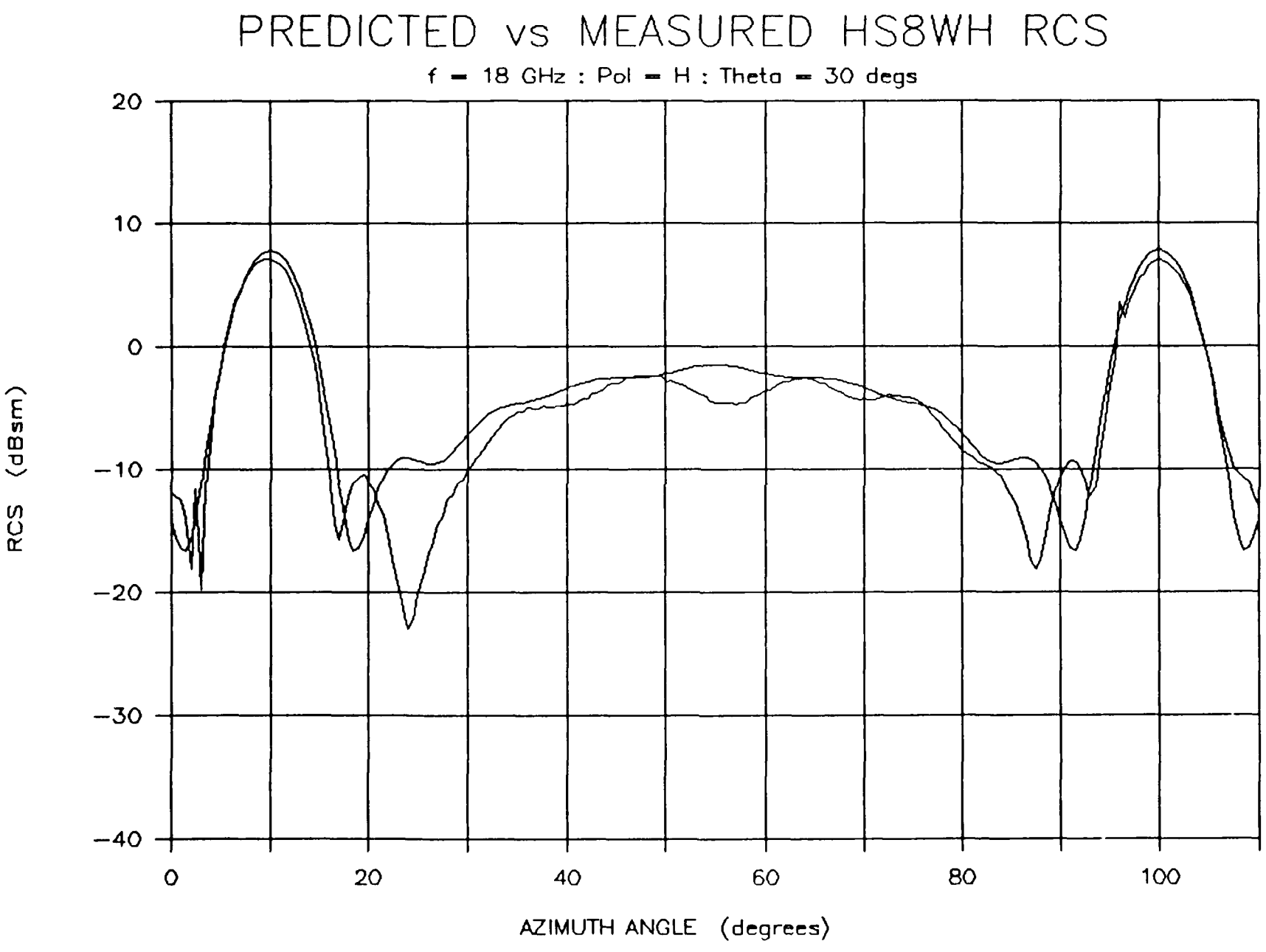

Figure G.21 Predicted vs Measured RCS: HS8WH, 18 GHz, Theta of 30 degs, Horz Pol

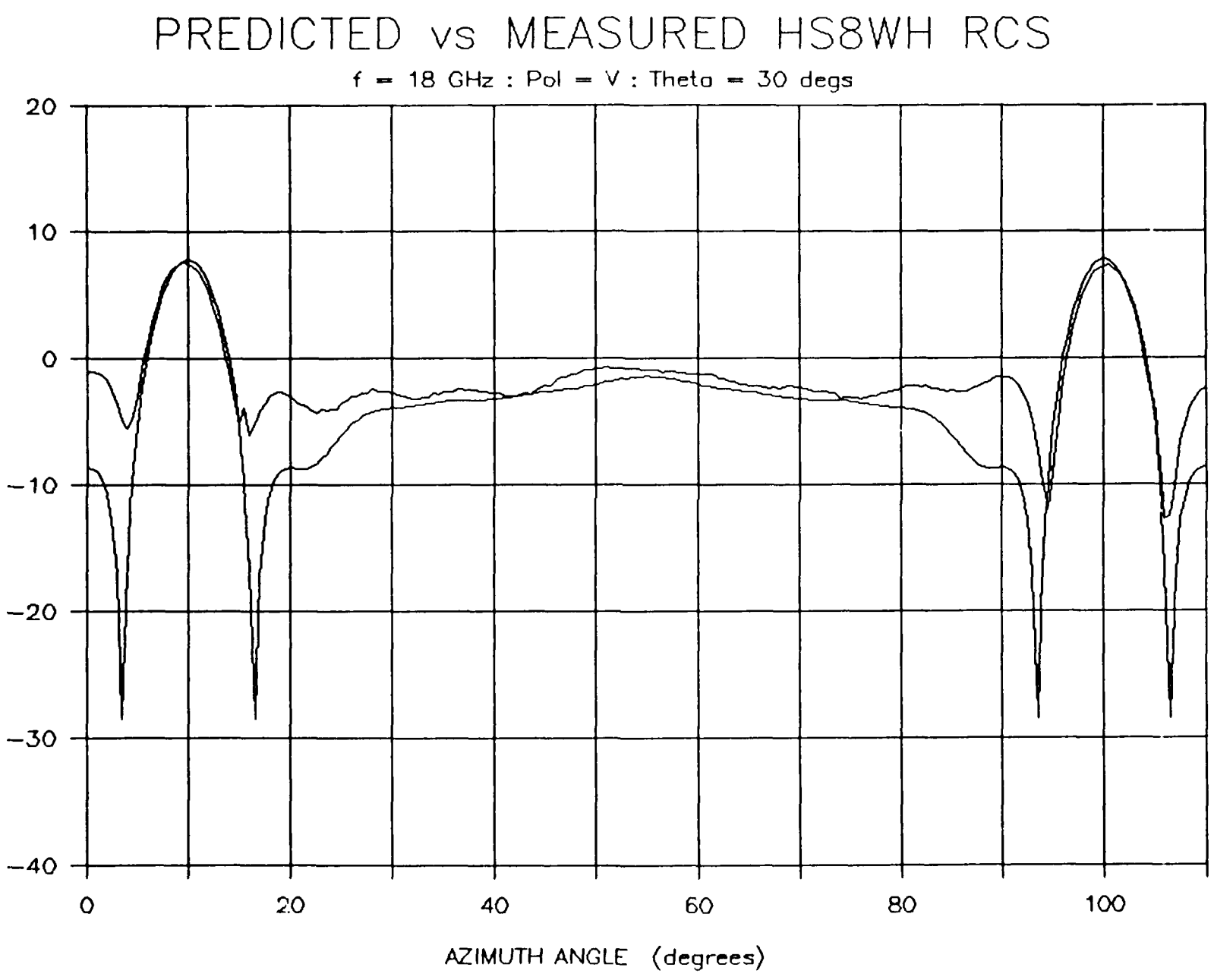

Figure G.22 Predicted vs Measured RCS: HS8WH, 18 GHz, Theta of 30 degs, Vert Pol

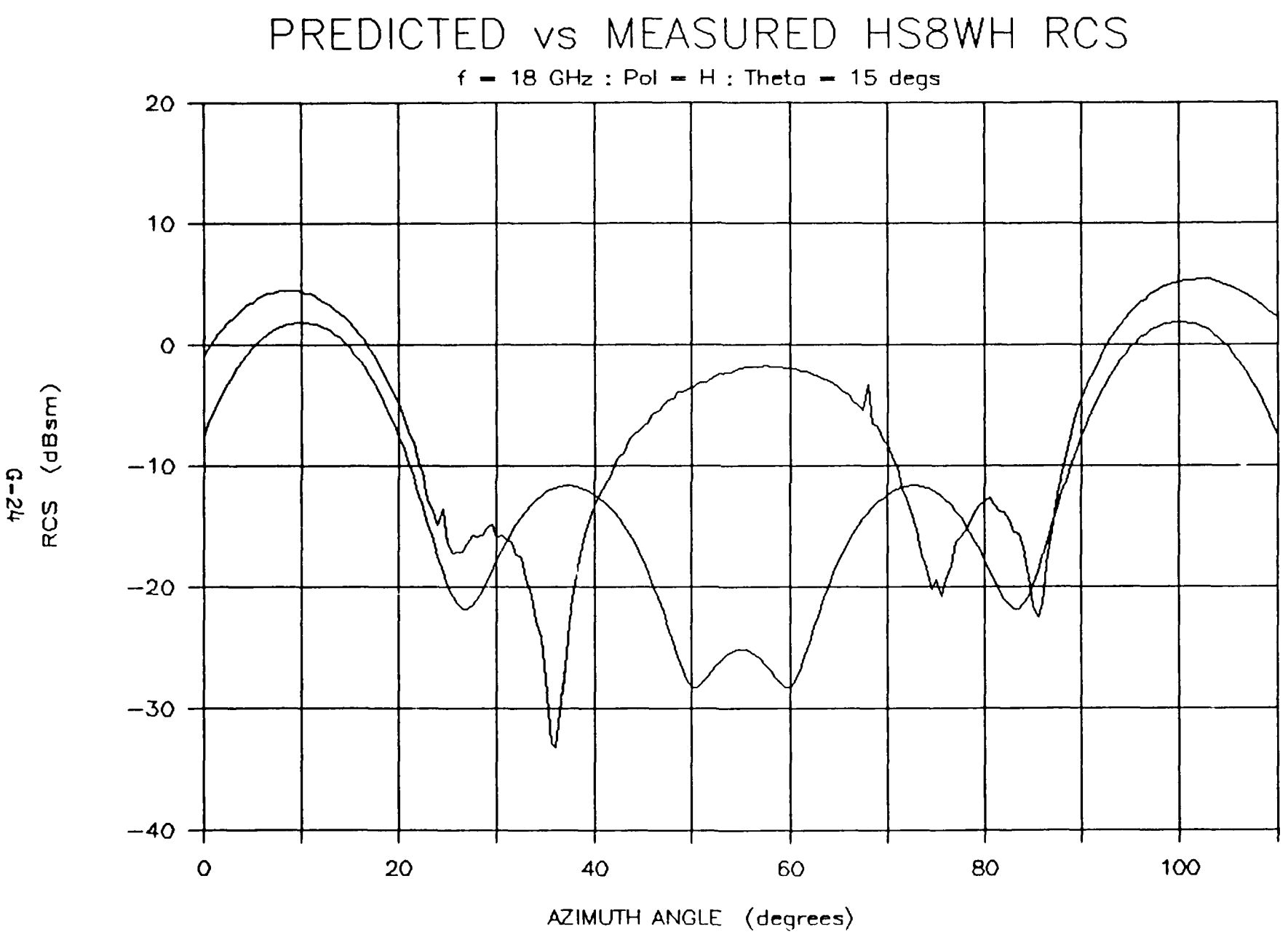

Figure G.23 Predicted vs Measured RCS: HS8WH, 18 GHz, Theta of 15 degs, Horz Pol

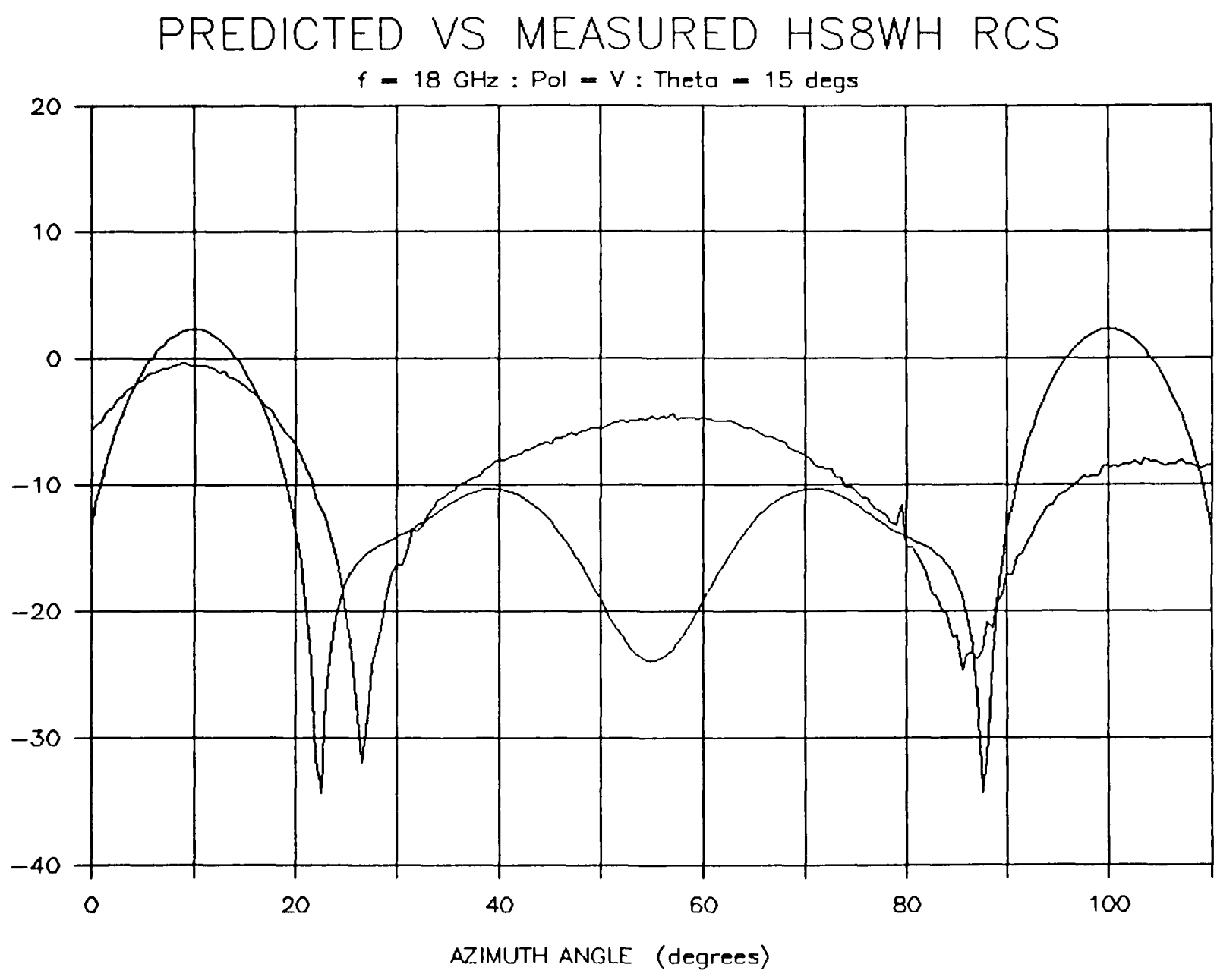

Figure G.24 Predicted vs Measured RCS: HS8WH, 18 GHz, Theta of 15 degs, Vert Pol

Bibliography

1. Berg, Richard M. "Exotic Geometries Yield High-Fidelity Chaff", Microwaves and RF, 64-70, (April 1983).

2. Decker E. E. "How a Geodesic Array of Retro-Reflectors Can Protect Your Ships, Harbors, & Facilities From Radar Guided Missiles" 14 July 1988.

3. Bachman, Christian G. Radar Targets. Lexington, Mass: Lexington Books, 1982.

4. Knott, Eugene F., John F. Schaeffer, and Michael T. Tuley. Radar Cross Section. Norwood, Mass: Artech House, Inc., 1985.

5. Skolnik, Merrill I. Introduction To Radar Systems. McGraw-Hill Book Company, 1980.

6. Blacksmith P. Jr., R. E. Hiatt, and R. B. Mack. "Introduction to Radar Cross-Section Measurements", Proceedings of the IEEE, 53, 901-920, (August 1965).

7. Kouyoumjian, R. G. and Peters L. Jr. "Range Requirements in Radar Cross-Section Measurements", Proceedings of the IEEE, 53, 920-928, (August 1965).

8. Owens, Capt Scott A. Automation of an RCS Measurement System and It's Application to Investigate the Electromagnetic Scattering from Scale Model Aircraft Canopies. MS Thesis, AFIT/GE/ENG/89D-38. School of Engineering, Air Force Institute of Technology (AU), Wright-Patterson AFB OH, December 1989.

9. Sinclair George. "Theory of Models of Electromagnetic Systems", Proceedings of the IRE, 36, 1364-1370, (November 1948).

10. McCool, Capt Stephen W. Bistatic Resonant Scattering Measurements of Special Shapes. MS Thesis, AFIT/GE/ENG/88D-27. School of Engineering, Air Force Institute of Technology (AU), Wright- Patterson AFB OH, December 1988.

11. Stutzman, Warren L. and Thiele, Gary A. Antenna Theory And Design, John Wiley and Sons, New York 1981.

VITA

Captain Richard E. Hamilton [redacted]. He attended high school in Lakeland, Florida. He enlisted in the U.S. Air Force in May 1975 and served as a Communication/Navigation/Electronic Countermeasures Integrated Avionics Systems Specialist at Mountain Home AFB, Idaho. While in Idaho, he attended Boise State University in the undergraduate engineering program. He was selected for the Airman Education and Commission Program in 1981. Under the program he attended the University of Central Florida and received his Bachelor of Science in Engineering (Electrical Engineering Option) in December 1983. He then attended Officer Training School receiving his commission in April 1984. He served as an Electronic Warfare Test Engineer for the 3246 Test Wing, Eglin AFB, Florida until entering the School of Engineering, Air Force Institute of Technology, in May 1988.

[redacted]

SECURITY CLASSIFICATION OF THIS PAGE

REPORT DOCUMENTATION PAGE

Form Approved
OMB No. 0704-0188

1a. REPORT SECURITY CLASSIFICATION Unclassified	1b. RESTRICTIVE MARKINGS
2a. SECURITY CLASSIFICATION AUTHORITY	3. DISTRIBUTION/AVAILABILITY OF REPORT Approved for public release; Distribution unlimited
2b. DECLASSIFICATION/DOWNGRADING SCHEDULE	
4. PERFORMING ORGANIZATION REPORT NUMBER(S) AFIT/GE/ENG/90M-3	5. MONITORING ORGANIZATION REPORT NUMBER(S)
6a. NAME OF PERFORMING ORGANIZATION School of Engineering 6b. OFFICE SYMBOL (*If applicable*) AFIT/ENG	7a. NAME OF MONITORING ORGANIZATION
6c. ADDRESS (*City, State, and ZIP Code*) Air Force Institute of Technology (AU) Wright-Patterson AFB OH 45433-6583	7b. ADDRESS (*City, State, and ZIP Code*)
8a. NAME OF FUNDING/SPONSORING ORGANIZATION 8b. OFFICE SYMBOL (*If applicable*)	9. PROCUREMENT INSTRUMENT IDENTIFICATION NUMBER
8c. ADDRESS (*City, State and ZIP Code*)	10. SOURCE OF FUNDING NUMBERS PROGRAM ELEMENT NO. / PROJECT NO. / TASK NO / WORK UNIT ACCESSION NO

11. TITLE (*Include Security Classification*)
MEASUREMENT AND ANALYSIS OF THE ELECTROMAGNETIC SCATTERING OF A GEODESIC ARRAY OF TRIANGULAR TRIHEDRAL CORNER REFLECTORS

12. PERSONAL AUTHOR(S)
Richard E. Hamilton, Capt USAF

13a. TYPE OF REPORT	13b. TIME COVERED	14. DATE OF REPORT (*Year, Month, Day*)	15. PAGE COUNT
MS Thesis	FROM _____ TO _____	March 1990	240

16. SUPPLEMENTARY NOTATION

17. COSATI CODES			18. SUBJECT TERMS (*Continue on reverse if necessary and identify by block number*)
FIELD	GROUP	SUB-GROUP	Radar Cross Section, Radar Corner Reflectors, Radar Decoys
17	09		
17	04	03	

19. ABSTRACT (*Continue on reverse if necessary and identify by block number*)

Thesis Advisor: Dr. Vittal P. Pyati
Associate Professor of Electrical Engineering

Abstract: See reverse side

20. DISTRIBUTION/AVAILABILITY OF ABSTRACT ☐ UNCLASSIFIED/UNLIMITED ☒ SAME AS RPT ☐ DTIC USERS	21. ABSTRACT SECURITY CLASSIFICATION Unclassified
22a. NAME OF RESPONSIBLE INDIVIDUAL Vittal P. Pyati, BSEE, MSEE, PhD	22b. TELEPHONE (*Include Area Code*) 513-255-3576 22c. OFFICE SYMBOL AFIT/ENG

DD Form 1473, JUN 86 *Previous editions are obsolete*

SECURITY CLASSIFICATION OF THIS PAGE

ABSTRACT

This thesis investigated the electromagnetic (EM) scattering of a Geodesic Array consisting of a cluster of twenty trihedral corner reflectors held together by hinges. This target was designed to provide a large radar return with a spatial coverage greater than that due to an array of eight corner reflectors.

Radar cross section (RCS), or echo area, was chosen as a means of investigating the EM scattering of a scaled model version of the Geodesic Array. The RCS of the individual components of the Geodesic Array (i.e. the single corner reflectors) and the RCS of the Geodesic Array were measured using a continuous wave measurement technique. For the purpose of comparison the RCS of an eight corner reflector array was also measured. In order to gather as much spatial scattering information as possible, a unique target support mount was designed, constructed, and used to collect conical cut RCS patterns. The measured RCS patterns of the targets are included in the appendixes of this document.

A comparative analysis between the measured RCS of the Geodesic Array and that of the eight corner reflector array was performed to determine how well the Geodesic Array met its designed goal. Based on certain criteria it was found that in almost all cases, the measured spatial RCS coverage for the Geodesic Array was equal to or better than the measured spatial RCS coverage of the array of eight corner reflectors. The only exception was for broadside incidence for which the Geodesic Array spatial coverage was slightly less.

The overall conclusion of this research effort was that the Geodesic Array is a viable target for the purpose of providing a large radar return over a large number of aspect angles. The recommendations stemming from this research are, to first compare the results presented in this document to results of other targets designed for this purpose, and based on this future comparison to decide if field testing of a full scale version of the Geodesic Array is warranted.